

Some pages of this thesis may have been removed for copyright restrictions.

If you have discovered material in Aston Research Explorer which is unlawful e.g. breaches copyright, (either yours or that of a third party) or any other law, including but not limited to those relating to patent, trademark, confidentiality, data protection, obscenity, defamation, libel, then please read our [Takedown policy](#) and contact the service immediately (openaccess@aston.ac.uk)

**BRAIN NETWORK APPROACHES TO CHARACTERISE STRUCTURE-FUNCTION
RELATIONSHIPS AFTER CHILDHOOD HEAD INJURY**

DANIEL J. KING

Doctor of Philosophy

ASTON UNIVERSITY

October 2019

© Daniel J. King, 2019

Daniel J. King asserts his moral right to be identified as the author of this thesis.

This copy of the thesis has been supplied on condition that anyone who consults it is understood to recognise that its copyright belongs to its author and that no quotation from the thesis and no information derived from it may be published without appropriate permission or acknowledgement.

BRAIN NETWORK APPROACHES TO CHARACTERISE STRUCTURE-FUNCTION RELATIONSHIPS AFTER CHILDHOOD HEAD INJURY

Daniel J. King, Doctor of Philosophy, 2019

THESIS SUMMARY

Traumatic brain injury (TBI) is a common leading cause of disability for children and young adults. Such an insult during development leads to a cognitive-behavioural syndrome of impairments post-injury however, the trajectory and magnitude of this syndrome at an individual-patient level are unknown. Pathological effects of a TBI on neuroanatomy can be quasi-quantitatively measured using magnetic resonance imaging (MRI). The current thesis highlights the current state of research into neuroanatomical differences post-TBI and identifies previous investigations of neuroanatomical correlates of later functioning adopt mostly reductionist and univariate approaches. It was posited that utilising MRI methodologies that respect the complex, interrelated nature of neuroanatomy across the cortex would provide better understanding of the neuroanatomical correlates of later cognitive functioning post-injury. The current thesis investigates novel network-level analyses of neuroanatomy, specifically structural covariance and morphometric similarity approaches, and its relationship with neuropsychological functioning, with a focus on executive functioning (EF) at 2 years post-injury. The data used included 107 survivors of paediatric TBI and 36 typically developing controls.

Using a structural covariance methodology the current thesis provides evidence that executive dysfunction is associated with atrophic neuroanatomical-changes to topologically important brain-regions within the network. Results also provided evidence that the magnitude of EF difficulties was associated with the extent to which an injury diverted the brain from the ‘typical’ organization of the neuroanatomical network. Using individual morphometric similarity approaches coupled with supervised machine learning, a pattern of morphology, centred in the pre-frontal cortex, predicted later EF.

Overall, these findings fit with the hypothesis that network-level neuroanatomical correlates of EF would be found. The current thesis concludes that, regarding the neuropsychological sequelae post-neurological insult, quantification of the complex organisation of neuroanatomy across the cortex is a useful biomarker. Future investigations integrating neuropsychology and neuroimaging to understand brain structure-function relationships should continue to utilise modern network approaches which capture the diffuse, disconnecting nature of injury.

Keywords: ‘Traumatic Brain Injury’, ‘Structural Covariance’, ‘MRI’, ‘Executive Function’, ‘neurodevelopment’

*To Nanna,
For always being proud of me*

*To Grandpa,
For believing in me*

And finally,

*To Dad,
For all of the support, love and encouragement*

ACKNOWLEDGEMENTS

I am grateful to all the participants and families who contributed their time and effort to the studies whose data was included in the current thesis.

Each experimental chapter in the current thesis was prepared for publication during the course of the PhD and I would like to thank all co-authors for their input on this process, including academics from the Murdoch Children's Research Institute in Melbourne, Australia, specifically Prof. Vicki Anderson, A/Prof. Cathy Catroppa and Dr Richard Beare. Additional information is provided at the start of the relevant chapters, including publication status and all author contributions declared.

I have had the great privilege of working with a number of amazingly talented academics and students as a part of the PROBI research team (and the wider entourage!) and would like to thank them all for making the last three years easier, more enjoyable and much tastier (there is always time for cake and science!).

I would also like to thank the inhabitants of the 5th-floor psychology post-graduate offices (both old and new), having such a kind group of people around makes the tribulations of the PhD journey a lot more bearable. A special mention to both Adam and Alena, thanks for your help, friendship and putting up with me for three years. The tea-room won't be the same for anyone without our frequent visits... !

A special thanks to my supervisors Dr Elaine Foley and Prof. Stefano Seri, for their support throughout this process. I would also like to give utmost thanks to my final supervisor, Prof. Amanda Wood, for helping me navigate the world of research, encouraging my scientific intrigue (when we get a chance to chat science!) and for mentoring me through the times where life has to come first. I look forward to doing more science together in the future!

Thank you also to my family in for putting up with me and what might seem to be an endless period of university education. And most importantly, I would like to thank my amazing wife-to-be. You've raised me up out of the bad times, celebrated with me in the good times and have always been there for all the times in between. We made it (although I can't promise that I won't still keep banging on about it all...)!

Funding Acknowledgements

The author of this thesis was supported by a studentship awarded by the School of Life and Health Sciences, Aston University, Birmingham UK. The current thesis was also supported by a European Research Council (ERC) - Consolidator Grant (ERC-CoG) to Professor Amanda Wood [grant number 682734].

Data from the 'Prevention and Treatment of Social Problems Following TBI in Children and Adolescents' study was made available via material transfer agreement by Prof. Vicki Anderson. Financial support for that study was provided by the Victoria Neurotrauma Initiative, Australia,

(Grant/Award Number: CO6E1); Victorian Government Operational Infrastructure Support Program, Australia to Prof. Vicki Anderson.

Autism Brain Imaging Data Exchange I data were made available by Adriana Di Martino supported by the (NIMH K23MH087770) and the Leon Levy Foundation. Primary support for the work by Michael P. Milham and the INDI team in relation to this data was provided by gifts from Joseph P. Healy and the Stavros Niarchos Foundation to the Child Mind Institute, as well as by an NIMH award to MPM (NIMH R03MH096321).

Human Connectome Project Data were provided [in part] by the Human Connectome Project, WU-Minn Consortium (Principal Investigators: David Van Essen and Kamil Ugurbil; 1U54MH091657) funded by the 16 NIH Institutes and Centers that support the NIH Blueprint for Neuroscience Research; and by the McDonnell Center for Systems Neuroscience at Washington University.

Table of contents

Thesis Summary	2
Dedication	3
Acknowledgements	4
Table of Contents	6
List of Tables	13
List of Fig	14
List of Appendices	15
Chapter 1 – General Introduction	16
1.1 Precis	16
1.2 Traumatic Brain Injury in Children	17
1.3 In vivo investigation of brain development with MRI	18
1.3.1 MRI of the Brain	18
1.3.2 Developing brain structure	19
1.3.3 Development of Brain Structure and Cognition	19
1.4 Executive Functions, MRI and pTBI	20
1.4.1 Neuropsychology of Executive Functions	20
<i>1.4.1.1 Working Memory and Updating</i>	21
<i>1.4.1.2 Inhibitory Control</i>	22
<i>1.4.1.3 Cognitive Flexibility</i>	23
1.4.2 Executive functions post-injury	23
1.4.3 Neural correlates of executive function following pTBI	24
1.5 Network analyses of in-vivo MRI	26
1.5.1 Network analyses	26
1.5.2 Network analyses of sMRI	27
1.6 Executive Summary	30

1.6.1 Main Thesis Aims.....	30
1.6.2 Thesis Outline.....	30
Chapter 2. A systematic review of cross-sectional differences and longitudinal changes to the morphometry of the brain following paediatric traumatic brain injury	32
2.1 Overview.....	32
2.2 Introduction.....	32
2.3 Methods.....	34
2.3.1 Review Strategy.....	34
2.3.2 Study quality.....	36
2.3.3 Data Visualisation.....	36
2.3.4 Overlapping samples.....	36
2.4 Results.....	36
2.4.1 Eligible studies.....	36
2.4.2 Cross-sectional studies.....	49
2.4.3 Longitudinal studies.....	57
2.4.4 Linking morphometry to cognition in TBI.....	58
2.5 Discussion.....	60
2.6 Concluding remarks.....	66
Chapter 3. Lesion induced error on automated measures of brain volume: Data from a paediatric traumatic brain injury cohort	68
3.1 Overview.....	68
3.2 Introduction.....	68
3.3 Methods.....	71
3.3.1 Participants.....	71
3.3.2 MRI Acquisition.....	76
3.3.3 Simulated Lesions.....	76
3.3.4 Automated structural segmentation using <i>Freesurfer</i>	78

3.3.5 Statistical Analysis.....	78
3.4 Results.....	80
3.5 Discussion.....	85
3.6 Limitations.....	89
3.7 Conclusion.....	90
Chapter 4. Structural Covariance Identifies Altered Network Topology in Children with Persistent Executive Function Impairments after Traumatic Brain Injury	91
4.1 Overview.....	91
4.2 Introduction.....	91
4.3 Methods.....	94
4.3.1 Ethics statement.....	94
4.3.2 Participants.....	94
4.3.2.1 TBI Cohort.....	94
4.3.2.2 ABIDE dataset.....	95
4.3.3 MRI Processing.....	98
4.3.4 Executive Functions (EF)	98
4.3.5 Statistical analysis.....	101
4.3.5.1 Differences in CT between pTBI and Controls.....	101
4.3.5.2 Differences in SC between pTBI and Controls.....	101
4.3.5.3 SC between regions with CT reductions in pTBI.....	102
4.4 Results.....	102
4.4.1 Differences in CT between pTBI and Controls.....	102
4.4.2 Differences in SC between pTBI and Controls	102
4.4.3 SC between regions with CT reductions in pTBI.....	105
4.4.3 Lesion Cases.....	107
4.5 Discussion.....	107
4.5.1 Differences in CT between pTBI and Controls.....	107

4.5.2 Differences in SC between pTBI and Controls.....	108
4.5.3 SC between regions with CT reductions in pTBI.....	108
4.6 Limitations.....	109
4.7 Conclusion.....	110
Chapter 5. Developmental Divergence of Structural Brain Networks as an Indicator of Future Cognitive Impairments in Childhood Brain Injury	111
5.1 Overview.....	111
5.2 Introduction.....	111
5.3 Methods.....	114
5.3.1 Ethics statement.....	114
5.3.2 Participants.....	115
5.3.2.1 TBI Cohort.....	115
5.3.2.2 ABIDE dataset.....	116
5.3.3 MRI Processing.....	118
5.3.4 Graphs of Structural covariance.....	118
5.3.4.1 Divergence Metrics.....	118
5.3.4.2 Reference Networks.....	119
5.3.4.3 Sliding-Window.....	120
5.3.5 Executive Functions (EF).....	121
5.3.5.1 Central Executive Network (CEN).....	123
5.3.6 Statistical analysis.....	123
5.3.6.1 Post-Hoc Analyses.....	124
5.4 Results.....	124
5.4.1 Age-invariant Network and DDI_{inv}	124
5.4.2 Age-matched Network and DDI_{age}	126
5.4.3 DDI of the CEN.....	130
5.4.4 Post-hoc exploratory analyses.....	130

5.5 Discussion.....	132
5.6 Conclusion.....	136
Chapter 6. Clinically-Feasible Brain Morphometric Similarity Network Construction Approaches with Restricted Magnetic Resonance Imaging Acquisitions and their Relationship with Cognition	137
6.1 Overview.....	137
6.2 Introduction.....	137
6.3 Materials and Methods.....	141
6.3.1 Participants - HCP data.....	141
6.3.1.1 HCP 1200 Release.....	141
6.3.1.2 HCP Test-Retest Release.....	141
6.3.2 Methods.....	141
6.3.2.1 Data Quality Control.....	141
6.3.2.1 MRI Processing.....	142
6.3.2.2 MSN Construction.....	144
6.3.3 Demographic and Behavioural Data.....	144
6.3.3.1 General Cognitive Ability.....	145
6.3.3.2 Executive Functioning.....	145
6.3.4 Statistical comparison.....	145
6.4 Results.....	148
6.4.1 Inter-model comparisons.....	148
6.4.1.1 Magnitude of morphometric similarity: graph-level strength.....	148
6.4.1.2 Edge Weights.....	150
6.4.2 Intra-model comparisons.....	152
6.4.2.1 Test-retest reliability of MSN models.....	152
6.4.2.2 Similarity with average MSN.....	152
6.4.3 Relationship with cognitive scores.....	154
6.5 Discussion.....	154

6.6 Conclusion.....	158
Chapter 7. Morphometric Similarity Networks of the Brain in Children Post-TBI Predict long-term Executive Functioning after Insult	160
7.1 Overview.....	160
7.2 Introduction.....	160
7.3 Methods.....	163
7.3.1 Ethics statement.....	163
7.3.2 Participants.....	163
7.3.3 MRI Processing.....	166
7.3.4 Morphometric Similarity Network Construction.....	166
7.3.5 Executive Functions (EF)	167
7.3.6 Statistical analysis.....	169
7.3.6.1 <i>Between-group differences in the magnitude of morphometric similarity...</i>	169
7.3.6.2 <i>Predicting EF outcome using MS in pTBI.....</i>	169
7.4 Results.....	170
7.4.1 Patient-control differences in the magnitude of morphometric similarity...	170
7.4.2 Predicting EF outcome using morphometric similarity in pTBI.....	170
7.4.3 Predicting EF outcome using individual morphometric features in pTBI...	171
7.5 Discussion.....	177
7.5.1 Patient-control differences in the magnitude of morphometric similarity...	177
7.5.2 Predicting EF outcome using morphometric similarity in pTBI.....	177
7.5.3 Predicting EF outcome using individual morphometric features in pTBI...	179
7.5.4 Limitations.....	180
7.6 Conclusion.....	181
Chapter 8. General Discussion	183
8.1 Overview.....	183

8.2 Findings and Thesis Aims.....	183
8.2.1 Current State of Morphometric Research in pTBI.....	183
8.2.2 Network approaches to Neuroanatomical Correlates of EF post-pTBI.....	185
8.3. Strengths, Limitations and Open Questions in pTBI.....	187
8.3.1 Sample Size, Open Data and Normative Development.....	187
8.3.2 ‘Trajectories’ of development - beyond cross-sectional imaging.....	190
8.3.3 Graph Theory as a ‘language’ of opportunity?.....	191
8.4 Conclusion.....	192
References	194
Appendices	227

List of Tables

Table 2.1 <i>Blocks of search terms used to query publication databases in the review strategy..</i>	35
Table 2.1a. <i>Study demographics for all cross-sectional studies included in the review.....</i>	39
Table 2.2b. <i>Study findings for all cross-sectional studies included in the review.....</i>	44
Table 2.2a <i>Study demographics for all longitudinal studies included in the review.....</i>	53
Table 2.3b <i>Study findings for all longitudinal studies included in the review.....</i>	55
Table 3.1. <i>Demographic variables for Control cases.....</i>	72
Table 3.2. <i>Demographic variables for Lesion cases.....</i>	74
Table 4.1 <i>Demographics for patients and controls.....</i>	97
Table 4.2. <i>Neuropsychological tests and subtests used to group patients on EF outcome....</i>	99
Table 4.3. <i>Demographics for patient subgroups.....</i>	99
Table 4.4. <i>Mean graph strength and bootstrapped 95% confidence intervals.....</i>	103
Table 4.5. <i>Regions with significant permutation differences in nodal strength between experimental controls and EF Poor groups.....</i>	103
Table 5.1. <i>Demographics for each cohort by group.....</i>	117
Table 5.2. <i>Neuropsychological tests and subtests used to calculate EF scores.....</i>	122
Table 5.3. <i>Pearson’s correlation coefficients (r).....</i>	131
Table 6.1. <i>Morphometric measures and the modality of MRI from which they were derived...</i>	143
Table 7.1. <i>Demographics for patients and controls.....</i>	165
Table 7.2. <i>Neuropsychological tests and subtests used to group patients on executive functioning.....</i>	168
Table 7.2. <i>Description of models where components were retained when predicting executive dysfunction from morphometric similarity.....</i>	172
Table 7.3. <i>Description of models where components were retained when predicting executive dysfunction from individual morphometric features.....</i>	173
Table A.1 <i>Imputed data used for visualization of cross sectional studies.....</i>	228
Table A.2 <i>Characteristics for all studies investigating relationship between cognition and morphometry.....</i>	229
Table B.1. <i>Outputs from linear mixed-models.....</i>	238
Table B.2. <i>Outputs from linear mixed-models.....</i>	239
Table B.3. <i>Outputs from linear mixed-models.....</i>	240
Table B.4. <i>Outputs from linear mixed-models.....</i>	241
Table D.1. <i>Details from analyses assessing appropriate window-size for primary analyses...</i>	251
Table D.2. <i>Differences in DDI between injury severity groups across whole-brain and CEN.....</i>	251
Table D.3. <i>Pearson’s partial correlation coefficients (r) between DDI and EF outcomes....</i>	254
Table F.1. <i>Results of GLM to test the effect of group on average nodal strength.....</i>	257
Table F.2. <i>Results of GLM to test the effect of group on nodal strength.....</i>	258
Table F.3. <i>Results of GLM to test differences across injury severity in average nodal strength.....</i>	260
Table F.4. <i>Results of GLM to test differences across EF impairment groups in average nodal strength.....</i>	261

List of Figures

Figure 2.1 <i>PRISMA flowchart</i>	38
Figure 2.2. <i>Descriptive plot of all eligible cross-sectional studies included for review</i>	52
Figure 3.1 <i>Visualisation of individual lesion masks in MNI space</i>	75
Figure 3.2. <i>Examples of original lesion cases</i>	77
Figure 3.3. <i>Plots of differences in cortex and cWM volume</i>	81
Figure 3.4. <i>Plots of PVD for both cortex and cWM volume</i>	83
Figure 3.5. <i>Plots of subject-level PVD for both cortex and cWM volume</i>	84
Figure 4.1. <i>Observed mean strength</i>	106
Figure 5.1. <i>Plots of DDI_{inv} for both TBI and control groups</i>	125
Figure 5.2. <i>Plots of DDI_{age} for both TBI and control groups</i>	127
Figure 5.3. <i>Scatter plots of the log of the DDI measures</i>	128
Figure 5.4. <i>Correlation between DDI of the CEN, and a) EF and b) BRIEF</i>	129
Figure 6.1 <i>Graph metrics describing average network strength for each MSN model</i>	149
Figure 6.2 <i>Violin plot of correlation of edge weights</i>	151
Figure 6.3 <i>Model comparisons across thresholds</i>	151
Figure 6.4 <i>Plots showing MSN similarity</i>	153
Figure 7.1. <i>Results of PLS regression.</i>	174
Figure 7.2. <i>Plot of top five positive/negative weighted predictors (degree of ROIs) of BRIEF GEC</i>	176
Figure B.1 <i>Workflow for generating simulated lesions</i>	237
Figure D.1. <i>Differences in DDI_{inv} and DDI_{age} for both the whole brain (first column) and only the CEN (second column) across injury severities</i>	252
Figure F.1. <i>The bootstrapped CI for PLS weightings for each ROI using individual morphometric features to predict BRIEF-GEC scores</i>	262
Figure F.2. <i>The bootstrapped CI for PLS weightings for each ROI using individual morphometric features to predict EF scores</i>	264

List of Appendices

Appendix A – Supplementary Materials for Chapter 2..... 227

Appendix B – Supplementary Materials for Chapter 3..... 235

Appendix C - Supplementary Materials for Chapter 4..... 242

Appendix D - Supplementary Materials for Chapter 5..... 247

Appendix E - Supplementary Materials for Chapter 6..... 255

Appendix F - Supplementary Materials for Chapter 7..... 256

Chapter 1 – General Introduction

“Of great value to both clinicians and to the families of TBI patients would be the ability reliably to predict the recovery of consciousness as well as the **evolution of cognitive and behavioural abilities in the long term** [emphasis added]. Such ability would dramatically change ... treatment and rehabilitation strategies ... reduce the financial burden of TBI upon the healthcare system ... more efficiently proportionate the level of care ... [and] inform families on rehabilitation goals” (Irimia, Wang, et al., 2012, p. 11).

1.1 Precis

Neuropsychological investigation of the cognitive and behavioural ramifications of brain disorders typically use psychometric evaluations to infer ‘damage’ to the neural systems that subsume those functions. The assumption implicit to the field is that brain structure underpins functions in a certain way. The advent of *in-vivo* imaging of the brain, using magnetic resonance imaging (MRI), allows the integration of these neuropsychological findings and a visualisation of the location and nature of the pathology in not only abnormal, but also typically developed or developing populations.

The technological advancement of MRI is ongoing but novel analytic frameworks offer scope to improve our understanding of structure-function relationships. The promising approach of brain network-level analysis, includes methodologies that incorporate metrics about the complexity of brain organization at the systems-level, where brain structure and function are modularly organised into networks of brain regions, rather than as unitary, isolated processing units. This has yet to be applied systematically to paediatric populations, but has potential relevance to children with acquired brain injuries.

Traumatic brain injuries lead to damage across brain networks that is not uniform between different patients, creating an opportunity to refine our understanding of the relationship between brain injury and functional outcomes by using a network-level analytic framework. This is particularly relevant for children who experience traumatic brain injury, in whom there is an ongoing development of brain structure and function. These network-level methodologies may allow us to place the neurological insult within the context of the wider system; damage does not exist in isolation from the rest of the developing brain. This approach represents a recent step-change in the field of neuropsychology, a contemporary approach that may, in future, be a valuable addition to the toolbox of neuropsychologists to quantitatively investigate symptomatic changes to neuroanatomy at the network-level. This is especially true given that many higher cognitive functions are subsumed by the synchronous functioning of diffuse neuroanatomical networks.

The research described in the current thesis presents a novel network approach where structural neuroanatomy is characterised with respect to its meso-scale organisation across the rest of the brain.

Within the context of this thesis, this approach has enabled a better understanding of the neuroanatomical correlates of long-term neuropsychological functioning in children who have experienced a TBI. In this introductory chapter, research pertinent to the reader is highlighted and the thesis is outlined in general terms.

1.2 Traumatic Brain Injury in Children

The overall incidence of traumatic brain injury (TBI) is estimated at between one and five people in every thousand (Sosin, Sniezek, & Thurman, 1996). TBI is a leading cause of disability for both children and young adults (World Health Organization, 2006). Estimates of incidence are much higher for the 0-25 year old age group, with ~30% of individuals experiencing a TBI by the time they reach young-adulthood (aged 25). Between the ages of 0-15 years, there is an estimated incidence between 1.10-1.85 cases per hundred (McKinlay et al., 2008). Thus, many injuries occur in the still-developing brain (Wilde, Hunter, & Bigler, 2012).

Although TBI has a clearly defined onset, as a polypathology (Smith, Johnson, & Stewart, 2013) the injury sets into motion a number of pathological effects including axonal pathology (Johnson, Stewart, & Smith, 2013; Johnson et al., 2016) and brain atrophy (particularly in frontal-temporal regions (Farbota et al., 2012; Keightley et al., 2014; Ross, 2011)), amongst others. In the case of paediatric TBI (pTBI), these pathological mechanisms dynamically interact with the ongoing neurodevelopmental maturation of the brain. This raises the question as to how the brain continues to develop after such an injury?

Around 100-154 in every 100,000 head injuries result in persistent disability at one-year post-injury (Thornhill et al., 2000). It is well documented that a pTBI typically leads to a cognitive-behavioural syndrome of impairments post-injury (Crowe, Catroppa, & Anderson, 2015). However, the trajectory, when an impairment may appear or resolve, and the magnitude, the degree of impairment experienced, of this syndrome is unclear at an individual-level. Ultimately, the risk of poor neuropsychological and functional outcomes for those with mild to severe paediatric TBI (pTBI) is not clearly understood, especially due to the many factors upon which the likelihood of ongoing sequelae may be predicated (Babikian & Asarnow, 2009; Crowe et al., 2015; Irimia et al., 2017; Polinder, Haagsma, van Klaveren, Steyerberg, & van Beeck, 2015).

With the high prevalence of TBI in paediatric populations and survival rates following pTBI increasing, there is an ever-increasing need for the accurate prediction of clinically relevant, long-term cognitive outcome (Crowe et al., 2015). Understanding the neurobiological impacts of TBI on the developing brain is important to this task (Genc et al., 2017).

Essentially, being able to make these predictions will allow us to better support families, and answer the question; what does the future look like for my child, after surviving a traumatic brain injury? (Irimia, Wang, et al., 2012). With this information, clinicians could begin to offer support and guidance to

parents from an early stage, manage expectations, and improve the family interaction over the long recovery period.

1.3 In vivo investigation of brain development with MRI

1.3.1 MRI of the Brain

During the developmental period, the brain undergoes major maturational changes that are observable in-vivo using MRI, specifically structural MRI (sMRI). MRI allows us to visualise the soft-tissue within the head. Images are generated by firstly aligning protons in hydrogen molecules found in the water of the brain to a static magnetic field within the bore of a powerful magnet. The alignment of these protons is perturbed by the application of a radiofrequency pulse, with the resultant rebound upon turning off of the RF pulse being measured across the brain, localised using spatially varying gradients. This rebound time, otherwise known as T1 relaxation time, varies according to a number of factors including density of protons and local tissue microstructure. Due to this, the resultant 3D image is characterised by different intensities in each voxel (a 3D pixel), allowing for the visualisation of different tissue types. For example, cerebrospinal fluid (CSF) in the ventricles has a dark appearance (hypointense) in a T1-weighted (T1w) MRI, due to the high water-content of CSF, which has a slow relaxation time. The cortical grey matter (GM) ribbon which constitutes the neocortical sheet, appears grey on a T1w MRI due to high iron content, which has slightly faster relaxation time, whilst white-matter (WM), comprised of the dense fiber tracts of myelinated axons which connect GM regions, has a high-fat content with the quickest relaxation time and appears bright (hyperintense) on T1w MRI.

T1w sMRI is most commonly used to investigate neuroanatomy due to the stark differences in contrast across the image. The differences in contrast allow the automatic tissue segmentation of the brain into the separate tissue types (GM/WM/CSF), detecting boundaries between tissues using the changing gradients of contrast. This, alongside the high spatial resolution of MR images, enables the quantification of the morphometry of the brain at different spatial locations on the cortex. For instance, volume or the thickness of the cortical ribbon within anatomical GM regions (as defined by anatomical atlases) can be estimated. Changes or differences in these measures can be indicative of neurobiological processes relevant to neurological plasticity, pathology and/or development, such as synaptic pruning, or atrophy, and are commonly used across neuroimaging research. In estimating these over a large population, we can begin to characterise ‘typical’ development over time.

MRI provides a clear and high spatial resolution image of the brain however, it is, in fact, an indirect measure of in-vivo neuroanatomy. The signal intensity within voxels is quasi-quantitative in the sense that they are dependent on both hardware and RF pulse sequence. However, measures such as cortical thickness or volume have been validated based upon histological and manual measures (Kuperberg et al., 2003; Rosas et al., 2002; Salat et al., 2004) and are thus an effective approach to understand the relevant biological basis of neurological conditions.

1.3.2 Developing brain structure

Developmental neuroscience has embraced neuroimaging studies of the morphology of brain structure to characterise how the brain matures over this period and to better understand how this gives rise to cognitive development, over childhood. Developmental neuroimaging studies have highlighted distinct developmental trajectories for the structure of differing brain tissues (WM/GM), across different regions of the cortex (Giedd & Rapoport, 2010). The volume of cortical GM specifically shows an ‘inverted U’, nonlinear trajectory (Giedd, 2004; Giedd & Rapoport, 2010; Gilmore et al., 2007; Knickmeyer et al., 2008), with pre-pubertal expansion of the cortical GM, peaking during childhood (Mills et al., 2016; Vander Linden, Verhelst, Verleysen, et al., 2019) followed by a post-pubertal sustained loss of GM volume (despite synaptic density plateauing after puberty according to molecular and cellular evidence (Mills et al., 2016)). Brain maturation occurs across specific regional trajectories; peak GM density and reductions in GM volume occur earliest in primary function areas, somatosensory and primary motor cortices, and latest in higher-order association areas, dorsolateral prefrontal cortex and superior temporal gyrus for instance (Giedd & Rapoport, 2010; Vander Linden, Verhelst, Verleysen, et al., 2019). Cortical thickness maturation over time also shows a similar pattern, with generalised reductions over time (Herting, Gautam, Spielberg, Dahl, & Sowell, 2015; Nie et al., 2014; Whitaker et al., 2016). These trajectories of GM change are in line with what would be expected from models of synaptic pruning and myelination (Whitaker et al., 2016). Both post-mortem and electrophysiology studies suggest that these changes may be due to synaptic pruning (Huttenlocher, 1994; Whitford et al., 2007).

Overall, the literature suggests that childhood and adolescence are characterised by highly programmed trajectories of GM development (Batalle, Edwards, & O’Muircheartaigh, 2018; Mills et al., 2016; Raznahan, Shaw, et al., 2011; Shaw et al., 2008). This programmed maturation may be driven in some part due to genetics for instance, with the heritability of cortical thickness and cortical thickness change being estimated at around 50-60% in some studies (Schmitt et al., 2007; Teeuw et al., 2019; Wallace et al., 2006). Hence, regions with similar genetic architecture show similar trajectories of developmental change on MRI (Fjell et al., 2015). Given this highly coordinated, genetically programmed, developmental ‘blueprint’ of brain maturation, neurological disruption to the structure of the brain during this period, such as a pTBI, is likely to have a significant, and potentially symptomatic, impact on the ongoing development of the brain.

1.3.3 Development of Brain Structure and Cognition

The protracted development of the brain during childhood and adolescence (Giedd & Rapoport, 2010) leaves the brain at risk of neurological insult throughout the paediatric period. The pathological effects of a TBI in childhood will necessarily interact with these normative developmental processes which also occur. The traumatic force of a TBI can result in cellular and tissue-related damage (Bigler, 2007b, 2016; Maxwell, 2012), compromise vasculature and physiology of the brain (Bigler, 2001), as well as

resulting in trauma-induced cell loss (Bigler, 2013). This atrophy can vary in relation to injury factors such as mechanism, severity and pathology (Bigler, 2013; Cullen, Vernekar, & LaPlaca, 2011; Maxwell, MacKinnon, Stewart, & Graham, 2010) and be realised on sMRI as changes to both regional volumes (Bigler, 2016) and cortical thickness (Urban et al., 2017). Thus, a pTBI during the developmental period means that the pathophysiological changes that occur as a result of injury interact with similar, ongoing, age-related changes to the cortex.

Due to the dynamic nature of both brain and cognitive maturation (Giedd & Rapoport, 2010), neurocognitive morbidities post-injury are likely due to the fact that the injury itself disrupts this neural development (Crowe et al., 2015). These controlled, spatially-specific developmental trajectories of regional morphometry (Taylor, Barker, Heavey, & McHale, 2015; Vander Linden, Verhelst, Verleysen, et al., 2019; Vijayakumar et al., 2016; Walhovd et al., 2016) and neuronal connectivity (Lamblin, Murawski, Whittle, & Fornito, 2017; Marek, Hwang, Foran, Hallquist, & Luna, 2015; Marrus et al., 2018), have strong correspondence with trajectories of acquisition of cognitive skills. Essentially, brain structure gives rise to cognitive and behavioural function. Thus, neurological disruption to this highly-controlled, developmental blueprint of the brain due to TBI is likely to be symptomatic, in terms of later cognitive functioning. It is, therefore, logical to assume that the assessment of the post-injury development of the brain, using in-vivo MRI approaches, will aid in the identification of those children that are at risk for persistent cognitive impairment (Wilde, Merkley, et al., 2012).

This concept of MRI methodologies to index brain development, and how this may be affected by a pTBI, is picked up throughout the current thesis, across all experimental chapters. Specifically, this is addressed in a systematic review of the effects of an injury on the morphometry of the brain, which is presented in Chapter 2.

1.4 Executive Functions, MRI and pTBI

1.4.1 Neuropsychology of Executive Functions

Executive functions (EF) are a collection of top-down control processes that allow an individual to be adaptive to novel situations in their environment (Diamond, 2013). EF has been used as an umbrella term in neuropsychology to describe a number of higher-order, interrelated cognitive functions that aid an individual to achieve this goal. In the common three-factor model, EF can be conceptualised of comprising three core cognitive skills; working memory, inhibitory control, and cognitive flexibility (Karr et al., 2018; Miyake & Friedman, 2012; Miyake et al., 2000). From these three core skills arise higher-order EFs such as planning and novel problem solving (Diamond, 2013; Krasny-Pacini et al., 2017). Whilst other models of EF exist, there are multiple reasons for which this model has been selected. Firstly, since the introduction of the three-factor model by Miyake et al. (2000), it has been one of the most widely studied. Due to this, there is significant data-driven evidence of the factorial structure of this model. The fact that this model has been widely studied also means that there is

significant understanding of the neurobiological correlates that underpin the cognitive skills outlined by this three-factor model (i.e. Smolker, Friedman, Hewitt, and Banich (2018) & McKenna, Rushe, and Woodcock (2017)).

There is evidence of a nested factor model of distinct constructs of updating/working memory, shifting and a common EF construct which spans skills of updating/working memory, shifting and inhibition (Karr et al., 2018). However, in childhood and adolescence, there is modest evidence for a unidimensional model of EF, with measures of these three skills most commonly loading onto a single, latent EF component. Even though there are models which define EF across a greater number of EF subdomains, this unitary structure is beneficial as; a) it provides a theoretical basis for the high level of inter-correlations between components of EF and b) reduces the number of multiple comparisons when investigating the neuroanatomical correlates of these cognitive functions. Essentially, this highlights both unity and divergence of EF skills; subdomains of EF are not necessarily orthogonal constructs (Karr et al., 2018), but heavily rely on one another in order to adaptively function.

The complexity and diversity of EFs make them particularly difficult to test using neuropsychological measures. A number of performance-based tasks exist, including some suitable for use in children (Welsh & Peterson, 2014), and tasks which have been used to elucidate EFs can be found in a number of existing test batteries (i.e. Tests of Everyday Attention – Children (TEA-Ch; (Manly, Robertson, Anderson, & Nimmo-Smith, 1999)), Delis-Kaplan Executive Function System (D-KEFS, (Delis, Kaplan, & Kramer, 2001)), and Wechsler Intelligence Scale for Children (WISC-IV, (Wechsler, 2003))). However, one difficulty is ‘task impurity’ (Miyake et al., 2000), the fact that many EF skills are dependent on one another, and therefore any one task is likely to tap many aspects of these different EF skills. EFs in children and adolescents can also be evaluated using behavioural reports. The Behavior Rating Inventory of Executive Function (BRIEF) was specifically designed to index these executive skills in everyday environments such as home and school (Gioia, Isquith, Guy, & Kenworthy, 2000). However, it has been suggested that this measure may index problem behaviours and concerns, rather than neuropsychological or cognitive ratings of executive functions (McAuley, Chen, Goos, Schachar, & Crosbie, 2010; Toplak, West, & Stanovich, 2013).

Due to the task impurity of neuropsychological testing and the fact that behavioural ratings seemingly tap different skills, results from any one measure will elucidate differing levels of impairment or executive dysfunction. Thus, the current thesis utilises multiple measures to index EF. The following section briefly outlines the three domains of functioning defined in the three-factor model and, in turn, describes the neuropsychological tests used in the current thesis to index each of these.

1.4.1.1 Working Memory and Updating

Working memory (also conceptualised as updating in some descriptions) is the ability to manipulate and work with the information currently held in mind/memory. This idea of being able to hold in mind what

has come previously but is no longer perceptually present is important for many higher executive functions such as planning and reasoning (Diamond, 2013). This is inherently linked to inhibitory control in the sense that, in order to know what to inhibit, you need to be able to hold the current goal in working memory. The current thesis utilises a single measure of working memory, the ‘Digit Span Backwards’ score from the WISC-IV (Wechsler, 2003).

a) ‘Digit span backwards’ – In this task a list of numbers is read by the examiner, with an increasing span of digits. Participants are required to hold these numbers in working memory and repeat them backwards to the examiner. This task requires both aspects of this factor, working memory storage to memorise the numbers, but also memory updating, once the numbers have been reordered to then recall them to the examiner (Coulacoglou & Saklofske, 2017).

1.4.1.2 Inhibitory Control

Inhibitory control is defined as the ability to control one’s attention, behaviour, thoughts, and/or emotions despite a strong predisposition to a given automatic, yet less adaptive, response. This allows us to conduct a repertoire of behaviours beyond that of habits, impulses and conditioned responses (Diamond 2013). This skill is inherently linked to both response inhibition, inhibition of behavioural responses and executive attention, representative of interference control via inhibition at the level of attention (Diamond 2013). However, this use of selective attention is also explicitly linked to the abilities of working memory, in order to stay focussed on the working memory contents of interest (Santa-Cruz & Rosas, 2017). The current thesis utilises three measures to index aspects of inhibitory control; the ‘Colour-Word interference’ task from the D-KEFS, and both the ‘Walk-don’t-walk’ task and the ‘Sky Search’ attention score from the TEA-CH.

a) ‘Colour-Word interference’ – This task consists of two different conditions used to index inhibition, an incongruent Stroop condition, where participants read the colour of the ink and not the word written, followed by a switching trial where they must read either the colour of the ink or the word written, depending on whether the word is displayed inside a box or not. It is pertinent to note that these measures may also be related to processing speed due to their ‘time-to-completion’ scoring (Karr, Hofer, Iverson, & Garcia-Barrera, 2019).

b) ‘Walk-don’t-walk’– This task is a classical go-no-go task where children are presented a path of squares and are played one of two tones, one which means the child should move forward by one space, the other tone means the child should not move forward. This task specifically indexes response inhibition, inhibitory control at the level of behaviour (Diamond, 2013).

c) ‘Sky Search’ attention score – This is a selective attention task where children are presented with a sky filled with pairs of space ships. Children must circle those pairs that comprise the

same space ship and ignore those with unmatched pairs. The attention score is the time taken on this task relative to time taken on a similar motor-based control task in which there are no distractors present (Manly et al., 1999), to isolate executive attention abilities. Although nominally a test in the ‘selective attention’ domain of the TEA-Ch, the measure correlates with and, in factor models, loads with, other measures of inhibition (Downing, 2015; Wu et al., 2011). Thus, in the current thesis it is included within the inhibitory control domain.

1.4.1.3 Cognitive Flexibility

Cognitive flexibility (sometimes referred as, but not limited to, set shifting) is the ability to adapt behaviour or responses to changing rules, demands or priorities in the immediate environment (Diamond, 2013). The current thesis indexes this using the ‘creature counting’ task from the TEA-Ch.

a) ‘Creature Counting’ – In this task, the child is asked to count creatures along a path. When an arrow is encountered (either upward or downward pointing) the direction of counting is changed. The current study uses both the accuracy and time taken as two separate indicators of cognitive flexibility.

1.4.2 Executive functions post-injury

Cognitive-skills are more likely to show dysfunction when damage occurs during the period of skill-maturation (Ewing-Cobbs, Prasad, Landry, Kramer, & DeLeon, 2004; Krasny-Pacini et al., 2017). As EFs show a protracted period of maturation and development (Diamond, 2013; Friedman et al., 2016; Perone, Almy, & Zelazo, 2018), they are likely to have an extended window of vulnerability to the effects of injury (Krasny-Pacini et al., 2017). This is seemingly the case following a pTBI, as EFs have been shown to be commonly impaired, both acutely and chronically post-injury.

Rates of parent-reported executive dysfunction are raised after pTBI (18-38%) during the first year post-injury (Sesma, Slomine, Ding, McCarthy, & Children's Health After Trauma Study, 2008), with greater EF related difficulties in daily living tasks seen in patients compared to controls (Krasny-Pacini et al., 2017; Mangeot, Armstrong, Colvin, Yeates, & Taylor, 2002; Vander Linden, Verhelst, Verleysen, et al., 2019). Whilst performance-based measures of EF seemingly show some improvement over time (Anderson, Damasio, & Damasio, 2005; Krasny-Pacini et al., 2017; Levin et al., 1997), these difficulties in daily living, essentially the application of EF skills to everyday life, do not show similar improvement (Keenan, Clark, Holubkov, Cox, & Ewing-Cobbs, 2018; Krasny-Pacini et al., 2017; Vander Linden et al., 2018). Although there is evidence of greater executive dysfunction seen for greater injury severities, outcomes are highly variable and degree of functional impairment is characterised by an inter-individual heterogeneity which is poorly understood (Anderson et al., 2005; Catroppa & Anderson, 2009; Konigs et al., 2018; Polinder et al., 2015). For instance, current reports have highlighted that data-driven approaches can identify at least three distinct clusters of pTBI patients based on EF performance

(Ringdahl et al., 2019). These impairments are likely to be more apparent over childhood as there are multiple, ever-increasing demands in school and social environments, such as attentional, social and academic demands, especially in middle childhood and adolescence (Hunter & Sparrow, 2012). Overall, this highlights EF as a key domain of impairment within the sequelae of pTBI however, there is large within-population heterogeneity.

EF is a cognitive domain of especially great importance for children, and thus, executive dysfunction has significant links to impairments in attainment of expected skills at a functional level, setting the scene for long-term developmental outcomes (Perone et al., 2018). EF abilities in children predict attainment, health and competencies (Diamond, 2013; McKenna et al., 2017; Perone et al., 2018), such as math and reading abilities (Blair & Razza, 2007), school readiness (Welsh, Nix, Blair, Bierman, & Nelson, 2010), later school accomplishment (Checa & Rueda, 2011), social understanding (Riggs, Jahromi, Razza, Dillworth-Bart, & Mueller, 2006) and a number of other aspects of daily living (Diamond, 2013; Gaines & Soper, 2018). Executive dysfunction is defined as;

“...deficits in the ability to inhibit well-learned patterns of behaviour and derive new ways of solving problems. Individuals become trapped in repetitive cycles of well-learned behaviour (perseveration) and lack flexibility to accommodate and re-accommodate their behaviour to novel situations” (Henry & Bettenay, 2010, p. 3).

It is therefore easy to see how dysfunction in these cognitive skills can lead to wider difficulties for children who have suffered a pTBI. Therefore, understanding how pathological brain changes may predicate and potentially subsume later executive dysfunction is of great importance, as it may have much wider implications on their day-to-day quality of life. Early prediction, and identification of those who are likely to experience difficulties in EF will allow us to better target individuals for early intervention to promote best-attainable outcomes.

Impairment to executive functioning abilities therefore represents a common and functionally significant consequence of a pTBI. Early identification of those individuals that are more likely to experience significantly greater executive dysfunction is a key aim for clinical research in this area. Early identification would promote targeting individuals for early intervention, and reduce stress for families by giving them early prognostic information as the trajectory for recovery. One way by which to achieve this is understanding how pathological brain change, as identified with MRI, may predicate and potentially subsume, later executive dysfunction.

1.4.3 Neural correlates of executive function following pTBI

In neuropsychology, the term ‘executive functioning’ has previously been used interchangeably with ‘frontal lobe functioning’ (Ardila, Fatima, & Rosselli, 2019). However, recent research has asserted that EFs are subsumed by a widely distributed network of neural regions (Beauchamp, Catroppa, et al.,

2011; Collette, Hogge, Salmon, & Van der Linden, 2006; Nowrangi, Lyketsos, Rao, & Munro, 2014; Slomine et al., 2002). These networks may be particularly at risk of the diffuse nature of morphometric changes post-TBI and the diffuse axonal injury which is likely to ‘disconnect’ distant cortical regions (Treble-Barna et al., 2017). EFs are also more likely to experience less complete recovery and difficulties in making age-appropriate gains (Anderson, Spencer-Smith, & Wood, 2011), due to this diffuse network.

Furthermore, studies that investigate the brain-behaviour correlates of executive dysfunction post-injury using sMRI have provided little evidence of regionally-specific damage subsuming these deficits. Contrary to adult literature, where EF is implicated following frontal-region pathology, EF deficit in early brain injury occurs irrespective of injury factors such as lesion location (Anderson et al., 2010; Jacobs, Harvey, & Anderson, 2011). Non-significant correlations are reported between thinner cortical thickness (greater atrophy) of EF supporting ROIs and increased parent-reports of executive dysfunction (Vander Linden, Verhelst, Verleysen, et al., 2019). No relationship was found between GM volume and a performance measure of working memory (Konigs et al., 2018), but parent-reported working memory problems were significantly associated with the cortical thickness of temporal and parietal ROIs (Merkley et al., 2008). Similarly, no relationship was found between frontal pole cortical thickness and performance-based measures of mental flexibility and working memory (Levan et al., 2016). However, in a group with mild pTBI, thinner cortical thickness of the dorsolateral prefrontal cortex was associated with slower reaction times in a high cognitive load working memory dual-task (Urban et al., 2017). Smaller parietal and cingulate volumes were also related to longer reaction times in a working memory task (Wilde et al., 2011). Cortical WM volume predicted long-term inhibition/cognitive flexibility outcomes at 16 years post-injury (Yu, Seal, et al., 2018). Cognitive training has improved EF outcomes for children post-injury, but no associated change in brain morphometry was observed, despite differences in EF ROIs pre-training compared to controls (Vander Linden, Verhelst, Deschepper, et al., 2019). Differences in cortical thickness of frontotemporal regions were related to case-control differences in performance on a novel social problem-solving VR task (Hanten et al., 2011) likely to involve multiple complex EF demands. A diffuse set of cross-sectional and longitudinal changes in volume were also related to performance on a composite cognitive functioning index which included both working memory and cognitive flexibility indices (Dennis, Faskowitz, et al., 2017; Dennis et al., 2016). This literature clearly highlights the fact that there is no apparent consensus in the brain behaviour-correlates of EF post-injury, across multiple methodologies and approaches.

However, it is also important to note that these studies have three key limitations. Firstly, they investigate populations with a very limited sample size (Hanten et al., 2011; Levan et al., 2016; Merkley et al., 2008; Urban et al., 2017; Vander Linden, Verhelst, Deschepper, et al., 2019; Vander Linden, Verhelst, Verleysen, et al., 2019) limiting statistical power to detect effects. Secondly, they perform analyses on highly reductionist ‘summary’ measures of sMRI (mean over multiple EF ROIs (Vander

Linden, Verhelst, Verleysen, et al., 2019); whole GM volume (Konigs et al., 2018); Cortical WM as proportion of eTIV (Yu, Seal, et al., 2018)) or across a very limited number of ROIs (Levan et al., 2016; Vander Linden, Verhelst, Deschepper, et al., 2019). These two issues are likely highly intertwined, with limited statistical power due to small sample sizes, analyses are unable to be conducted across multiple ROIs whilst still maintaining adequate control over the false positive rate.

The final key limitation of this work is the specific univariate approach to these analyses. The neuropsychological research highlighted above discusses at great length that damage to the diffuse networks that subsume the development and maturation of EF is what results in the failure to reach age-appropriate milestones. However, the univariate approaches assume that each region occurs and exists independently of all other regions, rather than interconnected components of the wider neural system, in contradiction of these neuropsychological assumptions.

Considering the morphometry of the brain post-TBI as a set of interrelated regions is not a new concept. Spanos et al. (2007) investigated volumetric correlations across cerebro-cerebellar regions and reported a significant positive relationship between DLPFC/cerebellum was found in the TD but not in the TBI group. Drijkoningen et al. (2017) adopted a similar approach by estimating the correlational structure of atrophy scores between regions. Moderate to very strong positive correlations were found for these relationships. Bigler (2016) suggests that a potential explanation for volume/cortical thickness changes distal to primary locales of injury post-TBI may be due to the loss of connectivity between regions following a TBI, with the connection dropout affecting the morphometry of the regions that were once connected, thus providing a potential mechanism by which these changes in morphological covariation and correlations of atrophy may be driven.

Bigler (2016) suggested that a systems biology approach to TBI is necessary to better understand pathological mechanisms after injury and prognostication of post-injury functioning. He stated that;

“... how pathology influences the organism at the systematic level... is the most important challenge because therein is the link between damage, neural networks, and behaviour” (Bigler, 2016, p. 16).

Therefore, the current thesis takes a systems-level approach to investigate the changes to the structural organisation of the brain post-injury, specifically utilising network-analysis approaches, and how this may be related to later EF.

1.5 Network analyses of in-vivo MRI

1.5.1 Network analyses

Recently there has been a rise in neuroimaging studies investigating the network structure of the whole-brain, modelling this ‘connectivity’ within a graph-theoretic framework. Graph-theoretic approaches to neuroscience stem from a seminal paper by Sporns, Tononi, and Kotter (2005) which described the

human connectome as “a comprehensive structural description of the network of elements and connections forming the human brain” (p. 245). Mathematical graphs are representations of these interactions, otherwise known as edges, between several individual, communicating units, referred to as nodes. This collection of nodes and edges constitutes the network. The topological organization of the produced networks can then be quantitatively described using a mathematical language from graph theory. For a more detailed explanation of graph theoretical analysis in the neurosciences, see Fornito, Zalesky, and Bullmore (2016). As cognitive functioning arises through the coordinated activation of disparate neural units which comprise neural networks these approaches are highly intuitive (Giedd et al., 2015).

Network-level investigations of the brain in-vivo using MRI imaging is usually conducted in the functional domain, using functional MRI (fMRI) to understand how brain ‘activity’ is synchronous between pairs of communicating regions, or using diffusion MRI (dMRI) to estimate the degree and direction of which free water molecules can diffuse in the brain, allowing us to infer the presence and location of bundles of myelinated axons within the white matter, connecting different brain regions together. In the field of paediatric TBI, both fMRI and dMRI have been used to investigate the network-level organization of the brain post-injury. This is unsurprising; given the diffuse damage which can occur across the brain after a pTBI (Fujiwara, Schwartz, Gao, Black, & Levine, 2008; King, Ellis, Seri, & Wood, 2019) and recent characterizations of TBI as a connectivity disorder (Hannawi & Stevens, 2016; Hayes, Bigler, & Verfaellie, 2016; Wilde, Hunter, et al., 2012).

However, a key limitation of these types of analyses is that the MRI sequences required to generate fMRI and dMRI datasets have long acquisition times and may therefore be less tolerable in clinical populations. Given the arguably greater appropriateness and ease of collecting T1w MRI data from participants over fMRI and dMRI, the current thesis adopts a network-level approach to the investigation of meso-scale brain organisation post-injury using sMRI, an approach that is novel to the field of pTBI.

1.5.2 Network analyses of sMRI

Instead of treating the morphometry of the brain as independently segmented regions, one way to probe the structural network following TBI is to investigate the relationships between these regions using a structural covariance (SC) network approach (Bigler, 2016; Lerch et al., 2017). An approach which gained traction following a paper by Mechelli, Friston, Frackowiak, and Price (2005), SC is the degree to which the macroscopic structure of brain regions, as measured by in-vivo MRI morphometric measures (such as cortical volume or thickness for instance), statistically co-varies with that of all other regions of the brain across individuals (Alexander-Bloch, Giedd, & Bullmore, 2013; Alexander-Bloch, Raznahan, Bullmore, & Giedd, 2013; Evans, 2013). As multiple participants are required to sample enough cortical measurements to generate a correlation between all possible regional pairs, this approach generates group-level brain networks, expressing population-level covariance in neuroanatomy

(Alexander-Bloch, Raznahan, et al., 2013). However, this whole-brain approach to sMRI particularly lends itself to graph theoretical analysis (Evans, 2013), allowing for the quantification of whole-brain, interregional relationships (Alexander-Bloch, Giedd, et al., 2013).

SC between regions is likely driven by a range of (non-mutually exclusive) biological phenotypes and thus represents a biologically-meaningful ‘signal’ in the brain. These drivers include genes, development, ageing or plasticity (Evans, 2013; Pagani, Bifone, & Gozzi, 2016). It is suggested that the covariance may also reflect maturational changes or maturational coupling (Alexander-Bloch, Giedd, et al., 2013; Evans, 2013; Raznahan, Lerch, et al., 2011) over time which is synchronized between connected regions. As the infant brain begins forming and reforming axonal connections with development (Cao, Huang, Peng, Dong, & He, 2016) this synchronous axonal activity could have a trophic effect on regional levels of growth (Alexander-Bloch, Raznahan, et al., 2013). SC may also be genetically influenced through the co-expression of similar genes between regions as developmental ‘cues’ (Raznahan, Lerch, et al., 2011; Romero-Garcia et al., 2018; Yee et al., 2017), with 9% variance in SC explained by co-expression of Human Supragranular Enriched (HSE) genes (Romero-Garcia et al., 2018). It has further been suggested that SC may arise due to the trophic effects of co-activation of regions sharing direct axonal connections (Gong, He, Chen, & Evans, 2012). However, there is a limited correspondence between tract-tracing or tractography and SC, although some variance in SC can be explained (Gong et al., 2012; Reid, Lewis, et al., 2016). Reid, Lewis, et al. (2016) highlight the variance in SC explained by resting-state fMRI (rsfMRI) between regions. SC also shows greater congruence within, rather than between, fMRI network modules (Alexander-Bloch, Raznahan, et al., 2013). These structural-functional relationships are despite obvious differences in temporal dynamics of these processes, with the BOLD signal rapidly evolving over time whereas the maturational or disease-related organization of morphology occurs over longer periods of time (Alexander-Bloch, Raznahan, et al., 2013; Evans, 2013; Zhang et al., 2011). These studies therefore support the idea of mutually trophic influences, due to functional connectivity, “sculpting” SC development (Geng et al., 2017, p. 1805) or, put more simply, the notion that “form follows function” (Reid, Bzdok, et al., 2016, p. 2).

It must be remembered that in-vivo assessment of SC is not a direct assessment of the architecture of the brain, and thus it is unclear to what extent these networks resemble actual anatomical networks within the brain (Batalle et al., 2013). Gong et al. (2012) argue that given limited correspondence between white-matter fibre connectivity and SC (replicated by Reid, Lewis, et al. (2016)), SC should not be used as a proxy for actual anatomical connections. However, as stated, these potential driving mechanisms may not be mutually exclusive from one another (Yee et al., 2017). Whilst it is accepted that the neurobiological basis for this network of inter-regional relationships is poorly understood (Romero-Garcia et al., 2018), evidence presented here suggests that variance in SC between regions may be best explained by multiple driving biological phenotypes (Reid, Lewis, et al., 2016; Yee et al., 2017). This diverse evidence-base highlights the fact that the SC between regions represents a

biologically-meaningful signal which captures variance across multiple connectivity phenotypes, potentially offering complementary and beneficial information with which to investigate the brain.

With potential relationships with genetic control of cortical development (Romero-Garcia et al., 2018) and the trophic effects of co-activation on maturation (Alexander-Bloch, Raznahan, et al., 2013) it is perhaps unsurprising that SC is seemingly sensitive to neurodevelopmental change over time. These SC networks maintain efficient, small-world organization across early and late childhood and adolescent age groups (Khundrakpam et al., 2013), even as early as one month postnatally (Fan et al., 2011), suggesting that the changes over development to the SCN are meaningful in the sense that they maintain the expression of this important network-topology. Change in SC shows weak association with changes to cortical thickness and myelination suggesting this age-related change is beyond that of well-researched processes such as thinning and myelination (Váša et al., 2017). SC in the brain also appears to be sensitive to diversions of cortical development and maturation. SC in children with malformations of cortical development (MCD) due to multiple mechanisms of cortico-genesis disruption, showed graduated differences, with more marked differences found for multiple MCD structural phenotypes which pathologically occur at similar late stages of cortico-genesis (Hong, Bernhardt, Gill, Bernasconi, & Bernasconi, 2017). These differences seemingly specific to timing of disruption suggest that SC can index diversions of the typical maturational trajectory of the cortex, such as that seen post pTBI.

Overall this evidence suggests SC is sensitive to neurodevelopment. However, a barrier to a true longitudinal investigation of this coordinated maturational change is the slow rates of cortical development (Raznahan, Lerch, et al., 2011; Shaw et al., 2008). Nonetheless, sensitivity to neurodevelopment makes this method particularly appropriate for paediatric populations. For example, studies have investigated the cross-sectional differences to the structural covariance of the cortex of a number neurodevelopmental disorders and neurological conditions presenting in the paediatric period, including ADHD (Griffiths et al., 2016), autism (Bethlehem, Romero-Garcia, Mak, Bullmore, & Baron-Cohen, 2017), dyslexia (Liu et al., 2015; Qi et al., 2016), epilepsy (Bonilha et al., 2014; Garcia-Ramos et al., 2016) and, as discussed previously, malformations of cortical development (Hong et al., 2017).

Previous studies of GM atrophy and change following pTBI have looked at focal/univariate changes that treat the morphometry of multiple ROIs as distinct, independent features. The brain represents an organ of extreme complexity, and yet this mass univariate approach assumes that each region occurs and exists independently of all other regions, rather than interconnected components of a multivariate whole. However, network neuroscience approaches may alleviate this reductionism, providing a low dimensional description of the relatedness of the brain across the cortex. Overall, the studies highlighted in this section indicate that the in-vivo measurement of SC provides information that is biologically meaningful in terms of this meso-scale organisation of morphometry between regions. Given the fact that SC approaches are also sensitive to the effects of neurodevelopment and neurological disruptions,

the current thesis investigates the role of network analyses of sMRI in better understanding the brain-behaviour correlates, and potential predictors, of executive dysfunction following pTBI.

1.6 Executive Summary

1.6.1 Main Thesis Aims

The major aim of the current thesis was to investigate the brain-behaviour correlates between acute investigations using sMRI and executive dysfunction at two-years post-injury in a relatively large cohort of children who have experienced a pTBI. Specifically, the current thesis adopts a novel, network-level analyses of sMRI data to better capture the complex, meso-scale organisation of the cortex in relation to both development, and pathological damage of diffuse regions across the cortex. This addresses the three key limitations of existing investigations of the brain-behaviour correlates of executive dysfunction post-pTBI; i) analyses mostly restricted to univariate assessments, ii) highly reductionist approaches to sMRI data over a limited number of ROIs and iii) limited sample sizes. In addressing these, the current thesis aims to reconcile inconsistent findings regarding brain-behaviour correlates of EF in pTBI, likely due to the fact that previous research has focussed on univariate analyses which treat the morphometry of multiple ROIs as distinct, independent features, despite evidence to the contrary, especially during brain development.

The specific aims of the current thesis of work were threefold:

- a) To assess the current state of the field in regard to changes to brain morphometry post-TBI and the brain-behaviour correlates of post-injury cognitive impairment,
- b) To validate methodologies for sMRI network analyses for investigating cognitive functioning and pTBI populations,
- c) To conduct novel experimental investigations of the sMRI network-level brain-behaviour correlates of future executive dysfunction in a pTBI population.

1.6.2 Thesis Outline

The current thesis presents six experimental chapters in which the stated thesis aims are addressed across both hypothesis-driven investigations and methodological validations. Chapter 2 presents a systematic review that highlights the current state of the literature regarding morphometric changes to the brain post-TBI and current evidence for brain-behaviour correlates of later cognitive impairment. This highlights current concerns for the field, including pathological lesions on sMRI processing pipelines, an issue which is explored further using experimental investigations in Chapter 3. In Chapters 4 & 5, group-level, structural covariance methodologies are investigated for the first time in the field of pTBI research, with the findings proposing network-level, neuropathological mechanisms that are associated with poorer executive functioning outcome post-injury. Chapter 6 represents a methodological

validation of an adaptation to the state-of-the-art analysis approach to sMRI data, the morphometric similarity network, using a large publicly-available dataset. Given the success of this validation, this approach (within a supervised learning framework) was employed in the investigation of the pTBI dataset within Chapter 7, in order to assess the predictive validity of this approach in regard to post-injury executive dysfunction. Finally, in Chapter 8, the main findings of this research are more generally discussed, alongside various limitations and implications for the field.

Chapter 2. A systematic review of cross-sectional differences and longitudinal changes to the morphometry of the brain following paediatric traumatic brain injury

2.1 Overview

The main aim of the current chapter was to review the current state of the field regarding morphometric changes to the brain following a pTBI. The systematic literature search found that there is limited spatial consensus as to how the MRI-derived morphometry of the brain changes after a traumatic brain injury within the childhood period, but longitudinal studies suggest that developmental trajectory over time is different post-injury compared to controls. A version of the work presented in this chapter is published as follows:

King, D. J., Ellis, K. R., Seri, S., & Wood, A. G. (2019). A systematic review of cross-sectional differences and longitudinal changes to the morphometry of the brain following paediatric traumatic brain injury. *NeuroImage. Clinical*, 23, 101844.

DJK designed, conducted the search and wrote-up the results of this work. KRE conducted the second screening of search results. SS reviewed and provided comments on the manuscript. AGW supervised the design of the study and reviewed and provided comments on the manuscript.

2.2 Introduction

Traumatic brain injury (TBI) is a leading cause of disability for both children and young adults (World Health Organization, 2006). Estimates of incidence are high for the 0-25 year old age group, with overall prevalence being estimated at approximately 30% of individuals experiencing a TBI by the time they reach young-adulthood (aged 25). Between the ages of 0-15 year olds there is an estimated incidence between 1.10-1.85 cases per hundred (McKinlay et al., 2008). Thus, many injuries occur to the still-developing brain (Wilde, Hunter, et al., 2012). Unfortunately, the risk of poor neuropsychological and functional outcomes for those with mild to severe paediatric TBI (pTBI) is not clearly understood, especially due to the many factors upon which the likelihood of ongoing sequelae may be predicated (Babikian & Asarnow, 2009; Crowe et al., 2015; Irimia et al., 2017; Polinder et al., 2015).

In particular, the interaction between injury mechanisms and brain maturation in childhood may underpin the long-term neuropsychological effects of TBI. The impact and extent of ongoing neural changes associated with TBI is likely to have significant implications for children's later functioning. That is, the disease process that occurs following a pTBI necessarily interacts with the trajectory of normal brain development. Thus, the extent to which the injury alters that normal process may be an important factor to consider when trying to understand the apparent vulnerability of children's brains to early TBI and producing clinically relevant and reliable predictions for long-term outcomes. The current systematic review aims to investigate the interaction of injury and development by examining studies which have measured the effects of injury on the paediatric brain through MRI.

Alterations in brain structure occur after TBI but also as a part of normal development. TBI is defined as a neurological condition in which a traumatic external force to the brain leads to deformation of tissue, resulting in cellular or tissue damage which can cause transient or permanent functional impairment (Bigler, 2007b, 2016; Maxwell, 2012). TBI can result in the compromise of vasculature and physiology of the brain (Bigler, 2001) as well as resulting in trauma-induced cell loss (Bigler, 2013). This atrophy can vary in relation to injury factors such as mechanism, severity and pathology (Bigler, 2013; Cullen et al., 2011; Maxwell et al., 2010). This can be realised as changes to both brain volume (Bigler, 2016) and cortical thickness (CT) measures (Urban et al., 2017). Morphometric brain changes are also a feature of typical brain developing throughout childhood and adolescence (Batalle et al., 2018; Mills et al., 2016; Raznahan, Shaw, et al., 2011; Shaw et al., 2008). Non-linear trajectories of grey matter (GM) and white matter (WM) maturation are apparent in measures of volume (Giedd, 2004; Gilmore et al., 2007; Knickmeyer et al., 2008), gyrification patterning (Dubois et al., 2008) and cortical thickness (Herting et al., 2015; Nie et al., 2014; Whitaker et al., 2016), usually showing reductions over time, in line with models of synaptic pruning and myelination (Whitaker et al., 2016). This means that the morphometric atrophy and developmentally-inappropriate apoptosis (Urban et al., 2017; Wilde et al., 2005) due to pTBI is occurring in the context of an already changing, age and development-dependent brain (Bigler, 2016; Maxwell, 2012). Therefore, long term effects of injury are likely due to these interactions of age, neuroinflammation and neurodegenerative effects (Bigler, 2013; Johnson et al., 2013).

Bigler (2013) suggested that changes to the volumetrics of the brain, as measured by MRI, beyond that of anticipated age-dependent differences, may act as a biomarker of the state of health of the brain following pTBI. Previous reviews and investigations of quantitative MRI have also suggested a more long-term neurodegenerative effect of TBI on volumetry of the brain, in both adult and childhood TBI (Bigler, 2013; Cole, Leech, Sharp, & Alzheimer's Disease Neuroimaging, 2015; Keightley et al., 2014; Masel & DeWitt, 2010; Ross, 2011). Given the sensitivity of MRI-derived morphometry of the brain to typical development (as highlighted above), assessments of the brain using MRI post-TBI could prove to be key in understanding the potential long-term neurobehavioural and cognitive sequelae of pTBI (Bigler, 2013; Levin et al., 2008).

The brain can be uniquely vulnerable to the primary effects of TBI depending on the developmental stage at which the insult occurs (Anderson et al., 2011; Goldstrohm & Arffa, 2005; McCrory, Collie, Anderson, & Davis, 2004; Wilde et al., 2006). For example, the state of development of myelinated axons at the time of injury influences the response of tissues to brain injury (Adelson & Kochanek, 1998; Kochanek et al., 2000; Maxwell, 2012). Degeneration of nerve fibres following TBI occurs at a faster rate for unmyelinated versus myelinated cells (Maxwell, 2012; Staal & Vickers, 2011). Therefore, the early developing brain may be uniquely vulnerable in this way, with injuries occurring at different critical periods of development experiencing potentially very different functional trajectories (Anderson et al., 2011). In addition to potentially deleterious effects of a brain injury, it is also important to consider

the potential of compensatory neural trajectories, through mechanisms such as neural plasticity, which may lead to restitution of function (Anderson et al., 2011; Bigler & Wilde, 2010).

With this in mind, the current systematic review aimed to evaluate studies in which MRI-derived morphometry was measured in comparison to typical development, or longitudinally in paediatric patients following a TBI. In this vein, we chose to only include those studies that report on both patients and controls, thus excluding studies which only report on morphometry of patients. Whilst still informative, studies that just compare morphometry across injury severity cannot necessarily tease apart difference due to the injury and those expected differences due to typical development. A previous scoping review of studies investigated evidence of neurodegenerative change following TBI in children (Keightley et al., 2014). However, recent expansion of the literature in this field warrants a re-investigation.

The current systematic review aimed to answer the question; following paediatric brain injury, over a range of severities, does the morphology of the brain exhibit either i) longitudinal change and/or ii) differences compared to healthy controls. We then sought to determine whether there was evidence of a relationship between these changes or differences in morphology and cognitive outcomes.

2.3 Methods

2.3.1 Review Strategy

Five sources were searched for the systematic review; Web of Science, Psycharticles, Cochrane Library, PubMed and Scopus. No limits on publication dates were applied. Three blocks of related search terms were used: block 1 for 'paediatric' terms, block 2 for 'TBI' terms and block 3 for 'neuroimaging' terms. Table 2.1 shows the full list of search terms for each block. Blocks were combined using the AND function for searching and terms within each block were combined with the OR function. The 'neuroimaging' block was left deliberately broad to capture studies where investigations of morphometry were carried out as a secondary outcome (i.e. alongside DTI investigations in Konigs et al. (2018)).

Table 2.1 *Blocks of search terms used to query publication databases in the review strategy*

Block	Terms
Block 1 - Children	(paediatric OR infant OR child* OR Adolescen* OR youth OR teenage* OR young)
Block 2 - TBI	(TBI OR Trauma*-brain-injury OR brain-injur* OR brain NEAR/3 injury OR brain-insult OR DAI OR diffuse-axonal-injur* OR axonal-injur*)
Block 3 - Imaging	(MRI OR magnetic-resonance-imag* OR neuroimag*)

Returned records from each database were combined and collated using Endnote (Tomson Reuters, 2013) and duplicate records were excluded. Publications were included in the synthesis if they; i) report on human participant data following non-penetrating TBI of any severity using; a. between groups analysis against an appropriate comparison group of either typically developing (TD) or orthopaedic injury (OI) controls or, b. within groups analysis investigating longitudinal change over time against controls, ii) presented isolated results of a paediatric sample (ages 0-19) at scanning, iii) presented original empirical quantification of the morphometry of the brain from T1-weighted (T1w) magnetic resonance images (MRI), and iv) written in English. Exclusion criteria included lack of control comparison group, reviews, conference abstracts, case studies, dissertations and/or book chapters.

Initial screening of abstracts for inclusion was conducted independently by two reviewers (DJK and KRE). Full-text articles of records identified by the two reviewers were independently assessed for inclusion by two reviewers (DJK and AGW) and consensus on eligibility was sought through discussion. Following identification of relevant records for inclusion, a further backwards (reference lists) and forwards (citations) search were conducted in the web of science platform to ensure identification of all relevant publications. This was done iteratively, i.e. new papers selected for inclusion were subjected to the same forwards and backwards searches, until no new publications were identified.

Information from the studies chosen for inclusion was systematically extracted into a pre-designed data pro-forma from full-text articles by two reviewers (DJK and KRE). The following data were abstracted; citation details, country of origin, inclusion/exclusion criteria, design, study aim, MR imaging timepoint(s) relative to time of injury, patient sample (size, gender, injury severity, age at MRI, age at injury), control sample (size, gender, age at MRI, control comparison group (ie. typically developing (TD) vs orthopaedic injury (OI) samples)), neuroimaging characteristics (magnet strength, scan parameters, scale of region-of-interest (ROI; i.e. whole brain, ROI, voxel-wise), software, statistical design, morphometric measure(s) derived), results, and cognitive tests (tests administered, statistical

approach, results). Where relevant and/or necessary, authors were contacted to request further information about the methodology or data.

2.3.2 Study quality

Assessment of study quality was conducted using the ‘Methodological Index for Non-Randomized Studies’ (MINORS; Slim et al. (2003)) tool (full 12-item checklist). Assessment was conducted by a single reviewer (DJK). Studies were given a rating of 0 (not reported), 1 (reported but inadequately), 2 (reported adequately) or N/A if deemed to be not relevant to the study design. An average score was calculated across all non-N/A items to produce a continuous measure of quality from 0 to 2. High quality was identified as 1.51+, moderate as 1-1.5 and low as 0-0.99.

2.3.3 Data Visualisation

Visualisation of dispersion of cross-sectional studies based upon sample characteristics of age at injury and injury-scan interval was achieved with the ggplot2 package in R (Wickham, 2009). This was to aid qualitative interpretation of the heterogeneity in the patient populations being tested. Details of the methodology used are included in supplementary materials (Appendix A).

2.3.4 Overlapping samples

Similar to Dennis, Babikian, Giza, Thompson, and Asarnow (2017), we attempted to identify overlapping samples across the eligible studies presented for qualitative synthesis. Some studies clearly referenced other instances where the dataset was used in other published works. However, due to gaps in reporting of demographic characteristic or differences in the exact selection of participants used from a wider sample, we may have missed some of these overlaps. Despite data reuse, we report on all studies as the hypotheses tested were substantially different enough to warrant inclusion.

2.4 Results

2.4.1 Eligible studies

The search strategy (including forwards and backwards searches) was conducted on 15/11/17 and the initial search identified 17,005 articles over the five databases. Figure 2.1 shows the PRISMA flowchart of this process. The iterative forwards and backwards searches concluded in two iterations (i.e. for the 2nd iteration, no new papers were identified).

Overall, 33 studies were deemed as meeting the inclusion criteria and were included in the narrative synthesis. Study characteristics of all eligible studies are reported in Table 2.2 for cross-sectional studies and Table 2.3 for longitudinal studies.

Of the included studies, two were rated as poor quality, 22 were rated as medium and nine as high. The individual ratings are reported in both Table 2.2 and Table 2.3. Many studies were rated low on items

pertaining to items of 'Unbiased assessment of study endpoint', where there may have been a lack of blinding practices. Low ratings also occurred for all studies for the item of 'Prospective calculation of the study size' due to lack of a-priori power calculations for sample size (Slim et al., 2003).

We were precluded from performing a formal quantitative meta-analysis because included studies utilised divergent approaches, both across dimensions of methods and anatomical partitions tested.

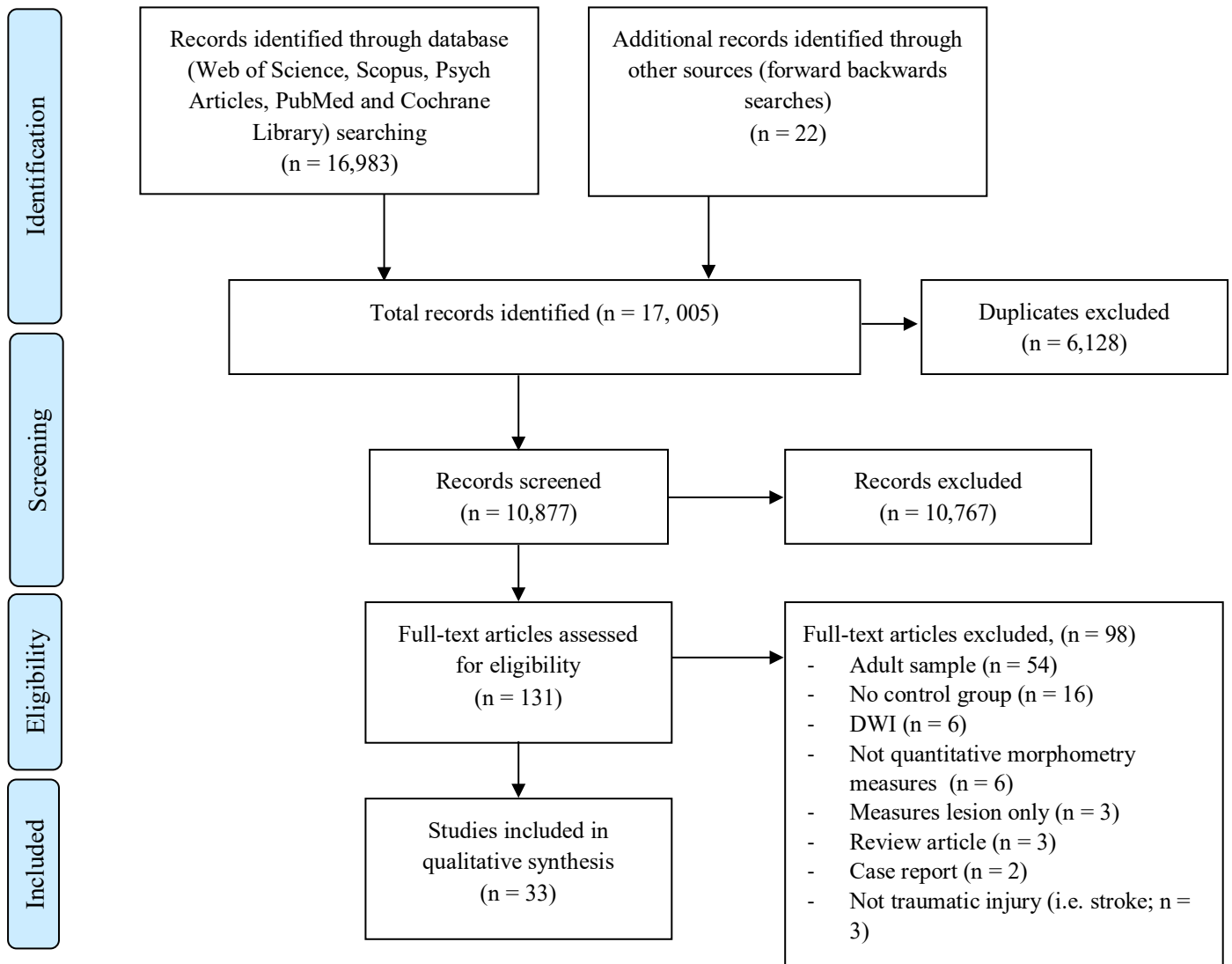


Figure 2.1 PRISMA flowchart, modified from (Moher, Liberati, Tetzlaff, Altman, & Grp, 2009)

Table 2.3a. *Study demographics for all cross-sectional studies included in the review*

Reference	Sample and age (age at scanning; years, M±SD)	Age at injury (years, M±SD)	Time since injury (days/months/years, M±SD)	Comparative Group and age at scan (years, M±SD)	Study quality
<i>Early stage (days to 1-year post injury)</i>					
Urban et al (2017), Canada	13 Mild TBI, 12.2 years ± 1.6, 13M	Not reported	120.69 days ± 2.05 (range 90.07-240.27)	14 TD controls, 12.6 years ± 1.6, 14M, (age and sex matched)	High (1.55)
Ryan et al (2017), AUS	57 Mild TBI, 10.80 years ± 2.33, 13F, 44M, 14 Mild complex TBI, 9.57 years ± 2.43, 6F, 8M, 26 Moderate TBI, 10.37 years ± 2.58, 10F, 16F, 15 Severe TBI, 10.41 years ± 3.10, 7F, 8M	Mild TBI, 10.67 ± 2.36, Mild complicated TBI, 9.47 years ± 2.44, Moderate TBI, 10.33 years ± 2.49, Severe TBI, 9.72 years ± 3.01	42.28days ± 29.53	43 TD controls, 10.41 years ± 2.76, 19F, 24M	High (1.73)
Ryan, Beauchamp et al (2016), AUS	67 Mild TBI, 10.54 years ± 2.39, 19F, 48M, 24 Moderate TBI, 10.37 years ± 2.58, 10F, 14M, 12 Severe TBI, 10.41 years ± 3.10, 4F, 8M	Mild TBI, 10.44 ± 2.40, Moderate TBI, 10.26 years ± 2.58, Severe TBI, 10.22 years ± 3.08	42.29days ± 29.53	34 TD controls, 10.41 years ± 2.76, 13F, 21M (matched on age, sex and SES)	High (1.73)
Ryan, Catroppa et al (2016), AUS	53 Mild TBI, 13F, 40M, 13 Mild complicated TBI, 5F, 8M, 22 Moderate TBI, 9F, 13M, 10 Severe TBI, 3F, 7M (Age at scan not reported)	Mild TBI, 10.69 ± 2.35, Mild complicated TBI, 9.65 years ± 2.45, Moderate TBI, 10.37 years ± 2.47, Severe TBI, 10.33 years ± 3.25	Mild TBI, 38.77days ± 21.84, Mild complicated TBI, 37.62days ± 17.91, Moderate TBI, 38.33days ± 19.34,	33 TD controls, 13F, 20M (Age at scan not reported)	High (1.64)

				Severe TBI, 57.31days ± 30.93		
Juranek et al (2012), USA	21 Moderate to Severe TBI, 12.08 years ± 3.58 (range 6.5-16.4), 6F, 15M	Not reported		Females 95.67days ± 42.34, Males 84.47days ± 39.73	20 OI Controls, 12.25 years ± 2.79 (range 8-15.9), 7F, 15M	High (1.64)
Max et al (2012), USA	27 Severe TBI, 7 Moderate TBI, 10 Complicated Mild, 14F, 30M (some patients excluded for cortical thickness analysis due to quality)	13.4 years ± 3.0	3 months		44 OI controls, 12.0 years ± 2.6, 12F, 32M	Medium (1.27)
Wilde et al (2011), USA	25 Severe TBI, 8 Moderate TBI, 7 Complicated Mild TBI, 12.1 years ± 2.4 (range 7-17), 14F, 26M	Not reported	4.0days ± 0.9		41 OI controls, 13.5 years ± 2.5 (range 7-17), 13F, 28M	High (1.55)
McCauley et al (2010), USA	40 Moderate to severe TBI, 13.8 years ± 2.5, 14F, 26 M	Range 7-17 years		124.8days ± 30.9	41 OI controls, 12.4 years ± 2.4, 11F, 30M	Medium (1.46)
<i>Chronic stage (1 – 5 years post injury)</i>						
Konigs et al (2017), Netherlands	20 Mild RF+ TBI, 10.5 years ± 1.8, 7F, 13M, 17 Moderate to Severe TBI, 10.0 years ± 1.4, 7F, 10M	Mild TBI RF+ 7.7 years ± 2.3, Moderate/Severe TBI 7.0 years ± 1.9	Mild TBI RF+ 2.8 years ± 1.1, Moderate/Severe TBI 3.0 years ± 1.4		Traumatic injury controls, 10.2 years ± 1.5, 15F, 12M	Medium (1.33)
Drijkoningen et al (2017), Belgium	19 Moderate to Severe TBI 13 years 11month ± 3 years 1m (range 8y6m-18y11m), 10F, 9M	10 years 1month ± 3y3m	3 years 8months ± 3y3m		30 TD controls, 14 years 10months ± 2y2m (range 9y5m-17y3m), 17F, 13M	Medium (1.18)

Bigler et al (2016), Canada & USA	82 Complicated Mild to Severe TBI, 72 scanned, refers to Bigler et al 2013 for demographics	Not reported	2.7 years	61 OI controls, 52 scanned, refers to Bigler et al 2013 for demographics (comparable on age and sex)	Poor (0.91)
Drijkoningen et al (2015), Belgium	18 Moderate to Severe TBI, 14 years 2months ± 2 years 11months, 9F, 9M	range 3.0-15.6	3 years 10months ± 3 years 3month (range 0.3-10.8)	30 TD controls, 14 years 2months ± 2 years 11months, 17F, 13M	Medium (1.18)
Yeates et al (2014), USA	82 Complicated Mild to Severe TBI, 10.36 years ± 1.50, 28F, 54M	7.83 years ± 1.94	range 12 - 63 months	61 OI controls, 10.62 years ± 1.68, 24F, 37M	Medium (1.18)
Cook et al (2013), USA	15 Moderate to Severe TBI, 16.66 years ± 2.22 (range 12.38-19.70), 7F, 8M	13.43 years ± 2.35 (range 9.16-16.66)	38.81months ± 10.47 (range 11.32-52.96)	13 TD controls, 16.87 years ± 2.1 (range 13.19-19.94), 7F, 6M	Medium (1.42)
Bigler et al (2013), USA	41 Complicated mild TBI, 10.67 years ± 1.42, 32%F, 68%M, (only 32 used in quantitative neuroimaging), 11 Moderate TBI, 10.16 years ± 1.35, 36%F, 64%M, (only 9 used in quantitative neuroimaging), 20 Severe TBI, 10.13 years ± 1.61, 45%F, 55%M, (only 18 used in quantitative neuroimaging)	Mild complicated TBI, 8.08 years ± 1.87, Moderate TBI, 7.40 years ± 1.74, Severe TBI, 7.85 years ± 2.04	Mild complicated TBI, 2.59 years ± 1.26, Moderate TBI, 2.77 years ± 1.35, Severe TBI, 2.28 years ± 1.14	61 OI controls, 10.66 years ± 1.64, 42%F, 58%M	Medium (1.36)
Dennis et al (2013), USA	57 Mild to Moderate TBI, 10.5 years ± 1.5, 19F, 38M, 25 Severe TBI, 9.9 years ± 1.5, 9F, 16M	Mild to Moderate, 8.0 years ± 1.9, Severe, 7.5 years ± 2.1	Mild to Moderate, 2.6 years ± 1.2, Severe, 2.5 years ± 1.2	61 OI controls, 10.6 years ± 1.4, 24F, 37M	Medium (1.36)
Hanten et al (2011), USA	15 Moderate to Severe TBI, 16.66 years ± 2.22 (range 12.38-19.70), 7F, 8M	13.43 years ± 2.35 (range 9.16-16.66)	38.81months ± 10.47 (range 11.32-52.96)	13 TD controls, 16.87 years ± 2.1 (range 13.19-19.94), 7F, 6M	Medium (1.17)
Krawczyk et al (2010), USA	12 Moderate to severe TBI, 16.51 years ± 2.14 (range 12.79-19.12, 5F, 7M)	Not reported	2.65 years ± 0.76	11 TD controls, 16.37 years ± 1.89, 5F, 6M	Medium (1.27)

Bigler et al (2010), USA	16 Moderate to Severe TBI, 12.9 years \pm 2.5 (range 9.0-16.8), 8F, 8M	9.75 years \pm 3.0 (range 3.7-13.8)	3.1 years \pm 2.4 (range 1.0-10.1)	16 TD controls, 12.8 years \pm 2.4 (range 9.0-16.4), 8F, 8M	Medium (1.36)
Fearing et al (2008)	16 Moderate to Severe TBI, 12.9 years \pm 2.5 (range 9.0-16.8), 8F, 8M	9.75 years \pm 3.0 (range 3.7-13.8)	3.1 years \pm 2.4 (range 1.0-10.1)	16 TD controls, 12.8 years \pm 2.4 (range 9.0-16.4), 8F, 8M (matched on ages, sex, ethnicity, handedness and maternal education)	High (1.64)
Merkley et al (2008), USA	16 Moderate to Severe TBI, 12.9 years \pm 2.5, 8F, 8M (SAME AS BIGLER 2010)	9.75 years \pm 3.0	3.1 years \pm 2.4	16 TD controls, 12.8 years \pm 2.4, 8F, 8M	Poor (0.91)
Spanos et al (2007), USA	16 Moderate to Severe TBI, 12.9 years \pm 2.5 (range 9.0-16.8), 8F, 8M (SAME AS BIGLER 2010)	Not reported	3.1 years \pm 2.4 (range 1.0-10.1)	16 TD controls, 12.8 years \pm 2.4 (range 9.0-16.4), 8F, 8M (matched on ages, sex, ethnicity, handedness and maternal education)	Medium (1.27)
Wilde et al (2007), USA	16 Moderate to Severe TBI, 12 years 10months \pm 2 years 6months (range 9-16 years 9month), 8F, 8M	Not reported	3 years \pm 2 years 5month (range 1-10yr)	16 TD controls, 12 years 10months \pm 2 years 5months (range 9-16 years 5months)	Medium (1.46)
Wilde et al (2006), USA	16 Moderate to Severe TBI, 12.9 years \pm 2.5 (range 9-16.8), 8F, 8M	9.75 years \pm 3.0 (range 3.7-13.8)	3.1 years \pm 2.4 (range 1.0-10.1)	16 TD controls, 12.8 years \pm 2.4 (range 9.0-16.4), 8F, 8M (age and gender matched)	Medium (1.36)
Wilde et al (2005), USA	16 Moderate to Severe TBI, 12.9 years \pm 2.5 (range 9.0-16.8), 8F, 8M	9.75 years \pm 3.0 (range 3.7-13.8)	3.1 years \pm 2.4 (range 1.0-10.1)	16 TD controls, 12.8 years \pm 2.4 (range 9.0-16.4), 8F, 8M	High (1.64)

Late chronic stage (9+ years post injury)

Beauchamp et al (2011), AUS	11 Mild TBI, 17.08 years \pm 3.77, 6F, 5M, 26 Moderate TBI, 17.24 years \pm 3.60, 8F, 18M, 12 Severe TBI, 16.34 years \pm 3.30, 4F, 8M	Mild TBI 7.04 years \pm 3.54, Moderate TBI 6.99 years \pm	Mild TBI 10.04 years \pm 1.39, Moderate TBI 10.25 years \pm	20 TD controls (from NIH repository), 15.80 years \pm 1.94, 7F, 13M (matched on age and gender)	Medium (1.17)
-----------------------------	--	--	--	---	---------------

	3.18, Severe TBI 5.29 years ± 2.77	1.44, Severe TBI 11.06 years ± 1.44	
Serra-Grabulosa et al (2005)	16 Severe TBI, 17.88 years ± 2.85, 2F, 14M	8.18 years ± 3.65	9.68 years ± 1.88
			16 TD controls, 16.94 years ± 3.21, 2F, 14M, (Gender, age, education and parental SES matched) (1.09)

Note. OI=Orthopaedic Injury, SES=socio-economic status

Table 2.2b. *Study findings for all cross-sectional studies included in the review*

Reference	Magnet Strength	Methodology (software, statistical approach, anatomical-level)	Measure of interest	Variables controlled for	Findings
<i>Early stage (days to 1 year post injury)</i>					
Urban et al (2017), Canada	3T	CIVET (GLM, Vertex-wise)	Cortical Thickness	None reported	Significantly thinner cortex found in TBI group compared to controls in the ldIPFC, right anterior IPL and posterior IPL (Cohen's d=.963, 1.152 and 1.002 respectively).
Ryan et al (2017), AUS	3T	Freesurfer (MANOVA, Network ROI summed for DMN, CEN, SN, MN and MNEN)	Volume	Age at Scanning and ICV, SES and sex	Time between injury and MRI was not significantly related to any measure of global or regional volumes. Volume of DMN, CEN, SN, CCMN and MNEN all significantly differed as a function of group, with significant differences found between severe TBI and all other severity/control groups. vmPFC, PCC, IPL, hippocampus, dlPFC, PPC, TH, vlPFC, ACC, A, STS, TPJ, TP, IPL, iFG-po had reduced volumes in the severe group.
Ryan, Beauchamp et al (2016), AUS	3T	FreeSurfer (ANCOVA, Network ROI summed for CSN)	Volume	Age and ICV	Significant effect of group on the volume of the total CSN, with smaller CSN for severe injury compared to control, moderate and mild groups. Of the CSN regions, only the severe group differed from controls in vmPFC, nucleus accumbens and ACC.
Ryan, Catroppa et al (2016), AUS	3T	Freesurfer (ANCOVA, global-brain and Network ROI summed for SBN)	Volume	ICV, age and SES	Across severity groups and controls, there was no multivariate effect of group on total brain, CC, WM and GM volumes. However, univariate effect of group was found on total WM volume and total SBN volume. SBN (specifically regions of STS, TP, mPFC, OFC, TPJ, cingulate, and insula) was significantly smaller only for severe TBI compared to controls.

Juranek et al (2012), USA	3T	Freesurfer (ANOVA, ROI)	Volume	ICV	No main effect of TBI/OI group (or gender or hemisphere) on the volume of the amygdala or hippocampus.
Max et al (2012), USA	1.5T	Freesurfer (MANCOVA, ROI)	Volume and Cortical Thickness	Age and ICV	No effect of group on structural volumes of cerebral GM and WM, cerebellar GM and WM, right and left frontal, right and left temporal, basal ganglia, amygdala, thalamus, corpus callosum and hippocampus.
Wilde et al (2011), USA	1.5T	Freesurfer (GLM, ROI, Vertex-wise)	Volume and Cortical Thickness	Volume corrected for ICV, age at testing	Smaller volumes were found for bilateral frontal regions, as well as right MFG in the TBI group compared to controls (Cohen's $f = .42, .37$ and $.35$ respectively). Reported group effects on cortical thickness across regions of frontal lobe (pTRI, pORB, LOF, MOF, rostral rMFG, FP, SFG) and right temporal lobe (STG, MTG, ITG and FFG).
McCauley et al (2010), USA	1.5T	Freesurfer (QDEC, vertex-wise)	Cortical Thickness	Age at testing	TBI showed significantly thinner cortex than controls bilaterally for anterior prefrontal (superior, middle, inferior, and medial cortices), temporal lobes and parahippocampal gyri, posterior cingulate, and parietal and precuneus regions.

Chronic stage (1 – 5 years post injury)

Konigs et al (2018), Netherlands	3T	SIENAX and FIRST (ANOVA, Global-brain, ROI)	Volume	Head size	Main effect of severity on the volume of total brain WM, but not GM. Mild and Moderate/Severe groups had significantly smaller WM volumes than controls (Cohen's $d = -.74$ and $-.80$ respectively). No significant differences were found for the tested subcortical structures.
Drijkoningen et al (2017), Belgium	3T	Freesurfer (ANOVA, Global-brain, ROI)	Volume	ICV	Total subcortical GM (not total cortical volume) was smaller in the TBI group compared to controls. No significant differences in cortical ROIs, but subcortically, thalamus, putamen, hippocampus and cerebellar cortex were significantly smaller in TBI.
Bigler et al (2016), Canada & USA	1.5T	Freesurfer (QDEC, vertex-wise)	Cortical Thickness	Sex, Age	No significant effect of group on vertex-wise cortical thickness. Age was significantly related to decreasing cortical thickness, with distribution of age-related changes being similar for TBI and OI.

Drijkoningen et al (2015), Belgium	3T	SPM8, SPM8, SUIT toolbox, DARTEL, MRICron (GLM, Global-brain, Voxel-wise)	Volume	ICV		No significant differences in total ICV. Reduced volume in TBI compared to OI for global infratentorial GM and WM. Cerebellar volume as a percentage of total ICV was significantly lower in TBI. A significant cluster of reduced WM volume in the infratentorial region for TBI compared to OI (but not for GM).
Bigler et al (2013), USA	1.5T	Freesurfer and VBM (voxel-wise)	Volume	None reported		Smaller CC volumes were found for severe injury compared to controls in anterior, mid-anterior, central, mid-posterior and posterior regions and total CC as well as total brain, total GM, total WM, thalamus, basal ganglia, amygdala and hippocampus. Posterior and anterior CC also showed reductions compared to controls in moderate and mild-complicated injuries. Severe injury group also had greater total ventricular volume and ventricle-to-brain ratio than controls. VBM showed largest significant reductions for severe injury compared to controls in CC, ventral frontal, basal forebrain regions and lateral ventricles.
Dennis et al (2013), USA	1.5T	Freesurfer (MANOVA, Network ROI summed for DMN, CEN, SN, MN and MNEN)	Volume	None reported		No significant differences in total ICV. Significant reductions in DMN, CEN, SN, MN and MNEN network volumes was found for severe TBI compared to OI and mild-moderate. Severe TBI group had significantly reduced volumes, compared to OIs, in PCC, HF, PPC, TH, I, A and STS.
Bigler et al (2010), USA	1.5T	Freesurfer and ANALYZE (ANCOVA, ROI)	Volume	Age at testing		TBI had reduced volume compared to controls in amygdala, brain stem, globus pallidus and thalamus, regardless of method (Freesurfer and ANALYZE). Putamen only smaller in TBI group when using ANALYZE method.
Fearing et al (2008)	1.5T	ANALYZE (MANCOVA and GLM, ROI)	Volume	Age at Scanning and ICV		TBI group showed reduced thalamic GM (but not WM) compared to controls (Cohen's $d = 1.050$), as well as total midbrain volume (Cohen's $d = 1.91$) and also its constituent parts, the tectum and tegmentum ($d = 0.999$ and 1.074 respectively). The pons, medulla and total brainstem did not significantly differ.

Merkley et al (2008), USA	1.5T	Freesurfer (ANCOVA, ROI)	Cortical Thickness	Age and gender	Significantly reduced cortical thickness in TBI compared to controls was found for ISFG, rpOPER, rFP, bilateral rostral MFG, bilateral caudal MFG, lpreC, bilateral supramarginal, IMTG, bilateral ITG, IFFG, bilateral postC, bilateral SPL, bilateral IPL, and bilateral precuneus regions.
Spanos et al (2007), USA	1.5T	ANALYZE (GLM, ROI)	Volume	ICV	TBI group showed reduced volumes compared to controls in cerebellar WM and GM (even after removing patients with focal cerebellar lesions). A significant interaction between groups was found, in which a significant positive correlation between DLPFC/cerebellum was found in the TD but not in the TBI group.
Wilde et al (2007), USA	1.5T	ANALYZE (ANCOVA, ROI)	Volume	Age and ICV	The TBI group showed volumetric reductions in bilateral hippocampus, amygdala and globus pallidus regions (Cohen's $d = 2.140, 0.801$ & 0.775 respectively) compared to controls, but not putamen and caudate.
Wilde et al (2006), USA	1.5T	Picture Archival System Software (ANOVA, ROI)	Volume	None	Showed the anterior-commissure volume was significantly smaller in the TBI group compared to controls.
Wilde et al (2005), USA	1.5T	ANALYZE (MANCOVA, ANCOVA, global brain and regional)	Volume	Age at testing	TBI group showed significantly reduced global brain measures of total brain and GM volumes, as well as increased ventricle to brain ratio, ventricle volume, whole brain, temporal and frontal CSF compared to controls. Regional reductions in the TBI group were found in lateral frontal WM, as well as ventromedial frontal, superior media frontal and temporal GM/WM.

Late chronic stage (9+ years post injury)

Beauchamp et al (2011), AUS	1.5T	FSL and ANALYZE (ANCOVA, Global brain and ROI)	Volume	Age at Scanning and ICV	A significant effect of group (TBI vs control) was found for total CSF, GM and WM volumes (Partial $\eta^2 = .54, .41$ and $.17$ respectively). Controls had less CSF and greater total GM and left hippocampus volume than all severity groups. Only severe injuries had smaller WM than controls. Right amygdala significantly bigger in controls than mild and moderate injury.
Serra-Grabulosa et al (2005)	1.5T	ANALYZE (t-test, ROI and global-brain)	Volume	None reported	The TBI group showed significant reductions in global WM (specifically frontal WM) volume and increases in CSF volume. No significant differences were found in total or frontal GM. Significant reductions were found in bilateral hippocampal volume in TBI compared to control.

Note. GLM=general linear model, ICV= Intra-cranial volume, OI=Orthopaedic Injury, QDEC=Query Design Estimate Contrast, ROI=Region of interest, SES=socio-economic status, VBM=voxel-based morphometry

2.4.2 Cross-sectional studies

Twenty-seven studies investigated cross-sectional differences in morphology between paediatric TBI groups and controls. Figure 2.2 plots the descriptive characteristics of these studies. Eligible studies sampled a range of ages at injury ($\text{mean}_{\text{pooled}} = 9.55^1$, range of means = 6.58 years - 13.86 years). The distribution of pooled ages fits into a bell curve, with few investigating very early childhood and late adolescence. The sample sizes for the majority of studies are small, with the average sample size for eligible studies being 38.96 participants ($\text{SD} = 29.74$, range = 12-112). The majority of studies investigated samples that were scanned within the first five years post injury. The minimum mean time post injury for which MRI's were obtained was 4.0 days \pm 0.9 (Wilde et al., 2011), with the maximum mean being 10.4 years \pm 1.45 post injury (Beauchamp, Ditchfield, Maller, et al., 2011). Table 2.2a lists all cross-sectional studies eligible for review and their sample demographics. Here we report on the most commonly replicated findings across studies. Table 2.2b summarises the results from all individual, cross-sectional studies included in this section.

At the early stage post-injury differences were found for total WM (Ryan, Catroppa, et al., 2016) and total GM (Ryan et al., 2017), but these findings were not reliably replicated across these studies. When comparing summed volume of ROIs comprising major brain networks (default mode network (DMN), central executive network (CEN), salience network (SN), cerebro-cerebellar mentalising network (CCMN) and mirror neuron empathy network (MNEN), cortico-striatal network (CSN) and social brain network (SBN); Ryan, Beauchamp, et al. (2016); Ryan, Catroppa, et al. (2016); Ryan et al. (2017)) as well as bilateral frontal regions (Wilde et al., 2011) smaller volumes were observed in the TBI groups compared to controls.

At the chronic stage post-injury, decreases to total brain and total GM (Bigler et al., 2013; Wilde et al., 2005), total WM (Bigler et al., 2013; Konigs et al., 2018), and increases to ventricles and ventricle to brain ratio were found in the TBI group (Bigler et al., 2013; Wilde et al., 2005). Specifically, whilst regional differences were understudied, volume differences were found in frontal and temporal GM/WM (Wilde et al., 2005) as well as the DMN, CEN, SN, MNEN and CCMN networks (Dennis et al., 2013), replicating findings from the early stage post-injury. Large WM tracts were also impaired across both corpus callosum (CC), and the anterior commissure (Bigler et al., 2013; Wilde et al., 2006). Commonly, replicated findings suggest that the thalamus, amygdala, hippocampus, putamen, global pallidus and cerebellar regions were smaller in volume cross-sectionally compared to controls (Bigler et al., 2013; Bigler et al., 2010; Dennis et al., 2013; Drijkoningen et al., 2017; Drijkoningen et al., 2015; Fearing et al., 2008; Spanos et al., 2007; Wilde et al., 2007). This period post-injury was specifically characterised by studies which had a mean time since injury between 2.53 years \pm 1.24 (Bigler et al., 2013) and 3.83

¹ This value does not consider the overlap of sample/datasets

years \pm 3.25 (Drijkoningen et al., 2015). However, the studies in this band of enquiry showed much greater variability in the time between injury and MRI at an individual study level. For example, Drijkoningen et al. (2015) reported a mean time since injury of 3.83 years \pm 3.25 but the reported range was 0.3 to 10.8 years post injury. Similarly, Bigler et al. (2010) reported a mean time post injury of 3.1 years \pm 2.4, but the range was 1.0 to 10.1 years. Thus, not all participants reported in this band of chronic stage post-injury are within this period, due to this large within-study variability. Given this large dispersion of time between injury and MRI/testing within-studies, we suggest greater caution when interpreting these findings and suggest that they may not be specific to the reported time post-injury.

It is pertinent to note that, of the cross-sectional studies included in the current review, only nine studies reported the range of time between injury and MRI/testing across time bands, and thus variability of time between injury and MRI may be greater than that reported in this review. In addition, even in studies that did not report the range of time between injury and MRI, standard deviations of this injury/MRI interval are particularly high.

At the late chronic stage, total cerebrospinal fluid (CSF) volume was greater for TBI patients (Beauchamp, Ditchfield, Maller, et al., 2011; Serra-Grabulosa et al., 2005), total GM was reduced (Beauchamp, Ditchfield, Maller, et al., 2011) and these changes were independent of severity, these differences were significant for all TBI severity sub-groups. However, total WM was found to be significantly lower only for severe injury group compared to controls (Beauchamp, Ditchfield, Maller, et al., 2011; Serra-Grabulosa et al., 2005). At the ROI level, studies reliably found hippocampal volume differences across studies with the injury group showing smaller volumes (Beauchamp, Ditchfield, Maller, et al., 2011; Serra-Grabulosa et al., 2005).

Morphometric investigations of the brain post-TBI were not limited to the volume of cortical regions, but also the cortical thickness. There were fewer investigations of cortical thickness, but early post-injury studies showed regions of dorso-lateral prefrontal cortex (dlPFC; McCauley et al. (2010); Urban et al. (2017); Wilde et al. (2011)) and other prefrontal regions (McCauley et al., 2010; Wilde et al., 2011) as well as superior temporal sulcus (STS; McCauley et al. (2010); Wilde et al. (2011)), cingulate regions (McCauley et al., 2010) and regions of the inferior parietal lobule (iPL; Urban et al. (2017)) to be significantly thinner in the TBI group compared to controls. However, these differences were not replicated at a later timepoint post injury (Bigler et al., 2016). This is not to say that these differences have 'recovered' over time (due to the cross-sectional nature of this evidence) but more likely due to differences in methodology and samples.

The evidence presented from these cross-sectional studies suggests that frontal, temporal and parietal regions areas are commonly (and persistently over time) impacted following a pTBI (Wilde et al., 2005). However, it is important to note that the regions identified by individual studies span multiple regions of the cortex and subcortical regions, suggesting in fact that the effects of pTBI can be seen diffusely

across the brain. This is specifically highlighted in studies investigating summed ROI volumes across distributed brain networks (Dennis et al., 2013; Ryan, Beauchamp, et al., 2016; Ryan, Catroppa, et al., 2016; Ryan et al., 2017).

However, some studies used innovative methodologies to investigate the diffuse nature of morphometric brain changes post-injury. Spanos et al. (2007) took an innovative approach to investigate volumes of the cerebro-cerebellar network (dlPFC, thalamus, pons and cerebellum) by estimating correlations between volumes of these structures. Significant correlations were found between volumes of the thalamus/dlPFC and the pons/cerebellum in both groups. A significant interaction between groups was found, in which a significant positive relationship between dlPFC/cerebellum was found in the TD but not in the TBI group. Drijkoningen et al. (2017) investigated the statistical relationship between regional subcortical-atrophy. Volume deviation score was calculated with a linear regression of subcortical volumes against intracranial volume (ICV) in the control group, with the linear model providing a predicted volume for regions given an ICV. Thus, the deviation score for any given patient was actual volume minus predicted volume. Correlations were assessed between the volume deviation scores across the TBI group. Moderate to very strong positive correlations were found for these relationships, with significant correlations found between deviation scores for multiple, subcortical regions. This interrelation between deviation scores suggests a diffuse pathology that affects wider subcortical volume, rather than specific areas (Drijkoningen et al., 2017).

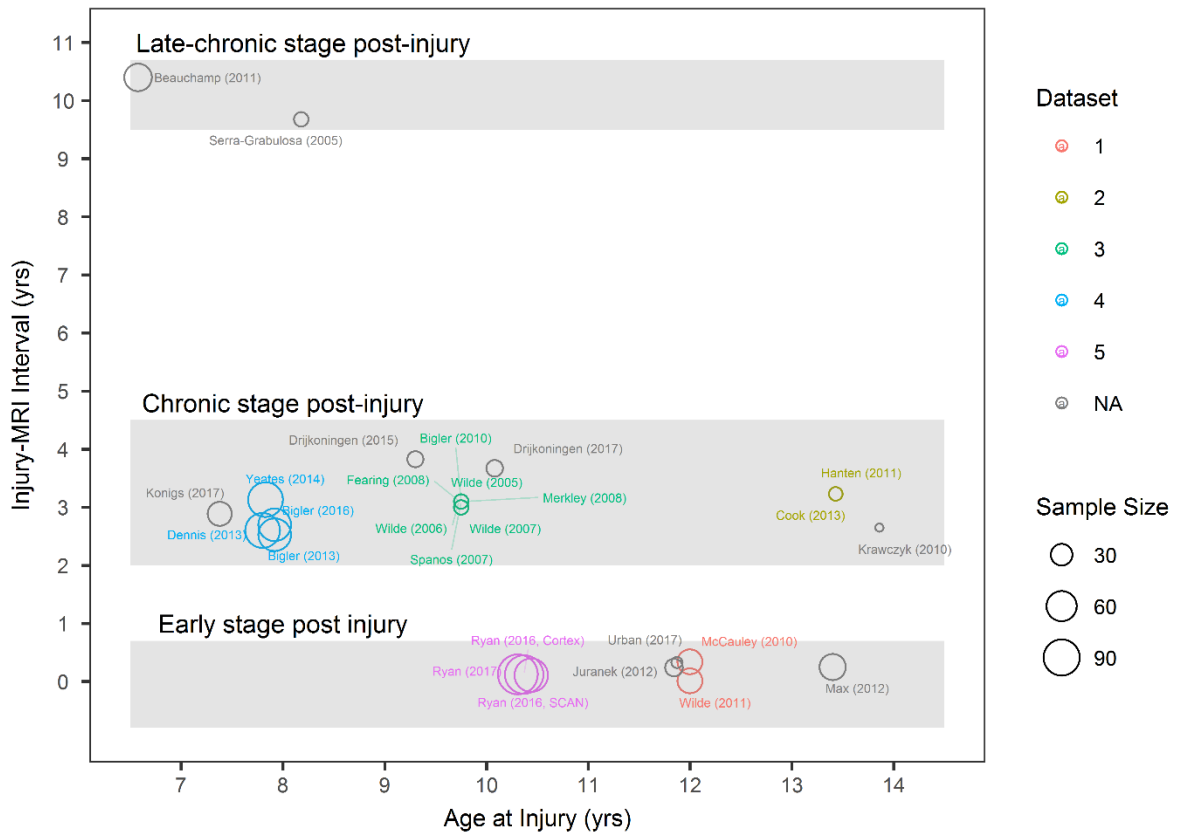


Figure 2.2. Descriptive plot of all eligible cross-sectional studies included for review. Studies are plotted based on mean age at injury of their sample against mean time between injury and MRI (years). Size of each point is proportional to the size of the TBI participant sample used in the study whilst the colour segregates clusters of studies that all use the same dataset of patients. To aid qualitative synthesis, studies were grouped into three major ‘bands’ of enquiry; i) an early stage (days to 1 year post-injury), ii) chronic stage (1-5 years post-injury) and iii) late chronic stage (9+ years post-injury). These band were qualitatively identified once studies were plotted in this way and are therefore based on the ‘natural’ grouping of the studies and therefore represent the current state of the literature.

Table 2.4a *Study demographics for all longitudinal studies included in the review*

Reference	Sample and age (age at scanning; years, M±SD)	Age at injury (years, M±SD)	Longitudinal Timepoints (days/months/years, M±SD)	Comparative Group and age at scan (years, M±SD)	Quality Rating
Dennis et al (2017), USA	11 TBI-slow IHTT, Timepoint 1: 14.1 years ± 1.9, 3F, 8M, Timepoint 2: 15.0 years ± 2.0, 10 TBI-normal IHTT, Timepoint 1: 16.0 years ± 2.6, 2F, 8M, Timepoint 2: 17.0 years ± 2.8	Not reported	Timepoint 1, TBI-slow IHTT 50.6days ± 5.9, TBI-normal IHTT 52.5days ± 9.7, Timepoint 2, 12 approximately 12 months post-timepoint 1 (Not reported)	26 Healthy Controls, Timepoint 1: 14.5 years ± 3.0, 11F, 15M, Timepoint 2: 15.6 years ± 3.0	Medium (1.33)
Wu et al (2018), USA	10 Sports concussion mTBI, Timepoint 1: 14.58 years ± 1.5, 4F, 6M, Timepoint 2: Not reported	Not Reported	Timepoint 1, <96hours post injury (range 21-116h), Timepoint 2, 3 months post injury (range 84-143days)	12 sports-related OI, 14.06 years ± 1.63, 3F, 9M (only 9 included for morphometric analysis at T1 and 12 at T2), 12 TD controls (no age or gender reported, only received single MRI)	Medium (1.25)
Dennis et al (2016), USA	36 (18 completed longitudinal testing) Moderate-Severe TBI, Timepoint 1: 14.1 years ± 2.7, 10F, 26M, Timepoint 2: 15.9 years ± 2.6, 5F, 13M (some participants were tested at only timepoint 1, others at only timepoint 2)	Not reported	Timepoint 1, post-acute phase (1-6 months post-injury), Timepoint 2, chronic phase (13-19 months post injury)	35 (22 completed longitudinal testing) TD controls, Timepoint 1: 14.8 years ± 2.8, 12F, 23M, Timepoint 2: 16.2 years ± 3.2, 7F, 15M (matched for age, sex, and educational level)	Medium (1.17)
Mayer et al (2015), USA	15 (11 completed longitudinal testing) Mild TBI, Timepoint 1: 13.47 years ± 2.20, 2F, 13M,	Not reported	Timepoint 1, within 21 days post injury (TBI 15.87days ± 4.93),	15 (12 completed longitudinal testing) TD controls,	High (1.58)

			Timepoint 2: Not reported	Timepoint 2, 4months post injury (TBI 127.82days ± 14.60)	Timepoint 1: 13.40 years ± 1.84, 3F, 12M (age and education matched), Timepoint 2: Not reported	
Wilde et al (2012), USA	13 Severe TBI, 4 Moderate TBI, 3 Complicated Mild TBI, Timepoint 1: 13.6 years ± 2.9 (range 8.2-17.5), Timepoint 2: 14.8 years ± 2.9 (range 9.3-18.7), 9F, 11M	Not reported		Timepoint 1, 3 months post injury (TBI 4.0months ± 1.0, OI 4.7months ± 2.6), Timepoint 2, 18 months post injury (TBI 18.5months ± 3.6, OI 18.4months ± 4.2)	21 OI controls, Timepoint 1: 12.3 years ± 2.5 (range 7.4-16.7), Timepoint 2: 13.2 years ± 2.6 (range 8.8-18.0), 6F, 15M	Medium (1.33)
Wu et al (2010), USA	3 Complicated Mild TBI, 4 Moderate TBI, 16 Severe TBI, Timepoint 1: 12.9 years ± 3.2 (range 7.8-17.2), 8F, 15M, Timepoint 2: Not reported	12.9 years ± 3.2		Timepoint 1, 3months post injury (TBI 4.0months ± 0.9, range 2.5-5.3, OI 4.2months ± 1.0, range 2.7-7.1), Timepoint 2, 18months post injury (TBI 18.9months ± 1.5, range 16.7-22.6, OI 18.8months ± 1.3, range 16.6-20.9)	25 OI controls, Timepoint 1: 11.8 years ± 2.7 (range 7.1-16.3), 7F, 18M, Timepoint 2: Not reported	Medium (1.50)

Note. CT=computed tomography, HTT=Inter-hemispheric transfer time, OI=Orthopaedic Injury

Table 2.3 b *Study findings for all longitudinal studies included in the review*

Reference	Magnet Strength	Methodology (software, statistical approach, anatomical-level)	Measure of interest	Variables controlled	Findings
Dennis et al (2017), USA	3T	Tensor based morphometry (linear regression, voxel-wise)	Volume	Age at scanning, sex, scanner, and ICV	Longitudinal regional volume changes differed significantly across a number of clusters between TBI-slow, TBI-normal and controls. Over time, TD children showed significant volume increases, but TBI-slow group showed mostly decreases across regions of splenium, CC, capsule and claustrum, posterior thalamic radiation and hypothalamus. The TBI-normal group had significantly greater reductions in including SFG, parietal operculum, PCC, thalamus, MFG, putamen, MTG, postC, internal OG, SFG and insula compared to controls and increases in internal capsule. TBI-slow showed greater volume reduction whereas TBI-normal showed longitudinal increase in internal capsule, thalamus and superior corona radiata. TBI-slow group had significantly greater atrophy than TBI-normal group in regions of SFG, inferior OG, SPL, cingulate, MFG, cuneus, PCUN and parietal operculum.
Wu et al (2017), USA	Not reported	Freesurfer (Between and paired T-test, ROI)	Volume	ICV	No cross-sectional or longitudinal differences in volume between TBI, and OI/TD groups.
Dennis et al (2016), USA	3T	Tensor based morphometry (linear regression, voxel-wise)	Volume	Age at scanning, sex, scanner, and ICV	Longitudinal effects not statistically assessed. At timepoint 1 significantly greater volume for the lateral ventricles in TBI (indicative of CSF expansion). Lower volumes found compared to controls in left LING, bilateral PCG, right FFG, right STG, left thalamus, left PCUN, left SFG, left OG, right PCG, cingulum, and parahippocampal gyrus. At timepoint 2 significantly increased ventricle size for the TBI group and smaller volumes for the TBI group compared to controls bilateral LING, right MTG, bilateral OrbG, right FFG, ACC and mid-cingulate cortex, left SPL, and left preC. However, greater volumes in TBI group in left IFG, and the bilateral posterior thalamic radiations, right superior longitudinal fasciculus, right OG, right AG, and right SPL.
Mayer et al (2015), USA	3T	Freesurfer longitudinal pipeline (GLM,	Volume and	None reported	No significant group differences in vertex-wise cortical thickness or volume of hippocampus and thalamus at timepoint 1. No significant effect of group on subcortical volume change. TBI group showed greater atrophy over time in the left SFG and MFG, left MTG, left postC running into IPL, left IPL, left cuneus, left MOG, right SFG and MFG.

		MANOVA, Vertex, ROI)	Cortical Thickness		
Wilde et al (2012), USA	1.5T	Freesurfer longitudinal pipeline (GLM, Vertex)	Cortical Thickness	None reported	At timepoint 1, smaller cortical thickness in TBI group compared to controls in bilateral rostral, MFG, SFG, lateral and medial OFC, anterior cingulate, and FP and unilaterally in the right pORB, right pTRI and right pOPER and at timepoint 2, bilateral rostral MFG, caudal MFG, FFG and lingual regions, and unilateral left SFG, preC, PCUN, isthmus cingulate, SPL and IPL, right pTRI, pORB, and lateral OFC. Longitudinally TBI group showed significant thinning in many cortical areas, with sparing of this effect seen in bilateral TP, and medial aspects of the frontal lobes, cingulate and left FFG. Significant longitudinal thinning in TBI versus OI group in SPL and right paracentral regions, but increase in medial OFC, bilateral cingulate, and right lateral OFC.
Wu et al (2010), USA	1.5T	Freesurfer longitudinal pipeline (GLM, t-test difference score, ROI)	Volume	ICV	At timepoint 1, TBI showed smaller midanterior CC compared to OI. Total CC volume significantly smaller in TBI group at timepoint 2 (but not timepoint 1) and anterior, midanterior, central and mid posterior CC. Longitudinally, the total, anterior, midanterior, midposterior, and posterior regions of the CC reduced in volume for the TBI group compared to slight increases in volume for OI group.

Note. GLM=general linear model, ICV= Intra-cranial volume, IHTT=Inter-hemispheric transfer time, OI=Orthopaedic Injury, ROI=Region of interest,

2.4.3 Longitudinal studies

Whilst there were significantly fewer studies eligible for inclusion that incorporated a longitudinal design compared to those who utilised a cross-sectional design, these longitudinal studies here showed that there were widespread differences in both volume and cortical thickness. Similarly small sample sizes were seen in the longitudinal studies as the cross-sectional studies with the average sample size for eligible studies being 20.83 (SD = 8.03, range = 10-36). A narrow distribution of age at scanning was seen (initial timepoint: $\text{mean}_{\text{pooled}} = 13.913^2$, range of means = 12.9 years-16.0 years), with no studies looking at the very extremes of childhood. However, it is important to note that this does not refer to the age at injury, but the age at MRI scanning. This is because all six longitudinal studies did not report the mean age at which the injury occurred. Table 2.3a describes the sample demographics of each study.

Differences in volume between timepoint one and two consistently changed as a function of group (patient vs control) across common regions of dlPFC (Dennis, Faskowitz, et al., 2017; Mayer et al., 2015), STS (Dennis, Faskowitz, et al., 2017; Dennis et al., 2016; Mayer et al., 2015), posterior parietal cortex (PPC) extending into iPL, cingulate regions (Dennis et al., 2016; Mayer et al., 2015; Wilde, Merkley, et al., 2012), and hypothalamic, thalamic and CC regions (Dennis, Faskowitz, et al., 2017; Wu et al., 2010). In these regions patients were more likely to show reductions or atrophy greater than that of the control group over the same time period, indicating that the rate of change in volume/cortical thickness differs between groups. However, whilst Dennis et al. (2016) and (Wilde, Merkley, et al., 2012) found significant differences between patients and controls in morphometry at both timepoint one and two, Wu et al. (2010) found differences at only timepoint two.

Interestingly, Dennis, Faskowitz, et al. (2017) used a longitudinal design (upon the same data as Dennis et al. (2016)) to investigate two sub-groups of the original moderate/severe injury group. Patients were divided based upon inter-hemispheric transfer time (IHTT); those that were slower than normal (TBI-slow) and those with normal IHTT (TBI-normal). Longitudinal regional volume changes differed significantly across a number of regional-clusters for pairwise comparisons of TBI-slow, TBI-normal and controls. When comparing TBI-slow and TD control groups, over time TD children showed significant increases in volume in regions, whereas the TBI-slow group mostly showed decreases. This was across mostly WM regions of splenium, CC (two clusters), external/extreme capsule and claustrum, posterior thalamic radiation and hypothalamus. The TBI-normal group had significantly greater reductions in a number of GM regions compared to controls, including superior frontal gyrus (SFG, four clusters), parietal operculum, PCC (three

² This value does not consider the overlap of sample/datasets

clusters), thalamus, middle frontal gyrus (MFG), putamen, middle temporal gyrus (MTG), post central gyrus (postC), internal- occipital gyrus (OG), SFG and insula. However, the TBI-normal group had two clusters of greater longitudinal volume change compared to controls in the internal capsule. When comparing the two TBI subgroups, TBI-slow showed more longitudinal reduction whereas the TBI-normal showed longitudinal increase in mostly WM tissue regions of internal capsule, thalamus and superior corona radiata. However, the TBI-slow group had significantly less longitudinal growth/greater atrophy than the TBI-normal group in mostly GM regions of SFG (four clusters), inferior- OG, superior parietal lobule (SPL), cingulate (two clusters), MFG, cuneus, precuneus (PCUN) and parietal operculum. Whilst the direction of causality remains unclear, this suggests potential relationships between both structural and functional changes.

Some studies utilise statistical methods controlling for effects such as total intracranial volume (Dennis, Faskowitz, et al., 2017; Dennis et al., 2016; Wu et al., 2018; Wu et al., 2010) or age at scanning (Dennis, Faskowitz, et al., 2017; Dennis et al., 2016) as proxies for the stage of brain development, or reported using age-matched samples (Dennis et al., 2016; Mayer et al., 2015). Theoretically, this would remove variance in morphometry due to the age-related development of the cortex, and group differences that survive removal of this covariance would be where the changes in morphology post-TBI are exceeding or fall short of typical development. However, in the current literature, when controlling for these proxies of development, the reported effects are not consistent across studies, with some studies still finding an interaction between group and timepoint on morphometry (Dennis, Faskowitz, et al., 2017; Wu et al., 2010) and others not (Wu et al., 2018). Although it is interesting to note that Wu et al. (2018) investigated a cohort of mild TBI due to sports concussion. This potential lack of consensus amongst studies limits assessment of whether or not the effects of injury are truly beyond that of expected developmental differences over time and warrants further study.

2.4.4 Linking morphometry to cognition in TBI

Of the eligible papers, 16 investigated the associations between morphometry after a TBI and cognitive/neuropsychological outcomes across multiple domains. Some studies investigated outcome measures that were not directly linked to cognitive ability (e.g. postural control (Drijkoningen et al., 2017; Drijkoningen et al., 2015)). Although we accept that these outcome measures are important and may be related to variation in cognition (such as postural control), we only review those outcomes that are direct measures of cognition (such as IQ). The results of these studies are summarised in supplementary materials (Table A.2, Appendix A) and are divided into the cognitive domains assessed. This table shows clearly the disparity in methods, measures and regions tested, thus highlighting the difficulty with which any significant qualitative synthesis can be achieved.

There were many ways in which studies designed analyses to probe brain-behaviour relationships post injury, and these are described in the design column of Table 2.4. The majority of studies used a correlational design, and did not model group differences, but instead looked at whole sample (across patients and controls) or just correlations within the TBI group. Other studies took a cross-sectional approach but varied in how vigorously they probed the cross-sectional differences between groups. In Table A.2 (Appendix A), cross-sectional (comparative) refers to studies which statistically investigated brain-behaviour relationships within both TBI and control groups but only qualitatively compared these relationships between the two groups, whereas cross-sectional (statistical) refers to those studies that statistically modelled differences in these brain-behaviour relationships between groups (for example modelling the main effect of group in a GLM of volume by performance relationship). Of the studies that used a cross-sectional design to probe these links between morphometry and cognition, the majority used the comparative approach.

The most common domain that was assessed was working memory, including a number of validated normed (i.e. WISC-III digit span test) and non-normed tests (i.e. Sternberg Item recognition tests (SIRT)). Reduced performance in the TBI group was seen repeatedly in relation to reduced volumes of parietal regions and cortical thickness of parietal and frontal regions (Merkley et al., 2008; Urban et al., 2017; Wilde et al., 2011). However, it is unclear if there are any meaningful differences in actual performance between patients and controls in working memory performance across the studies included in this review. Studies found significant reductions in performance for patients (Konigs et al., 2018), limited interaction effects of group and performance on certain task variables (Urban et al., 2017; Wilde et al., 2011) or did not report performance differences at all (Fearing et al., 2008; Merkley et al., 2008). Thus, without meaningful differences in performance it is difficult to realise the potential utility of these brain-behaviour relationships.

Multiple studies used a battery of tests to assess the relationship between cognitive (understanding false beliefs), affective (interpreting emotive communication) and conative (understanding social communication which influences others thinking i.e. irony) aspects of ToM morphometry after TBI (Dennis et al., 2013; Ryan et al., 2017; Yeates et al., 2013). Cognitive, conative and affective ToM abilities were all positively associated with total GM volume and negatively associated with ventricle to brain ratio (Yeates et al., 2013). Specifically cognitive ToM was related to total volume of the CCMN and affective to the SN (Ryan et al., 2017) Conative ToM was predicted by a model of DMN, CEN and MNEN volume (Dennis et al., 2013) and total MNEN volume (Ryan et al., 2017). Of the decomposed regional volumes of these networks only posterior cingulate/retrosplenial cortex and hippocampal formation remained significant following multiple comparison corrections (Dennis et al., 2013). VBM only found significant clusters of brain-behaviour relationship in the OI not the TBI group (Yeates et al., 2013).

Significant brain-behaviour relationships between morphometry and cognition post-injury were also found for other domains of executive functioning (Wilde, Merkle, et al., 2012), anticipating social consequences (Cook et al., 2013), social problem solving (Hanten et al., 2011), and analogous reasoning (Krawczyk et al., 2010). Across two studies, Dennis and colleagues (Dennis, Faskowitz, et al., 2017; Dennis et al., 2016) investigated the potential brain-behaviour relationships using a summary score of overall cognitive function (comprising a wide number of domains of processing speed, working memory, verbal learning, short term memory and attention switching), finding significant relationships both at a cross sectional and longitudinal basis, in the same sample. Domains of processing speed (Wu et al., 2010), IQ or verbal learning (Konigs et al., 2018) showed no significant relationships with morphometry. However, there were only a limited number of studies that measured each of these cognitive outcomes. As many of these studies had limited sample sizes and studies with significant findings utilised mass univariate approaches (i.e. voxel/vertex-wise analysis), there is a heightened risk of Type 1 errors even when controlling for multiple comparisons. Therefore, it is important to look at convergence of results across multiple studies to determine whether findings are reliable or not.

2.5 Discussion

The current review has found some consistency in the differences and changes to the brain following a TBI during childhood, with most findings reporting reduction of volume and cortical thickness at a whole brain and regional level compared to TD peers' between and across timepoints. This consistency across studies was found despite the considerable heterogeneity in the resulting neuropathology following a TBI (Dennis, Babikian, et al., 2017), and the additional complexity introduced by the fact that the injury occurs within the context of developing paediatric brain.

Overall, cross-sectional studies largely replicated the idea that frontal, temporal and parietal regions are particularly vulnerable following a pTBI (Wilde et al., 2005), likely due to the unique biomechanics of injury within the paediatric brain (Pinto, Poretti, Meoded, Tekes, & Huisman, 2012). However, regions of significant differences identified by individual studies can also be seen across the brain, suggesting a diffuse effect of injury on post-pTBI morphometry.

We synthesised the data from the reviewed cross-sectional studies into 'bands' post-injury to make longitudinal inference in regard to the time since injury. It is important to note that these bands were derived based upon the 'natural' grouping of studies in the literature (see Figure 2.2) and thus clinical relevance of these bands may be limited. This is especially true of the early-stage post-injury, given the very dynamic nature of evolving and resolving pathology. Differences in imaging methodology and participant cohorts did not allow for an alternative sub-grouping within this first year, however, some patterns still emerge. The

cross-sectional evidence presented suggests that TBI is related to atrophy of the brain post-injury and that some regions are more vulnerable to these effects. The regions affected, whilst broadly similar, still vary across these post-injury bands. These findings indicate that cross-sectional studies can provide information about the morphometric differences related to a given condition (Madan, 2017), in this case pTBI by highlighting, for example, regions at high potential risk of atrophy (Irimia et al., 2017). Nevertheless, these studies are limited as they provide only a snapshot of the highly dynamic process of lesion and pathology development (Bigler, 2016). It is not possible to disentangle whether differences across time periods could be attributed to either true longitudinal differences or variability in samples and/or methodologies (Kraemer, Yesavage, Taylor, & Kupfer, 2000; Vijayakumar, Mills, Alexander-Bloch, Tamnes, & Whittle, 2017). Hence, as we cannot imply a longitudinal process from the comparison of these cross-sectional studies, we may conclude that in fact these spatial differences arise as a function of the variability in injury; no two individuals, or even two patient populations, experiences the same biomechanics of injury, genetic context, and experience-dependant plasticity (Saatman et al., 2008). The key evidence presented here is that differences occur at each of the three bands post injury, from acutely to as far as 9-10 years post injury (Beauchamp, Ditchfield, Maller, et al., 2011). This suggests that there is a non-transient effect of paediatric traumatic brain injury, which neither recovers nor is compensated for over time.

The wide within-study variability of time between injury and MRI assessment affects interpretation of these cross-sectional data. The study with the greatest variability is Drijkoningen et al. (2015), with the range of time between injury and follow-up in their TBI cohort was 0.3 to 10.8 years post injury. Although this means that direct comparison between studies is not possible, it does not preclude studies from investigating time since injury as a covariate of analyses, an approach that no study included in this review took. Only Urban et al. (2017) investigated similar effects by looking at the correlation of time since injury on cortical thickness measures in the patient group, finding no significant relationship. This absence of evidence for an atrophic process differing as a function of time since injury would seem to disagree with a continuing, longitudinal injury process. However, it is important to consider that this univariate relationship does not consider other factors (such as age at time of injury) and would provide far more convincing evidence if conducted in a longitudinal cohort. Thus, at this point in time it is not possible to draw any conclusions about the influence of time since injury on brain morphometry on the basis of the cross-sectional data alone.

The longitudinal studies identified in the current systematic review point towards a divergence of the usual / expected developmental trajectory of the brain post-injury. Studies showed that change over time differed between groups (TBI vs Control) with patients more likely to show reductions or atrophy greater than that of the control group over the same time period. Given these data, and the presence of chronic cross-sectional differences between controls and patients highlighted previously (Beauchamp, Ditchfield, Maller, et al.,

2011), it is unlikely that the maturational processes which occur to the brain during childhood are able to ‘overwrite’ the original damage post-injury as proposed by Bigler and Wilde (2010), or even that brain development after a pTBI ‘catches up’ with that of healthy peers. However, the current literature is limited in understanding at an individual level where, how much and in which individuals these long-term changes occur, and how these relate to individual-level neuropsychological performance post injury.

The timing of both the initial brain injury and the resultant assessments that evaluate its effects, are known to be important factors in understanding the impact of TBI and subsequent neuropsychological sequelae in children (Anderson et al., 2011). Some research suggests that there are critical periods in development where the effects of injury are most severe (Anderson et al., 2011), potentially due to vulnerability to injury pathology that is specific to certain stages of brain development (Anderson et al., 2011; Goldstrohm & Arffa, 2005; McCrory et al., 2004; Urban et al., 2017; Wilde et al., 2006). This is also likely to go on to affect functional outcomes; if there is structural damage to still-developing brain networks which typically subsume given cognitive functions, then this may result in difficulties making “age-appropriate gains” (Ryan, van Bijnen, et al., 2016, p. 27) in the acquisition of these skills (Anderson et al., 2009; Ryan et al., 2015). There was, however, a limited number of studies in the current review which investigated the effects of age at injury on morphometric differences/variables. Three studies reported analyses that examined the effect of age at injury on morphometry (Bigler et al., 2016; Max et al., 2012; Urban et al., 2017). Urban et al. (2017) found no significant correlations between cortical thickness and age at or time since injury, whilst Max et al. (2012) found that structural volumes of regions did not differ as a function of age across both controls and TBI patients. Bigler et al. (2016) found a significant relationship between age and cortical thickness but this relationship did not statistically differ between groups (although they do not report if this is age at injury or age at MRI, it is likely to be age at scan). None of the longitudinal studies investigated morphometric changes differed as a function of age at injury. If we assume that there are critical periods of development when there is specific vulnerability to the pathology of injury, then TBI at these critical periods may result in changes to morphometric measures that are greater than if the injury occurs at other stages of development. Further to this, without thorough investigation of patient-control differences across the range of time post-injury it is difficult to assess the emergence of differences in the post-TBI developmental trajectory. That is to say, the exact timings of when this developmental ‘divergence’ is unknown, based on the present state of the literature.

Although age at injury is a salient variable when trying to understand the impact of TBI on brain development and later functional outcomes, the review demonstrates a paucity of studies in some age groups. At key stages of postnatal cortical development - in preschool age groups and late adolescence - the consequences of TBI on the morphometry of the brain are understudied. This is of particular concern given

that these are both periods of non-linear cortical change (Mills et al., 2016; Raznahan, Shaw, et al., 2011) in which developing brain networks are crucial for neurodevelopment. In order to understand the specific consequences and subsequently make treatment or rehabilitation recommendations for cognitive and behavioural impairments, a better understanding of age-related effects is needed. Thus, future studies should sample these age-bands.

A fundamental challenge for the field is to tease apart the various factors that interact with one another to determine brain morphology, such as the interaction between age at injury and the age at MRI scan. This is further complicated by the fact that these variables are unlikely to be independent, especially due to current practices of recruiting patients at an a-priori defined period post injury (i.e. acute, chronic). In such studies, the age at scanning will be systematically related to the age at injury (by the amount of the post-injury period). Future longitudinal studies (and even cross-sectional designs) may therefore be advised to take an accelerated longitudinal design approach to time since injury. By choosing a prospective study design which recruits at varying times post-injury (from acute to chronic stages) it will enable more effective statistical modelling of the independent trajectories that are determined by age at which an injury has occurred and the time since the injury, by giving suitable range of sampling of each of these variables.

One of the greatest challenges to the field is to understand how the whole-system level pathology to the brain gives rise to changes in functional behaviour (Bigler, 2016). The current review specifically investigated how gross brain atrophy in children with TBI may be associated with differences in post-injury cognition from TD controls. However, the lack of consistency in methods, measures and brain partitions used across the included literature makes synthesis of findings across studies difficult. The most commonly investigated association was between brain morphology and working memory. Specifically, regions of parietal and frontal lobe morphometry not only related to working memory measures (Merkley et al., 2008; Urban et al., 2017; Wilde et al., 2011), but also contributed to the difference in performance between controls and patients (McCauley et al., 2010). Longitudinal investigations of cognitive change over time also suggest that possible ‘divergence’ of morphometric maturation may be associated with differing development of and performance on a number of cognitive domains for the TBI group (Dennis, Faskowitz, et al., 2017; Dennis et al., 2016). However, it is important to note that, due to our inclusion criteria, we only looked at studies with a control group to assess morphometric change after injury. Papers that examined at brain-cognition relationships in solely a patient group were not included in the initial search.

The interrogation of any association between morphometry and cognition in children with TBI varies across studies. Individual differences in morphometry were typically correlated with individual differences in neurocognitive performance. Some studies did this solely in the TBI group (Konigs et al., 2018; Ryan et al., 2017; Wilde, Merkley, et al., 2012; Wu et al., 2010) and not in the TD control group. Thus, on the basis of

their reports, it was not possible to not separate out developmentally-appropriate brain behaviour relationships from those that are truly atypical. For example, if cognitive ability 'X' scales linearly/non-linearly as a function of the size of region 'Y' (or network 'Z') during development, then any brain-behaviour relationships between region 'Y'/network 'Z' and cognitive tasks assessing 'X' seen in a TBI population could potentially represent normative development, rather than informing us how damage and/or atrophy is potentially disrupting the development and retention of cognitive skills. Few papers in the current review approached this question using a cross-sectional approach, and even fewer statistically modelled the effect of group in these brain-behaviour relationships (i.e. through GLM using group as a between-subjects factor, (Dennis et al., 2013; Fearing et al., 2008; McCauley et al., 2010)). It is important to recognize that these differing approaches answer very different hypotheses on how the injured brain relates to cognitive development. It is our opinion that, in order to make clinically useful predictions about functional outcome based on morphometry measures of the brain, then it is important to see if the brain-behaviour relationships differ post-injury from those seen in typical development. If this is not the case, then it would be just as prudent to predict cognitive performance in the TBI group using morphometric models derived from healthy participants.

Synthesis of a large body of literature is important for understanding the nature of morphometric changes post-pTBI. However, there are methodological considerations within the field that must be considered both in the interpretation of this synthesis and in future studies. A key issue is the presence of macroscopic lesions on MR images as well as more subtle pathology. These include lesions due to WM deformation and shear, Wallerian degeneration, compromised vascular integrity, hemosiderin deposition and encephalomalacia, which are highly heterogeneous between individuals (Bigler, 2013; Bigler et al., 2016). In a study of a pTBI sample (used by multiple papers in the current review (Ryan, Beauchamp, et al., 2016; Ryan, Catroppa, et al., 2016; Ryan et al., 2017)) the presence of a lesion on MRI (T1w, T2w or FLAIR) was detected in 54% of cases (Beauchamp, Ditchfield, Babl, et al., 2011). This represents ~56% (n=20) of the cases for which the researchers had access to MRI, CT and susceptibility weighted imaging (n=36), and is therefore likely a slight overestimation. Despite the prevalence of lesions on MRI scans included in papers reporting global and regional morphometry following pTBI, only four studies discussed methodological approaches to deal with the presence of lesions. Spanos et al. (2007) replicated findings of cerebellar differences even when removing patients with focal cerebellum lesions, whilst Serra-Grabulosa et al. (2005) listed focal lesions as an exclusion criterion for their sample selection and still found cross-sectional differences between non-lesioned TBI cases and controls. Bigler et al. (2013) stated that, due to extreme structural damage in two patients, Freesurfer was unable to reconstruct the brain surfaces and thus these patients were excluded from analyses. The most proactive approach to controlling for the effect of lesion was that of Drijkoningen et al. (2017) who excluded regions where the presence of a focal lesion (>0.5 cm³) had resulted in distortion of

the segmentation or parcellation by Freesurfer, resulting in the exclusion of seven regions across two participants (although it is pertinent to note that only 1.8% of all ROI data across the whole TBI sample was excluded in this way). However, the remaining studies did not explicitly state how lesions were addressed in their quantitative neuroimaging pipelines or even if any lesions were present in their sample at all.

The presence of lesions may influence image processing pipelines, and therefore the resultant morphometric findings. This might lead to under- or over-reporting of TBI-control differences, depending on the approach adopted. For example, disruptions to voxel intensities (due to oedema for example) can lead to inappropriate solutions to cost-function algorithms (such as those in spatial normalization), causing observable distortion around the lesion (Brett, Leff, Rorden, & Ashburner, 2001; Goh, Irimia, Torgerson, & Horn, 2014; Irimia, Wang, et al., 2012). Gross anatomical lesions can also result in brain segmentation and surface reconstruction failures (Irimia, Goh, Torgerson, Vespa, & Van Horn, 2014; Merkley et al., 2008; Wang, Prastawa, Awate, et al., 2012; Wang, Prastawa, Irimia, et al., 2012). Anatomy can also be mislabelled by probabilistic-labelling when pathological lesions lead to gross and/or focal deformation of tissue, producing morphometric measures for ROIs which are not accurate (Dennis et al., 2016; Goh et al., 2014; Irimia, Chambers, et al., 2012; Irimia et al., 2014). Other methodologies, such as Freesurfer, are also semi-automated, and thus require manual intervention to ‘correct’ potential inaccuracies such as this. However, the degree to which manual intervention is conducted is solely at the discretion of the researcher and the details of which are often not transparently reported (Vijayakumar et al., 2017). None of the morphometric studies in the current systematic review reported how lesions were approached within this framework of manual editing, and there are no clear recommendations in software documentation as to how to approach such pathology.

The methods used to estimate morphometric estimates of the brain may not be robust in the presence of the lesions characteristic of TBI, and there is a lack of validation of these methods in TBI cohorts (Goh et al., 2014; Irimia et al., 2011; Irimia et al., 2014). This is especially true given the fact that many of these methodologies operate on detection of tissue boundaries within an MRI via changes in image contrast. In the presence of a TBI, tissue contrast of an MRI is suggested to be different to controls (Palacios et al., 2013). Even though some software allows (limited) integration of lesion masks into processing (ANTS allows users to perform cost-function masking during registration using a lesion mask), studies did not outline how the processing pipeline had been tested or optimised for use with MRI where there are traumatic lesions present. These methodological concerns raise questions about the credibility of the individual studies reported here, but also creates a critical question for our field; in order to accurately identify and report data on brain changes following pTBI it is important that our quantitative methodologies include pathological brains. Although excluding cases is an appropriate approach, and sometimes the only option available when

registration failures occur, these cases warrant inclusion in large, representative datasets. Future work needs to assess how lesions may impact the processing of neuroimaging data, however, due to the fact there is no one ‘universal’ TBI lesion (Bigler, 2016), this is unlikely to be a trivial endeavour.

The current review specifically focused on structural changes to the brain as measured with T1w structural MRI. Structural changes post pTBI have also been recognized using diffusion weighted imaging (DWI) and related WM-tract modelling (for an extensive review of this literature see Dennis, Babikian, et al. (2017)). The two methods provide unique information about differing injury mechanisms. For instance, fractional anisotropy of the diffusion signal can infer microstructural properties of WM following diffuse axonal injury (Dennis, Babikian, et al., 2017). GM measures of structure outlined in this review, such as cortical thickness or volume, aim to assess the potential atrophic effects of the cascade of mechanisms that occur post-injury (Bigler, 2013). Whilst indexing different injury mechanisms, these neuroimaging methodologies provide complementary information for the basis of understanding the brain post pTBI. For instance, multimodal imaging can enhance the segmentation of pathological lesions in pTBI (Irimia et al., 2011) with each modality detecting specific properties of the lesion (Zhang et al., 2016). Future research should therefore echo approaches of studies such as Konigs et al. (2018), by combining multiple modalities of imaging to better understand the brain post pTBI.

2.6 Concluding remarks

In the adult TBI literature, Cole et al. (2015) propose a model for changes to the ‘brain age’ of a patient after TBI. They prescribe that TBI does in fact cause a long-term chronic disease process, and these interact with the normative process of ageing of the brain. Thus, the resultant state of the brain can be expressed in terms of additive effects, the sudden departure of the brain from the ‘healthy’ brain state for an individual of that age, and interaction effects, which potentially accelerate the ageing process (particularly atrophy) due to the interaction of this process with the cascade of pathologies following injury. The studies shown in this review seem to paint a similar picture, but with the idea of ‘healthy ageing’ replaced instead with ‘normative development’. Our findings of the both volumetric and cortical thickness differences from controls in the initial stages of early injury highlight this potential ‘additive effect’ where the injury has caused sudden change to the morphometry to the brain. The current review also highlights the longitudinal effect of injury on development, supporting such a model of ‘interactive effects’ in paediatric TBI.

Overall the current systematic review draws the following conclusions from the existing literature on morphometric changes to the brain post pTBI; a) differences are apparent cross-sectionally at both acute and late-chronic timepoints post-injury, thus suggesting a non-transient effect of injury and b) morphometric

change over time is altered in TBI groups compared to patients, but it is currently unclear if this is an effect of disrupted development or a continuing ‘neurodegenerative’ effect of injury.

The current review also highlights challenges to the field in regard to within-study sample heterogeneity, limited investigations of the extreme tails of childhood, and the potential effect of lesions on analyses. In addition, further work is needed to effectively relate these morphometric measures to cognitive measures of post-injury functioning to firmly establish the role of TBI-related brain changes in long-term functional outcomes.

Chapter 3. Lesion Induced Error on Automated Measures of Brain Volume: Data From a Paediatric Traumatic Brain Injury Cohort

3.1 Overview

Chapter 2, highlighted a specific limitation of existing work into understanding the morphometry of the brain post pTBI, namely the effect that frank parenchymal lesions may have on processing pipelines. Given this, the current chapter further investigates how these may affect a standard, surface-based anatomical parcellation algorithm which is commonly used in the field of neuroimaging. The introduction of TBI lesions into pipelines commonly used to assess MRI-derived brain morphometry results in biased results. A version of the work presented in this chapter has been submitted for publication as follows;

King, D. J., Novak, J., Shephard, A. J., Beare, R., Anderson, V. A. & Wood, A. G. (Submitted).

Lesion induced error on automated measures of brain volume: Data from a paediatric traumatic brain injury cohort. *Frontiers in Neuroscience*.

DJK and AW contributed to the conception and design of the current study. VA contributed and collected data. JN contributed lesion masks whilst DJK and AS conceptualized the process of simulating lesions. DJK performed the processing of MRI data. DJK and RB conceptualized the statistical analysis. DJK performed the statistical analysis and wrote the first draft of the manuscript. All authors contributed to manuscript revision.

3.2 Introduction

Automated analysis to derive quantitative measures of brain structure offers significant benefit to large scale research endeavours that have clinical translation potential. In addition to reducing the time burden and potential error induced by manual methods (Bigler et al., 2010), quantitative approaches may be more sensitive to subtle but clinically relevant imaging biomarkers that are not apparent on routine visual reporting. Accordingly, successful use of these techniques has been demonstrated in disorders with relatively subtle global or regional changes (e.g., dementia of the Alzheimer's type (Frisoni, Fox, Jack, Scheltens, & Thompson, 2010)). Recent traumatic brain injury (TBI) research has utilised segmentation and analysis of T1-weighted (T1w) structural magnetic resonance images (MRI) to quantify these post-injury morphometric changes (Dennis, Faskowitz, et al. (2017); Ryan et al. (2017); Urban et al. (2017), see King et al. (2019) for a review). The accuracy of these methods in the context of gross lesions/pathology, however, may be reduced by errors introduced during the processing of such MRI. This then makes it difficult to ascertain whether differences between control and patient morphology are due to an injury-related pathology or due to systematic error which is specific to the patient cases with gross lesions (King et al., 2019).

The MRI features of TBI are heterogeneous due to injury mechanisms such as white matter deformation and shear, Wallerian degeneration, compromised vasculature, hemosiderin deposits and encephalomalacia (Bigler et al., 2013; Bigler & Wilde, 2010; Bigler et al., 2016), presenting as abnormal signal within the image, hereto referred to as ‘lesions’. The current study investigated these lesions in a cohort of paediatric TBI patients. In these TBI cases, these lesions occur within the context of a still-developing brain (Wilde, Hunter, et al., 2012), and accurate quantification of brain-morphology will allow us to assess the effects of these insults on the developmental trajectory of the brain.

In terms of prevalence, in a retrospective accidental paediatric TBI (pTBI) cohort (n=68), MRI within 2 weeks detected intraparenchymal lesions on ~29% of cases (Buttram et al., 2015). In a study of 36 patients, lesions were detected on MRI (T1w, T2w or FLAIR) for ~56% of cases (n=20, Beauchamp, Ditchfield, Babl, et al. (2011)). However, this is likely an inflated prevalence as Beauchamp et al. (2011) specifically included only those patients who explicitly had been clinically referred for CT.

These lesions are as unique between individuals as the precipitating injury, with no two individuals sharing the same biomechanics of injury, genetic context or experience-dependent plasticity (Saatman et al., 2008). This means that presentation of lesions on MR imaging is highly variable between-individuals, but also within-cases. The pattern of pathology varies across time post-injury: for example, white-matter shear is more common acutely, whilst Wallerian degeneration is a late manifestation of injury. Even for a given individual, lesion presentation on MRI is highly dependent on factors such as MR sequence and time post-injury (Bigler, 2007b; Bigler et al., 2013; Bigler & Maxwell, 2011). This heterogeneity means that lesion characterization presents a major challenge for neuroimaging software and analysis.

There are multiple potential sources of error in neuroimaging pipelines due to the presence of lesions. For instance, frank parenchymal lesions such as those seen in TBI are likely to distort the MR signal, causing abnormal voxel intensities (due to pathology such as gliosis and oedema), resulting in specific errors such as surface reconstruction errors which rely on intensity gradients for processing (Goh et al., 2014; Irimia, Wang, et al., 2012; Merkley et al., 2008). Poor registration is also seen in the presence of TBI lesions, resulting in modifying of voxel-mappings to the atlas space and thus inaccurate estimation of structural TBI volumetrics (Goh et al., 2014; Irimia, Wang, et al., 2012). Many of the automated approaches to segmentation are therefore likely to show lesion-induced error when used to process clinical populations where the pathology presents as lesions on MRI. Regardless of their exact origin within the processing pipeline, the effect of these errors is the potential to obscure or falsely identify findings of pathology-mediated changes to the morphology of the brain. For example, the focal white matter (WM) lesions seen in multiple sclerosis have been shown to bias measures derived from *SPM* (Penny, Friston, Ashburner, Kiebel, & Nichols, 2011), *FIRST* (Patenaude, Smith, Kennedy, & Jenkinson, 2011), *Freesurfer* (Fischl,

2012) and multiresolution segmentation methods (Chard, Jackson, Miller, & Wheeler-Kingshott, 2010; Gonzalez-Villa et al., 2017).

Freesurfer (Fischl, 2012) is a tool for the semi-automated segmentation of T1w structural MRI to estimate the morphometry of the brain. Documentation does not discuss how to approach surface-based segmentation of lesioned images, but does emphasize that the tool should not be used for clinical purposes. To date, little work has investigated *Freesurfer* performance in the presence of pathology-related MRI abnormalities. Despite these limitations, it has been used in several pTBI studies (e.g. Drikkoningen et al. (2017); Mayer et al. (2015); Ryan et al. (2017); Wilde, Merkley, et al. (2012); Wu et al. (2018)). The majority of the pTBI studies listed here report little detail on the implementation of *Freesurfer* in the presence of TBI-lesions, beyond the fact that manual-editing was performed. This paucity of detail, especially in the specific decisions in how manual editing was performed, restricts the ability to replicate study findings, and assess the effect lesions may have on the *Freesurfer* pipeline.

Despite a lack of research into methodologies to approach automated segmentation in the presence of lesions, previous studies investigating brain morphometry in pTBI have reported and adopted strategies to deal with the effect of lesions on their analyses. One utilised approach is to exclude cases with focal lesions from analyses (Serra-Grabulosa et al., 2005), however this both reduces statistical power (through reduced sample size) and limits clinical applicability and generalizability of findings to the full spectrum of injuries. Other studies have used post-hoc procedures to ‘correct’ for the effect of lesions on their analyses by replicating analyses with/without patients presenting with focal lesions in the region of interest (ROI) being tested (Spanos et al., 2007), or excluding ROIs where the presence of a lesion caused errors to the *Freesurfer* parcellation (Drikkoningen et al., 2017). These post-hoc methods rely on the assumption that the lesion-induced error is focal, however, it is important to consider whether this algorithmic error could be distributed more globally across the brain, causing error in regions not edited by these correction approaches.

We aimed to identify and quantify this potential global lesion-induced error by investigating morphometry in both the lesion and contralesion hemispheres. This was to disentangle the volumetric differences due to injury and those due to the algorithmic error within the surface-based output of *Freesurfer*, likely induced by the erroneous signal within the lesion (Chard et al., 2010). To achieve our aim, we ‘simulated’ TBI-lesions in a healthy paediatric cohort. Simulated lesions facilitate measurement of the effect of image processing in the presence of a lesion as compared to the ‘ground truth’, non-lesioned counterpart of the image. This is necessary in order to disentangle both the morphological changes due to algorithmic error and potentially ‘real’, globally-distributed pathological effects of injury.

We predicted that the presence of lesions would result in an error in morphometric measurement by *Freesurfer*, beyond that of the spatial extent of the lesion. We had three explicit hypotheses:

1. that for cases where we have simulated a lesion there will be a difference in measured volume from ground truth in both the lesion and the contralesion hemisphere,
2. that the magnitude of this difference will be greater in the lesion hemisphere than the contralesion hemisphere,
3. that this lesion-induced error (both in the lesion and contralesion hemisphere) will vary as a function of lesion characteristics (hypotheses a and b were defined a priori, whereas c was exploratory in nature).

3.3 Methods

3.3.1 Participants

The data used in the current study represent a subset of an existing dataset of paediatric TBI. This dataset contains a total of 157 children (patients $n=114$) who were recruited between 2007 and 2010 into a study on ‘Prevention and Treatment of Social Problems Following TBI in Children and Adolescents’. Further details of the study including details of the recruitment strategy have recently been published elsewhere (Anderson et al., 2013; Anderson et al., 2017; Catroppa et al., 2017). In brief, children with TBI were recruited on presentation to hospital at The Royal Childrens’ Hospital, Melbourne (RCHM), Australia. Children were eligible for the study if on presentation they: *i*) were aged between five and 16 years at the time of injury, *ii*) had recorded evidence of both a closed-head injury and at least two post-concussive symptoms (such as headaches, dizziness, nausea, irritability, poor concentration), *iii*) had sufficient detail within medical records (Glasgow Coma Scale (GCS; Teasdale and Jennett (1974)), neurological and radiological findings) with which to determine the severity of the injury, *iv*) had no prior history of neurological or neurodevelopmental disorder, non-accidental injuries or previous TBI, and *v*) were English speaking. TD controls were required to meet criteria *i*), *iv*) and *v*). MRI scans were acquired in the acute post-injury period for patients (for details, refer to Table 3.1). A favourable ethical opinion was granted from Aston University as a site for secondary analysis of neuroimaging data.

Control cases were selected from the overall dataset based on four criteria, to ensure that the control data used was of high quality: *i*) MRI data available, *ii*) no manual-editing of surfaces required after *Freesurfer* recon-all pipeline completed, *iii*) no MR-artefacts, and *iv*) no “failed” ratings (a ‘bad’ rating on any of ‘image sharpness’, ‘ringing’, ‘subcortical SNR’ or ‘GM + WM SNR’ scales) on a qualitative rating scale of T1w images (Backhausen et al. (2016); performed by DJK). Eleven (out of 36) control cases met this criteria for inclusion. Demographics of this group can be seen in Table 3.1.

Table 3.1. *Demographic variables for Control cases*

Control Case	Sex	Age at MRI (yrs)
1	Female	7.21
2	Male	10.73
3	Male	10.54
4	Male	6.82
5	Male	7.87
6	Female	8.38
7	Male	6.85
8	Female	14.62
9	Male	8.85
10	Female	11.88
11	Female	13.14

Patients were all investigated for visible lesions on T1w images, blind to severity ratings. Nineteen patient cases were identified as presenting with lesions which could be identified on these T1w images. However, three patients were excluded from this selection. The first was excluded due to the presence of bilateral lesions which therefore precludes comparison between the lesion and contralesion hemispheres. The second exclusion was due to the resolution of the T1w image being significantly different from the other images (0.8mm Isotropic). The final exclusion was due to the lesion being an incidental finding, rather than due to the TBI. Demographics of the lesion cases can be seen in Table 3.2. The included lesions were visualised as binary masks in MNI space in Figure 3.1. Lesion volumes (mm^3) were calculated as a count of the number of non-zero voxels in the associated lesion mask multiplied by the voxel size. This was calculated in native space of the lesion patient space (reported in Table 3.2) and once transformed into control space as a simulated lesion (see below).

Table 3.2. *Demographic variables for Lesion cases*

Study Case No.	Sex	Age at Injury (yrs)	Age at MRI (yrs)	Injury-MRI Interval (days)	Injury Severity	Cause of Injury	of Lesion Hemisphere	Lesion Volume (mm ³)
1	Male	5.75	5.88	35	Moderate	MVA	lh	25.00
2	Female	12.5	12.64	40	Moderate	MVA	lh	1030.00
3	Female	12.5	12.61	19	Moderate	MVA	rh	3063.75
4	Male	10.75	10.86	35	Moderate	MVA	lh	505.75
5	Male	6.5	6.53	7	Moderate	MVA	lh	12,081.50
6	Male	8.42	8.61	42	Mild-Complex	Fall	lh	60.25
7	Male	11	11.15	29	Mild-Complex	Fall	rh	63.00
8	Female	5.92	6.09	57	Severe	Fall	rh	35.00
9	Female	7.83	7.95	32	Mild-Complex	Fall	rh	2059.25
10	Male	10.92	11.13	71	Moderate	Fall	rh	8815.00
11	Male	10.5	10.68	38	Moderate	MVA	lh	83.50
12	Male	8.5	8.67	35	Severe	Fall	rh	3858.50
13	Female	13.67	13.75	20	Moderate	Fall	rh	391.50
14	Female	9.33	9.44	36	Moderate	Fall	lh	15.00
15	Female	12.33	12.51	43	Moderate	Fall	rh	37.50
16	Female	10.58	10.77	63	Moderate	MVA	rh	407.00

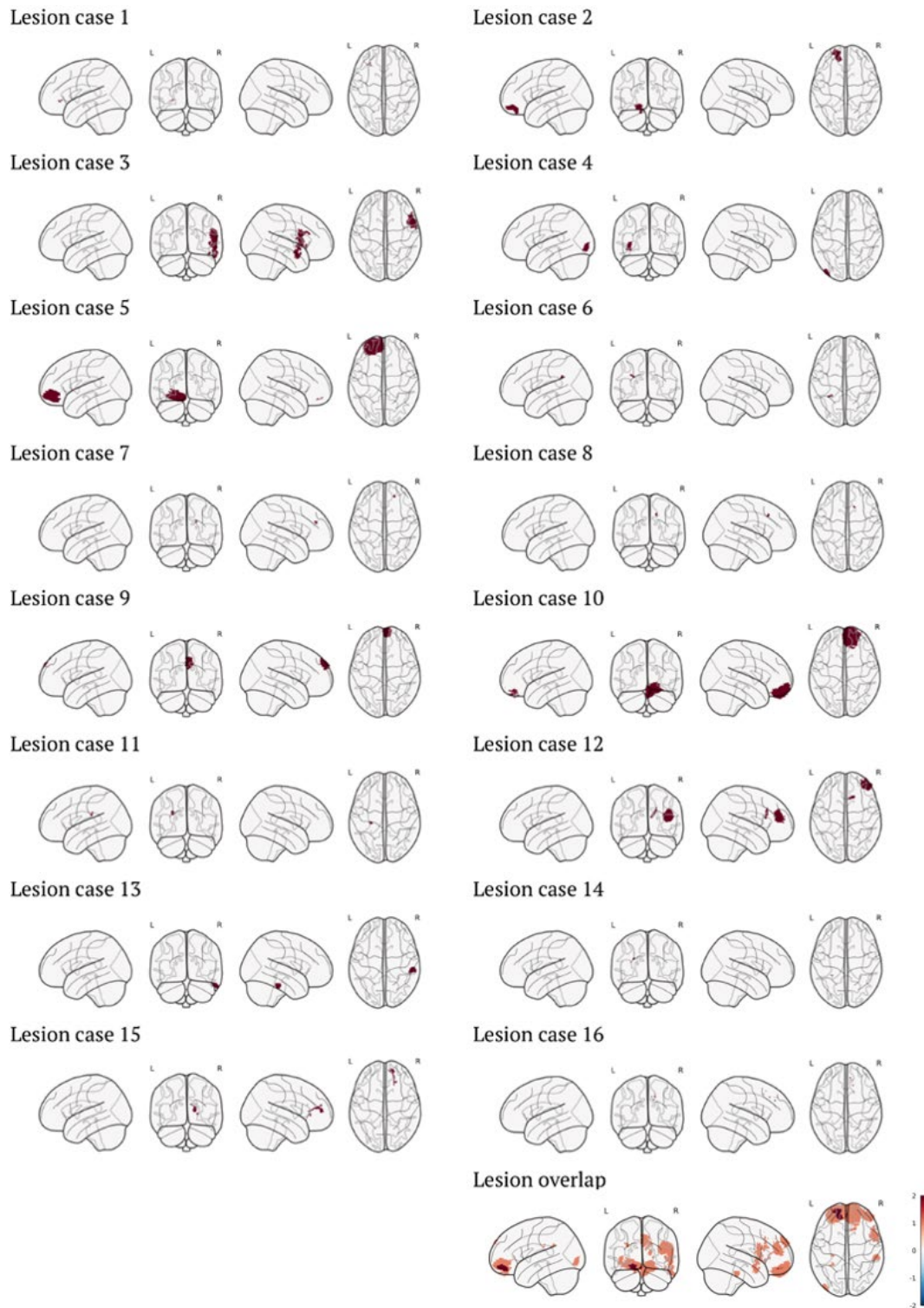


Figure 3.1 *Visualisation of individual lesion masks in MNI space, as well as overlap of all lesions used in the cohort (colourbar represents number of cases). Visualisation generated with code from Whitaker, Notter, and Morgan (2017).*

3.3.2 MRI Acquisition

MRI were acquired for the patient group acutely after injury (<90 days post-injury). MRI images were acquired at 3T as a part of an existing research protocol on a Siemens Trio scanner (Siemens Medical Systems, Erlangen, Germany) using a 32-channel matrix head coil. The acquisition sequence consisted of a sagittal three-dimensional (3D) MPRAGE [TR = 1900 ms; TE = 2.15 ms; IR prep = 900 ms; parallel imaging factor (GRAPPA) 2; flip angle 9 degrees; BW 200 Hz/Px; 176 slices; resolution $1 \times .5 \times .5$ mm], sagittal 3D T₂-w non-selective inversion preparation SPACE (Sampling Perfection with Application-optimised Contrast using different flip-angle Evolution) [TR = 6000 ms; TE = 405 ms; inversion time (TI) = 2100 ms; water excitation; GRAPPA Pat2; 176 slices; $1 \times .5 \times .5$ mm resolution matched in alignment to the 3D T1-weighted sequence].

3.3.3 Simulated Lesions

All MRI processing was conducted on a Linux system (UBUNTU 16.04.4 LTS). The lesions described above were initially segmented manually (by JN) using the *MRTrix (version 3.0)* software package (Tournier, Calamante, & Connelly, 2012), producing a binary lesion mask for each patient. Lesions were identified in our dataset by a single rater and masks drawn where visible lesions could be identified by eye on the T1w image, using FLAIR MRI to support lesion identification.

The approach in the current paper was similar to that proposed by Brett et al. (2001), and Gonzalez-Villa et al. (2017) using lesions from pTBI cases recruited on admission to an emergency department. The use of actual lesions provides distinct benefits over computer generated lesions, specifically reflecting the complexity of actual lesions, retaining natural characteristics such as texture and size (Seghier, Ramlackhansingh, Crinion, Leff, & Price, 2008). The full methodology is outlined in the supplementary materials (Appendix B). The resultant simulated dataset contained $n = 176$ cases, where every included lesion ($n = 16$) had been applied to every control image ($n = 11$) in all possible pairwise permutations. From here on, the control images with the simulated lesions applied will be referred to as the simulated lesion (*Sim_{lesion}*) cases ($n = 176$) and the control images without editing will be referred to as “ground truth” (*GT*) cases ($n = 11$). Examples of these lesion images and simulated cases can be seen in Figure 3.2.

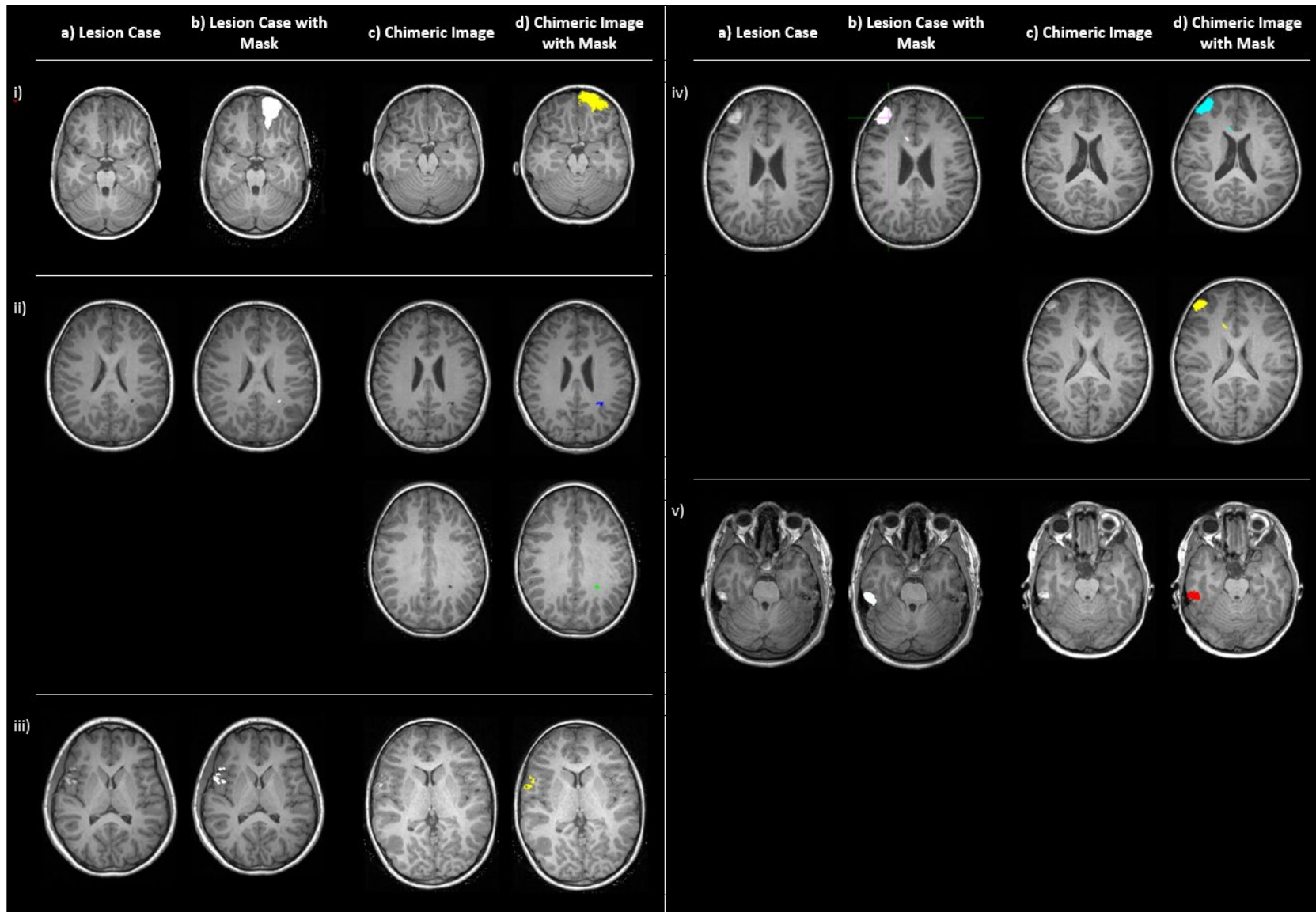


Figure 3.2. Examples of original lesion cases (i-v), with (a) and without (b) lesion masks and example chimeric images, the simulated cases where the corresponding lesion has been applied to a control subject (in native space) with the outlined methodology. Cases ii) and iv) show two example chimeric images to demonstrate that (in native space) simulated lesions show both morphological and spatial variation.

3.3.4 Automated structural segmentation using *Freesurfer*

Both the Sim_{lesion} and the GT cases were processed using the standard *Freesurfer* recon-all pipeline, which has good replicability and has been histologically validated (Han et al., 2006; Rosas et al., 2002). Explanations of the *Freesurfer* pipeline for 3D tissue segmentation and measurement of morphometry are given elsewhere (Fischl, 2012; Fischl et al., 2004). No manual editing was performed on either the simulated-lesion or control cases once segmented using *Freesurfer* in order to prevent any potential bias towards manual delineation (Perlaki et al., 2017).

Raw data was extracted using *Freesurfer* for both the Sim_{lesion} and GT cases pertaining to two volumetric measures; a) Cortex volume (left (lh) and right (rh) hemisphere) and b) Cerebral white matter (cWM) volume (lh and rh).

In light of the results of the primary analyses we were interested in whether the error in both the lesion and contralesion hemisphere ($hemi_{lesion}$ and $hemi_{contra}$ respectively) were related to the other characteristics of the simulated lesion. We were particularly interested in lesion size, mean intensity and SD of intensity values within the lesion. Due to the non-quantitative nature of T1w MR intensity values, the Sim_{lesion} cases were moved into a unit-variance space. Both mean intensity and SD of intensity values was calculated for the voxels within the brain mask, but whilst masking lesioned voxels. These values were used to demean and rescale the voxels within the brain mask (including the lesion) by subtracting the mean from all voxel intensities and then dividing by the SD. This image in unit-variance space was then used to calculate the mean and SD of intensity values within the lesion ROI.

3.3.5 Statistical Analysis

For each lesion applied to the control cases to generate the Sim_{lesion} cases, lesions masks were used to define whether lesions were located in the lh , rh or bilaterally. Using this information, and knowing which lesion is applied to each of the Sim_{lesion} cases, the raw volumetric measures for each case were recoded as the lesion hemisphere ($hemi_{lesion}$) and the contralesion hemisphere ($hemi_{contra}$). This is the case for all metrics calculated for the study. This allowed us to see if any lesion induced error is present in the hemisphere where no volumetric differences should occur in comparison to GT , as no image manipulation has occurred in the $hemi_{contra}$. For each Sim_{lesion} case, the appropriate referent GT case was matched and also recoded to maintain the mapping from lh/rh to $hemi_{lesion}/hemi_{contra}$. Thus, each repeated measure ‘datapoint’ contained a measure of both cortex and cWM volume for; *i*) $hemi_{lesion}$ in the Sim_{lesion} case, *ii*) $hemi_{contra}$ in the Sim_{lesion} case, *iii*) $hemi_{lesion}$ in the referent GT case and *iv*) $hemi_{contra}$ in the referent GT case.

All statistical analyses were conducted in R (R Core Team, 2016) using ‘lme4: Linear Mixed-Effects Models using ‘Eigen’ and S4’ (lme4 (Version 1.1); Bates, Machler, Bolker, and Walker (2015)). All analyses utilise linear mixed effect models (using the ‘lmer’ function and restricted maximum likelihood

(REML) estimation) to account for the crossed random effects of both the control MRI and lesion used to construct the Sim_{lesion} cases (lesion used was coded as 0 for the GT cases where no lesion was applied). The random effects of lesion and control MRI used were defined as crossed, rather than nested.

To test hypothesis a), cortex and cWM volumes were modelled as a function of the fixed effect of case (Sim_{lesion} vs GT cases) and the random effects of lesion and control MRI used to construct the Sim_{lesion} case. As per Barr et al.'s (2013) recommendations for best practices in mixed effect modelling, a maximal model was defined. Barr et al. suggest that random slopes are required for within-unit effects, but random intercepts are sufficient for between-unit effects. Therefore, random slopes were estimated for case across participant but not lesion or control. This model was tested for both the $hemi_{lesion}$ and $hemi_{contra}$, using the *lmer* 'subset' argument. When investigating the individual hemispheres, this decreased the number of observations per participant for the random effect of case across participants, and thus a random slope was no longer appropriate. Therefore, only a random intercept was used in the subset analyses.

As the second hypothesis pertains to the magnitude of differences, the outcome variable was switched to percent volume difference (PVD) between the Sim_{lesion} and GT cases. Percentage volume difference for $hemi_{lesion}$ and $hemi_{contra}$ between Sim_{lesion} and GT measurements was also calculated as:

$$PVD = 100 \times \frac{|V(Sim) - V(GT)|}{\frac{V(Sim) + V(GT)}{2}}$$

where V is the volume (calculated for both cortex and cWM volumes), with a greater PVD value representing greater volume differences between the Sim_{lesion} and GT cases (Perlaki et al., 2017). This is used for two reasons. Firstly, it is a well-accepted approach to segmentation comparison (Fischl et al., 2002) and is used in multiple existing studies of segmentation errors/biases (Amann et al., 2015; Katuwal et al., 2016; Morey et al., 2009; Perlaki et al., 2017). Secondly, it allows us to recode what would be a 2 x 2 interaction (Sim_{lesion}/GT x $hemi_{lesion}/hemi_{contra}$) when using raw volumes as a single factor (PVD of $hemi_{lesion}/hemi_{contra}$), meaning that the statistical results reported here are more interpretable. The 20% trimmed means (\bar{X}_t) and median values for PVD are also reported.

The mixed model was defined similarly to hypothesis a), but the fixed effect of hemisphere ($hemi_{lesion}$ and $hemi_{contra}$) was included rather than case. No random slope of hemisphere across participants was included as there were not sufficient observations per participant to warrant/enable this. Therefore, the maximal model in this case included only random intercepts.

As the random effect of control image and lesion significantly improved model fit for both hypothesis a) and b), we therefore conducted a final, exploratory analyses to investigate how specific characteristics of the lesion, such as lesion size and intensity (in native space), explain variance in PVD for both the $hemi_{lesion}$ and $hemi_{contra}$. This was done using a linear mixed model as per hypothesis a) and b), however

the random effect of lesion used was not included, as this variance should be explained by the fixed effects of the lesion characteristics added to the model. The outcome variable was PVD and fixed effects were: lesion size, mean lesion intensity and the SD of lesion intensity, whilst the only random effect was that of control image used to generate the *Sim_{lesion}* case. This model was estimated in the *hemi_{lesion}* and *hemi_{contra}* separately, using the *lmer* subset function. Therefore, the random effect of participant was not included as these models no longer represented repeated measures.

For all hypotheses, the mixed model (estimated with maximum likelihood rather than REML to facilitate model comparison) was compared to a linear model including only the fixed effects but none of the random effects to assess whether the random effects were warranted and significantly improved model explanation. All model comparisons were conducted using a Likelihood ratio test to assess whether the reduction in residual sum of squares was significant. To test the significance of fixed effects in relation to all hypotheses, *p*-values were estimated using the normal distribution of *t*-statistics. All results are presented using the ‘*ggplot2*’ (Wickham, 2009) and ‘*ggpubr*’ (Kassambara, 2018) packages.

3.4 Results

All models, including parameter estimates for all effects and associated *lmer* syntax, are described in supplementary materials (Appendix B). For hypothesis a) both cortex and cWM volume were predicted by the fixed effect of case (*Sim_{lesion}* and *GT*). When adding random effects, for cWM volume, the maximal model failed to converge and thus, as per Barr et al.’s (2013) recommendations, the random correlations between random slope and random intercept were removed from the model, as this performed similarly to the maximal model in simulations (Barr et al., 2013). The addition of the random effects to the model significantly improved model fit for both cortex and cWM volume ($\chi^2(5) = 2894.47$, $p < .0001$; $\chi^2(6) = 4025.22$, $p < .0001$), and thus the inclusion of random effects in the model was warranted.

For cortex volume, across both hemispheres, the fixed effect of case was non-significant ($B = -942.61$, $\text{std.Error} = 531.83$, $t = -1.77$, $p = .076$). When considered separately, surprisingly, the fixed effect of case was non-significant in the *hemi_{lesion}* ($B = -1324.46$, $\text{std.Error} = 1155.34$, $t = -1.15$, $p = .25$), but significant in the *hemi_{contra}* ($B = -560.76$, $\text{std.Error} = 136.47$, $t = -4.11$, $p < .0001$). In both hemispheres, the parameter estimates were negative for the simulated lesion case, suggesting that the cortex volume was lower when a lesion was simulated. The significant difference found in the *hemi_{contra}* was smaller than the non-significant difference in the *hemi_{lesion}*. For cWM volume, the effect of case was non-significant across hemispheres ($B = -161.75$, $\text{std.Error} = 261.88$, $t = -0.62$, $p = .54$), and within the individual *hemi_{lesion}* and *hemi_{contra}* respectively ($B = -308.84$, $\text{std.Error} = 619.14$, $t = -0.50$, $p = .62$; $B = -14.66$, $\text{std.Error} = 101.00$, $t = -0.15$, $p = .88$). See Figure 3.3 for plots of these effects.

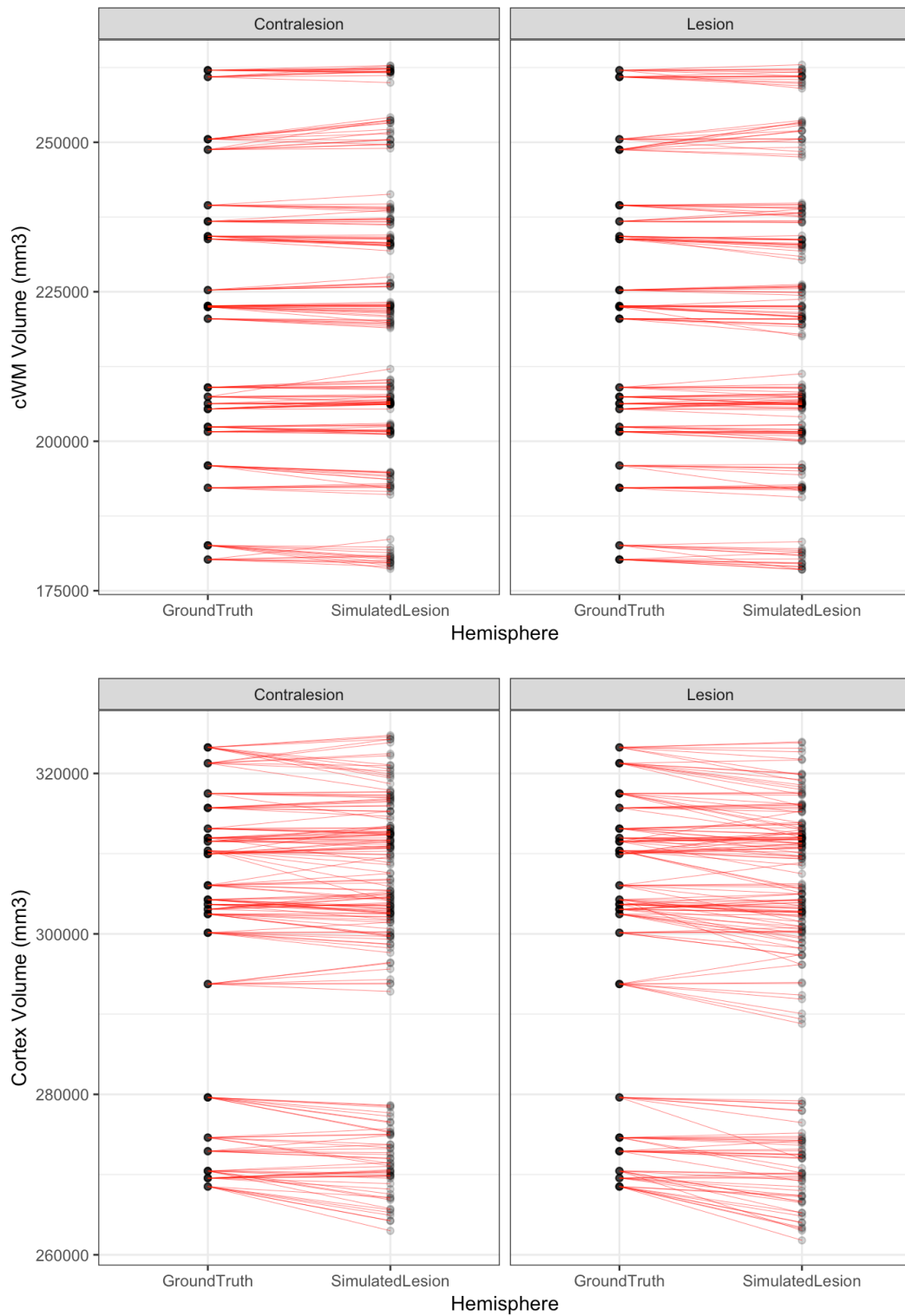


Figure 3.3. Plots of differences in cortex (top) and cWM volume (bottom) between Sim_{lesion} and GT cases across hemispheres.

As the second hypothesis pertains to the magnitude of differences, the outcome variable was switched to percent volume difference (PVD) between the *Sim_{lesion}* and *GT* cases. For cortex volume, PVD was slightly higher in the *hemi_{lesion}* ($\overline{X}_t = 0.47\%$, *median* = 0.39%) than the *hemi_{contra}* ($\overline{X}_t = 0.37\%$, *median* = 0.39%), but overall, the volume difference was minimal between *Sim_{lesion}* and *GT* cases. Only 44 cases showed PVD greater than 1% in the *hemi_{lesion}* and 27 in the *hemi_{contra}*, with maximum PVD being 2.78% and 2.07% respectively. For cWM volume, PVD were similar between the *hemi_{lesion}* ($\overline{X}_t = 0.34\%$, *median* = 0.31%) and *hemi_{contra}* ($\overline{X}_t = 0.34\%$, *median* = 0.33%).

For hypothesis b) the baseline model (including no random effects) was defined similarly as per hypothesis a). No random slope of hemisphere across participants was utilised as there were not sufficient observations per participant to warrant/enable this. Therefore, the maximal model in this case included only random intercepts and represents a significant improvement over a model with just the fixed effect of hemisphere (cortex volume: $\chi^2(3) = 62.19$, $p < .0001$; cWM volume: $\chi^2(3) = 53.71$, $p < .0001$). Due to the varying scales across the fixed effect variables, these were converted to z-scores (centred and scaled) to facilitate model convergence.

For PVD of cortex volume, the fixed effect of hemisphere was significant ($B = .140$, *std.Error* = .047, $t = 2.96$, $p = .003$), with parameter estimates suggesting that the *hemi_{contra}* had a smaller PVD. However, the effect of hemisphere on cWM PVD was non-significant ($B = -.007$, *std.Error* = .039, $t = -.18$, $p = .86$). This can be seen in Figure 3.4 below. For PVD of both cortex volume and cerebral white matter volume, the random effect of control and lesion used significantly improved model fit. This suggested that there was some variance significantly attributable to the specific lesion used to generate the simulated lesion MRI, as can be seen in Figure 3.5 below.

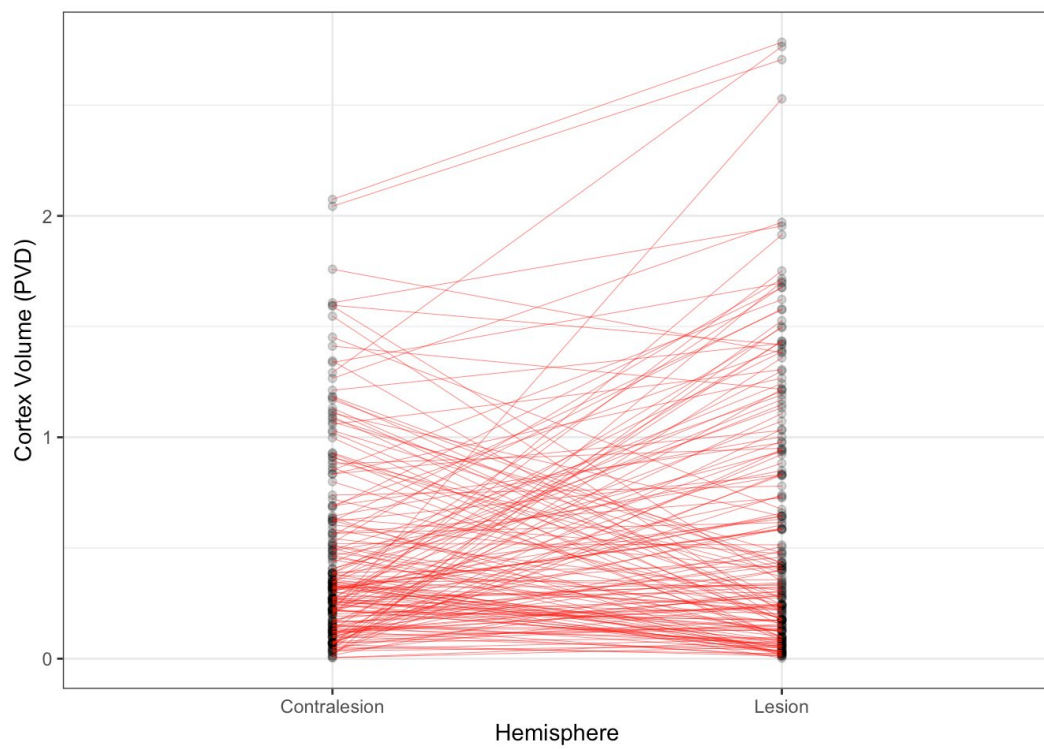
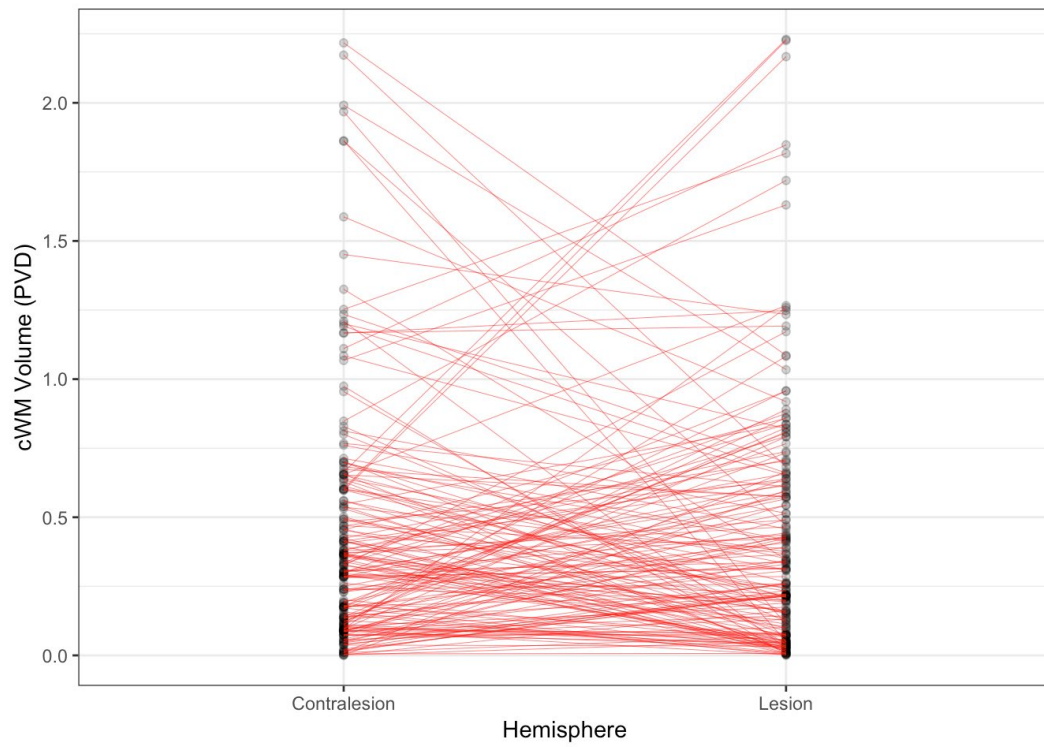


Figure 3.4. Plots of PVD for both cortex (top) and cWM volume (bottom) across hemispheres for each individual subject.

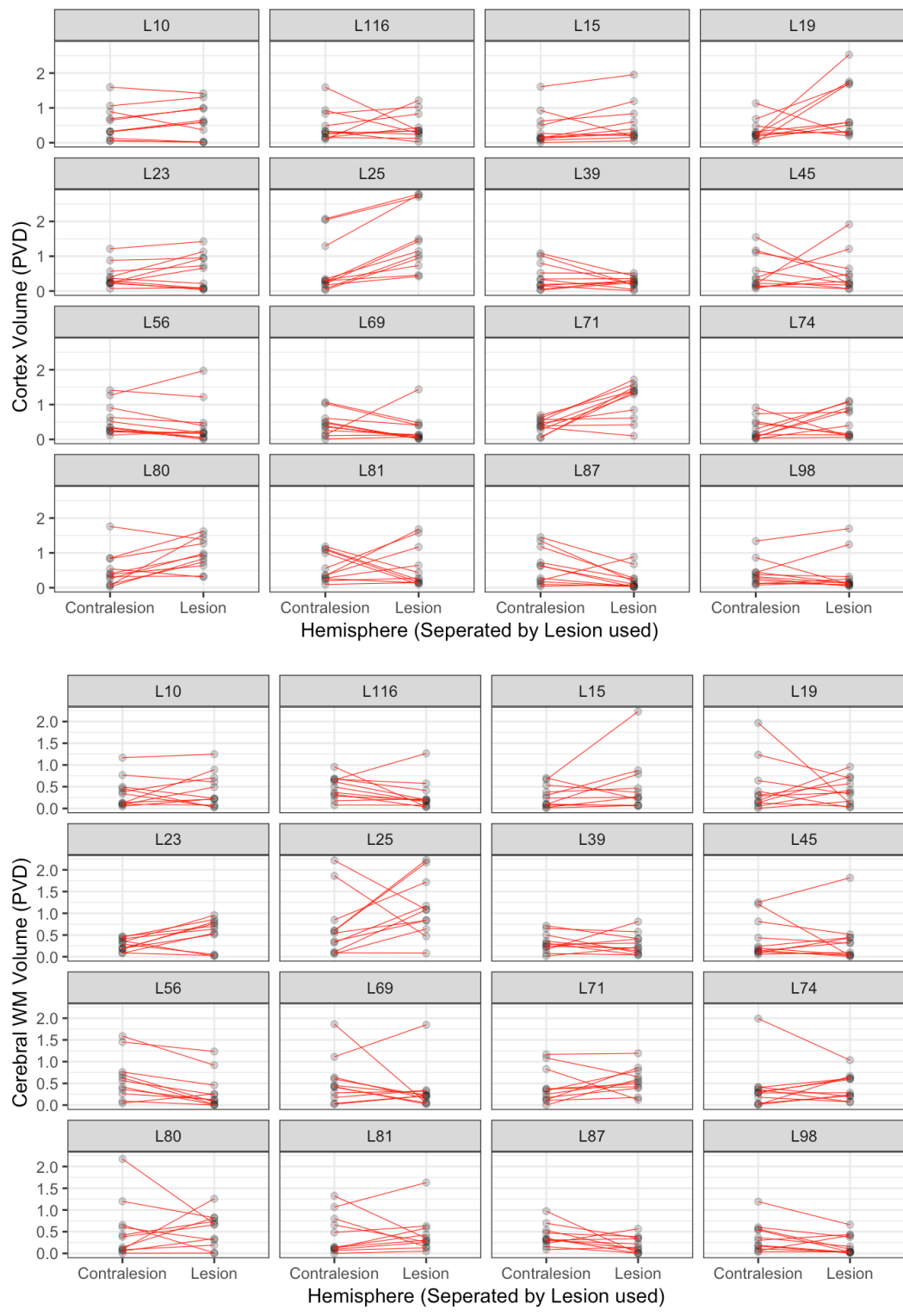


Figure 3.5. Plots of subject-level PVD for both cortex (top) and cWM volume (bottom) across hemispheres plotted by lesion used.

Therefore, an exploratory analysis investigated the effects of certain lesion characteristics on PVD. For cortex volume, in the $\text{hemi}_{\text{lesion}}$, the fixed effects of lesion volume and SD of lesion intensity were significant ($B = .28$, $\text{std.Error} = .038$, $t = 7.35$, $p < .0001$; $B = -.23$, $\text{std.Error} = .088$, $t = -2.60$, $p = .0094$ respectively). However in the $\text{hemi}_{\text{contra}}$, only the fixed effect of SD of lesion intensity was marginally significant ($B = -.16$, $\text{std.Error} = .080$, $t = -2.02$, $p = .044$). For cWM, the only significant fixed effect found was the effect of volume on PVD of cWM in the $\text{hemi}_{\text{lesion}}$ ($B = .15$, $\text{std.Error} = .030$, $t = 5.08$, $p < .0001$).

3.5 Discussion

Frank parenchymal lesions as a result of pTBI pathology result in surface reconstruction errors due to abnormal MRI features, such as distortions to the voxel-intensity (Goh et al., 2014; Irimia, Wang, et al., 2012; Merkley et al., 2008). The current study investigated the accuracy of surface-based, morphometric measurement from T_1 -w images containing TBI-lesions, using a paediatric cohort of simulated lesions and their base control images as a referent. Specifically, we examined whether the lesion-induced error within the *Freesurfer* pipeline was globally distributed by assessing this error in both the lesion and contralesion hemispheres of the brain.

Statistically significant differences were only found for cortex volume between $\text{Sim}_{\text{lesion}}$ and GT cases within the $\text{hemi}_{\text{contra}}$, with the simulated lesions cases having reduced volume. This suggests a significant measurement error introduced to the cortex volume measurement by the lesion, distal to the location of the pathology itself. Surprisingly, no significant differences were found in the $\text{hemi}_{\text{lesion}}$ for either cortex or cWM volume suggesting that the estimated volumes did not differ when a lesion was simulated. However, this is likely due to the large variance in the effect seen across participants, as shown by the large standard error of the parameter estimates for case in these models. Overall, these findings suggest that there is not a reliable lesion-induced error in the $\text{hemi}_{\text{lesion}}$ as we had predicted, however this may vary from case to case. It is important to consider that, within the $\text{hemi}_{\text{lesion}}$, differences from ground truth segmentations can be thought of as being due to both algorithmic error and ‘actual’ changes: for instance where lesioned tissue is successfully no longer included in the cortical ribbon. However, in the $\text{hemi}_{\text{contra}}$, there has been no image manipulation of the MRI, and thus these reliable, significant differences from the ground truth image are attributable to the lesion-induced error.

Despite the lack of significant differences for cWM volume, descriptive statistics of PVD values, as a measure of deviation of the $\text{Sim}_{\text{lesion}}$ from GT cases, did suggest that in fact there is deviation, albeit relatively minimal, from the ground truth volumes seen in the cases where a lesion had been simulated. This is seemingly present in both the lesion and contralesion hemispheres and for both cortex volume and cWM. This is in line with our hypothesis of a globally distributed lesion-induced error. However, when comparing PVD between hemispheres to compare the magnitude of these differences, only significant results were found for cortex volume, suggesting that the PVD was greater in the lesion

hemisphere. In terms of the magnitude of differences, we found a maximal PVD from ground truth in the hemispheric cortex and cWM volume of around 2.07-2.78% respectively. Whilst this represents the extreme cases (\overline{X}_t and median values were in the order of around 0.5%), this maximal magnitude of difference is comparable to that seen for the error induced by minor motion in adult MRI (Reuter et al., 2015).

Overall, the pattern of results we report suggest that, whilst the lesion produces large magnitudes of PVD across subjects (PVD was significantly larger in the lesion hemisphere), this is not consistent across subjects (non-significant differences in cortex volume for the lesion hemisphere between Sim_{lesion} and GT) whilst in the contralesion hemisphere, the magnitude of PVD is smaller but is seen consistently across subjects (significant differences in cortex volume for the contralesion hemisphere between Sim_{lesion} and GT). This holds true for cortex, but not cWM volume.

We also investigated how MR characteristics of the lesion explained variance in the PVD of our morphometric measures in both the $hemi_{lesion}$ and $hemi_{contra}$. We found that cortex and cWM PVD variance was significantly explained by lesion volume in the $hemi_{lesion}$, and this was expected as a large lesion will deform the surface to a greater extent, causing greater differences in morphometric measurements. However, more interestingly, we found that in both the $hemi_{lesion}$ and $hemi_{contra}$, there was a significant effect of SD of voxel intensities within the lesion on cortex PVD. Specifically, there was a greater difference in cortex volume for lesions with a lower SD of voxel intensities.

One plausible mechanism by which this may be the case is that, where the SD of voxels intensities is high within the lesion, the number of any given ‘outlier’ intensities is low and thus doesn’t exceed the noise in the dispersion of voxel intensities across the entire T1w image. However when the SD is low, there is a higher concentration of potentially ‘outlier’ intensities (especially in lesions of greater volume), and thus these intensities within the lesion may be enough to affect and bias any of *Freesurfer*’s operations which rely on the dispersion of voxel intensities across the image. One example of this may be in the intensity normalisation step. Therefore, it is not necessarily the heterogenous-appearing lesions that would induce the greatest lesion-induced error in both the affected ($hemi_{lesion}$) and unaffected ($hemi_{contra}$) hemispheres, but in fact those lesions which are more homogenous in intensity. However, given the exploratory nature of these correlations, it will be important to perform confirmatory tests on these within an independent pTBI dataset.

Given that *Freesurfer* processes the two hemispheres separately for a vast proportion of its later pipeline (especially in processing cortical thickness measures), the fact that we see these lesion induced errors in the hemisphere where there has been no image manipulation of the MRI, suggests that the bias due to lesion-induced error is early in the pipeline. This is in keeping with our findings that the SD of voxel intensities within the lesion effects cortex PVD in both hemispheres, as it is in these early pipeline stages

that multiple intensity normalisation and correction steps (including an Non-parametric Non-uniform intensity Normalization (N3) correction (Sled, Zijdenbos, & Evans, 1998)).

The global lesion-induced error was detected in the current study using very coarse measures of brain volume, looking at the entire volume of each hemisphere. It may in fact be the case that our estimates of the ‘error’ are conservative overall, and individual ROIs in the $\text{hemi}_{\text{contra}}$ may experience greater error, in differing directions of over- and under- estimations. The current investigation precluded ROI analysis of the lesion-induced error across hemispheres due to the fact that the $\text{hemi}_{\text{lesion}}$ varies between left and right hemispheres for differing lesions. Thus, because many atlases, including those used by *Freesurfer* do not parcellate the hemispheres with identical homologues, it would be difficult to compare all ROIs between the $\text{hemi}_{\text{lesion}}$ and $\text{hemi}_{\text{contra}}$. Also, in the presence of gross pathology, probabilistic labelling (such as that performed by *Freesurfer* to produce ROI volumes) may fail and produce inaccurate registration between the individual and the atlas.

It is important to consider how this may affect previous and future investigations of case/control differences at the group level. Within previous investigations of the pTBI cohort used in the current study, group means for total grey matter differed between specific severities of pTBI patients and typically developing controls by a PVD value of a similar order of magnitude to the current findings (mild .38%, mild-complex 4.8%, moderate 2.7% and severe TBI .77% (Ryan, Catroppa, et al., 2016); mild 3.1%, mild-complex .93%, moderate .66% and severe TBI 8.1% (Ryan et al., 2017)). No differences between controls and any TBI severity groups were significant (Ryan et al., 2017). Due to the similar magnitude of changes seen in both real and error based cases, group-level differences may be contaminated by this error and may erroneously be attributed to pathology-related changes.

It is also important to consider the dynamic state of these lesions in the brain. It is likely that lesioned tissue within the MRI will change in appearance as a function of time, due to effects such as the stabilising of pathological mechanisms after the acute period, but also potential recovery mechanisms over time. As the lesion changes over time (lesion presentation on MRI is highly dependent on time post-injury (Bigler & Maxwell, 2012)), this will result in differences in the lesion-induced error we have detected in the *Freesurfer* pipeline. These errors may then be misattributed to longitudinal changes to the morphometry of the brain post-pTBI, confounding therapy effects, or “real” recovery measures.

However, it is important to note that not all patients within pTBI studies will present with pathological lesions on T1w MRI and thus the cumulative error from these cases may not exceed the typical ‘noise’ in group-level comparisons. The lesion-induced error therefore poses the greatest threat to group-level analysis in those cases where there are small sample sizes, such as can be seen in the existing literature of pathology-related morphometric change to the brain post-pTBI ($n=12$ (Krawczyk et al., 2010), and $n=13$ (Urban et al., 2017)), and the relatively few lesion-cases will have a greater artefactual effect on

the findings due to limited power to detect true group-differences above and beyond this additional ‘noise’.

These ideas can be seen in (Spanos et al., 2007), who found that group-level reductions in cerebral white matter in a pTBI group compared to typically developing controls were still apparent when excluding those cases where there was a focal lesion. This is an example where, at the group-level, the lesion-induced error we have quantified in this paper seemingly has little effect. We therefore recommend that for all group analyses where there are MR lesions present, that a robustness check where lesion-cases are removed and analyses rerun, would be a prudent step to take in assessing the impact of this lesion-induced error on findings. This would be relatively easy to adopt across the field as standard practice, the only difficulty being in those studies where sample sizes are small, and the reduction of statistical power would be too great if these cases were removed.

Of greater concern however, is the impact of this error on individual-level prediction. Prognostication of outcome at the individual level is a key goal of many studies investigating TBI, attempting to understand how brain pathology give rise to changes in functional behaviour (Bigler, 2016) and therefore aid prediction of long-term outcomes for individuals. However, as noted by Irimia, Wang, et al. (2012), and subsequently supported by the results of the current study, lesions inappropriately bias the morphometric measurements from automated software packages, thus leading to erroneous measurements of potentially useful biomarkers. In terms of recent methods in medical prognostication using machine learning approaches, this could bias training data in a way which leads to unsuccessful prediction and/or classification of cases. Therefore, the current lesion-induced error renders the subset of pTBI cases which present with pathological lesions on MRI unreachable in terms of prognostication using morphometric measurements of the brain.

Devising a solution to allow for the correction of these individual-level errors in segmentation due to the presence of lesions is non-trivial. Foulon et al. (2017) proposed an approach to study cortical thickness in patients with stroke lesions. They took an approach whereby they enantiomorphically fill the lesion (Nachev, Coulthard, Jager, Kennard, & Husain, 2008) followed by masking cortical thickness within the lesion. Briefly, the enantiomorphic filling is based on the assumption of hemispheric structural symmetry, a chimeric image is produced with the corresponding reflected section of the non-lesion hemisphere overlaid on the lesion hemisphere, essentially ‘filling’ the lesion (Nachev et al., 2008). This image is used for calculating the solution to the cost-function in the normalisation process, producing a transformation or warp which can later be applied to the non-manipulated T1w image. Thus, the lesion can be transformed without it influencing the spatial normalization process (see (Brett et al., 2001) for a further investigation of the effect of lesions on spatial normalisation). Finally, voxels within the lesioned tissue were removed from maps of cortical thickness, thus preventing this ‘contamination’ of measurements. This means that, for an ROI where 50% is covered by lesion tissue, there is still 50% of non-lesioned tissue by which to estimate a mean cortical thickness value for the region. Whilst this

was a different software package to *Freesurfer*, it is important to consider that, within the context of the findings presented here, this approach is unlikely to deal with the global lesion-induced error seen across the brain.

We therefore recommend a *Freesurfer* pre-processing approach, similar to the approach by Foulon et al. (2017), whereby the lesioned T_{1w} image is enantiomorphically-filled and this is the image which is processed by *Freesurfer*. Given our finding that the hemi_{contra} lesion-induced error seems to be associated with the SD of voxel intensities within the lesion region, it is prudent to think that, by replacing the intensities of this region with homologous intensities from the normal-appearing voxel intensities from within the contralesion regions of the brain, the contralesion lesion-induced error would be mitigated. Therefore, dependent on the quality of the lesion-filling, this would ensure more biologically-meaningful morphometric measurements of the whole-brain to be calculated. As a further *Freesurfer* post-processing step, individual-subject level atlas parcellations could then be masked as per Foulon et al.'s (2017) approach, whereby region labels which are completely or partially occluded by lesion tissue will be edited. Morphometric measures (such as cortical thickness, volume etc.) could be calculated using the standard *Freesurfer* approaches but due to this masking, the output of this pipeline would be cortical morphology measurements which are not contaminated by a) lesion-tissue within the original image or b) filled with estimated/imputed voxel intensities in the enantiomorphically filled T_{1w} images. Future studies should investigate the potential of such an approach.

3.6 Limitations

One particular limitation was the drawing of lesion masks. Lesions were identified in our dataset by a single-rater and masks drawn by hand (as is the typical 'gold standard' for lesion segmentation of MR images) where visible lesions could be identified by eye using T_{1w} and FLAIR images (by JN). It may in fact be the case that some smaller, more subtle lesions were missed and therefore not used in the simulated cases. This, alongside the fact that the array of lesions used as source material for the simulated dataset was small in size ($n=16$), we cannot ascertain for certain that this effect is ubiquitous to all pTBI cases which present with lesions. However, the purpose of these lesion masks were to allow the extraction of lesion tissue for use in the simulated dataset. Therefore, the issue of false-negatives in the binary voxel masks are less of a concern as lesion tissue was still able to be extracted. Although, it must be acknowledged that potential false-positive identification of lesion voxels in the binary lesion mask is a potential cause for concern, especially as we did not conduct inter- or intra-rater reliability tests.

We aimed to provide a specific commentary on the types of lesions observed in TBI, specifically in our paediatric population. The idea of a 'lesion-induced error' to structural segmentation and measurement of morphometry is neither new nor specific to the field of pTBI, and we therefore accept that the specific quantification of error presented here is only generalisable to the current population.

Despite this, the fact that we have utilised ‘real’ lesion cases is beneficial in the sense that it provides us a lesion which retains those characteristics which may be harder to replicate artificially such as texture and the complexity of the distribution of lesions (Seghier et al., 2008). Multilevel models presented in the current study showed greater model fit on the inclusion of a random effect of the ID of the lesion used to generate the simulated case. This suggests that the effect of lesions on volume vary across specific lesions. However, the use of these ‘real’ lesions does mean we are limited in the ability to systematically investigate specific lesion characteristics (Chard et al., 2010), such as locale (GM vs WM vs Both), size or number (focal vs multifocal) in comparisons to artificially generated lesions. Figure 3.1 shows that the spatial distribution of the lesions was in the expected regions (fronto/temporal (Bigler et al., 2016)) but was still varied. There was also large variation in size of lesion also. This in turn makes it difficult to assess which types of lesion are characteristic of this lesion-induced error, or whether location of the lesion is of any consequence.

3.7 Conclusion

Many previous studies investigating morphometric differences in the brain post-TBI have reported very little information as to how *Freesurfer* manual-edits have been performed to deal with lesion tissue in some TBI cases. Of those that did, the methods used were post-processing approaches, which dealt with potential error considering only focal errors in the *Freesurfer* algorithm (Drijkoningen et al., 2017; Spanos et al., 2007). The current study is the first empirical investigation to show that, for cortex volume in particular, these approaches may not be sufficient, with a small, but consistent lesion-induced error being found in the contralesion hemisphere. Thus, this may call into question previous work which has found group differences in brain morphometry, with lesion-induced error being misattributed to pathology-related changes. Future work investigating TBI using morphometric investigations of the brain should be aware of the potential for lesion-induced errors beyond the lesion and be more robust in the reporting of their methods.

Chapter 4. Structural Covariance Identifies Altered Network Topology in Children with Persistent Executive Function Impairments after Traumatic Brain Injury

4.1 Overview

This chapter marks the beginning of three experimental investigations implementing network-level analyses of sMRI data in those children who experienced a pTBI. The experimental investigations described in this chapter utilise structural covariance approaches at the group-level to investigate the multivariate relationship between sMRI measures across the cortex and its relationship with later executive functioning. In doing so, this chapter proposes a plausible topological mechanism by which is associated with the transition to poor executive functioning outcome post-injury. In Chapter 3, the potential error that lesions may have on the Freesurfer processing pipeline was emphasised. The current chapter addresses this and utilises an approach similar to that suggested in the previous chapter, to enable a greater number of participants to be included in the current analysis. Overall, the changes to brain-morphometry post-injury are spatially patterned with regard to the normal network structure of the typically developing brain in those cases where executive functioning shows long-term impairment. A version of the current work is currently being prepared for publication as follows;

King, D. J., Seri, S., Catroppa, C., Anderson, V. A. & Wood, A. G. (In Prep.) Structural Covariance Identifies Altered Network Topology in Children with Persistent Executive Function Impairments after Traumatic Brain Injury.

DJK and AW contributed to the conception and design of the current study. VA and CC contributed and collected data. DJK performed the processing of MRI data, conceptualized and performed the statistical analysis and wrote the first draft of the manuscript. All authors contributed to manuscript revision.

4.2 Introduction

Traumatic brain injury (TBI) in childhood and adolescence is a leading cause of disability (World Health Organization, 2006), with these injuries occurring in the individual-context of a still-developing brain (Wilde, Hunter, et al., 2012). Paediatric TBI (pTBI) has a reported incidence between 1.10-1.85 cases per hundred for the 0-15 age range (McKinlay et al., 2008) and has specific adverse effects on neurodevelopment. When the brain is exposed to a traumatic, external force, this can result in pathology at a micro and macroscopic level, leading to both transient and permanent impairments (Bigler, 2007b, 2016; Maxwell, 2012). Damage can be realised as trauma-related, developmentally inappropriate atrophy (Bigler, 2013; Urban et al., 2017; Wilde et al., 2005) which, when imaged using techniques such as structural magnetic resonance imaging (sMRI), can appear as relative changes in both brain volume (Bigler, 2016) and cortical thickness (CT, Urban et al. (2017)). However, in pTBI, these negative consequences of injury occur during a period of ongoing age- and development-dependent changes to the brain (Bigler, 2016; Maxwell, 2012)

Previous sMRI studies have shown that, from early to post-chronic timepoints post-injury, the morphometry of the injured brain differs from that of typically developing children (see King et al. (2019) for a systematic review of findings). These cross-sectional differences are found even up to 10 years post-injury (Beauchamp, Catroppa, et al., 2011; Serra-Grabulosa et al., 2005) suggesting alterations that are non-transient, neither recovering nor being compensated for over time. These cross-sectional differences are evidence of a long-term effect of TBI on the morphometry of the brain.

Previous studies have suggested that, from the perspective of clinical characteristics, two TBI's can superficially appear similar but result in vastly different outcomes (Bigler, 2007a; Schneider et al., 2014). Whilst MRI has been used to try to elucidate the reasoning for this disparity in outcomes, the location and extent of focal lesions to the brain following a pTBI are seemingly insufficient to fully explain post-injury neuropsychological deficits (Bigler, 2001). There is also limited evidence of brain-behaviour relationships between brain morphometry differences and functional outcomes (King et al., 2019). The paucity of reliable relationships between brain structural biomarkers and long-term outcomes of neuropsychological functions may be explained in part by the fact morphometric changes can be highly distributed across the cortex even within a single patient, and these changes vary across individuals (Bigler, 2007a; Bigler et al., 2013; Bigler & Maxwell, 2011). This spatial heterogeneity of damage and post-injury changes may limit the potential of univariate investigations of morphometry, which are therefore unable to tell us about the subtleties of the more diffuse effects of an injury. Therefore, looking more widely at the global effects of injury and how focal damage can change the wider 'system' of the brain may explain greater variance in functional outcomes post-injury. One way to explore this hypothesis is to investigate changes to the global neural-network following injury due to pTBI, in keeping with recent characterizations of TBI as a disorder of brain connectivity (Hannawi & Stevens, 2016; Hayes et al., 2016), utilising a graph-theory framework to quantitatively describe these networks. This will capture the multifaceted nature by which the brain can experience pathological change post-injury.

Patterns of grey matter morphometry across the cortex can be captured as a biologically-meaningful brain network. This structural covariance (SC) network models the degree to which the morphology (measured with CT) of brain regions statistically co-varies across all possible pairs of ROIs (Alexander-Bloch, Giedd, et al., 2013; Alexander-Bloch, Raznahan, et al., 2013; Evans, 2013; Mechelli et al., 2005), capturing meso-scale organisation of brain structure. These networks are sensitive to neurodevelopmental and age-related change (Alexander-Bloch, Raznahan, et al., 2013; Fan et al., 2011; Khundrakpam et al., 2017; Khundrakpam, Lewis, Zhao, Chouinard-Decorte, & Evans, 2016; Khundrakpam et al., 2013; Raznahan, Lerch, et al., 2011; Váša et al., 2017), with regions showing similar/shared developmental trajectories being more similar in morphometry (Alexander-Bloch, Raznahan, et al., 2013), likely driven by the gene-controlled patterning of CT and SC across the cortex (Romero-Garcia et al., 2018; Yee et al., 2017).

Given this highly coordinated, genetically programmed developmental ‘blueprint’ of brain development, neurological disruption to the structure of the brain during this period, is likely to have a significant impact on the ongoing development of the brain, and it is unsurprising that this would be detectable as an abnormality in SC across the cortex. For instance, SC has been investigated in other forms of paediatric brain insult, including malformations of cortical development and cortico-genesis disruption in neonates, with degree of differences changing as a function of the specific gestational-timing of disruption (Hong et al., 2017). Therefore, the SC approach may be a biologically meaningful phenotype with which to investigate functional outcomes, sensitive to the effects of pTBI on the developmental trajectory of the brain, whilst respecting the complex organisation of the GM across the whole cortex, rather than univariate ROIs.

Previous papers have adopted such an approach and investigated the correlational structure of regional-level morphometry post-pTBI in comparison to controls. Spanos et al. (2007) investigated volumetric correlations across cerebro-cerebellar regions and found a significant positive relationship between DLPFC/cerebellum was found in the TD but not in the TBI group. Drijkoningen et al. (2017) adopted a similar approach by estimating the correlational structure of atrophy scores between regions. Moderate to very strong positive correlations were found for these relationships. These interrelations between regional morphology/atrophy support the hypothesis of a diffuse pattern of pathology post-injury. The current paper attempts to expand on these previous findings by investigating these relationships across the whole brain utilising SC which is novel to the field of TBI.

The topology of brain networks ordinarily makes them inherently robust to insult (Hillary & Grafman, 2017). However, targeted damage to topologically central regions may have a disproportionate impact on the network and is more likely to be behaviourally symptomatic (Crossley et al., 2014; Hillary & Grafman, 2017). In the clinical setting, neurological and psychiatric disorders which may have aetiologies during the childhood period may also be linked to abnormal development of hub regions (Morgan, White, Bullmore, & Vertes, 2018). During development, there is very early formation of hubs in the structural network (a stable scaffold to build-upon during subsequent development). Later, maturational change is focussed upon hub regions, with hub locations becoming more adult-like across childhood (Csermely, London, Wu, & Uzzi, 2013; Morgan, White, et al., 2018; Oldham & Fornito, 2019). The protracted development of SC hubs over childhood and adolescence, with those responsible for higher integrative functions developing most slowly (Khundrakpam et al., 2013; Whitaker et al., 2016), may put them at greatest risk to pathology which may result in delayed or disrupted development (Morgan, White, et al., 2018). Integral to the development of the brain, damage to regions central to the network during this period, therefore, may result in behaviourally-relevant changes to the developmental trajectory of the brain.

Across multiple neurologic disorders, the probability of a region showing case-control differences in grey matter morphology is significantly related to the degree, the summation of the number of

connections, of the node (based on DTI-derived networks, (Crossley et al., 2014)). Similarly, voxels with significant case-control differences in grey matter volume/density, indicative of potential atrophy, belonged to regions with a greater median degree than ‘undamaged’ voxels (Crossley et al., 2014). In adult TBI specifically, reductions in ‘hubness’ of nodes (betweenness and eigenvector centrality) derived from a tractography network were related to greater cognitive impairment, including executive functions (Fagerholm, Hellyer, Scott, Leech, & Sharp, 2015). These results highlight the fact that the behavioural consequences of damage to the brain are highly dependent on the topological position of the damage within, and the organization of, neural networks (Aerts, Fias, Caeyenberghs, & Marinazzo, 2016; Hillary & Grafman, 2017).

The aims of the current study were twofold; 1) to capture global, diffuse nature of the effects of TBI on the still-developing brain using multivariate-network methodologies, and 2) to investigate whether the cortical topography of post-pTBI neurodegeneration/atrophy (as indexed by CT reductions) in relation to the typical topology of the brain is related to poor cognitive functioning at two year follow-up.

We examined three hypotheses:

1. Patient groups (including those subgroups with good/poor executive function (EF) outcome) would show significant CT reductions in comparison to healthy controls,
2. Patient groups would show differences in SC compared to controls,
3. For those patients who exhibited poor EF outcomes at 2 years post-injury, CT reductions would have occurred in regions that have higher SC than randomly selected regions. We predicted that this relationship would not be observed in patients who exhibited good EF outcomes at 2 years post-injury.

4.3 Methods

4.3.1 Ethics statement

Data from the TBI cohort in the current study was obtained under a material transfer agreement between the Murdoch Children’s Research Institute and Aston University originally acquired for a study that had previously received ethical approval via the Human Research and Ethics Committee of Royal Children’s Hospital, Melbourne, Australia. We also acquired additional control data through the public Autism Brain Imaging Data Exchange (ABIDE) database, as shared by the Preprocessed Connectome Project (PCP). A favourable opinion was granted by Aston University ethics panel for the secondary analysis of both the TBI and ABIDE datasets.

4.3.2 Participants

4.3.2.1 TBI Cohort

The data used in the current experiment are a subset of an existing dataset of children who have experienced a TBI between the ages of five and 16 years of age. 157 children (patients n=114) were recruited between 2007 and 2010 into a study on ‘Prevention and Treatment of Social Problems Following TBI in Children and Adolescents’. Further details have recently been published elsewhere (Anderson et al., 2013; Anderson et al., 2017; Catroppa et al., 2017). In brief, children with TBI were recruited on presentation to the emergency department at the Royal Children’s Hospital, Melbourne, Australia. Eligibility for the study was determined if they: i) were aged between five and 16 years at the time of injury, ii) had recorded evidence of both a closed-head injury and also two post-concussive symptoms (such as headaches, dizziness, nausea, irritability, poor concentration), iii) had sufficient detail within medical records (Glasgow Coma Scale (GCS; Teasdale and Jennett (1974)), neurological and radiological findings) with which to determine the severity of the injury, iv) had no prior history of neurological or neurodevelopmental disorder, non-accidental injuries or previous TBI, and v) were English speaking. TD controls were also recruited and were required to meet criteria i), iv) and v).

MRI images were acquired at 3T as a part of an existing research protocol on a Siemens Trio scanner (Siemens Medical Systems, Erlangen, Germany) using a 32-channel matrix head coil. The standard acquisition included a sagittal three-dimensional (3D) MPRAGE [TR = 1900 ms; TE = 2.15 ms; IR prep = 900 ms; parallel imaging factor (GRAPPA) 2; flip angle 9 degrees; BW 200 Hz/Px; 176 slices; resolution $1 \times .5 \times .5$ mm] and sagittal 3D T2-w non-selective inversion preparation SPACE (Sampling Perfection with Application-optimised Contrast using different flip-angle Evolution) [TR = 6000 ms; TE = 405 ms; inversion time (TI) = 2100 ms; water excitation; GRAPPA Pat2; 176 slices; $1 \times .5 \times .5$ mm resolution matched in alignment to the 3D T1-weighted sequence].

We applied a number of inclusion criteria to the dataset, only including subjects who; a) met strict quality control criteria of Freesurfer outputs (see supplementary materials (Appendix C) for further details), and b) had MRI data available and were scanned <90 days post-injury. This resulted in a subset of n = 116 subjects (TBI patients (n = 83) and healthy controls (n = 33)), with patients who had MRI acquired acutely after injury (range = 1-88 days). Group demographics can be seen in Table 4.1.

4.3.2.2 ABIDE dataset

In order to provide a second healthy reference group for validation of findings, we employed the open-access data from the Autism Brain Imaging Data Exchange (ABIDE, Di Martino et al. (2014)), specifically the pre-processed version of the dataset made available by the Preprocessed Connectome Project (PCP, Bellec et al. (2013), for full details see <http://preprocessed-connectomes-project.org/>). The ABIDE dataset consists of a large sample of 532 individuals with autism spectrum disorders and 573 typical controls, composed of MRI (functional and structural) and phenotypic information for each subject, accumulated across 17 independent sites. The scan procedures and parameters are described in more detail elsewhere (http://fcon_1000.projects.nitrc.org/indi/abide/).

We applied similar inclusion criteria to this dataset, only including subjects who; a) passed a strict MRI quality control criteria of raw structural MRI (see supplementary materials, Appendix C), b) were recorded as controls within the ABIDE database, c) at time of scan were aged < 17 years and d) had pre-processed Freesurfer data available as part of the PCP release. This resulted in a final reference group of $n = 327$ (M/F = 259/68, median age (yrs) = 12.49, age range (yrs) = 6.47 – 16.93). The list of IDs for ABIDE subjects included in these analyses can be found in supplementary materials (Appendix C), as per ABIDE's recommendations.

Both controls in the experimental cohort and the ABIDE cohort had qualitatively similar mean IQ ($M = 105.4$ and $M = 109.8$) as measured across multiple age-appropriate IQ tests (in the experimental cohort IQ was assessed by WASI 2-scale IQ whereas the measures used by the ABIDE dataset were varied, see ABIDE documentation for details).

Table 4.1 *Demographics for patients and controls*

Group	pTBI	Controls	Comparison
N	83	33	-
M/F	54/29	20/13	OR= .83, p=.67 ^a
Age at Scanning (median, yrs)	10.92	9.99	F(1,114)= .262, p=.61 ^b
(range, yrs)	6.09-14.82	6.53-15.47	-
Age at Injury (median, yrs)	10.92	-	-
(range, yrs)	5.92-14.67	-	-
Injury-Scan Interval (median, days)	34	-	-

Note. ^a Fisher's exact test (OR = odds-ratio), ^b One-Way ANOVA

4.3.3 MRI Processing

3D tissue segmentation and estimation of cortical thickness (CT) and estimated total intracranial volume (eTIV) from T1-weighted (T1w) MR images were conducted using an established pipeline (Freesurfer version 6.0; see Fischl (2012) for review). The steps involved are documented elsewhere (Fischl et al., 2004) but briefly, T1w images were stripped of non-brain tissues (Segonne et al., 2004), grey matter (GM) / white-matter (WM) boundaries were tessellated and topology was automatically corrected (Fischl, Liu, & Dale, 2001; Segonne, Pacheco, & Fischl, 2007). Finally, deformation of this surface was performed, to optimally define the pial (Cerebro-spinal fluid/GM) and white (GM/WM) surfaces using intensity gradients to estimate where intensity maximally shifts to define boundaries of these tissue classes (Dale, Fischl, & Sereno, 1999; Dale & Sereno, 1993; Fischl & Dale, 2000). Where available, 3D T2-weighted (T2w) FLAIR MRI were used to refine the boundary between the pial surface and dura. In this study, Freesurfer was used to estimate the cortical volume/thickness for 34 regions-of-interest per hemisphere, based upon the cortical parcellation of the Desikan-Killiany atlas (Desikan et al., 2006). This parcellation was chosen over a more fine-grained parcellation scheme due to concerns over statistical power if a greater number of ROIs were analysed.

The quality of Freesurfer outputs was assessed using Qoala-T (Klapwijk, van de Kamp, van der Meulen, Peters, & Wierenga, 2019) as a decision support tool to guide the systematic and replicable selection of which cases required manual editing. Multiple cases within the original TBI cohort also had frank parenchymal lesions to the grey matter ribbon. For these cases, Freesurfer has limited applicability with its standard processing pipeline and thus an adjusted pipeline was utilised and is described in Supplementary Materials (Appendix C). Eight lesion cases were retained for analysis using this pipeline.

Processing using the Freesurfer pipeline had already been done for the ABIDE dataset within the PCP, using the standard pipeline as described above (however using an older version of Freesurfer (version 5.1)). Details of quality assurance of the anatomical processing using Freesurfer for the ABIDE data, and steps to control for ABIDE site effects, can be found in Supplementary materials (Appendix C).

4.3.4 Executive Functions (EF)

EF was assessed for patients in the TBI cohort (patients and controls) at 24-months post injury/recruitment using performance-based neuropsychological testing. Several standard, age-appropriate neuropsychological tests were administered to participants to index EF skills, and these were from three typical, age-appropriate test batteries; i) Tests of Everyday Attention – Children (TEA-Ch; (Manly et al., 1999)), ii) Delis-Kaplan Executive Function System (D-KEFS, (Delis et al., 2001)), and iii) Wechsler Intelligence Scale for Children (WISC-IV, (Wechsler, 2003)). These measures were selected from a wider battery of administered neuropsychological tests as part of the wider study. Specific subtests used in the current study were selected to represent components of a three-factor EF model (Miyake et al., 2000) and can be found in Table 4.2.

An approach to define those individuals exhibiting clinically relevant cognitive impairment was selected (a-priori) to group patients in terms of executive (dys)function at 2 years post-injury. The current study adopted the neuropsychological impairment (NPI) rule proposed by Beauchamp et al. (2015). This rule has previously been shown to be sensitive to TBI with an increase in identification of impaired individuals (Beauchamp et al., 2015), and has been used to detect behavioural impairment (Donders & DeWit, 2017), and cognitive inefficiency (Beauchamp et al., 2018) following paediatric TBI and concussion respectively.

Briefly, performance scores for the neuropsychological test batteries were converted to age-scaled scores ($M=10$, $SD=3$). To identify those with a clinically relevant impairment in executive functioning a cut-off of 1 SD outside 'average' functioning in the direction of worse performance. To be assigned to the group who were experiencing clinically relevant cognitive impairment (poor EF outcome (EF_{Poor})), participants had to have shown impaired functioning on two or more individual EF measures, whereas those who were impaired less than two measures were assigned to the without cognitive impairment group (good EF outcome (EF_{Good})). A minimum of two cases of impairment identifies a pattern of deficit, unlikely to be due to typical variability due to individual differences or measurement error for instance. We only calculated the NPI rule for those cases that had the full battery of EF tests. The demographics of these two subgroups (EF_{Poor} and EF_{Good}) are shown in Table 4.3.

Table 4.2. Neuropsychological tests and subtests used to group patients on EF outcome 2 years post-injury

EF Domain	Battery	Subtest	Measure
Set Shifting	TEA-Ch	Creature counting	Accuracy (no. correct)
	TEA-Ch	Creature counting	Time taken
Inhibition	D-KEFS	Colour-word interference – condition 3	Time Taken
	D-KEFS	Colour-word interference – condition 4	Time Taken
	TEA-Ch	Walk-don't-walk	Score
	TEA-Ch	Skysearch	Attention Score
Working Memory	WISC-IV	Digit span backwards	Score

Table 4.3. Demographics for patient subgroups

Group	Control	EF _{Good}	EF _{Poor}	Statistical comparison
N	33	42	17	-
M/F	20/13	27/15	12/5	p=.78 ^a
Age at Scanning (median, yrs)	9.99	10.95	11.13	F(2,89)= .366, p=.70 ^b
(range, yrs)	6.53-15.47	6.69-14.82	6.09-14.17	-
Age at Injury (median, yrs)	-	10.75	11.00	F(1,57)= .027, p=.87 ^b
(range, yrs)	-	6.58-14.67	5.92-14.00	-
Injury-Scan Interval (median, days)	-	35.5	30.0	F(1,57)= 1.971, p=.17 ^b
Injury Severity				
Mild	-	23	10	p= .58 ^a
Mild-Complicated	-	4	3	
Moderate	-	11	4	
Severe	-	4	0	

Note. ^aFisher's exact test, ^bOne-Way ANOVA

4.3.5 Statistical analysis

The analysis plan of the current study was inspired by that of Wannan et al. (2019). All analyses were conducted with a series of packages in R (R Core Team, 2016), with network analyses being specifically conducted using ‘brainGraph’ version 2.2 (Watson, 2016b), which is an expansion of the iGraph package (Csardi & Nepusz, 2006). All analyses were conducted over three group-contrasts; i) pTBI patients vs. controls, ii) pTBI EF intact vs. controls and iii) pTBI EF impaired vs. controls. These contrasts specifically only represent case-control differences, rather than within-patient analyses. This is because we specifically wanted to investigate pathological deviations to the typical development of the brain.

4.3.5.1 Differences in CT between pTBI and Controls

Firstly, we investigated cross-sectional differences in CT between patients and our experimental controls. For each ROI (n=68) a general linear model (GLM) was generated to test the effect of group (patient vs control) on CT, whilst controlling for the effects of age at scanning, sex, and estimated total intracranial volume (eTIV). A t-test was used to test the directional hypothesis of cortical thickness reductions in the patient group compared to controls. When calculating p-values, the false discovery rate was maintained at $\alpha_{\text{fdr}} = 0.05$ using the Benjamini and Hochberg (1995) correction to control for multiple comparisons across all ROIs. The effect size was reported as Hedges’ g (Hedges & Olkin, 2014) corrected for unequal sample sizes as per Rosnow, Rosenthal, and Rubin (2000). This was repeated for the three pairwise contrasts.

4.3.5.2 Differences in SC between pTBI and Controls

Structural covariance networks were generated using the Freesurfer-derived structural parcellation as the nodes (n=68) and the edges of the network the similarity of cortical thickness between as pairs of ROIs. As is common in the SCN literature, CT was used as the dependant variable for general linear models run across all ROIs with covariates of age at scanning, sex, and estimated total intracranial volume. This is to control for the fact that CT has been shown to decrease with age (Magnotta, 1999), and increase with total intracranial volume (Im et al., 2008) and to differ across genders (Sowell et al., 2007). The studentised residuals were then retained for analysis and used to generate graphs of structural covariance. Pearson’s correlations between residuals of each ROI generated a single 68 x 68 adjacency matrix data. This will represent an undirected, unthresholded, weighted network, with ROIs as the nodes and correlation coefficients as the edge-weights between nodes. This network represents age-invariant structural covariance (Váša et al., 2017) with age at scanning controlled for in the model.

For each graph/network, the ‘magnitude’ of structural covariance for each node was measured as node strength. For node i , this is the sum of the connectivity weights of all edges connected to node i (Fornito et al., 2016). We did not normalize these measures based on number of edges as we utilised the fully-

connected, unthresholded networks and thus the number of edges connected to each node was equal across all nodes. To calculate an estimate of graph-level strength, we calculated the average nodal strength over all nodes. To generate confidence intervals for each group, these measures were bootstrapped over 5000 resamplings. In order to assess significant differences in structural covariance, permutation testing (5000 permutations) generated a null distribution of differences (t-values) in graph metrics between two groups with a two-tailed α -level of .05. These comparisons were conducted for each of the three pair-wise contrasts and were conducted at the graph-level (mean graph strength) and at the nodal level. p -values for nodal-level comparisons were also FDR-corrected over the 68 nodes, whilst the graph level comparisons were FDR-corrected over the three comparisons.

4.3.5.3 SC between regions with CT reductions in pTBI

To assess whether SC was significantly greater between regions with cortical thickness reductions in pTBI compared to randomly selected regions, we conducted permutation testing. Briefly, for each contrast, ROIs were ranked in terms of the effect size of CT reductions in the patient group compared to controls. For the top n -regions in terms of effect size, mean nodal strength was calculated (where $n = 2,3,4\dots68$) based on the SC graph calculated for the control group only. A null distribution of this mean nodal strength was generated by calculating mean SC for 5000 sets of randomly selected sets of n -nodes (without replacement). For each value of n , a one-tailed p -value was calculated as the proportion of permutation cases where the mean nodal strength of randomly selected nodes exceeded that of the observed mean nodal strength. p -values were corrected across values of n using the FDR-correction. A significant result suggests that SC of regions where CT reductions exist is significantly greater than expected for randomly selected regions. We also repeated this analysis using the larger ABIDE cohort with which to provide an estimate of age-invariant structural covariance across a larger, more representative dataset compared to the experimental controls.

4.4 Results

4.4.1 Differences in CT between pTBI and Controls

When comparing pTBI patients to experimental controls, adjusted mean differences (mean_{adj} (pTBI minus control), adjusted for age at scanning, sex, and eTIV) in CT across regions ranged from -.104 in rTP to .077 in lcACC. When comparing EF_{Good} and EF_{Poor} to experimental controls, mean_{adj} difference ranged from -.109 in rrACC to .084 in liCC and -.285 in ITP to .123 in lcACC respectively. However, across all contrasts, no regional CT reductions in the TBI group were significant (after FDR correction).

4.4.2 Differences in SC between pTBI and Controls

Mean graph strength for each of the groups and subgroups can be found in Table 4.4. No significant difference in mean graph strength was found between patients and our experimental controls (observed

difference (ObsDiff) = -10.9, $p_{\text{fdr}} = .062$). When investigating subgroups, significant differences were found between experimental controls and EF_{poor} but not EF_{Good} (ObsDiff = -20.0, $p_{\text{fdr}} = .008$, and ObsDiff = -10.9, $p_{\text{fdr}} = .062$ respectively). After fdr correction, no nodal differences remained significant between control and the whole pTBI group or EF_{Good} subgroups. However, when comparing the EF_{Poor} group to controls, multiple regions (44/68) showed significantly greater nodal strength in the patient group. These regions can be found in Table 4.5. These regions were widely distributed across the cortex, yet a high proportion of these significant regions were found in the frontal lobe (41% frontal lobe, 25% temporal lobe, 20% parietal lobe, 9% cingulate, 5% occipital lobe). However, it is important to note that, whilst the observed between-group difference between EF_{Poor} and experimental controls was significant in comparison to the permuted-distribution, the confidence intervals of the differences all crossed zero.

Table 4.4. Mean graph strength and bootstrapped^a 95% confidence intervals

Group	Graph Strength	CI _{Low}	CI _{High}	ObsDiff ^b	$p_{\text{fdr}}^{\text{b}}$
Controls	17.1	11.8	22.6	NA	NA
pTBI	28.0	21.9	34.8	-10.9	.062
EF _{Good}	28.0	19.5	37.5	-10.9	.062
EF _{Poor}	37.1	27.9	48.1	-20.0	.008

Note. ^a 5000 resamplings, ^b compared to experimental controls.

Table 4.5. Regions with significant permutation^a differences in nodal strength between experimental controls and EF_{Poor} groups

Region	ObsDiff ^b	p_{fdr}	Region	ObsDiff ^b	p_{fdr}
lcMFG	-25.3	0.025	rpORB	-19.2	0.025
lIPL	-21.9	0.025	rpostC	-38.9	0.025
lLOF	-24.7	0.025	rpreC	-27.1	0.025
lMOF	-21.1	0.025	rpTRI	-24.1	0.025
lMTG	-29.9	0.025	rSFG	-21.6	0.025
lPCUN	-21.8	0.025	rSMAR	-22.9	0.025
lpOPER	-26.3	0.025	rSTG	-26.3	0.025
lpostC	-30.4	0.025	lpreC	-22.2	0.025
lSFG	-23.5	0.025	lpTRI	-22.9	0.025
lSMAR	-23.9	0.025	lLOG	-21.8	0.031
lSPL	-19.1	0.025	lSTG	-25.9	0.031
lITP	-22.1	0.025	rSPL	-18.5	0.031
rBSTS	-29.4	0.025	rTT	-26.4	0.031
rcMFG	-23.9	0.025	lpORB	-25.6	0.031
rFUS	-23.1	0.025	lrACC	-23.2	0.031
riCC	-32.2	0.025	liCC	-25.8	0.032
rIPL	-20.8	0.025	rparaC	-12.5	0.032
rLOF	-24.8	0.025	IPARH	-19.7	0.034
rMOF	-25.9	0.025	rLOG	-20.4	0.037
rMTG	-31.7	0.025	IFUS	-19.9	0.041
rPCC	-29.0	0.025	lparaC	-15.2	0.042
rpOPER	-22.2	0.025	lITG	-23.6	0.043

Note. ^a 5000 permutations, ^b Control minus EF_{Poor}

4.4.3 SC between regions with CT reductions in pTBI

We conducted permutation testing to estimate whether, for either the whole group or either of the two subgroups, regions which showed cortical thickness reductions compared to controls were those regions which, in the typically developing population (i.e. using the experimental controls or ABIDE data controls), show higher levels of SC. When considering the whole group of pTBI patients, for no value of n number of regions with greatest CT reductions was the mean strength of regions in the experimental control group significantly greater than that of n randomly selected regions. This was also true of the EF_{Good} subgroup.

However, for the EF_{Poor} group, the mean strength in the experimental controls of the greatest n nodes with cortical thickness reductions was significantly greater than the mean strength of n randomly selected regions for 59/67 values of n ($n = 8, 10 - 67$, $p_{\text{fdr}} \text{ all} < .05$). This can be seen in Figure 4.1. When repeating the analysis using the ABIDE dataset to estimate mean strength of nodes in the typically developing brain, these results were largely replicated; mean node strength was significantly greater than that of n randomly selected regions for multiple values of n in the EF_{Poor} group ($n = 19 - 65, 67$, $p_{\text{fdr}} \text{ all} < .05$), but neither the whole pTBI sample or the EF_{Good} subgroup.

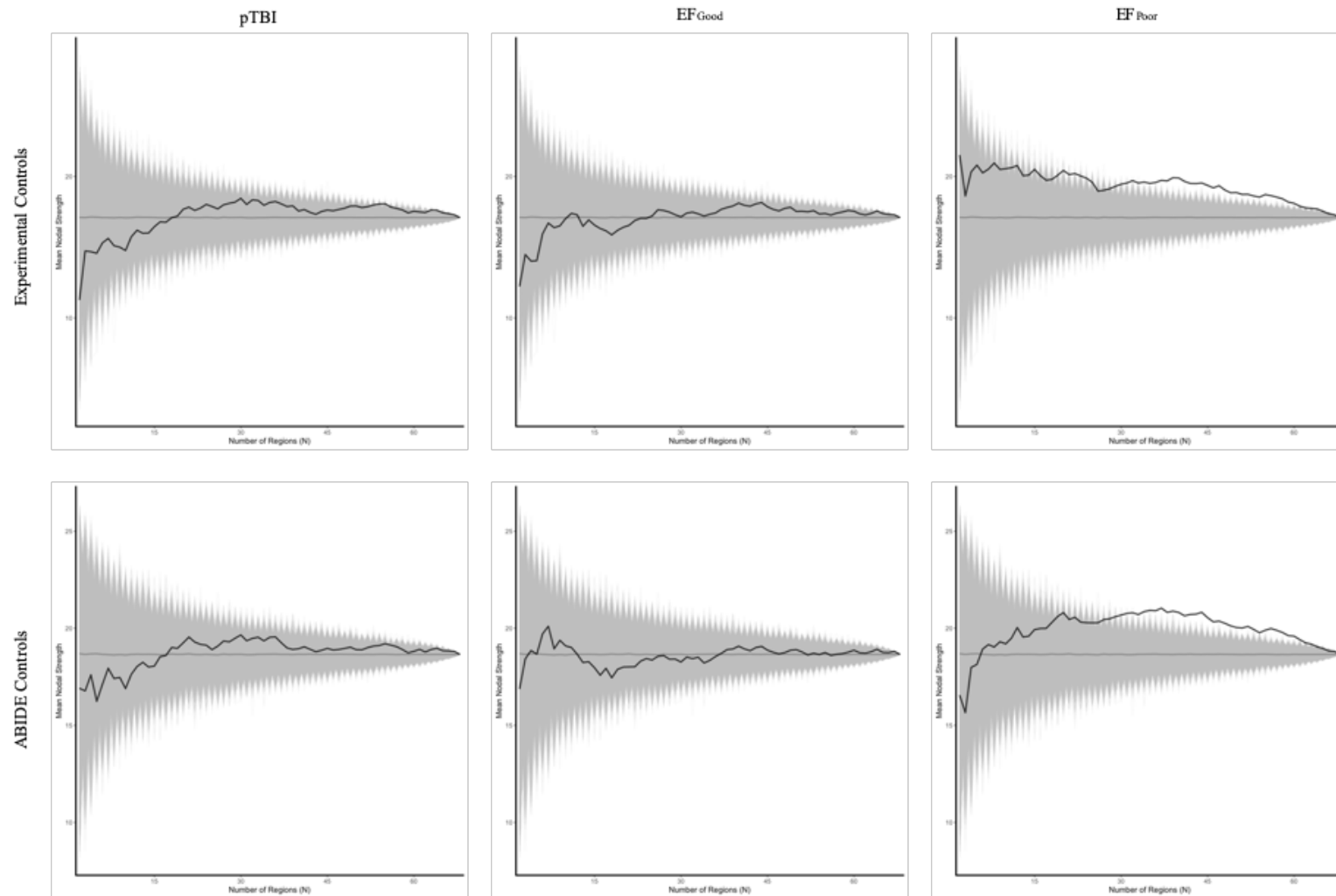


Figure 4.1. Observed mean strength (in the experimental control group (top row) and the ABIDE control group (bottom row)) across n nodes ($n = 2-68$) with greatest CT reductions in the whole pTBI group and both the EF_{Good} and EF_{Poor} subgroups, grey region represents the mean nodal strength for 5000 permutations of n randomly selected nodes.

4.4.3 Lesion Cases

To examine whether the results were driven by a bias towards cases with cortical grey matter lesions who were processed using our custom Freesurfer pipeline, we repeated all analyses excluding the lesion cases. The results can be seen in supplementary materials (Appendix C) but, briefly, these were qualitatively the same as the results presented above, with effects seen in the EF_{Poor} group but not the whole group or the EF_{Good} group.

4.5 Discussion

The location and extent of focal brain lesions, as well as post-injury brain morphometry, are seemingly insufficient to fully explain the neuropsychological deficits that persist post-injury (Bigler, 2001; King et al., 2019). Thus, the current paper presents an entirely novel analysis to the pTBI literature, investigating the structural covariance (SC) network of the brain post-pTBI, in order to better capture the diffuse, global effects of injury on the brain.

4.5.1 Differences in CT between pTBI and Controls

We predicted that patient groups (including those subgroups with good/poor EF outcome) would show significant CT reductions in comparison to healthy controls, replicating previous findings at this acute time-point post injury (McCauley et al., 2010; Urban et al., 2017; Wilde, Merkley, et al., 2012). Whilst cortical thickness was, on average, reduced in patients compared to controls across a large proportion of regions of the brain, no singular region showed differences deemed to be statistically significant after correction for multiple comparisons. This was true of comparisons between our experimental controls and those patients with or without EF impairments.

This challenges previous research suggesting that cortical thickness differences from controls are seen both acutely and chronically post-injury (King et al., 2019), with the post-injury cortical thickness being specifically related to executive functioning (Wilde, Merkley, et al., 2012). Observed differences were generally in the direction expected for pathology-related tissue loss, with patients having thinner cortices, but effect sizes were very small across regions. It may, in fact, be the case that the atrophic changes seen this acutely post-injury are too subtle to detect at these sample sizes, especially over multiple ROIs. However, the only two studies to report CT reductions in patients compared to controls at a similarly acute timepoint post injury conducted vertex-wise analyses (McCauley et al., 2010; Urban et al., 2017). It may in fact be that the univariate atrophy is highly focal and averaging these changes over the rest of a region for ROI-based analyses makes these harder to detect.

CT reductions as measured with MRI aim to assess the potential atrophic effects of the cascade of mechanisms that occur post-injury (Bigler, 2013). However, it is important to note that, due to the cross sectional, rather than longitudinal, nature of the sampling in the current study, it is hard to ascertain

whether these changes are in fact due to atrophy. These types of longitudinal analyses will inform us as to whether any thinning of cortex is beyond that of typical thinning due to cortical development.

4.5.2 Differences in SC between pTBI and Controls

Despite the non-significance of these univariate tests, we hypothesised that the cumulative effect of all the subtle differences across individual regions could still have a functionally meaningful effect on the developing brain post-injury. Hence, in a novel set of analyses, we investigated the structural covariance network as a method to investigate the multivariate relationships between cortical thicknesses across the cortex. We found that differences in the mean graph strength, the average magnitude of SC across all nodes, was not different when comparing pTBI patients to our experimental controls, however, when stratifying based on EF outcome, significant differences from controls were found for the EF_{Poor} but not the EF_{Good} group. This suggests that the SCN is only ‘abnormal’ in the impaired group, with the non-impaired group showing a network structure similar to controls. This pattern was repeated for the nodal-level findings and, interestingly, the significant differences in the EF_{Poor} group were overly represented by nodes in the frontal and temporal lobes, regions commonly implicated in brain morphometry differences post-pTBI (King et al., 2019).

At both the nodal and graph level, the magnitude of SC was greater in the impaired patient group than our experimental groups. This would suggest that, in these patients, the morphometry of regions across the cortex was less differentiated. Whilst it remains unclear how this may translate into changes to the underlying cytoarchitecture of the brain, this represents a marked change from the gene-controlled patterning of SC across the cortex (Romero-Garcia et al., 2018; Yee et al., 2017). Given the acute timing of the MRI in this study, it is unclear how this may alter the ongoing development of the morphometry of the brain after the injury, however future longitudinal research would be well positioned to answer this.

4.5.3 SC between regions with CT reductions in pTBI

For those patients who exhibited poor EF outcomes, we predicted that CT reductions would be localised to regions that have higher SC than randomly selected regions in the healthy population. The findings supported this hypothesis. In other words, we found that, at the group-level, for cases where long term executive function outcome is poor, cortical damage (measured as cortical thickness reductions) is seemingly preferentially loaded onto regions high in structural covariance in the typically developing population, but not when EF is spared.

Executive functions are supported by widely distributed neural networks (Beauchamp, Catroppa, et al., 2011; Collette et al., 2006; Nowrangi et al., 2014; Slomine et al., 2002) and are therefore particularly vulnerable to the distributed, multifocal mechanisms of TBI (Treble-Barna et al., 2017). Thus, our

findings were specific to those patients with ongoing EF impairment is strong evidence that early biomarkers at network-level are sensitive to functionally relevant brain changes.

Although no one region showed significant cortical thickness reductions, on average the largest of these smaller, more subtle differences are loaded onto high structural covariance regions in healthy controls. This, therefore, suggests that rather than the topography (the physical distribution across cortex) of specific alterations being important to functional outcomes, it is the topology (the connectivity of a node) of these regions in the wider cortical network which is important. There is spatial inconsistency in alterations to brain morphometry associated both between and within clinical manifestations of neurologic disorders (Cauda, Mancuso, Nani, & Costa, 2019), and this is also true of pTBI (King et al., 2019). This may be because spatially-disparate lesions and/or atrophy may occupy similar topological positions in the network and in these cases result in a similar neuropsychological profile. Damage to topologically central regions likely has a disproportionate impact on the broader network than if the damage occurred in other regions, and this in turn renders it more likely to be behaviourally symptomatic (Crossley et al., 2014; Hillary & Grafman, 2017), as seen in our results. Also, given that regional nodes which are topologically central are particularly relevant to the development of the brain (Csermely et al., 2013; Morgan, White, et al., 2018; Oldham & Fornito, 2019) and that damage loading onto these regions is more likely to result in EF impairment, it is unsurprising that divergence from the typically developing SCN is related to EF abilities (King et al., 2020).

The connectivity of the brain is underpinned by white matter fibre bundles which are specifically vulnerable to the effects of pTBI, specifically due to diffuse axonal injury. Diffusion MRI (DWI) is the current standard for estimating this structural white matter connectivity between brain regions (Batalle et al., 2018). DTI-based connectivity studies have also shown topological differences after injury, compared to controls acutely after mild pTBI (Yuan, Wade, & Babcock, 2015) but also across wider injury severities chronically after injury (Caeyenberghs et al., 2012; Konigs et al., 2017; Yuan, Treble-Barna, Sohlberg, Harn, & Wade, 2016). However, high quality DWI sequences have long acquisition lengths and thus may not be suitable for paediatric populations (Batalle et al., 2013). Previous research has also highlighted the potential role of WM connectivity as a driver of structural covariance between regions (Gong et al., 2012; Reid, Lewis, et al., 2016) as regions which are similar in cytoarchitectural organisation are more likely to be anatomically connected (Goulas, Uylings, & Hilgetag, 2017; Wei, Scholtens, Turk, & van den Heuvel, 2019). Therefore, the current study highlights the SCN as a potential alternative to studying structural network phenotypes after pTBI, which may in fact capture not only pathological grey-matter atrophy, but also the effects of DAI. Future studies may combine these methodologies in multimodal studies of the cortex post-injury to better understand how they capture injury mechanisms

4.6 Limitations

One key strength of the current study is the fact we were able to validate the relationship between CT reductions in the patient group and the SC network of healthy controls. The SCN is limited to the application to population-level covariance in neuroanatomy (Alexander-Bloch, Raznahan, et al., 2013). We specifically investigate the age-invariant SCN (Váša et al., 2017), since the analysis combines data across childhood and adolescence, modelling the common network structure across development. The limited numbers in our experimental control group could result in limited accuracy of the estimation of this age-invariant SCN. Utilising the ABIDE reference group allowed us to replicate the results using a more reliable estimate of the age-invariant SCN due to the much larger sample size. However, it is important to note that hubs of the SCN have distinct developmental trajectories over the timecourse of childhood and adolescence (Khundrakpam et al., 2013; Whitaker et al., 2016). Therefore, future research should try to resolve the relationship between CT reductions post-TBI and SC across age-matched SCN. We focused on nodes with high topological strength in the network, namely regions that have high summed structural covariance with all other regions of the brain. This metric is a relatively simplistic, although intuitive, measure of ‘hubness’ but may not capture the more nuanced aspects of the centrality of a node in a network (Oldham & Fornito, 2019; van den Heuvel & Sporns, 2013). However, due to the fact that the SC networks do not adhere to typical assumptions of networks (edges representing definitive real connections) we utilised strength as a simpler metric which makes fewer assumptions about the underlying neurophysiology of the network. Once a more complete understanding of communication dynamics throughout the SCN has been understood, future studies may investigate other, more nuanced measures of nodal centrality, which may capture greater information about their role in the wider network.

4.7 Conclusion

There is strong theoretical support for future studies of brain insults to focus on generating hypotheses about underlying pathophysiology to the neural network biology (Aerts et al., 2016). Here we provide a novel methodological advance in support of this goal, offering an analysis of the SCN post-TBI in which we specifically proposed that the topology of nodes which were damaged would be important for understanding which children go on to experience functionally relevant impairment post-injury. Given disparity in outcomes after a pTBI, these results have specific implications for predicting which children go on to experience significant impairment post-injury as opposed to those who will recover well. Future research needs to expand these findings to investigate the causal nature of these relationships, and to see whether these patterns expand beyond the SC network of the brain (i.e. DTI). This network-based approach of covariance between disparate regions is in keeping with recent characterizations of TBI as a disorder of brain connectivity (Hannawi & Stevens, 2016; Hayes et al., 2016; Wilde, Hunter, et al., 2012).

Chapter 5. Developmental Divergence of Structural Brain Networks as an Indicator of Future Cognitive Impairments in Childhood Brain Injury

5.1 Overview

The current chapter addresses a potential limitation of the SCN approach, the fact that it can only make inference at the group level, as seen in **Chapter 4**. In **Chapter 2**, it was highlighted that the brain ‘diverges’ from the normal developmental trajectory post-injury. Therefore, the current chapter proposes a developmental divergence index (DDI) which is used to relate individual-level divergence from the SC of typically developing children to better understand the neuroanatomical correlates of executive dysfunction post-injury. The DDI represents a potential measure of injury ‘magnitude’ in regard to meso-scale changes to the cortex post-injury, a tool that may be useful across the field. The results of this chapter suggest that distance of the network structure of the morphometry of the brain post-TBI from that of typically developing controls, as a proxy measure for developmental divergence, is a useful predictor of executive functioning post-injury. A version of the work presented in this chapter has been submitted for publication as follows;

King, D. J., Seri, S., Beare, R. Catroppa, C., Anderson, V. A., Wood, A.G. (Submitted).
Developmental Divergence of Structural Brain Networks as an Indicator of Future
Cognitive Impairments in Childhood Brain Injury: Executive Functions.
Developmental Cognitive Neuroscience.

DJK and AW contributed to the conception and design of the current study. DJK wrote and performed analyses and then wrote the first draft of the manuscript. VA and CC contributed and collected data. All other authors contributed to the critical review and revision of the manuscript.

5.2 Introduction

The pathological effects of neurological conditions occurring during childhood, necessarily interact with the highly-programmed maturation of the brain, perturbing the trajectory of normal brain development, which is in itself non-linear (Gogtay et al., 2004; Shaw et al., 2008). Previous research has suggested that deviations from the developmental trajectory of the brain may act as a marker of brain health, neurological disorders and cognitive functioning (Bigler, 2013; Cole & Franke, 2017; Erus et al., 2015). Thus, the degree to which the injury alters normal development may be an important factor to consider when trying to understand subsequent cognitive sequelae post-insult including impairments to intellectual and executive functioning, as well as attention and processing speed (Crowe et al., 2015). The current study investigates this idea using a measure of divergence of the structural network to investigate levels of post-insult cognitive impairment, with a focus on executive functioning.

Specifically, the current study focuses on traumatic brain injury (TBI) in childhood and adolescence, a leading cause of disability (World Health Organization, 2006). Many injuries occur in the context of a

still-developing brain (Wilde, Hunter, et al., 2012), with an incidence between 1.10-1.85 cases per hundred for the 0-15 age range (McKinlay et al., 2008). Paediatric TBI (pTBI) has specific adverse effects on neurodevelopment. The traumatic, external force to the brain can result in pathology at both a cellular and tissue level, leading to transient or even permanent impairment (Bigler, 2007b, 2016; Maxwell, 2012). Some damage is realised as trauma-related, developmentally inappropriate atrophy (Bigler, 2013; Urban et al., 2017; Wilde et al., 2005) which, when imaged using techniques such as structural magnetic resonance imaging (sMRI), can appear as relative decreases to both brain volume (Bigler, 2016) and cortical thickness (CT) measures (Urban et al., 2017). However, in pTBI, these negative consequences of injury occur against a backdrop of ongoing age- and development-dependent changes to the brain (Bigler, 2016; Maxwell, 2012) leading to differential vulnerability to TBI depending on the developmental stage at which injury occurs (Anderson et al., 2011; Goldstrohm & Arffa, 2005; McCrory et al., 2004). For example, the state of development of myelinated axons at the time of injury influences the magnitude of degeneration of nerve fibres (Adelson & Kochanek, 1998; Kochanek et al., 2000; Maxwell, 2012; Staal & Vickers, 2011). Thus, disruption at different ‘critical’ periods of the developmental trajectory could result in very different functional outcomes long term (Anderson et al., 2011; Resch et al., 2019).

Previous sMRI studies have shown that, from early to post-chronic timepoints post-injury, the morphometry of the injured brain differs from that of typically developing children (see King et al. (2019) for a systematic review of findings). These cross-sectional differences are found even up to 10 years post-injury (Beauchamp, Catroppa, et al., 2011; Serra-Grabulosa et al., 2005) suggesting alterations which are non-transient, neither recovering nor being compensated for over time. These cross-sectional differences are evidence of a long-term effect of TBI on the morphometry of the brain.

Whilst these cross-sectional studies can provide evidence that differences exist, longitudinal studies are needed to provide explanation of the basis of these changes (ie whether pathologic-injury related change or developmental change) and if they resolve over time. Longitudinal morphometric studies of paediatric cohorts have investigated changes between patients and controls across multiple timepoints post-injury (Dennis, Faskowitz, et al., 2017; Dennis et al., 2016; Mayer et al., 2015; Wilde, Merkley, et al., 2012; Wu et al., 2018; Wu et al., 2010). The majority of these studies show a reduction in volume or cortical thinning over time in the TBI group, as well as cross-sectional differences from controls. Interestingly however, they also show an interaction between group (patient vs. controls) and time post-injury on CT measures (Mayer et al., 2015; Wilde, Merkley, et al., 2012) and corpus callosum volumes (Wu et al., 2010), with greater atrophy over time seen post pTBI. Dennis, Faskowitz, et al. (2017) also found differences in longitudinal morphometric change between a TBI patient group who experienced slowed inter-hemispheric communication, compared to those with a normal inter-hemispheric transfer time, suggesting that these structural differences are not only a result of an injury, but also relevant to post-injury functioning of the brain. Due to the highly programmed trajectories of white matter (WM) and

grey matter (GM) development during childhood and adolescence (Batalle et al., 2018; Mills et al., 2016; Raznahan, Shaw, et al., 2011; Shaw et al., 2008), these group differences in longitudinal change (between TBI patients and controls) suggest that the developmental trajectory of the brain is in fact altered to some degree by a TBI. However, previous research has not investigated the magnitude to which a pTBI interferes with the developmental trajectory at an individual level or how this may change as a function of age at which the injury occurs. Overall, these studies suggest that pTBI has potentially lifelong consequences, owing to the persistent and ongoing differences to the structural development of the cortex post-injury.

The effects of a pTBI on the brain are highly diffuse with morphometric differences found across widespread brain regions (in both cortex and subcortically) even within a single individual (Bigler, 2007b; Bigler et al., 2013; Bigler & Maxwell, 2011). This diffuse (rather than focal) injury can also vary in location across individuals, samples and studies, although commonly fronto-temporal regions are affected (King et al., 2019). Thus, previous studies investigating regions of interest (ROIs) with a univariate approach, may not capture the multivariate and heterogeneous nature of injury. One way to interrogate the multivariate structure of the brain is the structural covariance (SC) network approach (Bigler, 2016; Lerch et al., 2017), modelling the degree to which the morphology of brain regions statistically co-varies across all possible pairs of ROIs (Alexander-Bloch, Giedd, et al., 2013; Alexander-Bloch, Raznahan, et al., 2013; Evans, 2013; Mechelli et al., 2005).

These whole-brain, network approaches to morphometric data, within a graph theoretic framework (Bullmore & Sporns, 2009), will allow us to investigate additional information beyond that which is offered by univariate, local approaches (Bullmore & Sporns, 2009; Pagani et al., 2016).

SC is both biologically meaningful and sensitive to changes to the developing-brain. The topological organization of these networks are quantifiably non-random and complex (Alexander-Bloch, Giedd, et al., 2013; Evans, 2013), similarly to brain connectivity networks estimated from both resting-state fMRI and diffusion-weighted imaging (DWI). SC across the cortex changes as a function of neurodevelopment, age and maturational change (Alexander-Bloch, Raznahan, et al., 2013; Fan et al., 2011; Khundrakpam et al., 2017; Khundrakpam et al., 2016; Khundrakpam et al., 2013; Raznahan, Lerch, et al., 2011; Váša et al., 2017) and may be related to shared expression of genes related to controlling cortical development between ROIs (Romero-Garcia et al., 2018). Age-related change in SC captures variation in changes to the brain beyond that of neurodevelopmental processes such as thinning and myelination (Váša et al., 2017). These networks are also sensitive to differences due to other types of paediatric brain insult, including malformations of cortical development and cortico-genesis disruption in neonates, with degree of differences changing as a function of the specific gestational-timing of disruption (Hong et al., 2017), suggesting that SC can index divergence of the typical maturational trajectory of the cortex. Thus, these approaches may allow us to capture the developmental-

divergence of morphology after a pTBI and investigate its relationship to functional outcomes post-injury.

However, as multiple participants are required to sample enough cortical measurements to generate a correlation between all possible regional-pairs (each participant can only contribute a single measurement per region), this SC network approach can only generate group-level brain networks, expressing population-level covariance in neuroanatomy (Alexander-Bloch, Raznahan, et al., 2013). Thus, studies have tried to develop methods that can translate this information to the individual-subject level (for example Seidlitz et al. (2018) or Tijms, Series, Willshaw, and Lawrie (2012)). We specifically utilise the individual contribution metric (proposed by Saggar et al. (2015)), as a potential solution to this problem, which allows us to estimate distance of a patient from a group-level, reference SC network.

We aimed to measure subject-level divergence of the SC network following brain insult and potential perturbation of brain development. Specifically, we investigate deviation in a cohort of paediatric TBI patients from a reference network of typically developing control participants by leveraging a large-scale, open-access MRI database. Our approach adopts a novel analytic framework of a sliding-window approach to calculate these developmentally-appropriate reference networks. We predict that there will be greater divergence of structural networks for cases with a pTBI compared to control cases. We also aimed to use these divergence metrics as a proxy of perturbations in brain development and as a predictor of long-term functional outcome, specifically hypothesising that greater structural divergence will be associated with greater executive dysfunction. The current study focused upon executive functioning (EF) because cognitive-skills are more vulnerable to damage occurring during the period of skill-maturation (Ewing-Cobbs et al., 2004; Krasny-Pacini et al., 2017), thus the protracted period of EF development (Diamond, 2013; Friedman et al., 2016; Perone et al., 2018) means EF is likely to have an extended window of vulnerability (Krasny-Pacini et al., 2017).

We also hypothesised that stronger associations would be found between structural divergence and executive dysfunction when investigating a sub-graph of the whole-brain SC network, which consists of regions known to subserve core executive function skills.

5.3 Methods

5.3.1 Ethics statement

Data from the TBI cohort in the current study was obtained under a material transfer agreement between the Murdoch Children's Research Institute and Aston University for a study which had previously received ethical approval via the Human Research and Ethics Committee of Royal Children's Hospital, Melbourne, Australia. The reference data used in this research was acquired through the public Autism Brain Imaging Data Exchange (ABIDE) database, as shared by the Preprocessed Connectome Project (PCP). The database has de-identified all the patient health information associated with the data. A

favourable ethical opinion was granted by Aston University for the secondary analysis of both the TBI and ABIDE datasets.

5.3.2 Participants

5.3.2.1 TBI Cohort

The data used in the current experiment are a subset of an existing dataset of children who have experienced a TBI between the ages of five and 16 years of age. 157 children (patients $n=114$, controls $n=43$) were recruited between 2007 and 2010 into a study on ‘Prevention and Treatment of Social Problems Following TBI in Children and Adolescents’. Further details have recently been published elsewhere (Anderson et al., 2013; Anderson et al., 2017; Catroppa et al., 2017). In brief, children with TBI were recruited on presentation to the emergency department at the Royal Childrens’ Hospital, Melbourne, Australia. Eligibility for the study was determined if they: i) were aged between five and 16 years at the time of injury, ii) had recorded evidence of both a closed-head injury and also two post-concussive symptoms (such as headaches, dizziness, nausea, irritability, poor concentration), iii) had sufficient detail within medical records (Glasgow Coma Scale (GCS; (Teasdale & Jennett, 1974)), neurological and radiological findings) with which to determine the severity of the injury, iv) had no prior history of neurological or neurodevelopmental disorder, non-accidental injuries or previous TBI, and v) were English speaking. TD controls were also recruited and were required to meet criteria i), iv) and v).

TBI severity was categorized as follows: mild TBI: GCS 13 to 15 on hospital presentation, no evidence of mass lesion on CT or clinical MRI and no neurologic deficits (if there was evidence of intra-cranial pathology, these were classified as mild complicated); moderate TBI: GCS 9 to 12 on hospital presentation, and/or mass lesion or other evidence of specific injury on CT/MRI, and/or neurological impairment; and, severe TBI: GCS 3 to 8 on hospital presentation, and/or mass lesion or other evidence of specific injury on CT/MRI, and/or neurological impairment.. Due to small group sizes in relevant analyses, the mild-complicated, moderate and severe groups were collapsed for analyses.

MR-Images were acquired for the patient group acutely after injury (<90 days post-injury, range = 1-88 days). MRI images were acquired at 3T as a part of an existing research protocol on a Siemens Trio scanner (Siemens Medical Systems, Erlangen, Germany) using a 32-channel matrix head coil. The standard acquisition included a sagittal three-dimensional (3D) MPRAGE [TR = 1900 ms; TE = 2.15 ms; IR prep = 900 ms; parallel imaging factor (GRAPPA) 2; flip angle 9 degrees; BW 200 Hz/Px; 176 slices; resolution $1 \times .5 \times .5$ mm] and sagittal 3D T2-w non-selective inversion preparation SPACE (Sampling Perfection with Application-optimised Contrast using different flip-angle Evolution) [TR = 6000 ms; TE = 405 ms; inversion time (TI) = 2100 ms; water excitation; GRAPPA Pat2; 176 slices; $1 \times .5 \times .5$ mm resolution matched in alignment to the 3D T1-weighted sequence].

We applied a number of inclusion criteria to the dataset, only including subjects who; a) met strict quality control criteria of Freesurfer outputs, b) had no gross/frank pathology/lesions identified within the grey matter ribbon (as this may bias image processing with Freesurfer (Chapter 3))(King et al., In prep.), c) had available MRI data and were scanned <90 days post-injury. This resulted in a subset of $n=108$ subjects (TBI patients ($n=75$) and healthy controls ($n=33$)). Group demographics can be seen in Table 5.1.

5.3.2.2 *ABIDE dataset*

In order to provide a healthy reference group for the calculation of our divergence metric, we employed the open-access data from the Autism Brain Imaging Data Exchange (ABIDE, Di Martino et al. (2014)), specifically the pre-processed version of the dataset made available by the Preprocessed Connectome Project (PCP, Bellec et al. (2013), for full details see Pre-processed Connectome Project website <http://preprocessed-connectomes-project.org/>). The ABIDE dataset consists of a large sample of 532 individuals with autism spectrum disorders and 573 typical controls, composed of MRI (functional and structural) and phenotypic information for each subject, accumulated across 17 independent sites. The scan procedures and parameters are described in more detail on the ABIDE website (http://fcon_1000.projects.nitrc.org/indi/abide/).

We applied similar inclusion criteria to this dataset, only including subjects who; a) passed a strict MRI quality control criteria of raw sMRI (see supplementary materials (Appendix D) for further details), b) were recorded as controls within the ABIDE database, c) at time of scan were aged < 17 years and d) had pre-processed Freesurfer data available as part of the PCP release. This resulted in a final reference group of $n = 327$. As per ABIDE's recommendations to share the data ID list used for primary analyses, this can be found in supplementary materials (Appendix D). Group demographics can be seen in Table 5.1.

Both controls in the experimental cohort and the ABIDE cohort had similar mean IQ ($M = 105.4$ and $M = 109.8$ respectively) as measured across multiple age-appropriate IQ tests (in the experimental cohort IQ was assessed by WASI 2-scale IQ (Wechsler, 1999) whereas the measures used by the ABIDE dataset were varied, see ABIDE documentation for details).

Table 5.1. *Demographics for each cohort by group*

Cohort/Group	TBI Cohort -Patients	TBI Cohort - Controls	ABIDE
N	<i>n</i> = 75	<i>n</i> = 33	<i>n</i> = 327
M/F	51/24	20/13	259/68
Age at MRI (median, yrs)	10.81	9.99	12.49
(range, yrs)	6.18-14.91	6.53-15.47	6.47-16.93
Age at Injury (median, yrs)	10.58	-	-
(range, yrs)	6.08-14.67		
Injury-MRI interval (median, days)	34		
(range, days)	1-88		
Injury Severity			
Mild	47	-	-
Moderate/Severe ^a	28	-	-

Note. ^a Mild Complicated TBI + Moderate TBI + Severe TBI

5.3.3 MRI Processing

3D tissue segmentation and estimation of CT from T1-weighted (T1w) MR images was conducted using an established pipeline (Freesurfer version 6.0; see Fischl (2012) for review). The steps involved are documented elsewhere (Fischl et al., 2004) but briefly, T1w images were stripped of non-brain tissues (Segonne et al., 2004), GM/WM boundaries were tessellated and topology was automatically corrected (Fischl et al., 2001; Segonne et al., 2007). Finally, deformation of this surface was performed, to optimally define the pial (Cerebro-spinal fluid/GM) and white (GM/WM) surfaces using intensity gradients to estimate where intensity maximally shifts to define boundaries of these tissue classes (Dale et al., 1999; Dale & Sereno, 1993; Fischl & Dale, 2000). Where available, 3D T2-weighted (T2w) FLAIR MRI were used to refine the boundary between the pial surface and dura. In this study, Freesurfer was used to estimate the cortical volume/thickness for 34 regions-of-interest per hemisphere, based upon the cortical parcellation of the Desikan-Killiany atlas (Desikan et al., 2006). The quality of Freesurfer outputs was assessed using Qoala-T (Klapwijk et al., 2019) as a decision support tool to guide systematic and replicable selection of which cases required manual editing. Processing using the Freesurfer pipeline had already been done for the ABIDE dataset within the PCP, using the standard pipeline as described above (however using an older version of Freesurfer (version 5.1). Details of quality assurance of the anatomical processing using Freesurfer for the ABIDE data, and steps to control for ABIDE site and cohort effects (TBI cohort vs ABIDE), can be found in Supplementary materials (Appendix D).

5.3.4 Graphs of Structural Covariance (SC)

All network analysis were conducted with a series of packages in R version 3.5.0 (R Core Team, 2016), specifically brainGraph version 2.2.0 (Watson, 2016b), which is an expansion of the iGraph package (Csardi & Nepusz, 2006).

As is common in the SC literature, CT was used as the dependant variable for general linear models (GLM) run across all ROIs with covariates of age at scanning, sex and estimated total intracranial volume. This is to control for the fact that CT has been shown to decrease with age (Magnotta, 1999), and increase with total intracranial volume (Im et al., 2008) and to differ across genders (Sowell et al., 2007). The studentised residuals were then retained for analysis and used to generate graphs of structural covariance. Pearson's correlations between residuals of each ROI generated a single 68 x 68 adjacency matrix for the ABIDE reference data. This will represent an undirected, unthresholded, weighted network, with ROIs as the nodes and correlation coefficients as the edge-weights between nodes.

5.3.4.1 Divergence Metrics

Since SC networks are derived from correlations between regions within participants, graphs are compiled at a group level. Our hypotheses suggest that the individual deviation from 'typical' maturation will be an important variable in the prediction of executive function. Therefore, it is important to identify

methods by which to extract estimates of this deviation at the individual subject level as a proxy of perturbations in brain development. A developmental-divergence index (DDI) is therefore generated for each patient using the ‘Add-One-Patient’ (AOP) approach (Saggar et al., 2015). This measure is further outlined below. Saggar et al. (2015) term this ‘individual contribution’ to the group-level network. From our perspective, those that are most different from the group/reference network will be those whose development is furthest from typical, expected trajectories. Hence, we refer to this ‘individual contribution’ metric as a (developmental) divergence index.

The AOP approach allows the direct comparison of the weighted SC network by assessing the matrix of CT residuals. The approach compares the structural network of a reference group and a second matrix comprising of the reference group, plus a single patient (hence AOP). This means that the existing correlation matrix for a reference control group, denoted R_{cont} , will be combined with each patient individually, to generate a new matrix, denoted $R_{cont+Pi}$ (where i is the individual patients, $i = 1, 2, ..n$). Subsequently, a normalized Mantel test (Mantel, 1967) is conducted to assess similarity of these matrices calculated as;

$$Mantel\ test\ r(X, Y) = \frac{1}{n-1} \sum_{i=1}^n \sum_{j=1}^n \frac{x_{ij} - \bar{x}}{Sx} \cdot \frac{y_{ij} - \bar{y}}{Sy}$$

Where X and Y represent R_{cont} and $R_{cont+Pi}$ respectively, x and y are elements of these matrices, Sx and Sy are the standard deviations for the matrices and n is the number of nodes (in the case of this study, 68 ROIs) for each correlation matrix (Saggar et al., 2015). This metric of similarity (whereas r increases this represents two matrices with higher similarity) is subtracted from one to compute the divergence from the reference group matrix where;

$$DDI(P_i) = 1 - r(R_{cont}, R_{cont+Pi})$$

These divergence metrics will provide individual-level distance (at the level of the whole graph) from the reference group. If R_{cont} and $R_{cont+Pi}$ are similar (Mantel test trending toward 1), subj(i) has not altered the group-level network, and therefore Subj(i) does not show divergent morphology, thus DDI will be low. If highly dissimilar (Mantel test trending toward 0), addition of subj(i) has significantly altered the group-level network, thus subj(i) is different from typically developing peers (and DDI is greater). Essentially, if the patient exhibits developmentally-appropriate morphometry, the reference-plus-patient network will be similar to that of the reference group alone. Therefore, the less similar the networks, the more developmentally divergent the patient’s morphometry. Thus, for each patient the analysis will output a single DDI to estimate divergence across the whole cortex.

5.3.4.2 Reference Networks

In order to calculate developmental divergence for both the control and TBI cases from the TBI cohort, we used the ABIDE dataset as a reference group to generate the R_{cont} SC network. We calculated developmental divergence from the typically-developing SC network using two approaches, an age-invariant SC network and an age-matched SC network. For the age-invariant network, the all participants selected for our ABIDE cohort were utilised as a reference group. Similarly to Váša et al. (2017), we termed this the age-invariant SC network since the analysis combines data across childhood and adolescence, with participants of all ages in the ABIDE sample included. Age-invariant DDI ($DDI_{inv.}$) was therefore calculated for each subject in the TBI cohort (both patients and controls) from this whole-group reference. Previous studies have adopted this approach of using a single reference group to calculate Saggari et al.'s (2015) 'individual contribution' metric. A single reference group combines a wide range of ages and thus ignores known variations in developmental changes of grey and white matter across childhood and into adolescence (Gogtay et al., 2004; Sowell et al., 2004). Thus, we also adopted a novel analytic framework in which developmentally-appropriate reference networks to calculate an age-matched DDI (DDI_{age}) were generated from control participants from the ABIDE dataset using a sliding-window approach (outlined below).

5.3.4.3 Sliding-Window

Similarly to Váša et al. (2017), we used a sliding window approach in order to calculate developmentally appropriate, age-matched reference SC networks. In brief, subjects from the ABIDE dataset were ordered by age at scanning. Subject-level CT residuals were then correlated within equal-sized windows of participants, with the window being 'slid' across the age-range of participants (Váša et al., 2017). A window-size of 26 participants and a step-size of 15 participants was selected, subsequently 21 half-overlapping windows across the ABIDE cohort were selected, resulting in a single reference SC network per window.

Window-size was selected against a number of criteria: a) based on recommendations by Saggari et al. (2015) in relation to stability of their AOP metric, b) maximised the difference-statistic for control vs TBI differences in DDI_{age} measure, and c) which resulted in an n^{th} window (where number of windows is 1: n) which was as close to the defined window size as possible (due to the remainder from the calculation of:

$$no. of windows = \frac{no. of ABIDE(I) subjects}{window size}$$

the final window was not guaranteed to have the full number of subjects). Details of this window-size selection process can be found in supplementary materials (Appendix D).

Once reference SC networks for each window were generated, the median age of participants within the window were calculated. Each participant within the TBI cohort (patients and controls) was

individually-matched to the reference window which minimised the difference between their age at scanning and the median-age of the reference-window. This matched reference window was then used to calculate the DDI_{age} for that individual.

5.3.5 Executive Functions (EF)

We investigate EFs as they are commonly impaired, both acutely and chronically post-injury, but also because they show a protracted period of maturation and development (Diamond, 2013; Friedman et al., 2016; Perone et al., 2018) and are therefore likely to have an extended window of vulnerability to the effects of injury (Krasny-Pacini et al., 2017). EF was assessed for pTBI patients at approximately 24-months post injury ($M(SD) = 754(80)$ days post-injury). EF was assessed in controls relative to their MRI scan ($M(SD) = 367(135)$ days post-MRI). EF was assessed both using performance-based neuropsychological testing and a parent-reported measure.

Several standard neuropsychological tests were administered to participants to index EF skills, and these were from three typical, age-appropriate test batteries; i) Tests of Everyday Attention – Children (TEA-Ch; Manly et al. (1999)), ii) Delis-Kaplan Executive Function System (D-KEFS, Delis et al. (2001)), and iii) Wechsler Intelligence Scale for Children (WISC-IV, (Wechsler, 2003)). These measures were selected from a wider battery of administered neuropsychological tests as part of the wider study. Specific subtests used in the current study were selected to represent components of a three-factor EF model (Miyake et al., 2000) and can be found in Table 5.2.

Performance scores for the neuropsychological test batteries were converted to age-scaled scores ($M=10, SD=3$). To provide a summary score for common EF performance, we summed these age-scaled scores across subtests, with higher scores representing better performance. The EF summary score was calculated for 80 subjects (TBI $n = 52$, controls $n = 28$) who had data for all subtests available, as well as sufficient data to calculate the DDI. This summary score was used for two main reasons; firstly, due to a limited sample size and the use of correlational analyses, we have limited power to look at each domain separately. Secondly, due to the fact we are using a whole-brain measure of developmental-divergence, it is likely that the measure is too coarse to capture the nuances across multiple sub-domains of executive functioning.

Table 5.2. Neuropsychological tests and subtests used to calculate EF scores

EF Domain	Battery	Subtest	Measure
Set Shifting	TEA-Ch	Creature counting,	Accuracy (no. correct)
	TEA-Ch	Creature counting	Time taken
Inhibition	D-KEFS	Colour-word interference – condition 3	Time Taken
	D-KEFS	Colour-word interference – condition 4	Time Taken
	TEA-Ch	Walk-don't-walk	Score
	TEA-Ch	Skysearch	Attention Score
Working Memory	WISC-IV	Digit span backwards	Score

The Behaviour Rating Inventory of Executive Function (BRIEF, Gioia et al. (2000)) measures EF in daily life, using purposeful, goal-directed behaviours to solve and adapt to problems (Donders & DeWit, 2017). The current study specifically uses the ‘Global Executive Composite’ T-score (GEC; $M=50$, $SD=10$), with higher scores representing greater difficulties in behavioural EF (measured in TBI $n = 52$, controls $n = 32$). By using two differing measures of EF (performance-based vs behavioural/parent report) we are able to assess concordance of our results across multiple measures.

5.3.5.1 Central Executive Network (CEN)

The DDI represents the divergence of a subject’s morphology from the typical SC network across all cortical nodes/ROIs. However, this may reduce the signal to noise ratio when looking at associations between DDI and EF, as not all regions may be relevant to subsuming EF. Thus, we also investigated DDI_{inv} and DDI_{age} across a subgraph of the SCN, specifically regions within the CEN. The CEN is a neural network that shows heightened activity during typical tasks of EF (Seeley et al., 2007; Sherman et al., 2014; Thomason et al., 2011). We defined the CEN anatomically as per the Desikan-Killany (Desikan et al., 2006) atlas regions identified in Ryan et al. (2017), which comprised regions of dorsolateral pre-frontal cortex and posterior parietal cortex. Specifically, regions were bilateral caudal and rostral middle frontal gyrus, inferior and superior parietal lobule, precuneus and superior frontal gyrus. These regions have been identified (amongst others) as supporting common EF activation in adolescence and childhood (Horowitz-Kraus, Holland, & Freund, 2016; McKenna et al., 2017) and adulthood (Niendam et al., 2012).

5.3.6 Statistical analysis

All analysis were performed in R (R Core Team, 2016) using the ‘stats’ packages. Analyses were planned a-priori as follows. Due to the non-normal distribution of the DDI metrics, both DDI_{inv} and DDI_{age} were compared between patients and controls from the TBI cohort using a one-tail Mann-Whitney test (with the alternative hypothesis of the location shift of mean DDI from controls to the patient group is greater than 0). Pearson’s correlations were calculated between DDI measures (both DDI_{inv} and DDI_{age}) and each EF measure EF (EF score and BRIEF). This was calculated for both DDI calculated on the whole network and calculated on the CEN sub-graph. Correlations were calculated for the whole sample, and independently for patient and control groups. The sample sizes for the current study were larger than many current pTBI MRI studies (King et al., 2019) however, we acknowledge that this could still influence statistical analyses. Thus, both resampling approaches and false discovery rate (FDR) correction were used to mitigate these risks. The bootstrapped (100 iterations) 95% confidence intervals (CIs) were calculated for all point estimates of correlation coefficients. Raw p-values calculated using a permutation resampling approach (5000 permutations, calculated using the `jmuOutlier` package in R version 2.2) are reported. Significance was assessed using an FDR correction

(Benjamini & Hochberg, 1995). Results are presented using the ‘ggplot2’ (Wickham, 2009) and ‘ggpubr’ (Kassambara, 2018) packages.

5.3.6.1 Post-Hoc Analyses

A number of analyses were conducted post-hoc to assess the robustness of the approach. Firstly, split-half analyses were conducted to assess the internal reliability off the DDI_{inv} across different subsets of the normative reference group. Briefly, the ABIDE dataset was randomly split into two groups ($n=164$ & 163) and DDI_{inv} was calculated for all pTBI patients using both the 1st and 2nd halves of the ABIDE sample and the Pearson’s correlation between these is reported. This was repeated for 500 random split halves. Additional comparisons investigated whether DDI_{inv} and DDI_{age} differed as a function of injury severity. To maintain statistical power, mild-complex, moderate and severe injury classifications were grouped into a ‘Moderate/Severe’ group for comparisons. Clinical presentation between injury severities is very different and thus treating the patient group as a single cohort in patient vs control analyses of the divergence index may miss clinically meaningful differences. Finally, partial correlations (Pearson’s) were conducted between whole-brain DDI_{inv}/DDI_{age} and EF/BRIEF whilst controlling for age at scanning (yrs), to control for potential age-related biases in these measures and also simultaneously controlling for both age at scanning (yrs) and the interval between MRI and EF assessment (days).

5.4 Results

5.4.1 Age-invariant Network and DDI_{inv} .

Median DDI_{inv} for the TBI and control group were $5.16e-05$ (min = $1.08e-05$, max = $8.47e-04$) and $3.97e-5$ (min = $1.37e-05$, max = $1.90e-04$), respectively. Violin plots of DDI_{inv} for each group can be seen in Figure 5.1a. The difference of DDI_{inv} from the TBI group compared to the control group was not significantly greater than zero ($W = 1046$, $p = .890$). Given that divergence from the whole-group reference SC network may be due to the difference between age of subjects and the median age of the reference network, we plotted this absolute difference against DDI_{inv} . No apparent relationship was found (in the TBI or control group), as can be seen in Figure 5.1b. No significant association was found between DDI_{inv} and age at injury in the patient group. In terms of association with EF at two years post-injury, DDI_{inv} was significantly negatively correlated with EF performance across the whole sample ($r = -.300$, $p = .009$), but specifically in the TBI population ($r = -.319$, $p = .024$), and not controls. DDI_{inv} was significantly, positively correlated with BRIEF GEC in the whole sample ($r = .277$, $p = .021$). No significant relationships were found with the BRIEF GEC in the TBI group (see Figures 5.1c and d).

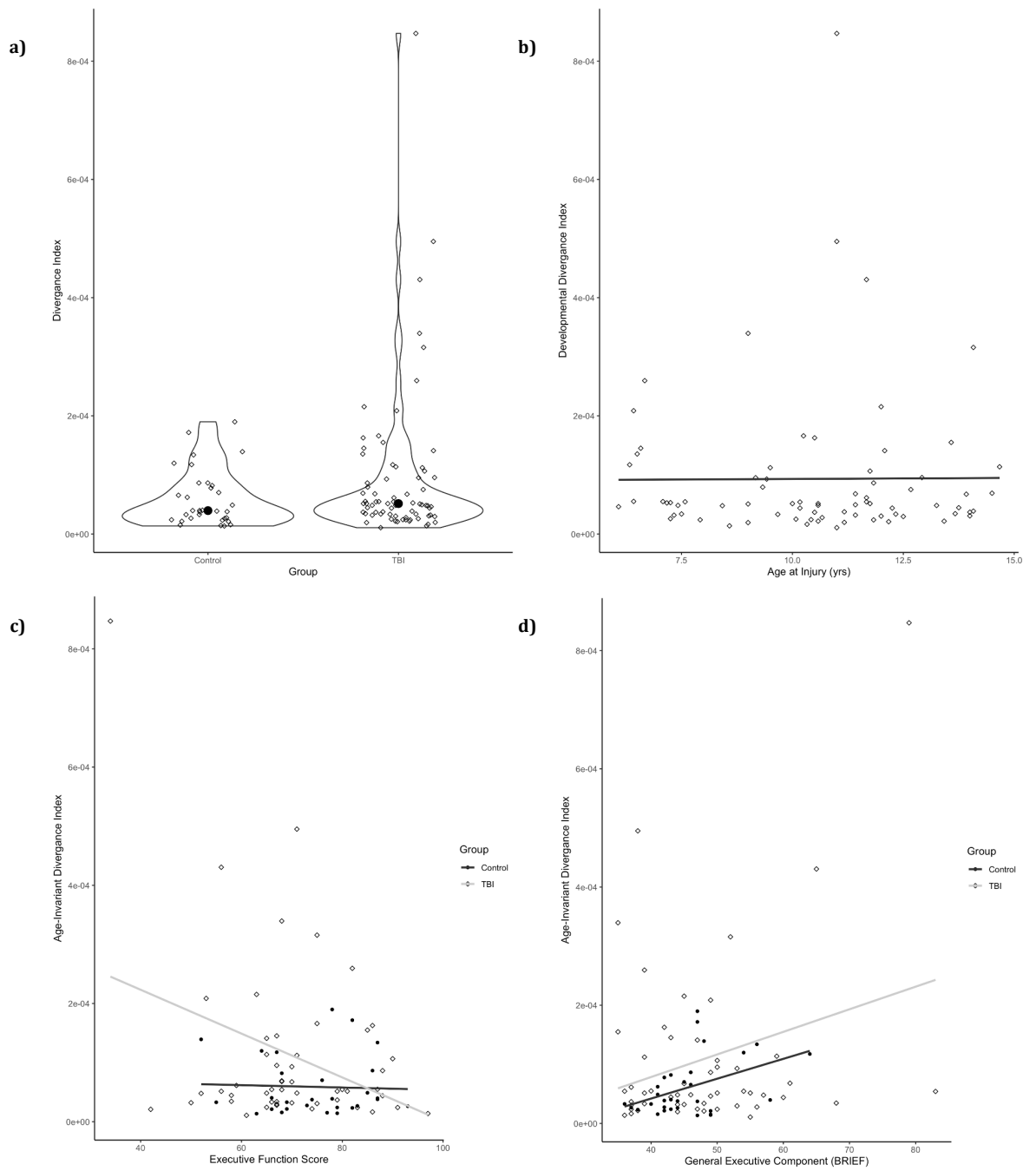


Figure 5.1. a) Violin plots of $DDI_{inv.}$ for both TBI and control groups, b) correlation between age at injury and $DDI_{inv.}$, and correlations between EF and $DDI_{inv.}$, specifically c) executive function score and d) BRIEF GEC, for both the TBI and control groups.

5.4.2 Age-matched Network and DDI_{age}

Median DDI_{age} for the TBI and control group were $4.583e-03$ (min = $9.75e-04$, max = $7.33e-02$) and $4.14e-03$ (min = $1.38e-03$, max = $1.56e-02$), respectively. Mean absolute difference between age at scanning of the subject and the median age of the window that they were matched to was .30 yrs for both TBI (SD = .50) and control (SD = .43) groups. Violin plots of DDI_{age} for each group can be seen in Figure 5.2a. The difference between DDI_{age} from the TBI group and the control group was not significantly greater than zero ($W = 1181$, $p = .648$). No significant association was found between DDI_{age} and age at injury in the patient group. In terms of association with EF at two years post-injury, DDI_{age} was significantly negatively correlated with EF performance across the sample ($r = -.308$, $p = .007$), and in the TBI population ($r = -.330$, $p = .021$), but not controls. Significant positive relationships were found with the BRIEF GEC ($r = .277$, $p = .021$) but not the TBI or control populations (see Figures 5.2c and 5.2d).

Due to the non-normal distribution of our DDI measures, for visualisation purposes, Figure 5.3 displays the relationship between our DDI measures and the indexes of EF where the log of the DDI variables are plotted, rather than the observed values.

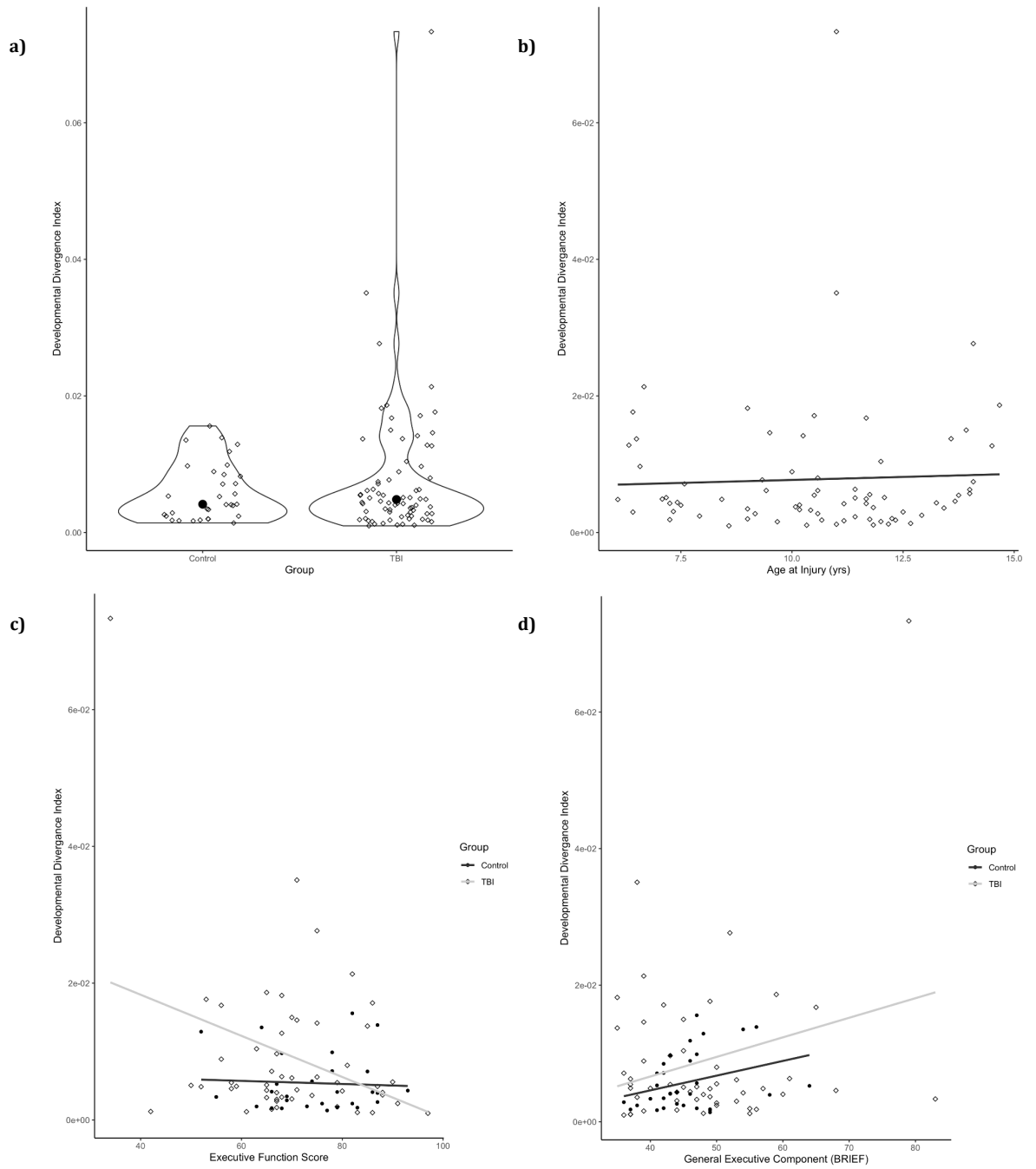


Figure 5.2. a) Violin plots of DDI_{age} for both TBI and control groups, b) correlation between age at injury and DDI_{age} , and correlations between EF and DDI_{age} , specifically c) executive function score and d) BRIEF GEC, for both the TBI and control groups.

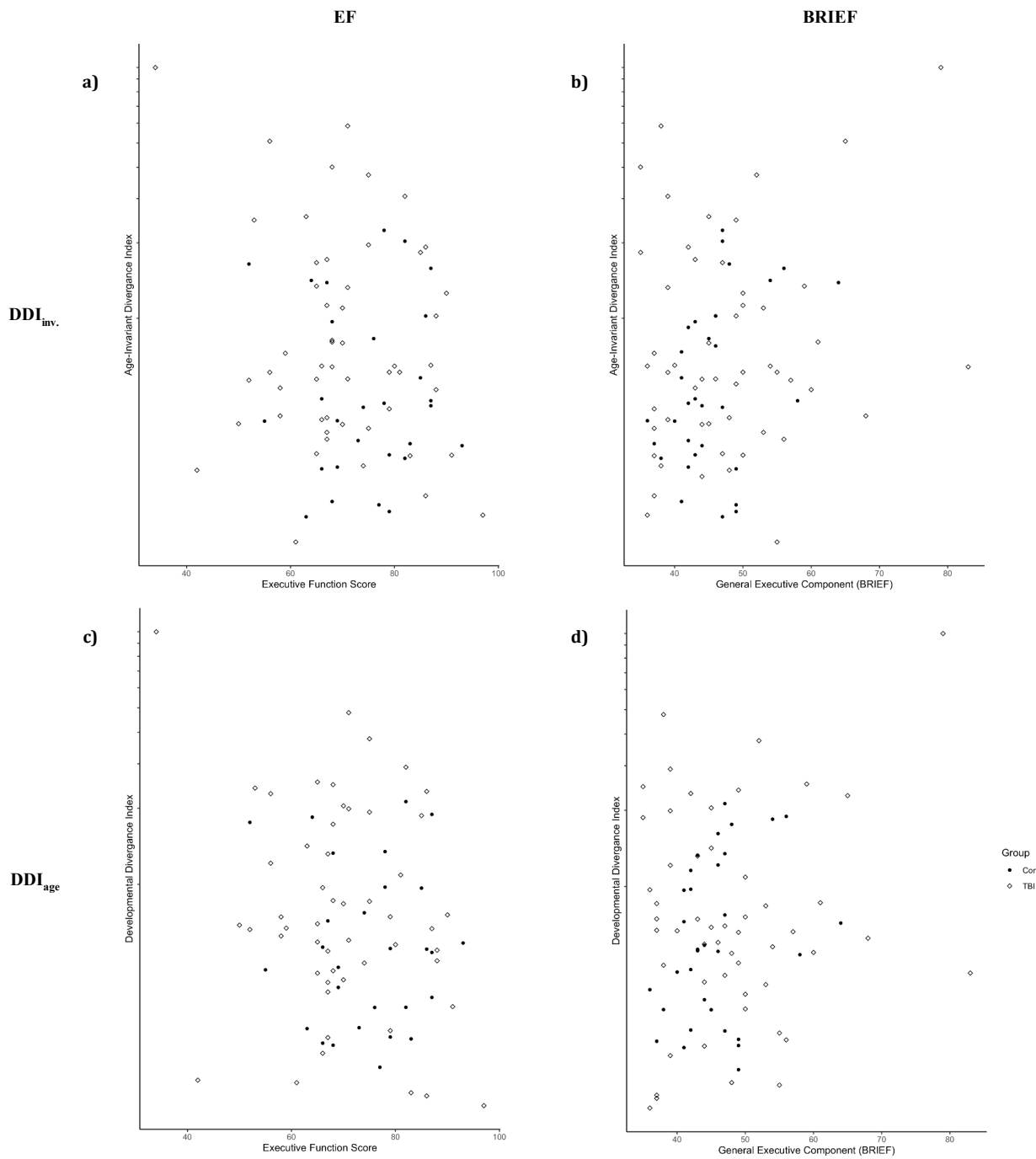


Figure 5.3. Scatter plots of the log of the DDI measures (top row DDI_{inv} , bottom row DDI_{age}) plotted against the EF measures (first column EF score, second column BRIEF)

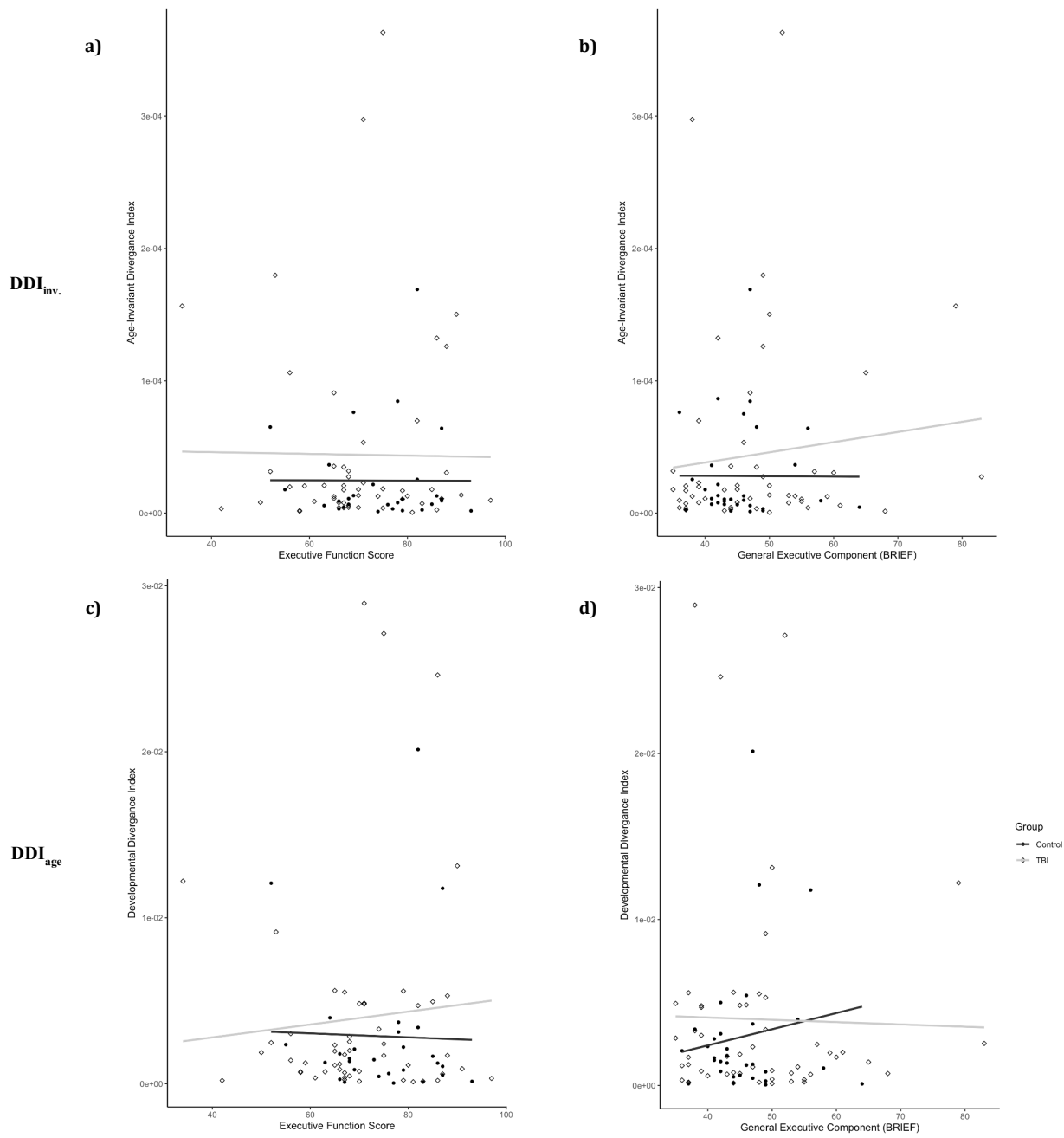


Figure 5.4. Correlation between DDI_{inv} of the CEN, and a) EF and b) BRIEF, and correlation between DDI_{age} of the CEN, and c) EF and d) BRIEF for both TBI and control groups.

5.4.3 DDI of the CEN

When investigating DDI calculated from a subgraph consisting of regions of the CEN, the difference of DDI_{inv} from the TBI group compared to the control group was not significantly greater than zero ($W = 1146, p = .730$). The difference of DDI_{age} from the TBI group compared to the control group was not significantly greater than zero ($W = 1302, p = .335$). For the CEN, across DDI_{inv} and DDI_{age} , no tested association with EF was found to be significant, as seen in Figure 5.4.

5.4.4 Post-hoc exploratory analyses

We conducted post-hoc analyses to assess robustness of these findings. When the DDI_{inv} was calculated using 500 random split halves from the ABIDE data, there was considerable agreement between DDI calculated from the first and second halves of the sample (DDI_{inv} mean pearson's $r = .988$, mean spearman's $\rho = .981$).

For both DDI_{inv} and DDI_{age} , we compared our DDI measure between controls and injury severity groups (mild and moderate/severe). Across the DDI_{inv} and DDI_{age} calculated for both the whole brain and CEN, no significant differences are reported. These results are seen in the supplementary materials (Appendix D). Partial correlations between whole-brain DDI_{inv}/DDI_{age} and EF/BRIEF controlled for multiple factors that may have biased analyses. When controlling for age at MRI, correlation coefficients remained qualitatively similar to those found previously. This was also true when simultaneously controlling for age at injury and interval between MRI and EF assessment. These results are seen in the supplementary materials (Appendix D).

Table 5.3. Pearson's correlation coefficients (r), 95% bootstrapped confidence intervals and associated permutation-based p -values for each group and the sample as a whole

DDI Measure	DV	Regions	TBI Patients				Controls				Whole Sample			
			r	Lower <i>CI</i>	Upper <i>CI</i>	p	r	Lower <i>CI</i>	Upper <i>CI</i>	p	r	Lower <i>CI</i>	Upper <i>CI</i>	p
DDI _{inv}	Age at Injury ^a	Whole Brain	.007	-.203	.168	.956	-	-	-	-	-	-	-	-
		CEN	.054	-.206	.261	.659	-	-	-	-	-	-	-	-
	EF ^b	Whole Brain	-.319	-.589	.085	.024*	-.040	-.388	.322	.839	-.300	-.565	.081	.009*
		CEN	-.011	-.371	.241	.939	-.003	-.428	.337	.987	-.037	-.246	.187	.746
	BRIEF ^c	Whole Brain	.272	-.221	.623	.053	.421	.155	.631	.020*	.299	-.130	.635	.013*
		CEN	.111	-.089	.384	.418	-.004	-.261	.280	.981	.108	-.093	.336	.316
DDI _{age}	Age at Injury ^a	Whole Brain	.041	-.198	.202	.730	-	-	-	-	-	-	-	-
		CEN	.093	-.137	.259	.426	-	-	-	-	-	-	-	-
	EF ^b	Whole Brain	-.330	-.604	.203	.021*	-.054	-.426	.304	.786	-.308	-.563	.082	.007*
		CEN	.077	-.178	.363	.586	-.027	-.564	.339	.893	.035	-.147	.217	.764
	BRIEF ^c	Whole Brain	.260	-.309	.648	.058	.309	.035	.622	.083	.277	-.144	.661	.021*
		CEN	-.023	-.276	.219	.878	.138	-.045	.426	.418	.018	-.150	.206	.865

^a. Cases for correlation is $n = 75$, ^b complete cases for correlation are $n = 52$ for TBI group and $n = 28$ for controls, ^c complete cases for correlation are $n = 52$ for TBI group and $n = 32$ for controls. Upper and lower 95% confidence intervals for the correlation coefficients are calculated using a bootstrap approach with 100 iterations, *CI*s which do not cross zero are highlighted in bold. p values are raw, uncorrected values calculated using a permutation approach with 5000 resamplings.

5.5 Discussion

Previous research suggests a TBI during childhood can result in the deviation of the brain from the typical developmental trajectory (Dennis, Faskowitz, et al., 2017; King et al., 2019; Mayer et al., 2015; Wilde, Merkley, et al., 2012; Wu et al., 2010) and that these deviations may act as a marker of brain health, neurological disorders and cognitive functioning (Cole & Franke, 2017; Erus et al., 2015). We aimed to quantify. The current study utilises a modified version of Saggar et al. (2015) add-one-patient approach, termed the developmental divergence index, to calculate individual-level divergence from the typical SC network (estimated from a large paediatric dataset) for a cohort of patients who have experienced a TBI during childhood. This was a proxy measure of the level of divergence, with greater divergence hypothesised to be associated with poorer functional outcome. For the first time, the current study combined both this measure of divergence with a ‘sliding-window’ approach to generate developmentally-appropriate, age-matched, reference networks.

The current study found significant correlations between an index of divergence, calculated both against a general paediatric reference group but also an age-matched reference group, and executive functioning, measured with both performance and behavioural measures. These were in the expected direction; greater distance from a typical reference network was related to worse executive function skills and increased behavioural-problems related to poor EF. We found these relationships in both the whole sample and the subgroup of TBI patients only and not the control group. These results are in spite of the considerable heterogeneity in the neuropathology which occurs as a result of TBI (Dennis, Babikian, et al., 2017), and the global, whole brain nature of the DDI metric. This may highlight the benefit of considering the broader impact of the injury and subsequent development beyond the individual regions.

The greater strength of association seen in the TBI group is somewhat unsurprising. Whilst in the patient group developmental divergence due to injury is likely to explain much of the variation in EF outcomes, in the control sample, it is likely that other individual differences explain a greater proportion of variance. The magnitude of these relationships between the DDI and EF are small. However, due to the limited sample size, estimating accurate point estimates of the correlation coefficients is difficult, as seen in the confidence intervals listed in Table 5.3. These wide confidence intervals also prohibited investigating whether the correlational relationships were significantly different between controls and TBI patients. Given the brain-behaviour relationships being seen in the whole sample, it is important to tease apart whether the DDI measure represents ‘normative’ development in the TBI group, rather than informing us how neuropathological effects (such as developmental divergence) are potentially disrupting the development of cognitive skills.

However, no significant differences were found between controls and patients within the TBI cohort in estimated DDI, across $DDI_{inv.}$ and DDI_{age} for both whole brain and in the CEN. This was despite optimising our window-size to maximise between group differences (Supplementary materials,

Appendix D). The sample of pTBI patients used for the current study was recruited across all injury severities, from mild to severe, with the majority of cases falling within mild injury. Whilst there is evidence for morphometric change due to injury across moderate to severe injury classifications (King et al., 2019) there is less evidence for this difference in mild injury cases (i.e. Ryan et al. (2017)). We therefore compared DDI metrics between injury severity groups in a post-hoc analyses, and yet no differences were found. Whilst there are no significant group differences in DDI, even at this very early stage post-injury, the DDI measure showed predictive validity with regard to executive functions. It is important to note the timings of both the MRI (<90 days post-injury) and neuropsychological assessment (24 months post-injury). The existing literature shows that neuroanatomical changes that occur post-injury persist over time (King et al., 2019). Given this, and the fact that we are still able to find these significant relationships (despite their weak magnitude) between relatively acute neuroanatomy and chronic functional outcome, one explanation is that these acute changes to the brain in response to injury, seemingly have a persistent effect which may guide the subsequent neurodevelopment required to subsume these executive functions. However, it is important to remember the evidence presented here is not causal in nature, but it does provide strong grounds upon which to further explore these relationships in independent cohorts. Overall, the current study shows that early imaging can assist in prognosis for cognition and therefore guide early intervention planning.

Cognitive-skills are particularly vulnerable to dysfunction due to damage during the period of skill-maturation (Ewing-Cobbs et al., 2004; Krasny-Pacini et al., 2017). Thus, the protracted development of EF (Diamond, 2013; Friedman et al., 2016; Perone et al., 2018) is likely to result in an extended window of vulnerability of EF to brain insult (Krasny-Pacini et al., 2017). Mechanistically, this vulnerability is likely due to damage within still-developing brain networks that subsume EF development (Khundrakpam et al., 2013). Essentially, a key principle is that, developmental processes happening at the time of insult are those which are the most vulnerable (Spencer-Smith & Anderson, 2009).

SC has an ongoing developmental trajectory throughout the neonatal period, childhood and adolescence (Alexander-Bloch, Raznahan, et al., 2013; Fan et al., 2011; Khundrakpam et al., 2016; Khundrakpam et al., 2013; Raznahan, Lerch, et al., 2011; Váša et al., 2017), and SC across association-cortex networks such as those supporting EF has a yet more protracted development (Khundrakpam et al., 2013). Thus, we investigated whether deviation of SC across regions of the CEN (which are commonly reported as supporting common EF activation in adolescence and childhood (Horowitz-Kraus et al., 2016; McKenna et al., 2017)), was related to executive dysfunction. The fronto-parietal regions included in the CEN are commonly affected by pTBI (King et al., 2019; Wilde et al., 2005), likely due to unique biomechanics of injury in the context of the paediatric brain (Pinto et al., 2012). Also, cross-sectional differences in cortical CT with significant correlations between CT of frontal brain regions and BRIEF (Wilde et al., 2012). Despite these findings, divergence from the age-appropriate SC in the CEN was not associated with later EF. Overall, our findings support previous conclusions that the integrity of development in

the entire brain is necessary for achieving age-appropriate, intact EF (Anderson et al., 2010), rather than early vulnerability due to specific damage to the networks that subsume EF development (Anderson, 2002). Taken together, these findings underscore the importance of considering metrics of connectivity when attempting to understand how brain insults impact on functional outcomes in a developmental context.

We used a composite measure of EF scores to explore structure-function relationships and this may contribute to the patterns of results reported. We adopted this approach to mitigate the relatively small sample size and the need to preserve statistical power. Thus, we were unable to investigate these skills with more granularity by examining discrete sub-components of EF. Such an approach would enable us to uncover whether regional / network deviations explain variance in specific EF impairments and future research should consider these more complex relationships. This is especially important given the variability in the age at which these different sub-domains of functioning (i.e. inhibitory control) come on-line during childhood (Miyake et al., 2000) and thus may differentially ‘react’ at different ages at which the injury occurs.

If we make the assumption that there are critical periods of vulnerability to the mechanical and pathological effects of injury then we might assume that greater divergence may be seen at one age versus another (Anderson et al., 2011; King et al., 2019). This may be due to the effects of injury differentially interacting with the myriad of developmental process that occur at different points throughout childhood brain development. Interestingly however, we found no linear relationship between age at injury and our proxy measure of brain perturbation. This is inconsistent with the idea of critical-periods of vulnerability, with no age at injury showing greater propensity to greater developmental divergence. Previous research investigating potential ‘age at injury’ effects post-TBI, do not primarily consider the magnitude of the perturbation the brain post injury (i.e. Resch et al. (2019)). Thus, the current research opens up new opportunities in this area, offering a quantitative measure of brain perturbation (the DDI) by which we can investigate the individual and potentially interactive effects of both age at injury and magnitude of injury. This will better inform our understanding of critical-periods of vulnerability to TBI.

Generating an SC network allows the investigation of population-level covariance in neuroanatomy (Alexander-Bloch, Raznahan, et al., 2013). The individual contribution metric (proposed by Saggat et al. (2015)), enables an estimate of the distance of a patient from a group-level, reference SC network, to allow subject-level analyses. Previous studies show that greater divergence from the ‘typical’ SC network is related to worse neuropsychological performance (Saggat et al., 2015; Watson, 2016a).

In the context of the current study of pTBI, we ‘rebrand’ this metric as a measure of ‘developmental divergence’. This focus is primarily based upon our approach adopting a novel analytic framework whereby we use developmentally-appropriate control groups to calculate a reference network for the

typically-developing SC network, using a sliding window approach. With the advent of large-scale, publicly-accessible neurodevelopmental studies such as ABIDE (Di Martino et al., 2014), ABCD (Casey et al., 2018) and HCP-development (Somerville et al., 2018) we are able to better understand the normative variation in brain development across age. The current study capitalised on this by calculating age-appropriate reference networks using MRI of typically-developing children from the ABIDE dataset.

The benefits of this are two-fold. Firstly, the variance of age within the window still allows us to better capture typical developmental variance within age bands, which here means that our reference groups from the ABIDE data captures variation due to individual differences in morphometry. By using discrete windows, which act similarly to age-bins, we also account for non-linearity in the changes to the SC network over time, as opposed fitting a continuous/linear reference trajectory. Previous studies have used a single control group to calculate Saggat et al.'s (2015) individual contribution metric, potentially conflating 'normal' differences due to discrepancies in age between the participant and the reference network with what is proposed to be pathologically-related divergence.

However, there is a limited number of cases at much younger ages in ABIDE. Thus, estimation of the DDI at these younger ages may be less reliable. A further limitation of the window-based approach is the small number of subjects with which each window was constructed ($n = 26$), given the size of the correlation matrix being estimated (68x68). The size of this window was selected empirically, based on maximising the between group-difference and the recommendations of Saggat et al. (2015). Future research could use a larger reference group to allow 'denser' age-windows to be generated with more subjects. However, this could result in the 'mean' network generated from the age-matched window being highly robust to the addition of new participants, and thus, based on the addition of the patient (AOP), the distance between R_{cont} and $R_{cont + Pi}$ would be minimal, and the DDI measure is therefore likely to scale with the size of the reference group. This makes between study comparisons difficult.

We posited that deviation from a developmentally-appropriate reference group represents developmental-divergence and that in the context of a preceding brain injury, this reflects a negative perturbation or abnormality of expected brain development at a macroscopic-level. However, compensatory responses to brain injuries may also contribute to observed measurements of developmental divergence. The potential capability of the brain to experience adaptive or compensatory morphometric change, due to mechanisms such as neural plasticity, could potentially lead to restitution of function (Anderson et al., 2011; Bigler & Wilde, 2010). Therefore, one potential limitation of the DDI methodology is that it fails to disentangle change due to pathology and that which is compensatory and assists in recovery. Because MRI scans were conducted acutely (<90 days post-injury), divergence from typical morphometry, at this stage post-injury, is likely to be related to injury mechanisms, rather than recovery mechanisms. However, previous research observes both a persistent morphometric difference from controls, even at 10 years post-injury (Beauchamp, Catroppa, et al., 2011), but also an

ongoing neurodegenerative effect of injury (Keightley et al., 2014), typically related to worse cognitive performance (King et al., 2019). Therefore, we believe that the majority of variance in DDI is due to injury-related change. Future research may also investigate DDI pre- and post- neurorehabilitation, in order to investigate the role of divergence from typically-developing reference groups as a potential indicator of positive divergence supporting recovery of function. Differences in pre-processing steps used in our own experimental sample and that of the ABIDE reference group may influence the pattern of findings we observed. The ABIDE data was pre-processed using Freesurfer version 5.1 whilst our data was processed using the newer 6.0 release. Previous studies (and the Freesurfer developer community) recommend not comparing morphometric results between versions, with significant differences in measures being found for the same MRI scans (Chepkoech, Walhovd, Grydeland, Fjell, & Neuroimaging, 2016; Gronenschild et al., 2012). However, these differences will be systematic across all participants, in which case the DDI measure will comprise of a combination of systematic version-error and the ‘true’ divergence. Also, no direct comparisons have occurred between the morphometric measures calculated on different versions. The SC networks were produced from the inter-correlations of these measures and then these SC networks are then compared, rather than the raw data. Future research may wish to consider this as a potential area of concern needing greater study.

5.6 Conclusions

We calculated individual-level divergence from the SC network (estimated from a large paediatric dataset) for a cohort of pTBI patients and found an association whereby greater divergence from the normative SC network was related to poorer executive functioning two years later. By investigating the CEN we took a neural-systems perspective to cognitive dysfunction, on the assumption that ‘damage’ to the network of regions supporting EF will relate to executive dysfunction (Anderson, 2002). However, the lack of correlation between CEN DDI and executive dysfunction in the TBI group highlights the nuanced role of immature networks subsuming neuropsychological functioning in childhood and that whole-brain integrity is required for age-appropriate EF abilities.

We propose that the DDI of the whole cortex may provide unique insights into the effects of brain injury on typical neurodevelopmental outcomes following early life brain injuries, and could be used in predictive models that seek to identify more accurately those children at greatest risk of long-term difficulties.

Chapter 6. Clinically-Feasible Brain Morphometric Similarity Network Construction Approaches with Restricted Magnetic Resonance Imaging Acquisitions and their Relationship with Cognition

6.1 Overview

In **Chapters 4 & 5**, structural covariance methodologies were utilised to model sMRI data post-TBI as a complex network, allowing the inference of potential network-level, neuropathological mechanisms related to executive dysfunction post-injury. However, these methodologies operate at the group level, and the individual-level DDI metric is limited to a more global understanding of the network. In the current chapter morphometric similarity networks were adopted as a potential individual-level equivalent to structural covariance. The current chapter conducts a validation of this approach, specifically investigating an adaption where only sMRI data is utilised and assess the MSN methodology for use within a pTBI cohort, where multiple sequences, with long acquisition times are unfeasible. Overall, it is concluded that methodologies to generate morphometric brain networks at the individual level are still suitable when only T1w MRI images are used to index brain morphometry. A version of the current work has been submitted to a journal as follows;

King, D. J. & Wood, A. G. (Submitted). Clinically-Feasible Brain Morphometric Similarity Network Construction Approaches with Restricted Magnetic Resonance Imaging Acquisitions and their Relationship with Cognition. *Network Neuroscience*.

and a preprint is already available here;

King, D. J., & Wood, A. (2019). Clinically-Feasible Brain Morphometric Similarity Network Construction Approaches with Restricted Magnetic Resonance Imaging Acquisitions and their Relationship with Cognition. <https://doi.org/10.31234/osf.io/vks3u>.

DJK and AW contributed to the conception and design of the current study. DJK wrote and performed analyses and then wrote the first draft of the manuscript. Both authors contributed to the revision and review of the manuscript.

6.2 Introduction

Cortical grey-matter (GM) structural covariance (SC) networks model the degree to which the morphology of brain regions (measured by a single morphometric feature, cortical thickness (CT) or volume for instance) statistically co-varies across all possible pairs of regions of interest (ROIs; (Alexander-Bloch, Giedd, et al., 2013; Alexander-Bloch, Raznahan, et al., 2013; Evans, 2013; Mechelli et al., 2005). Whilst these types of networks represent region to region similarity of GM region metrics rather than causal interactions or tracked anatomical connections (Zheng et al., 2019), they are built on the premise that regions which are morphometrically similar across these structural features are more likely to be anatomically connected (Goulas et al., 2017; Wei et al., 2019). These whole-brain network

approaches to morphometric data, within a graph theoretic framework (Bullmore & Sporns, 2009), allow us to investigate additional information beyond that which is offered by univariate, local approaches (Bullmore & Sporns, 2009; Pagani et al., 2016).

The potential role of disruption to the SCN to understanding functional outcomes has been explored within a graph theoretic framework in relation to a range of conditions. These include broad psychiatric diagnoses such as bulimia, depression and schizophrenia (Chen et al., 2017; Mak, Colloby, Thomas, & O'Brien, 2016; Palaniyappan, Park, Balain, Dangi, & Liddle, 2015; Tijms et al., 2015; Westwater, Seidlitz, Diederer, Fischer, & Thompson, 2017), neurodegenerative disorders, such as Alzheimer's disease (AD) and multiple sclerosis (Kim et al., 2016; Pereira et al., 2015; Pereira et al., 2016; Raamana, Weiner, Wang, Beg, & Alzheimer's Disease Neuroimaging, 2015; Tewarie et al., 2014), epilepsies (Garcia-Ramos et al., 2017; Sone et al., 2016; Yasuda et al., 2015) and autism spectrum disorders (Balardin et al., 2015). In all of these studies, the methodology requires multiple participants to sample enough cortical measurements to generate a correlation between all possible regional pairs. Thus, this framework approach generates group-level brain networks, expressing population-level covariance in neuroanatomy (Alexander-Bloch, Raznahan, et al., 2013). This limits the ability of these approaches to quantify network- and system- level deficits within individual patients, which would benefit stratified diagnosis and prognosis (Zheng, Yao, Xie, Fan, & Hu, 2018).

Existing methodological approaches have attempted to investigate these structural relationships between regions at the individual-patient level (i.e. (Kim et al., 2016; Kong et al., 2015; Kong et al., 2014; Tijms et al., 2012; Yu, Wang, et al., 2018)). The majority of these methodologies have two major limitations; they either divide ROIs into sub regions that do not respect the underlying structure and convolutions of the cortex (Tijms et al., 2012), or the edge weights are defined as the simple subtraction of the feature in region A minus region B, rather than covariance. Both of these methodological deviations represent marked changes to the SC paradigm under which many of the previous SC network validation studies have operated, potentially limiting the validity of these studies.

An alternative approach to investigate the covariance structure between multiple morphometric features can provide individual-level networks of covariance. Morphometric Similarity Networks (MSNs; Seidlitz et al. (2018)) estimate meso-scale organisation of the cortex as a biologically meaningful set of similarities between anatomical properties at both the macro- and micro- structural level (Morgan, Seidlitz, et al., 2018). This is achieved through combination of features derived from a large set of imaging sequences, which may not always be possible in clinical settings. Data include morphometry measurements (such as CT, volume, curvature etc from T1w structural MRI), tissue diffusion properties (such as fractional anisotropy (FA) and mean diffusivity (MD) from diffusion-weighted images) and myelination indices (i.e. magnetization transfer from a multi-parameter mapping sequence or T1w/T2w ratio).

MSNs have been shown to be clinically useful, predicting ~40% variance in IQ, as well as being biologically meaningful, with edges of the MSN highly aligned with gene co-expression between regions in human data and with axonal tract tracing data in the rhesus macaque (Seidlitz et al., 2018). These findings likely reflect the fact that cortical regions that are less cortically differentiated from one another (that is, more anatomically similar) are more likely to also be anatomically connected (Goulas et al., 2017; Wei et al., 2019). Given the alignment between MSNs and other biological networks, these networks represent a new imaging phenotype that may provide additional biologically relevant information beyond existing network approaches.

MSNs have already been utilised in a small number of studies in clinical populations. For example, Morgan, Seidlitz, et al. (2018) used the multi-feature (GM volume, surface area, CT, Gaussian curvature, mean curvature, FA, and mean diffusivity) network approach using both T1w and DWI MRI and found a robust and replicable pattern of differences in cortical grey-matter networks for patients with psychosis compared to controls. Galdi et al. (2018) used a similar multi-feature model with macrostructural (volume and T1/T2 ratio) and multiple microstructural features (diffusion tensor-derived metrics and Neurite Orientation Dispersion and Density Imaging (NODDI) parameters). They trained a model to predict the post-menstrual age of infants born at term or pre-term. This model was able to detect a dysmaturation of the brain in the preterm infants, consistent with previous findings in similar cohorts. Seidlitz et al. (2019) also used MSNs to empirically test a ‘transcriptional vulnerability model’ of neurodevelopmental disorders of known genetic origin, with anatomical disruptions being spatially associated with regional gene expression within the region of the causal copy number variant. Overall, these findings seem to suggest that MSNs appear to offer a useful and clinically-relevant, individualised imaging phenotype.

Despite these existing clinical applications, it is important to note that multiple, high quality MRI sequences are required to recreate such methodologies. These may not be feasible for all research requirements and/or settings. For instance, in large existing clinical (‘legacy’) cohorts, the availability of this ‘advanced’ imaging may be limited or only a minimal number being consistent across multiple sites for instance. Also, due to the longer acquisition time of these MRI scans (especially DWI), the risk is that these MRI are more vulnerable to being of lower quality due to potential of movement artefacts over time for instance, especially in some paediatric or clinical applications where movement is more prevalent (Rosen et al., 2018).

Subsequently, estimating meso-scale organisation across the cortex based on metrics from a single T1w 3D anatomical MRI, which is quickly and commonly acquired in clinical settings, is attractive to the fields of clinical and developmental neuroscience (Batalle et al., 2018). Both Seidlitz et al. (2018) and Li et al. (2017) estimated morphometric similarity in this way and found the edge weights of these networks to be similar to the multi-modal MSNs ($r = .68$, Seidlitz et al. (2018)), with ‘good’ test-retest reliability in terms of network topology ($ICC = .60$, Li et al. (2017)). However, these networks had

reduced precision in their estimation with greater standard deviation of edge-level weights seen across participants (Seidlitz et al., 2018). Of these previous studies, limited assessment has been conducted of the performance of these methods across characteristics of reliability, consistency with group-networks, biological validity and predictive ability. However, very little attention has been given to directly comparing the performance of models with a reduced number of structural features with which the network is estimated. No previous study has conducted an assessment of the reliability and performance of models across a number of models, each using reduced number of structural features indicative of a more restricted MRI acquisition sequence. These networks using only T1w MRI have already been seen in clinical applications. Zheng et al. (2019) generated networks using seven morphological features from T1w MRI. These networks were used to predict classification of ASD and controls. A machine learning approach using individual morphological features produced near-chance prediction accuracy, however, utilising only connection-weights from multi-feature networks there was a significant improvement in the model's prediction. Zheng et al. (2018) conducted a similar classification task and found that multi-feature MSNs classify patients with AD and mild cognitive impairment against controls, with a very high accuracy (~96%).

However, without an evidence-based comparison of MSNs constructed from only T1w MRI features and those constructed from a wider selection of MRI acquisitions, it is unclear as to whether the addition of added MRI sequences would necessarily lead to more reliable estimates of the network. If this were the case, then one would also posit that the increased reliability of morphometric similarity estimation would better position MSNs as a biomarker of brain structure, with less measurement error, and thus provide better prediction than simpler, T1w only models such as those in Zheng et al. (2019) and Zheng et al. (2018).

Recent research has shown that multi-feature MSNs are biologically meaningful and have potential clinical applicability, but MSNs generated with T1w features may be more amenable to certain patient groups/samples. The current study aimed to determine whether reduced-feature approaches approximate the 'original' MSN model as a potential tool to investigate brain structure. We extended previous investigations of reduced-feature MSNs by comparing not only T1w-derived networks, but additional MSNs generated with fewer MR sequences to their full-acquisition counterparts. No previous work has specifically investigated three MSN models, each using fewer metrics from a reduced number of specific MRI scan acquisitions, assessing a number of replication properties. These models were hierarchically organised, with reduced acquisition complexity from model a) to c) seen below;

- a) MSN (T1w + T1w/T2w ratio + DWI; ten-features (MSN_{10-feat.})),
- b) MSN (T1w + T1w/T2w ratio; eight-features (MSN_{8-feat.})),
- c) MSN (T1w; seven-features (MSN_{7-feat.}))

Model a), hereto referred to as $MSN_{10\text{-feat.}}$, is the best approximation of the Siedlitz (2018) approach, with magnetization transfer replaced with T1w/T2w ratio mapping (Glasser & Van Essen, 2011) in the current study. Thus, for each participant, three connectivity matrices (one per model) were estimated, across multiple thresholds. We predicted that, for each measure of reliability/replicability, performance would be ordered in a hierarchical fashion, with $MSN_{10\text{-feat.}}$ outperforming $MSN_{8\text{-feat.}}$ which subsequently outperforms $MSN_{7\text{-feat.}}$. However, we also predicted that between model comparisons would suggest that the models themselves were highly similar. We also predicted that we would conceptually replicate previously found associations between cognition and MSN organisation (Siedlitz et al., 2018) and that we could generalise this finding to a novel domain of cognition, specifically executive functioning.

6.3 Materials and Methods

6.3.1 Participants - HCP data

The current study uses open access, 3T MRI data provided by the Human Connectome Project (Van Essen et al., 2013), shared via ConnectomeDB (<https://db.humanconnectome.org>) under the HCP1200 and HCP Test-retest release. Favourable ethical approval for the secondary analysis of this data was granted by the Aston University ethics panel.

6.3.1.1 HCP 1200 Release

The HCP 1200 release contains data from $n = 1206$ subjects (550 Males, 656 Females). Subjects are grouped into age bins from '22-25' to '36+' (median age = 26-30). Whilst $n = 1206$ subjects provided behavioural data, only 1113 subjects had MRI data available. These were the subjects for which data was accessed and downloaded from ConnectomeDB for the current study.

6.3.1.2 HCP Test-Retest Release

For 46 subjects from the HCP-1200 release, a second 'retest' dataset is available to assess test-retest reliability of analyses. These second MRI visits occurred within time bins from '1-2 months' to '11 months' post initial scanning session. The median retest-interval bin was '5 months'. Of these subject 45 had available MRI data, and these were the subjects used for subsequent analyses.

6.3.2 Methods

6.3.2.1 Data Quality Control

Subjects were selected for inclusion if, in the 1200-subject HCP release, they had T1w, T2w and diffusion data uploaded. This led to exclusion of $n = 76$ cases.

Also, utilising QC data shared by the HCP project, any data labelled as with QC issue code B (which flags cases as having focal segmentation and surface errors when the corresponding Freesurfer outputs

were checked) was further excluded from the current study ($n = 33$). The final dataset consisted of $n = 1004$ subjects. In the test-retest cohort, only one subject was excluded as flagged with QC issue B by the HCP project.

6.3.2.1 MRI Processing

The current study utilises data shared in its pre-processed format, including the output of the HCP Freesurfer pipeline (Fischl et al., 2002; Glasser et al., 2013; Jenkinson, Bannister, Brady, & Smith, 2002; Jenkinson, Beckmann, Behrens, Woolrich, & Smith, 2012), processed DWI (gradient non-linearity, eddy-current and EPI distortion corrected (Andersson, Skare, & Ashburner, 2003; Andersson & Sotiropoulos, 2015, 2016), and calculated T1/T2w ratio myelin maps (Glasser & Van Essen, 2011). For further details of HCP processing pipelines see Glasser et al. (2013).

Once cases were selected, measures indexing underlying neuroanatomical structure were derived from multiple imaging modalities (see Table 6.1). Seidlitz et al. (2018) leverage near-identical MRI-derived metrics for the construction of the MSN network. However, we are using the T1/T2 ratio as a proxy for myelin content, rather than the magnetization transfer scan used by Seidlitz et al. (2018). The rationale for this modification was both pragmatic and clinically-driven; i) the T1/T2w ratio maps are already implemented by the HCP project and thus this data is available for use with the rest of the high-quality HCP acquisition data and ii) in clinical populations, for which the methods may provide greatest benefit, multi-parameter mapping MRI sequences may not be acquired as part of a clinical protocol, whereas T1w and T2w sequences are.

Table 6.1. *Morphometric measures and the modality of MRI from which they were derived*

Modality	Metrics
T1w	Cortical thickness (CT), surface area (SA), mean (extrinsic) curvature (MC), Gaussian (intrinsic) curvature (GC), folding index (FI), curvature index (CI) and grey matter volume (GMV)
T2w	Myelination (T1/T2w ratio)
DWI	Fractional Anisotropy (FA), Mean Diffusivity (MD)

Preprocessed DWI ($b = 1000$) in T1w space were fitted to a tensor model using FMRIB's 'dtifit' function, and the subsequent FA and MD maps were mapped to the individual subject's Freesurfer generated surface model in MNI space, using the connectome workbench (Marcus et al., 2011) function 'volume-to-surface-mapping'. These, and the Tw1/T2w ratio myelin maps, were parcellated based on the Desikan-Killany atlas (Desikan et al., 2006), by generating a dense-cifti (using the 'cifti-create-dense-from-template' function) and parcellating the output (using 'cifti-parcellate'). Freesurfer metrics were also extracted for each parcellated region using the 'aparcstats2table' function.

6.3.2.2 MSN Construction

To generate MSNs we apply the methods of Seidlitz et al. (2018) to the HCP data. The Desikan-Killany atlas was mapped to the individual subjects with a surface-based registration, using the Freesurfer pipeline. The Desikan-Killany atlas ROIs were used as the nodes for all network construction (Desikan et al., 2006).

Morphometric features (parcellated to the Desikan-Killany atlas) for each participant can be expressed as a set of n vectors of length 10, with each vector as a different anatomical region ($n = 68$), and each element of the vector a different morphometric measure. However, these features are not all measured at the same magnitude of scale. For instance, volume (mm^3) is measured at the order of 10^3 , whereas folding index is measured to the order of 10^1 . Thus, to normalize within this length 10 vector, each of these morphometric features is normalized across the 68 regions, using Z-scores (demeaned and SD scaled). This brings the measures across the feature vector into a comparable range.

Using the normalized features, a correlation matrix is generated for each participant, where each element of the matrix is the correlation between the feature vectors for every possible pairwise combinations of regions. Because each feature is zero-centred, the resultant distribution of correlation coefficients is normally distributed about zero. This correlation matrix represents the MSN-estimated connectivity for each participant. This procedure was repeated across the three MSN models ($\text{MSN}_{10\text{-feat.}}$, $\text{MSN}_{8\text{-feat.}}$, and $\text{MSN}_{7\text{-feat.}}$), each using fewer metrics from a reduced number of scan acquisitions.

6.3.3 Demographic and Behavioural Data

Demographic variables were selected from the unrestricted data table accessed via 'ConnectomeDB'. These included age bin, sex recorded at birth and recorded quality control issues. Behavioural data were also extracted to assess the relationship between the MSNs and both general cognitive ability (measured with both fluid and crystallized intelligence measures) and executive functioning. These neuropsychological assessments were conducted contemporaneously in relation to the MRI scans. Further details of the tasks and measures acquired in the HCP dataset can be found in (Barch et al., 2013).

6.3.3.1 General Cognitive Ability

General cognitive functioning is measured with the Cognitive Function Composite (CogComp) score (Heaton et al., 2014), derived from the average of the normalized, scaled scores of Fluid and Crystallized cognition measures, then subsequently age-adjusted, and scaled. The Fluid Cognition Composite score is derived by averaging the normalized scores of each of the fluid ability measures in the NIH-toolbox (Flanker, Dimensional Change Card Sort, Picture Sequence Memory, List Sorting and Pattern Comparison), whilst the Crystallized Cognition Composite score is derived by averaging the normalized scores of each of the crystallized measures in the NIH-toolbox (Picture Vocabulary and Reading Tests). Higher Cognitive Function Composite scores indicate higher levels of cognitive functioning.

6.3.3.2 Executive Functioning

Behavioural executive function (EF) measures were selected based on an evidence-based, 3-factor model of executive function (Karr et al., 2018); measures selected from the HCP cognitive battery to model EF were the same as previous studies of EF utilising the HCP data (Lerman-Sinkoff et al., 2017; Nomi et al., 2017). These tests assessed multiple cognitive aspects of executive functioning including cognitive flexibility/shifting (Dimensional Change Card Sort test, (Zelazo, 2006; Zelazo et al., 2014)), inhibition (Flanker Inhibitory Control and Attention task, (Zelazo et al., 2014)), working memory (List Sorting task, (Tulsky et al., 2013)). Age-adjusted scores were used for all behavioural data.

Due to the fact we have only one neuropsychological measure per sub-domain of EF and there is therefore potential risk of measurement error, a principal component analysis (using the ‘prcomp’ function in the R ‘stats’ base package (R Core Team, 2016)) was used to find a common EF component across all three EF measures. This produced a single principal component with an eigenvalue above 1, upon which all measures positively loaded onto, and thus this component was used as a ‘summary’ score of EF (see supplementary materials (Appendix E) for further details). Higher summary EF scores reflect greater EF functioning.

6.3.4 Statistical comparison

When comparing weighted networks produced by each model, we use multiple metrics to assess the (dis)similarity of the subsequent covariance matrices.

To reduce number of comparisons and, based on our premise that the $MSN_{10-feat.}$ is the most precise estimation of the MSN network (as shown by Seidlitz et al. (2018)), all inter-model comparisons were done in a hierarchical fashion in comparison to this ‘gold-standard’ network. That is to say that model $MSN_{10-feat.}$ was compared to the $MSN_{8-feat.}$ and then the $MSN_{10-feat.}$ was subsequently compared to the $MSN_{7-feat.}$.

In order to test differences in the topological organisation of the networks produced by each model, we calculate average nodal strength for each graph. Nodal strength is the ‘magnitude’ of structural covariance for each node, this is the sum of the connectivity weights of all edges connected to node i (Fornito et al., 2016). We did not normalize this measure based on number of edges as we averaged the nodal measures over the graph, where the number of edges was consistent across models due to density thresholding. This metric was calculated per subject, per density for each MSN model. For each comparison, we calculate the difference in distributions of graph strength using a paired t-test test. Due to the large number of comparisons (across densities, and contrasts) we do not report p-values, but instead report the effect sizes for comparisons.

We also calculate the Pearson correlation coefficient between all edge weights for both models (as per Seidlitz et al. (2018)), and also specifically between all non-zero edge weights (those elements where a zero is present in the correlation matrix for each model are excluded). However, because of the symmetric, undirected nature of the correlation matrix, this correlation coefficient may inflate/bias the supposed ‘similarity’ between the sets of edge weights. Thus, we also employed the Mantel test, which calculates the Pearson correlation on either half of the off-diagonal elements of the correlation matrix (Mantel, 1967).

To compare the binary networks produced by each model at each density (where edges retained after thresholding are set to 1 and those excluded are set to zero), we assessed the number of edges in the reduced model which replicated as a proportion of the fuller model, as per the following formula:

$$\frac{\sum(x_i \neq 0 \ \& \ y_i \neq 0)}{\sum(x_i \neq 0)}$$

where x_i and y_i represent the correlation matrices estimated from two of the MSN models for a given subject i .

Secondly, we calculate these similarity measures between the subject-level network and the group average network, across all densities and models. This allows the assessment of the inter-subject reliability of the networks being constructed by each model. Thirdly, we similarly test the intra-subject reliability of the produced networks, based on test-retest data from a subset of the overall dataset. Due to the categorical and inaccurate nature of the ‘binned’ measurement of time between initial and retest scan, this was not controlled for in this analysis.

In order to assess the functional relevance of these networks, we assess their ability to predict CogComp and EF scores using a supervised-learning approach, namely partial least squares (PLS) regression (similarly to Seidlitz et al. (2018)) using the ‘plsRglm’ package in R (Bertrand & Maumy-Bertrand, 2018). This multivariate approach finds the optimal low dimensional relationship between a high dimensional set of predictors (in this case the MSN networks) and a univariate predictor variable (either

CogComp or EF). This approach is commonly use when the number of predictors exceeds the number of observations (Krishnan, Williams, McIntosh, & Abdi, 2011).

A PLS regression was used to find the maximal low-dimensional covariance between components derived from the MSN and cognitive outcomes. The PLS regression was used to decompose the predictor variables into latent variables (components) which simultaneously model the predictors and predict the response variable (Krishnan et al., 2011). The predictor matrix consisted of either the degree or strength of each node of the MSN, for each participant. Using a linear model, the potential confounding effect of age, gender and age*gender interaction was regressed out of values for nodal degree/strength (but not our cognitive outcome variable as these were already age-adjusted within the HCP dataset). For each model (at each threshold), a PLS regression model was fitted between principal components derived from the resultant predictor matrix (68 x 991) and the outcome variable. This was repeated across 100 instances of 9-fold cross-validation.

Cross-validated R^2 (R^2_{CV}) otherwise known as the Q^2 statistic (Consonni, Ballabio, & Todeschini, 2010; Stone, 1974), was used to select the number of components to retain in the predictor matrix. Q^2 was defined as:

$$Q^2 = R^2_{CV} = 1 - \frac{PRESS}{TSS} = 1 - \frac{\sum_{i=1}^n (\hat{y}_i - y_i)^2}{\sum_{i=1}^n (y_i - \bar{y})^2}$$

where PRESS is the predictive residual error sum of squares and TSS is the total sum of squares.

The number of components to retain in the predictive model was selected as the number of components which resulted in the greatest Q^2 value. This was repeated over the cross-validations and resulted in a count measure of the number of times a model with a given number of components were selected. Hence the final model was the given number of components which was most commonly selected as having the greatest Q^2 statistic. Given the model with the retained number of components, we report the variance explained by the model and the bias corrected and accelerated bootstrapped (Bastien, Vinzi, & Tenenhaus, 2005) weightings of each predictor. This allows us to assess which brain regions are contributing most to the prediction.

Due to the normal distribution of the cognitive measures (CogComp and EF) data, there may be an issue of class-imbalance for more ‘extreme’ cases (Torgo, Branco, Ribeiro, & Pfahringer, 2015). As there are fewer subjects who fall within the tails of the continuous distribution on our cognition measures, the cross-validation approach may lead to training samples where there are too few ‘extreme’ cases (those with particularly high/low cognitive abilities) to ‘learn’ from. This may result in a model where there is accurate prediction around the mean but not at the tail ends of the distribution. To ensure the training samples contain subjects from stratified sampling approach, we repeated the analyses discretizing the performance on cognitive measures into four discrete bins across the distribution and training a model based on equally-sized, random samples from each bin.

6.4 Results

6.4.1 Inter-model comparisons

6.4.1.1 Magnitude of morphometric similarity: graph-level strength

In terms of the topology of the networks, global graph strength for each model, across densities, can be seen in Figure 6.1. This plot shows the similar trajectories across densities for all models tested, however the observed average graph strength was different between models, with lower strength being seen in the MSN models with greater features. The effect size of differences (estimated with a paired t-test) between $MSN_{10\text{-feat.}}$ vs $MSN_{8\text{-feat.}}$ and $MSN_{10\text{-feat.}}$ vs $MSN_{7\text{-feat.}}$ can be also be seen in Figure 6.1. Effect sizes (r) were extremely large, especially between $MSN_{10\text{-feat.}}$ vs $MSN_{7\text{-feat.}}$.

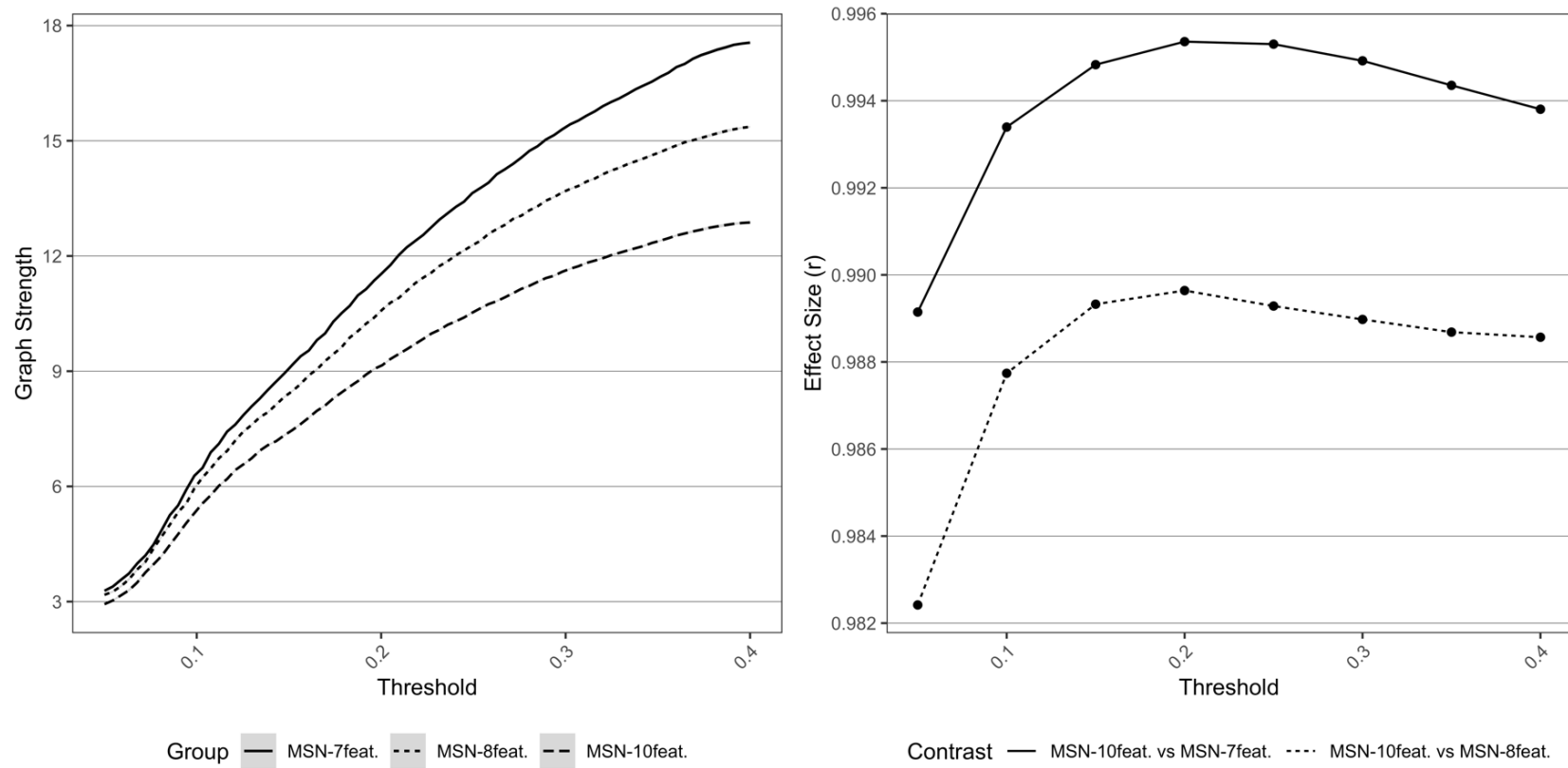


Figure 6.1 Left: *Graph metrics describing average network strength for each MSN model, across all densities. Right: Effect sizes of differences between a) MSN_{10-feat.} vs MSN_{8-feat.} and b) MSN_{10-feat.} vs MSN_{7-feat.} for differing graph metrics, across densities.*

6.4.1.2 Edge Weights

Figure 6.2 shows the inter-model comparisons between $MSN_{10\text{-feat.}}$ and $MSN_{8\text{-feat.}}$, and between $MSN_{10\text{-feat.}}$ and $MSN_{7\text{-feat.}}$. There is a gradual increase in correlation of edge weights across densities with the peak mean correlation being found between $MSN_{10\text{-feat.}}$ and $MSN_{8\text{-feat.}}$ at a 40% threshold ($r(M\pm SD) = .849 (\pm .025)$), with slightly weaker correlations found between $MSN_{10\text{-feat.}}$ and $MSN_{7\text{-feat.}}$ ($r(M\pm SD) = .736 (\pm .031)$). When considering only the non-zero edge weights (only edge weights remaining after thresholding), a slightly weaker peak correlation was found for both contrasts at 5% threshold ($MSN_{10\text{-feat.}}$ vs $MSN_{8\text{-feat.}}$ $r(M\pm SD) = .738 (\pm .053)$; $MSN_{10\text{-feat.}}$ vs $MSN_{7\text{-feat.}}$ $r(M\pm SD) = .670 (\pm .066)$). However, as the threshold increased, the dispersion of individual level non-zero edge correlation decreases, especially in the $MSN_{10\text{-feat.}}$ vs $MSN_{7\text{-feat.}}$ contrast.

When considering correlation coefficients calculated using the Mantel test, similarly strong correlations were found between edge weights across all models however, as predicted, the $MSN_{10\text{-feat.}}$ vs $MSN_{8\text{-feat.}}$ were most similar (At 40% threshold: $MSN_{10\text{-feat.}}$ vs $MSN_{8\text{-feat.}}$ Mantel $r(M\pm SD) = .835 (\pm .028)$; $MSN_{10\text{-feat.}}$ vs $MSN_{7\text{-feat.}}$ Mantel $r(M\pm SD) = .715, (\pm .034)$). For the binarized networks, the proportion of edges replicated also peaked at 40% threshold ($MSN_{10\text{-feat.}}$ vs $MSN_{8\text{-feat.}}$ proportion of replicated edges = 85%, ($\pm 2\%$); $MSN_{10\text{-feat.}}$ vs $MSN_{7\text{-feat.}}$ proportion of replicated edges = 77%, ($\pm 2\%$).

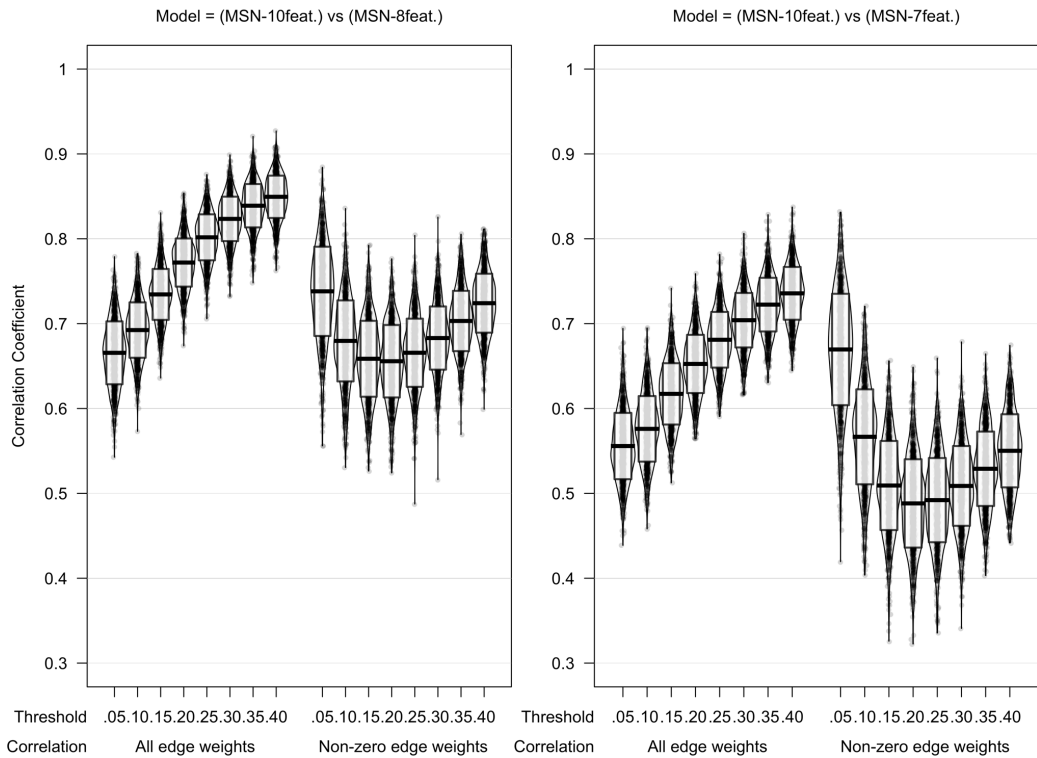


Figure 6.2 Violin plot of correlation of edgeweights between a) $MSN_{10-feat.}$ vs $MSN_{8-feat.}$ and b) $MSN_{10-feat.}$ vs $MSN_{7-feat.}$. Midline of the box-plot component of the violin represents the mean of all correlation coefficients, with the box itself representing the SD of this mean. Individual data points are also plotted.

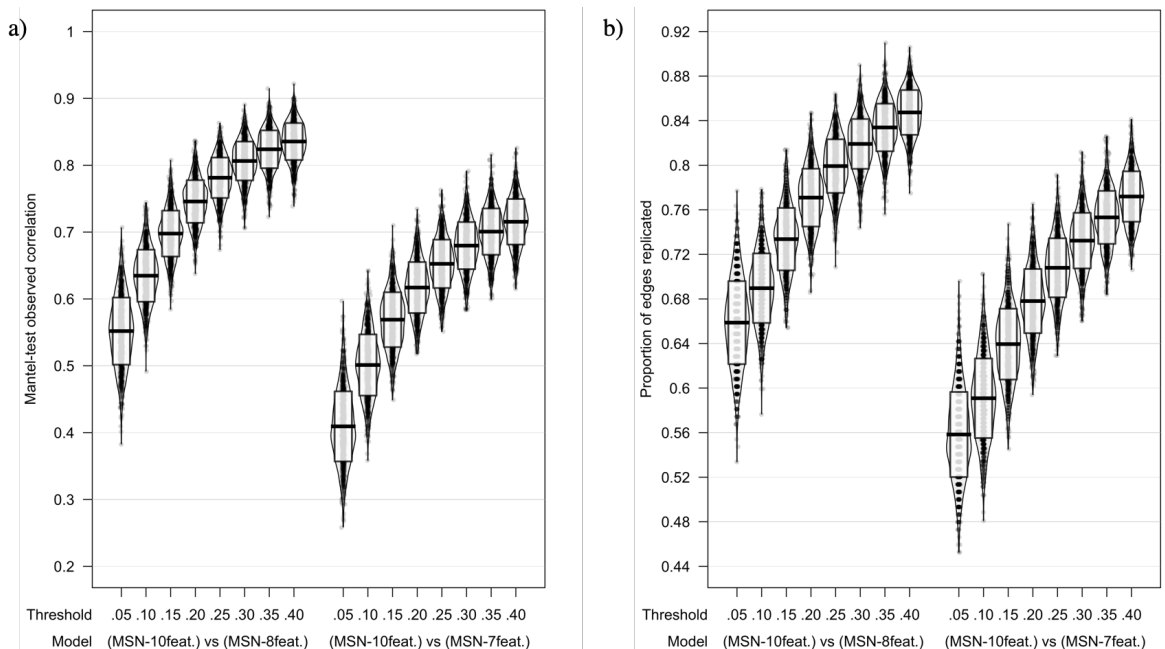


Figure 6.3 Model comparisons across thresholds using a) Mantel-test correlation coefficient and b) proportion of edges replicated as measures of model similarities. Midline of the box-plot component of the violin represents the mean whilst the box itself representing the SD

6.4.2 Intra-model comparisons

6.4.2.1 Test-retest reliability of MSN models

We compared the MSN models at the initial scan with those calculated from test-retest scans acquired between 1 and 11 months after the initial MRI. All models showed high test-retest reliability of the MSN (correlation of all edge weights at 40% threshold: MSN_{10-feat.} $r(M \pm SD) = .902 (\pm .032)$; MSN_{8-feat.} $r(M \pm SD) = .881 (\pm .040)$, MSN_{7-feat.} $r(M \pm SD) = .857 (\pm .043)$). This high test-retest reliability of networks held even when networks were binarized (At 40% threshold: MSN_{10-feat.} proportion of replicated edges = 87 % ($\pm 3\%$); MSN_{8-feat.} proportion of replicated edges = 87% ($\pm 3\%$), MSN_{7-feat.} proportion of replicated edges = 86% ($\pm 3\%$)). See Figure 6.3 for plots.

6.4.2.2 Similarity with average MSN

For each model, at each threshold, a group-level network was produced as the mean of the correlation matrices for all subjects. Across all models (MSN_{10-feat.}, MSN_{8-feat.}, and MSN_{7-feat.}), regardless of similarity metric used, the individual-level MSNs were highly similar to the group-mean network (see Figure 6.4). Interestingly, the MSN_{8-feat.} model showed greatest correlation between edge weights (At 40% threshold: MSN_{10-feat.} $r(M \pm SD) = .843 (\pm .032)$; MSN_{8-feat.} $r(M \pm SD) = .875 (\pm .029)$, MSN_{7-feat.} $r(M \pm SD) = .850, (\pm .031)$). Similar to the inter-model analyses, correlation peaked at the highest threshold tested (40%) for all models.

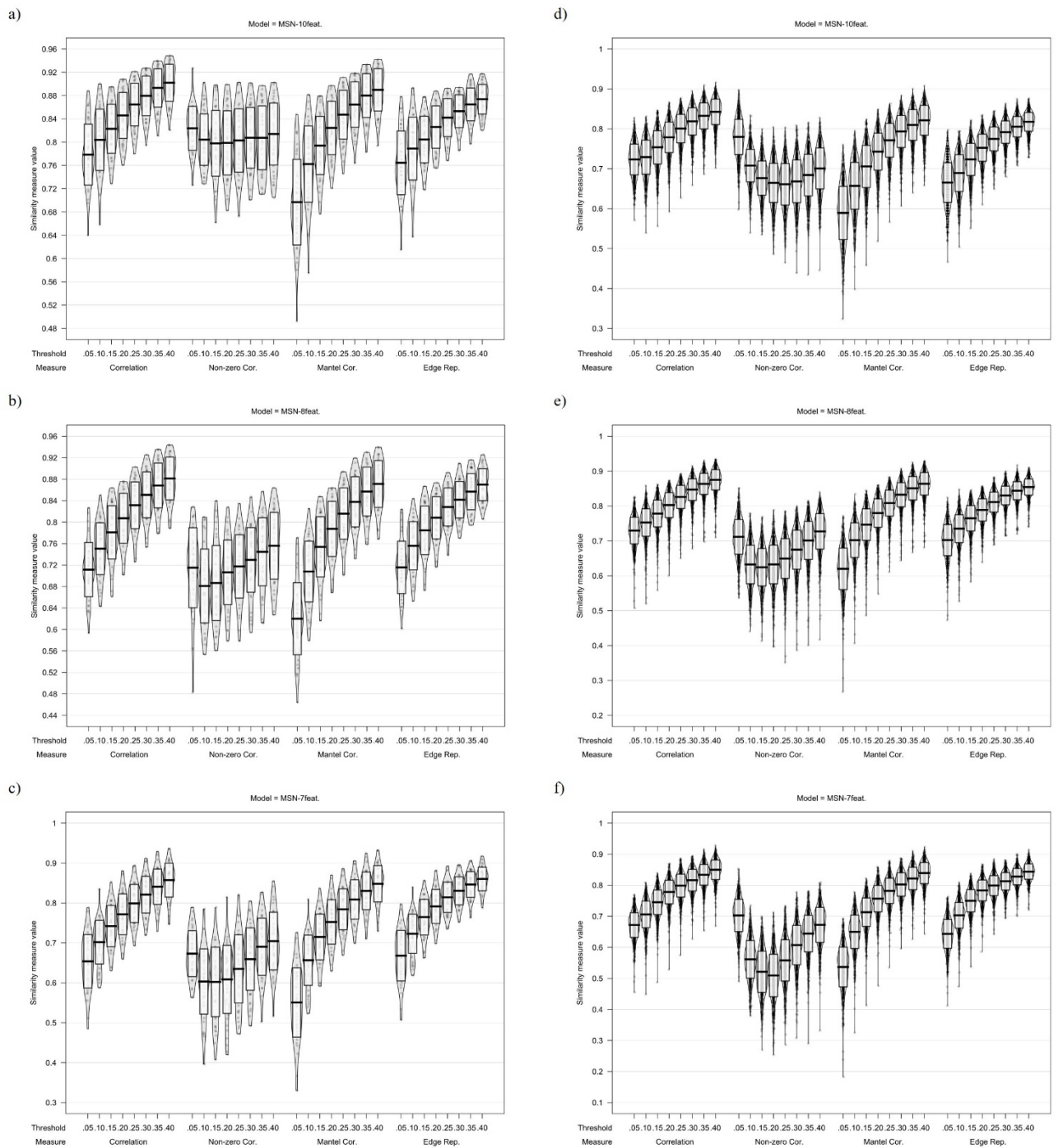


Figure 6.4 Plots showing MSN similarity (across thresholds, with multiple similarity measures) between a,b,c) individual MSNs generated with test-retest MRI scans and d,e,f) individual-level MSNs and the group-average MSN network.

6.4.3 Relationship with cognitive scores

Only participants who had available a full dataset comprising of the three EF subtests and the CogComp measure were included in the following analyses ($n = 991$). For both cognitive variables, using 100 instances of 9-fold cross validation, the greatest Q^2 was found most frequently when zero-components were retained and thus no models were built.

This suggests that no PLS-derived components of nodal degree, strength or normalised strength of the MSN provided greater explanation than the intercept alone. After the stratified sampling of the training cohort, there was no improvement in the result outlined above; cross-validation still recommended retention of zero components for all MSN models.

6.5 Discussion

Within the morphometric similarity network model, we assume that those regions which are high in morphometric similarity have high concordance of cyto- and myelo- architectural features at a resolution unobservable in-vivo with current MRI capabilities (Morgan, Seidlitz, et al., 2018). These cortico-cortico regions which are less cortically differentiated from one another are more likely to be anatomically connected (Goulas et al., 2017; Wei et al., 2019). However, the methods presented here are not causal, they represent the region to region similarity in terms of the GM morphology of the cortex (Zheng et al., 2019). Whilst Seidlitz et al. (2018) and Li et al. (2017) performed some assessment of T1w MSNs, the current study is the first to formally investigate the potential for generation of multiple MSNs based on a reduced number of macro- and micro- structural features dependant on the complexity of the MRI acquisition sequence. We found that the weighted networks generated from these models are highly similar, across a number of correlation measures investigating edge weightings. Overall our results suggest that these meso-scale relationships can be captured (to a considerable degree) within a more limited number of features from a lesser number of MR-sequences.

Seidlitz et al. (2018) investigated the similarity of a T1w MSN (using only 5 morphometric features compared to our 7) with the full $MSN_{10\text{-feat.}}$ model and found a high level of similarity, although the $MSN_{10\text{-feat.}}$ model had a greater level of precision with a lower standard deviation of edge weights. Seidlitz et al. (2018) also did not systematically investigate the consequences of removing MRI acquisitions from the features with which to estimate the MSN model.

In the current study we expanded previous comparisons of T1w MSNs to the ‘original’ MSN model to include multiple MSN models. We found that the between-model similarity was nearly always hierarchical between models, with greater similarity seen between $MSN_{10\text{-feat.}}$ and $MSN_{8\text{-feat.}}$ compared to that between $MSN_{10\text{-feat.}}$ and $MSN_{7\text{-feat.}}$. Weaker similarity was found for sparser networks at a much lower density (i.e. .05). Even when binarized (that is to say the edge weightings were ignored) the replication rates were high, suggesting that the models are sensitive to specific edges within the network.

However, our results show that, in terms of average network strength, the three models differed significantly in their topology. Whilst previous studies had investigated the correlation between nodal similarity for full and reduced models of MSN estimation (Seidlitz et al., 2018), this is the first study to investigate differences in this topology. On average, the magnitude of morphometric covariance across the nodes of the graph are higher when fewer features are used to generate the network. The topology of networks generated from different MSN models is fundamentally different and, dependant on metric used, this difference can be of a large effect size. Hence, as more cytoarchitectural features are added to the MSN, specifically estimated myelin content (T1w/T2w ratio) and macro-structural diffusion properties (FA & MD), regions appear less similar and more differentiated, hence the lower average graph strength. This may be because these features index structural properties which show greater variation, and are more discriminatory between regions, across the cortex. This difference in network topology is important to consider, as it means that network topology between these models is not comparable across studies.

Each model seemed to achieve high-levels of congruence with the group average network, suggesting that we are able to use these methods to index individual differences from a relatively consistent meso-scale phenotype of the structure of the brain. Li et al. (2017) found high levels of test-retest reliability of the T1w MSN, we replicated this and found that each of the reduced-feature MSNs seemingly had similar reproducibility in terms of test-retest MRI.

It is important to consider that none of the models tested in the current manuscript showed perfect or even near-perfect concordance across these measures of performance. These between-model differences may be due to the fact that these models are generated with less features, rather than being specific to the modality of feature being dropped. Beyond the scope of the current paper but could look at this in future by generating MSN with 10, 8 and 7 randomly selected features, irrespective of modality of MRI sequence used to derive said feature. If this is the case, then the ‘gap’ between the $MSN_{10-feat.}$ and $MSN_{7-feat.}$ models could potentially be rectified using software such as ‘mindboggle’ to generate/sample a larger number of morphometric features from the T1w image.

Overall, our findings suggest that, even with a reduced number of structural features, the MSN seems to capture a group-level phenotype of the structure of the brain which shows a reasonable level test-retest reliability. However, whilst these models may capture enough shared variance to be meaningful in a number of fields, it must be considered that the loss of information due to a reduced number of MR-acquisitions may result in a ‘noisier’ measure of the connectivity phenotype being indexed by the MSN approach. This will inherently limit generalisability across findings utilising these methods.

However, the main benefit of the reduced MR-acquisition approaches (specifically the $MSN_{7-feat.}$ model) is the applicability to those populations where multiple MR sequence acquisition is more challenging or difficult. For instance, in clinical populations where research MRI are acquired alongside routine

examination and therefore time is limited, or in developmental populations where acquisition time needs to be kept short in order to ensure child participants can remain still for the length of the scan to ensure the images are free of motion artefact. Estimating morphometric similarity based on metrics from a single T1w 3D anatomical MRI, which is commonly and quickly acquired clinically, is therefore particularly attractive to the field of clinical and developmental neuroscience (Batalle et al., 2018). It also validates these models for use in legacy datasets for instance, where the full array of MRI acquisition sequences required to estimate the ‘original’ MSN were not acquired and are therefore not available. Overall, the current study validates the use of these reduced-feature networks in recent studies estimating cytoarchitectural similarity utilising the MSN (Galdi et al., 2018; Li et al., 2017; Morgan, Seidlitz, et al., 2018; Seidlitz et al., 2019; Zheng et al., 2019; Zheng et al., 2018).

One could argue that one-acquisition connectivity is already available in the form of DWI tractography, or even fMRI resting state connectivity. However, these are still much longer sequences compared to a 3D T1w MPRAGE for instance and therefore face inherent difficulties in the face of clinical realities of restricted time and potentially greater motion. Also, both fMRI and DTI inevitably suffer from a lower signal-to-noise ratio and a greater sensitivity to motion artefacts compared to anatomical MRI (Wang, Jin, Zhang, & Wang, 2016). It could also be argued that, in terms of legacy/existing datasets, it is more likely that a high quality, 3D T1w MRI has been acquired than the specific DWI/fMRI protocol required. Overall, this therefore positions MSNs as a useful in-vivo connectivity phenotype for studying both clinical and developmental populations, with the T1w-only model potentially being of greatest potential benefit.

These approaches have potential utility in these fields of research, with one use being assessing relationships between brain structure and neuropsychological functioning. The current zeitgeist in the field of cognitive neuroscience is that the topological organization of the brain networks (across multiple MR modalities), as quantified within a graph theoretic framework, captures physiologically relevant information (Bullmore & Sporns, 2009; Fornito, Zalesky, & Breakspear, 2013; Hahn, Lanzenberger, & Kasper, 2019). However, a recent study failed to replicate one of the most prominent findings for the field relating resting-state fMRI connectivity to fluid and crystallized intelligence in the HCP dataset (Kruschwitz, Waller, Daedelow, Walter, & Veer, 2018). The current study investigated this by assessing the relationships between cognition and organisation of the MSN models.

We assessed the predictive validity of the MSN models in the current study by comparing the predictive validity of the three MSN models in relation to general intelligence, with previous research suggesting the organization of the MSN network (modelled similarly to the MSN_{10-feat.}) was able to predict ~40% variance in WASI IQ (verbal and non-verbal, (Seidlitz et al., 2018)). We were unable to replicate the predictive validity of the MSN with regard to general cognitive functioning or generalize previous relationships to a novel domain of cognitive functioning (in this case executive functioning). Our results

showed that, when using 9- fold cross-validation, no model (at any density) recommended retention of any PLS components.

One important strength of the current study is the fact that we used a quantitative methodology of cross-validation to validate retained number of components whereas previous studies have retained either a single or two components which explains the greatest amount of variance (Seidlitz et al., 2019; Seidlitz et al., 2018). This may mean that previous findings are less generalizable to new datasets, hence why we were unable to replicate findings of Seidlitz et al. (2018), and instead found that nodal topological characteristics (i.e. strength) did not predict cognitive abilities in the current sample.

However, there are several other potential hypotheses as to why we were unable to replicate the previous findings. Most importantly, there were developmental differences between our sample and that of Seidlitz et al. (2018). The current study investigated a healthy young adult population between the 3rd and 4th decades of life whereas Seidlitz et al. (2018) studied a late adolescent (15-25yrs) sample. The brain undergoes substantial structural change over development with this adolescent period being a time of peak maturation (Gogtay et al., 2004; Sowell et al., 2004) It is across these years in which some of the neurocognitive skills investigated in the current study, executive functioning for instance, are fully established. For instance, the NIH-toolbox total cognition composite highlights this quite clearly with a greater magnitude of age effects seen in childhood compared to adulthood (Akshoomoff et al., 2013; Heaton et al., 2014). This is likely because, throughout childhood, the regions subsuming these functions are reaching structural maturity. Therefore, it is reasonable to believe that, it is within the child/adolescent period where the most variance in these neurocognitive skills can be explained by structural networks (as seen by the ~40% variance in IQ explained by the MSN in Seidlitz et al. (2018)).

In the age-range that the current study has sampled, the brain should have reached structural maturity (with only mild age related effects in this age-group) and so there is likely less between-individual variance in the MSN. This was seen in the fact that there was greater congruence between individual MSNs and the group-average MSN in the current study compared to previous adolescent MSNs (correlation of all edge weights: mean $r = .60$, (Seidlitz et al., 2018)). Therefore, the limited variance in the MSN within this age group may mean that there is not enough variance to relate to cognitive functioning, hence our current findings.

We therefore propose that the MSN may in fact be a useful phenotype for assessing neuropsychological functioning, but only in populations where there is sufficient variation in the structure of the brain. This may be populations in the infant/child/adolescent period where structural networks are likely to see greatest variability due to developmentally-mediated change (such as Galdi et al. (2018) & Seidlitz et al. (2018)) or clinical populations where atypical brain structure is seen in the pathophysiology of the disorder (such as Seidlitz et al. (2019), Morgan, Seidlitz, et al. (2018) & Zheng et al. (2019)). It may be the case that these networks hold utility in populations such as these, rather than healthy, matured

populations (where measures of brain structure are likely to heavily regress to the mean), where these methodologies may be of much lesser utility in explaining cognitive functioning.

However, it is also important to consider that the variation in our results could be due to other variations in analysis. Firstly, differences may be driven as an artefact of using differing measures of general intelligence, with Seidlitz et al. (2018) utilising the Weschler Abbreviated Scale of Intelligence (WASI; (Wechsler, 1999)), whilst we used the NIH Toolbox Cognition composite scores (Heaton et al., 2014). However, it is important to remember that the composite score shows high convergent validity with other Weschler assessments of general intelligence (with the Weschler Adult Intelligence Scale (WAIS-IV, (Wechsler, 2008)) $r = .89$ (Heaton et al., 2014), and with the Weschler Intelligence Scale for Children (WISC-IV; (Wechsler, 2003)) $r = .88$ (Akshoomoff et al., 2013).

Also, we calculated the MSN at a much lower spatial scale (68 ROIs) compared to this previous work (308 ROIs). This lower spatial resolution may result in more regionally specific effects being difficult to detect, however it may also have allowed us to detect more subtle effects due to increased power. Yet it is important to note that the 308 ROIs are derived by subdividing the 68 ROI atlas used in the current study into equally sized ‘patches’ and thus still respects the anatomy of the brain in the same way. Therefore, it is highly unlikely that this would explain our non-replication of previous findings.

One potential issue with these metrics is that these similarity measures only investigate graph properties which only partially describe the whole network (Schieber et al., 2017). By using correlational measures of ‘replicability’ we only consider edge-weightings, rather than the structure of the network, hence why we also included comparisons of network strength to begin to investigate this in terms of network topology. We could have investigated additional metrics which characterize network topology (i.e. global efficiency) however, due to the fact that the SC networks do not adhere to typical assumptions of networks (edges representing definitive real connections) we utilised strength as a simpler metric which makes less assumptions about the underlying neurophysiology of the network. Thus, we have taken the assumption that SC represents a graph of higher-order inter-relationships between morphometry and not necessarily ‘connectivity’.

6.6 Conclusion

We have demonstrated that, when we generate the MSN based on a reduced/limited number of MR features, we produce correlation matrices which are highly similar to those generated with multi-modal imaging. However, the networks generated are differentially, topologically organised based on the number of features. We also find that, regardless of number of features, these networks have limited predictive validity of generalised cognitive ability scores, although this may be specific to the current age range under study. Overall, our study recommends that, in situations where multi-modal imaging is not available or clinically/developmentally inappropriate, T1w-restricted MSN construction may give a

useful estimate of the MSN, however between model comparisons should be aware of potentially methodologically-driven changes to network topology.

Chapter 7. Morphometric Similarity Networks of the Brain in Children Post-TBI Predict long-term Executive Functioning after Insult

7.1 Overview

Chapter 6 highlights the potential use of morphometric similarity as an individual-level methodology for investigating sMRI data. This final experimental chapter utilised such a methodology to investigate the neuroanatomical correlates of executive functioning at an individual level. Given that there is a large number of predictors able to be extracted from such networks, the current chapter adopts a data-driven approach to analysis, investigating the neuroanatomical correlates of later executive dysfunction using supervised-learning. Using this approach it was found that the MSN is able to predict later executive functioning in daily living, with a relatively good performance and thus it is concluded that the MSN may be a useful tool for investigating these neuroanatomical correlates.

King, D. J., Seri, S., Catroppa, C., Anderson, V. A. & Wood, A. G. (In Prep.) Morphometric Similarity Networks of the Brain in Children Post-TBI Predict long-term Executive Functioning after Insult.

DJK and AW contributed to the conception and design of the current study. VA and CC contributed and collected data. DJK performed the processing of MRI data, conceptualized and performed the statistical analysis and wrote the first draft of the manuscript. All authors contributed to manuscript revision.

7.2 Introduction

Executive dysfunction is a common and persistent impairment following a paediatric traumatic brain injury (pTBI), even at longer periods post-injury (Babikian & Asarnow, 2009; Sesma et al., 2008). Executive functions (EF) can be conceptualised of comprising three core skills; working memory, behavioural inhibition and cognitive flexibility (Karr et al., 2018) and from these arise higher-order EFs such as planning and novel problem solving (Krasny-Pacini et al., 2017). The executive dysfunction seen in children after TBI is not only evidenced by impairments to performance-based EF measures (Babikian & Asarnow, 2009; Resch et al., 2019; Roncadin, Guger, Archibald, Barnes, & Dennis, 2004; Sesma et al., 2008; Urban et al., 2017) but also on measures of higher-order, everyday EF (Krasny-Pacini et al., 2017; Mangeot et al., 2002; Vander Linden, Verhelst, Verleysen, et al., 2019) that can be indexed via parental report. This ecologically-relevant impairment in daily-living persists over time (Keenan et al., 2018; Krasny-Pacini et al., 2017; Vander Linden et al., 2018) despite improvements in scores on performance-based EF skills (Anderson & Catroppa, 2005; Krasny-Pacini et al., 2017; Levin et al., 1997). However, there still exist distinct, inter-individual trajectories of executive dysfunction after injury (Anderson & Catroppa, 2005; Catroppa & Anderson, 2009; Konigs et al., 2018; Polinder et al., 2015; Ringdahl et al., 2019). Executive dysfunction has significant links to impairments in the attainment of other, linked skills, thus setting the scene for long-term poor developmental outcomes (Gaines & Soper, 2018; Perone et al., 2018). Given this, and the importance of early intervention to

promote best-attainable outcomes, it is important to investigate models by which we can predict the children and adolescents who go on to experience EF-related difficulties.

MRI is a potential biomarker of brain health and level of damage following a TBI (Bigler, 2013). Morphometric analyses of structural T1w MRI show that the brains of children and adolescents who have experienced a pTBI are different to that of typically developing controls, with evidence of differing trajectories from normative brain maturation (King et al., 2019). EFs require intact frontal-striatal circuits (Giedd et al., 1999; Luciana & Nelson, 1998), with the maturation of a cortical-subcortical network needed for the appropriate unfolding of EF skills over the childhood and adolescent period (Bettcher et al., 2016). Therefore, EFs are particularly vulnerable to the damage that occurs in pTBI, because those same brain networks are still undergoing maturational changes necessary to subsume these developing skills. Therefore, MRI ‘biomarkers’ of these networks should provide insight into the degree of executive dysfunction experienced post-injury at the individual-level. However, the current literature shows mixed findings of the association, and predictive utility, between structural brain imaging and EF in pTBI. For instance, in a group with mild pTBI, thinner cortical thickness (CT) of the dorsolateral prefrontal cortex was associated with slower reaction times in a high cognitive load working memory dual-task (Urban et al., 2017). Smaller parietal and cingulate volumes were related to longer reaction times in a working memory task (Wilde et al., 2011) and parent-reported working memory problems were significantly associated with the CT of temporal and parietal regions-of-interest (ROIs Merkle et al. (2008)). Whole brain white-matter (WM) volume predicted long-term inhibition/cognitive flexibility outcomes at 16 years post injury (Yu, Seal, et al., 2018). Despite these findings, others have found no relationship between total grey-matter (GM) volume or frontal pole CT and performance measures of working memory and cognitive flexibility (Konigs et al., 2018; Levan et al., 2016). Morphometric changes are not associated with the improvement of EF following cognitive training (Vander Linden, Verhelst, Deschepper, et al., 2019) or parent-reports of executive dysfunction (Vander Linden, Verhelst, Verleysen, et al., 2019). These results highlight the high variability in the purported relationship between indexes of post-injury brain morphometry and EF.

A number of limitations may account for inconsistencies in these findings. Existing literature utilises limited sample sizes (Levan et al., 2016; Merkle et al., 2008; Urban et al., 2017; Vander Linden, Verhelst, Deschepper, et al., 2019; Vander Linden, Verhelst, Verleysen, et al., 2019), and either highly reductionist measures of brain morphology across multiple regions/hemispheres (Konigs et al., 2018; Vander Linden, Verhelst, Verleysen, et al., 2019; Yu, Seal, et al., 2018) or a limited number of ROIs that are tested (Levan et al., 2016; Vander Linden, Verhelst, Deschepper, et al., 2019) These factors are likely due to the restricted statistical power with which to test more complex or a greater number of brain regions, given the small sample sizes in the field of pTBI.

A key limitation of this previous work is the abundance of univariate analyses that treat the morphometry of multiple ROIs as distinct, independent features, rather than interconnected components of a

multivariate whole. A promising technique to establish a link between TBI related changes to the complex organization of morphometry of the brain and later executive functioning outcomes is Morphometric Similarity (MS, Seidlitz et al. (2018)). These networks quantify the meso-scale organisation of the cortex as a biologically meaningful set of statistical similarities between the macro and microstructural architectural properties of all regions of the brain, which can be measured in-vivo, using MRI (Morgan, Seidlitz, et al., 2018). Approaching the morphometry of the cortex as a complex network allows us to investigate additional information beyond that of univariate, local approaches to brain structure (Bullmore & Sporns, 2009; Pagani et al., 2016). These approaches have produced meaningful networks of meso-scale cortical organisation, which are able to discriminate between controls and patients with autism spectrum disorder (Zheng et al., 2019), Alzheimer's disease (Zheng et al., 2018) and early psychosis (Morgan, Seidlitz, et al., 2018). These networks have also successfully been applied to neurodevelopmental cohorts, detecting structural brain dysmaturity in premature infants (Galdi et al., 2018), and anatomical disruptions due to regional expression of the abnormal copy number variants (CNVs) in a number of neurodevelopmental disorders (Seidlitz et al., 2019). Whilst these networks have been used to predict variance in IQ (Seidlitz et al., 2018), no previous work has used these networks to predict clinically-relevant, neuropsychological outcome. However, recent research has highlighted that individual differences in morphometric similarity, specifically levels of similarity of regions in the prefrontal cortex, were able to predict inhibitory control more accurately than any individual morphometric features in a large sample of adults (He, Rolls, Zhao, & Guo, 2019). This highlights the potential use of this method in both paediatric populations with pathological changes to the brain and investigating the neuroanatomical basis of executive functioning.

Given recent characterisations of TBI as a diffuse disorder of brain connectivity, and the limited findings of local, univariate approaches to brain structure function relationships post-injury, we utilised morphometric similarity as a novel tool with which to investigate executive dysfunction post pTBI. We predicted that, in children who have experienced a pTBI, due to the additive effects of both pathology-related abnormalities and disrupted neural development, that the highly controlled morphometric similarity of cortical regions will be different compared to controls. We also predicted these differences would be primarily found in fronto-temporal regions which are most commonly found to be abnormal following pTBI (King et al., 2019). We also predicted that quantitative measures of morphometric similarity in patients would be related to later functioning and predict later EF outcomes beyond that of any one feature alone.

The specific hypotheses were that:

1. the magnitude of morphometric similarity in patients would be different from that of controls and this difference would be regionally focussed in the fronto-temporal regions,

2. the magnitude of morphometric similarity of regions will predict later executive dysfunction at two years post-injury in pTBI patients,
3. the morphometric similarity of regions will provide greater information than any one individual morphometric feature and thus will generate a more accurate prediction than that with individual features.

7.3 Methods

7.3.1 Ethics statement

Data from the TBI cohort in the current study was obtained under a material transfer agreement between the Murdoch Children's Research Institute and Aston University originally acquired for a study which had previously received ethical approval via the Human Research and Ethics Committee of Royal Children's Hospital, Melbourne, Australia. A favourable opinion was granted by Aston University ethics panel for the secondary analysis of this dataset.

7.3.2 Participants

The data used in the current experiment are a subset of an existing dataset of children who have experienced a TBI between the ages of five and 16 years of age. 157 children (patients n=114) were recruited between 2007 and 2010 into a study on 'Prevention and Treatment of Social Problems Following TBI in Children and Adolescents'. More detailed descriptions have been published elsewhere (Anderson et al., 2013; Anderson et al., 2017; Catroppa et al., 2017). In brief, children with TBI were recruited on presentation to the Melbourne Royal Childrens' Hospital's emergency department. Patients were eligible if they: i) were aged between five and 16 years at the time of injury, ii) had recorded evidence of both a closed-head injury and also two post-concussive symptoms (such as headaches, dizziness, nausea, irritability, poor concentration), iii) had sufficient detail within medical records (Glasgow Coma Scale (GCS; (Teasdale & Jennett, 1974)), neurological and radiological findings) with which to determine the severity of the injury, iv) had no prior history of neurological or neurodevelopmental disorder, non-accidental injuries or previous TBI, and v) were English speaking. TD controls were also recruited and were required to meet criteria i), iv) and v).

MRI images were acquired at 3T as a part of an existing research protocol on a Siemens Trio scanner (Siemens Medical Systems, Erlangen, Germany) using a 32-channel matrix head coil. The acquisitions pertinent to the current study included a sagittal three-dimensional (3D) MPRAGE [TR = 1900 ms; TE = 2.15 ms; IR prep = 900 ms; parallel imaging factor (GRAPPA) 2; flip angle 9 degrees; BW 200 Hz/Px; 176 slices; resolution 1 × .5 × .5 mm] and sagittal 3D T2-w non-selective inversion preparation SPACE (Sampling Perfection with Application-optimised Contrast using different flip-angle Evolution) [TR = 6000 ms; TE = 405 ms; inversion time (TI) = 2100 ms; water excitation; GRAPPA Pat2; 176 slices; 1 × .5 × .5 mm resolution matched in alignment to the 3D T1-weighted sequence].

We only included subjects who; a) met strict quality control criteria of Freesurfer outputs (see later), and b) underwent MRI scanning <90 days post-injury. This resulted in a subset of n = 116 subjects (TBI patients (n = 83) and healthy controls (n = 33)). Group demographics can be seen in Table 7.1.

Table 7.1. *Demographics for patients and controls*

	Group	pTBI	Controls	Comparison
	N	83	33	-
	M/F	54/29	20/13	OR= 1.21, p=.67 ^a
Age at Scanning (median, yrs)		11.07	9.99	F(1,114)=.262 , p=.61 ^b
(range, yrs)		6.09-14.82	6.53-15.47	-
Age at Injury (median, yrs)		10.92	NA	-
(range, yrs)		5.92-14.67	NA	-
Injury-Scan Interval (median, days)		34	NA	-
(range, days)		1-88	NA	-
Injury Severity				
	Mild	47	NA	-
	Moderate/Severe ^c	36	NA	-

Note. ^aFisher's exact test (OR = odds-ratio), ^bOne-Way ANOVA, ^cMild Complicated TBI + Moderate TBI + Severe TBI

7.3.3 MRI Processing

3D tissue segmentation and estimation of brain morphometry from T1-weighted (T1w) MR images were conducted using an established pipeline (Freesurfer version 6.0; see Fischl (2012) for review). The steps involved are documented elsewhere (Fischl et al., 2004) but briefly, T1w images were stripped of non-brain tissues (Segonne et al., 2004), GM/WM boundaries were tessellated and topology was automatically corrected (Fischl et al., 2001; Segonne et al., 2007). Finally, deformation of this surface was performed, to optimally define tissue boundaries using intensity gradients (Dale et al., 1999; Dale & Sereno, 1993; Fischl & Dale, 2000). Where available, 3D T2-weighted (T2w) FLAIR MRI were used to refine the boundary between the pial surface and dura within the Freesurfer algorithm, to good effect. In this study, Freesurfer was used to estimate multiple morphometric features for 34 ROIs per hemisphere, based upon the cortical parcellation of the Desikan-Killiany atlas (Desikan et al., 2006). This parcellation was chosen over a more fine-grained parcellation scheme due to concerns over statistical power if a greater number of ROIs were analysed. This allowed us to estimate seven metrics with which to estimate the morphometry and shape of the cortex. This included surface area, curvature index, folding index, Gaussian curvature, mean curvature, cortical thickness, and cortical volume. The quality of Freesurfer outputs was assessed using Qoala-T (Klapwijk et al., 2019) as a decision support tool to guide systematic and replicable selection of which cases required manual editing. Multiple cases within the original TBI cohort also had frank parenchymal lesions to the grey matter ribbon. For these cases, Freesurfer has limited applicability with its standard processing pipeline and thus an adjusted pipeline was utilised as used in our previous studies of this dataset (Chapter 4). Eight cases with lesions were retained for analysis using this pipeline.

7.3.4 Morphometric Similarity Network Construction

In the initial validation experiments of morphometric similarity, Seidlitz et al. (2018) estimated networks from morphometric features measured in vivo by both structural and diffusion. However, in previous work, we highlighted significant correspondence between this morphometric similarity and that estimated with only features obtainable from a T1w MRI (King & Wood, 2019) and recent papers have similarly adopted this T1w-only approach (He et al., 2019). Therefore, the current study adopts this approach.

To estimate morphometric similarity, the nodes for network construction were the ROIs from the Desikan-Killiany atlas. At an individual-level, the seven morphometric features estimated for each node can be expressed as a set of n vectors of length 10, with each vector as a different anatomical region ($n = 68$), and each element of the vector a different morphometric measure. To normalize measures within this length 10 vector, each morphometric feature is demeaned and SD scaled across the 68 regions, using Z-scores. A correlation matrix was generated for each participant, where each element of the matrix is the correlation between the feature vectors for every possible pairwise combination of regions. This

correlation matrix represents the morphometric similarity derived meso-scale cortical organisation for each participant. These were thresholded across multiple network density thresholds ($x = 5$ to 40 in increments of 5), retaining only x % strongest absolute values of morphometric similarity across the graph. We also investigated the unthresholded graph. This has the effect of removing potential false-positive estimates of morphometric similarity.

For each node/ROI, we calculated both nodal degree and nodal strength. Nodal degree was the number of edges that had survived thresholding for each node. Normalised nodal strength was calculated as the ‘magnitude’ of morphometric similarity for each node. This is defined as the sum of the morphometric similarity weights of all of the edges of node i (Fornito et al., 2016), normalised by the degree of the node (nodes with a higher number of edges will by definition have a greater magnitude of morphometric similarity). We also calculated the average nodal strength across the network to provide a global measure of the magnitude of morphometric similarity.

7.3.5 Executive Functions (EF)

EF was assessed for patients in the TBI cohort (patients and controls) at approximately 24-months post injury ($M(SD) = 754(80)$ days post injury) using performance-based neuropsychological testing. Several standard, age-appropriate neuropsychological tests were administered to participants to index EF skills, and these were from three typical, age-appropriate test batteries; i) Tests of Everyday Attention – Children (TEA-Ch; (Manly et al., 1999)), ii) Delis-Kaplan Executive Function System (D-KEFS, (Delis et al., 2001)), and iii) Wechsler Intelligence Scale for Children (WISC-IV, (Wechsler, 2003)). These measures were selected from a wider battery of administered neuropsychological tests as part of the wider study. Specific subtests used in the current study were selected to represent components of a three-factor EF model (Miyake et al., 2000) and can be found in Table 7.2. Performance scores for the neuropsychological test batteries were converted to age-scaled scores ($M=10$, $SD=3$). To provide a summary score for common EF performance, we summed these age-scaled scores across subtests, with higher scores representing better performance. The Behaviour Rating Inventory of Executive Function (BRIEF, Gioia et al. (2000)) measures EF in daily life, using purposeful, goal-directed behaviours to solve and adapt to problems (Donders & DeWit, 2017). The current study specifically uses the ‘Global Executive Composite’ T-score (GEC; $M=50$, $SD=10$), with higher scores representing greater difficulties in behavioural EF. Fifty-nine participants had completed neuropsychological testing to calculate EF summary scores and 59 (not identical) participants had BRIEF-GEC scores available. By using two differing measures of EF (performance-based vs behavioural/parent report) we are able to assess the concordance of our results across multiple measures.

Table 7.2. Neuropsychological tests and subtests used to group patients on executive functioning outcome 2 years post-injury

EF Domain	Battery	Subtest	Measure
Set Shifting	TEA-Ch	Creature counting	Accuracy (no. correct)
	TEA-Ch	Creature counting	Time taken
Inhibition	D-KEFS	Colour-word interference – condition 3	Time Taken
	D-KEFS	Colour-word interference – condition 4	Time Taken
	TEA-Ch	Walk-don't-walk	Score
	TEA-Ch	Skysearch	Attention Score
Working Memory	WISC-IV	Digit span backwards	Score

7.3.6 Statistical analysis

7.3.6.1 Between-group differences in the magnitude of morphometric similarity

Firstly, we investigated differences in the magnitude of morphometric similarity between patients and controls. For each threshold, we conducted a GLM to test the effect of group (TBI vs Controls) on average nodal strength, whilst controlling for age at scanning, sex, age*sex, and estimated total intracranial volume (eTIV). This was repeated for all ROIs of the unthresholded network to investigate the effect of group on nodal strength. For all GLM analyses, the t-statistic for the estimated effect of group on was used to estimate the effect size using Hedge's *g* (reference) corrected for unequal sample sizes (Rosnow et al., 2000). All p-values reported are FDR-corrected (Benjamini & Hochberg, 1995) across the number of thresholds or the number of ROIs.

7.3.6.2 Predicting EF outcome using MS in pTBI

To assess whether MS was related to later function EF outcomes in the patient group, we utilised a supervised learning approach using partial least squares regression ('plsRglm' package in R, Bertrand and Maumy-Bertrand (2018)). This multivariate approach finds the maximal low-dimensional covariance between components derived from a high dimensional set of predictors (in this case morphometric similarity across ROIs) and a univariate predictor variable (either EF score or BRIEF). This approach is commonly used when the number of predictors exceeds the number of observations (Krishnan et al., 2011) and has previously been used to examine the relationship of brain structural changes and behaviour (Phan et al., 2010).

Firstly, we decompose the predictor variables into latent variables (components) which simultaneously model the predictors and predict the response variable (Krishnan et al., 2011). The predictor matrix consisted of either the degree or normalised strength of each node of the morphometric similarity network, for each participant. Using a linear model, the potential confounding effect of eTIV, age, gender and age*gender interaction was regressed out of values for nodal degree/strength. Then, at each network threshold, a PLS regression model was fitted between principal components derived from the resultant predictor matrix and the outcome variable. Components were derived and the number of components to retain in the final model was decided based upon the local minima of AIC, calculated using corrected degrees of freedom of the model (Krämer & Sugiyama, 2011). Given the model with the retained number of components, we report the variance explained by the model, and both the Pearson correlation and mean absolute error (MAE) between actual and predicted outcome scores. We also calculate the bias corrected and accelerated bootstrapped (Bastien et al., 2005) weightings of each predictor by conducting 1000 bootstraps of the model. This allows us to assess which brain regions most consistently load onto the components and are therefore contributing most to the explanation of variance in the final model.

In order to validate the model, we carried out leave-one-out cross validation. The PLS regression was applied once for each patient, using all other patients as a training set and using the selected patient as a single-item test set. This results in a numerical prediction of outcome for each participant, which is independent of the supervised learning procedure. The performance was again assessed with Pearson correlation and MAE between actual and predicted outcome scores.

Following these analyses, we conducted similar predictions using the individual morphometric features at each region as the predictors, to determine whether morphometric similarity provided greater information for prediction than the features alone.

7.4 Results

7.4.1 Patient-control differences in the magnitude of morphometric similarity

When comparing pTBI patients against controls, mean difference in the magnitude of morphometric similarity (adjusted for age at scanning, sex, age*sex, and eTIV) across the brain was not significant following FDR correction, across all network thresholds tested (all $p_{\text{fdr}} > .05$). This non-significant difference was echoed when looking at the nodal strength across the 68 regions in the unthresholded network. These results can be seen in supplementary materials (Appendix F).

We posited that these lack of significant differences were potentially due to the inhomogeneity of the patient group and thus we conducted exploratory, post-hoc analyses of multiple patient-control differences, specifically across groups of clinically relevant EF impairment and injury severity groups. Still, no significant differences were found. These results can also be seen in supplementary materials (Appendix F).

7.4.2 Predicting EF outcome using morphometric similarity in pTBI

Qualitatively, there appeared to be a range of performance on our indexes of EF, for both EF summary scores ($M = 70$, $SD = 12$, range = 34 – 97) and BRIEF GEC ($M = 48$, $SD = 11$, range = 35 – 83) across the pTBI group. We conducted PLS regression to separately predict these scores from the ROI-level magnitude of morphometric similarity estimated across all nine network thresholds tested.

For EF, across all thresholds, the AIC indicated the retention of zero predictor components in the model, thus no models were generated. This suggests that morphometric similarity is unrelated to later performance EF.

However, for BRIEF scores, AIC suggested retention of 1 component, across network densities of .25, .30, .35, & .40. In these models, highly significant positive correlations were found between actual and predicted BRIEF scores, with the PLS models explaining around 40% variance in BRIEF scores ($R^2 = .36 - .42$), with a relatively low error between predicted and actual scores ($MAE = 6.08-6.49$). When validated using a LOO-CV approach, there were significant positive correlations between predicted and

actual outcomes (see Table 7.2) and error was still low (MAE = 7.85-8.25). Figure 7.1 highlights these predictions graphically. When predictor weightings were bootstrapped to provide CIs of weightings, the CIs appeared narrow but some overlap between regions was present. Figure 7.2 illustrates, across network densities, a consistent set of regions that were most highly weighted in the generation of components, therefore explaining the greatest proportion of variance in BRIEF outcome.

7.4.3 Predicting EF outcome using individual morphometric features in pTBI

Table 7.3 shows the results of PLS models using individual morphometric features to predict both EF summary and BRIEF GEC scores. Unlike for morphometric similarity, PLS models were generated for curvature index, Gaussian curvature and cortical volume in predicting EF score. There was a large variation in performance of these models across the structural features when internally validated with LOO-CV across evaluations of variance of EF score explained and MAE ($R^2 = .03 - .13$, MAE = 9.67 - 10.56). In predicting BRIEF-GEC curvature index, folding index, Gaussian curvature, cortical thickness and cortical volume produced models where components were retained. For these models, training produced models which explained less variance than the morphometric similarity models, with weaker correlations between observed and predicted outcomes and slightly higher MAE ($R^2 = .10 - .19$, MAE = 6.99 – 7.61, See Table 7.3 for more details). The LOO-CV generated predictions from these models also explained less variance than the morphometric similarity model ($R^2 = .02 - .04$). As shown in the supplementary materials (Appendix F), the bootstrapped CIs for regional predictors for all individual features were much wider than those in the morphometric similarity PLS model.

Table 7.2. Description of models where components were retained when predicting executive dysfunction from the morphometric similarity of those following a pTBI

Outcome	Graph Metric	Network Density	N. Comp.	Full Dataset			LOO-CV		
				R ² Model	r(y _{pred.} , y _{actual})	MAE	R ² Model	r(y _{pred.} , y _{actual})	MAE
BRIEF-GEC	Degree	.25	1	.42	r = .65, p < .0001	6.12	.07	r = .27, p = .038	8.15
		.30	1	.41	r = .64, p < .0001	6.08	.09	r = .30, p = .021	7.97
		.35	1	.38	r = .62, p < .0001	6.30	.12	r = .35, p = .006	7.85
		.40	1	.36	r = .60, p < .0001	6.49	.08	r = .28, p = .033	8.25

Note. N. Comp. = Number of components retained in the model, LOO-CV = Leave-one-out cross-validation, MAE = Mean Absolute Error between predicted values and actual values

Table 7.3. Description of models where components were retained when predicting executive dysfunction from individual morphometric features of those following a pTBI

Outcome	Morphometric Feature	N. Comp.	Full Dataset			LOO-CV		
			R ² Model	r(y _{pred.} , y _{actual})	MAE	R ² Model	r(y _{pred.} , y _{actual})	MAE
EF Score	Curvature index	1	.17	r = .41, p = .001	8.71	.13	r = -.37, p = .004	10.56
	Gaussian Curvature	1	.17	r = .41, p = .001	8.98	.03	r = .24, p = .066	9.67
	Cortical Volume	1	.20	r = .45, p < .001	8.79	.05	r = .23, p = .073	9.79
BRIEF-GEC	Curvature index	1	.14	r = .37, p = .004	7.61	.04	r = -.21, p = .11	8.62
	Folding Index	1	.18	r = .43, p < .001	7.48	.03	r = -.16, p = .22	8.78
	Gaussian Curvature	1	.15	r = .39, p = .002	7.50	.04	r = .20, p = .14	8.09
	Cortical Thickness	1	.10	r = .32, p = .013	7.57	.02	r = .14, p = .30	8.03
	Cortical Volume	1	.19	r = .43, p < .001	6.99	.03	r = .17, p = .20	7.82

Note. N. Comp. = Number of components retained in the model, LOO-CV = Leave-one-out cross-validation, MAE = Mean Absolute Error between predicted values and actual values

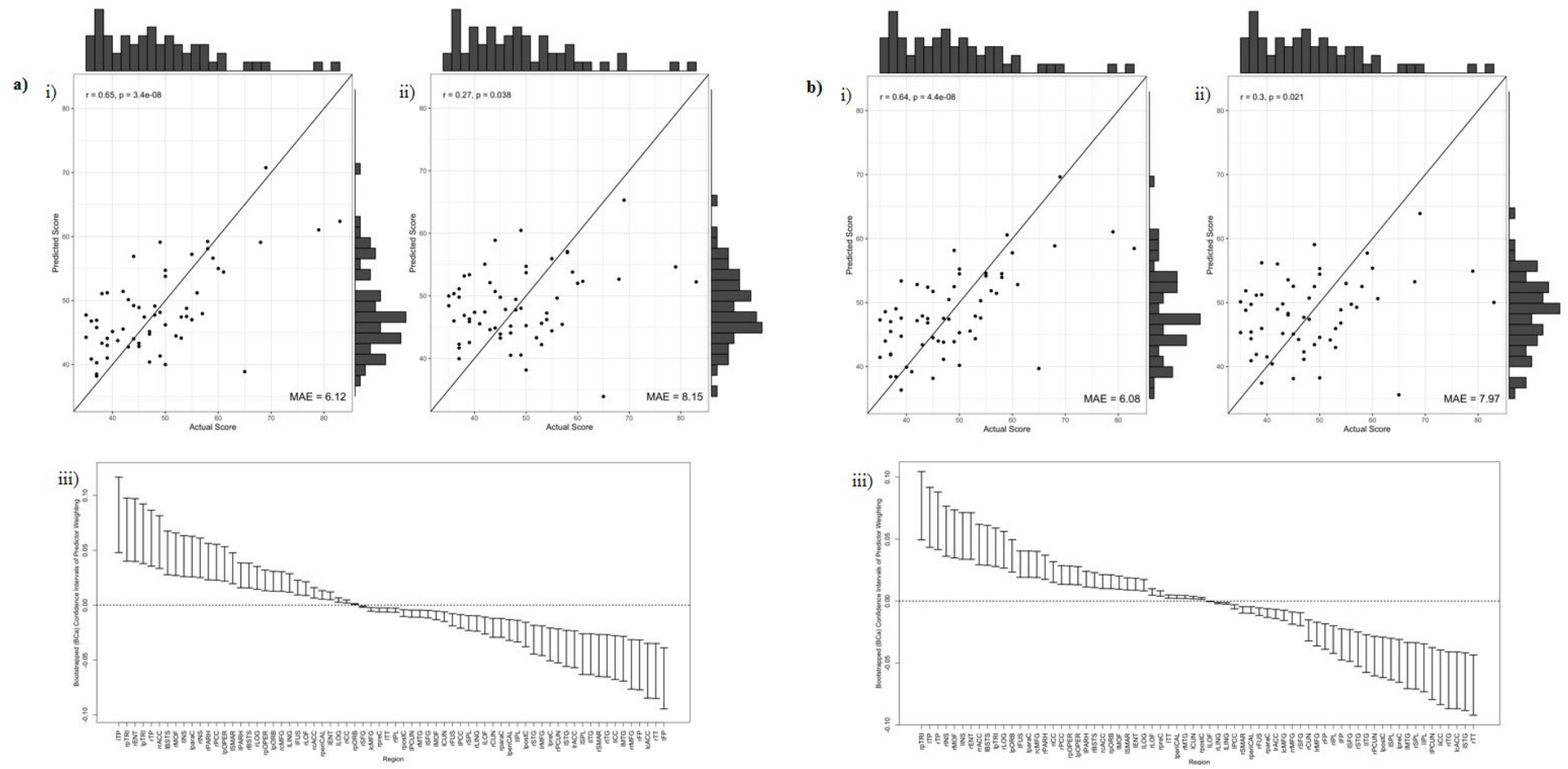


Figure 7.1. Continued overleaf

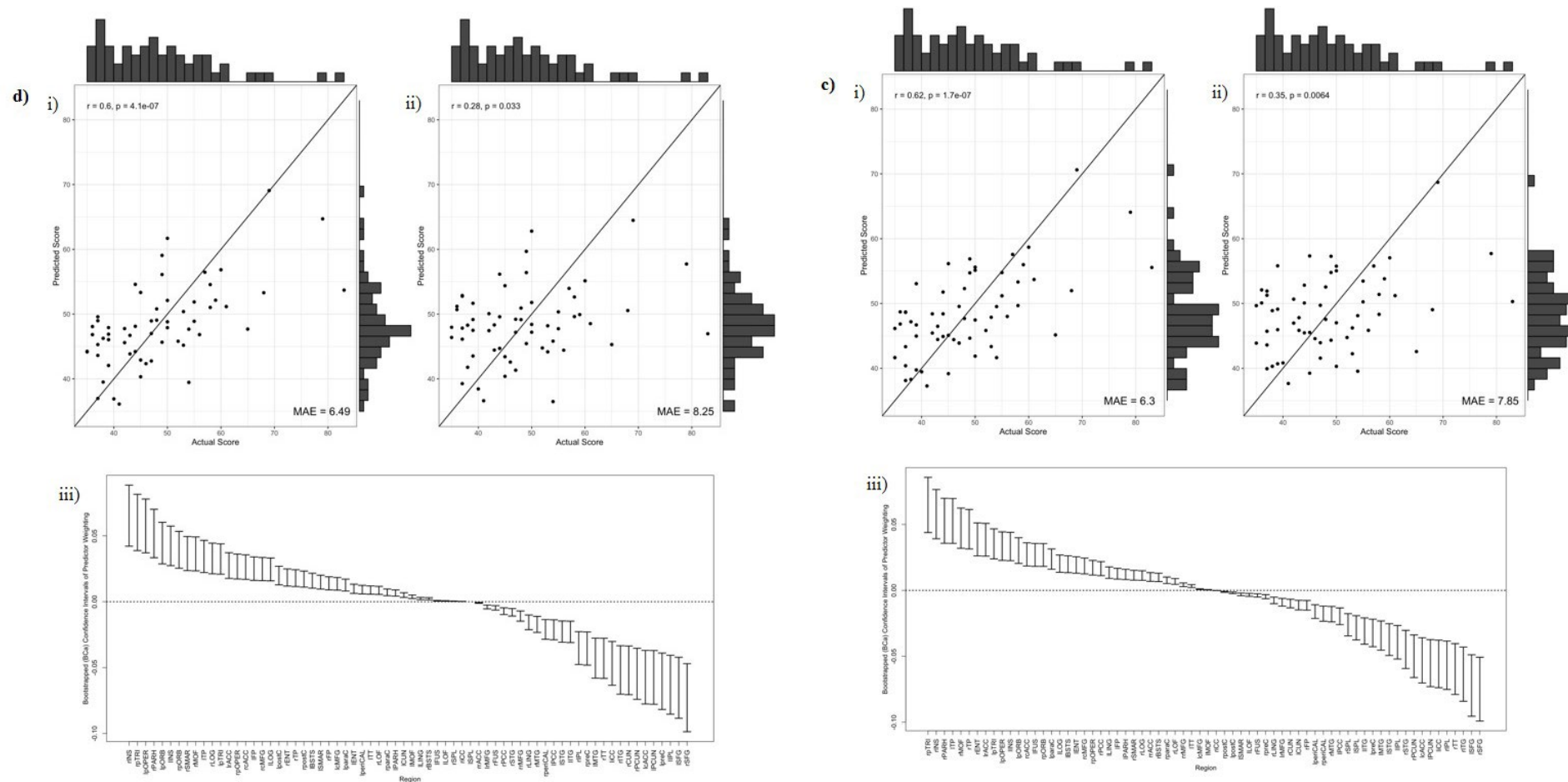


Figure 7.1. Results of PLS regression. Results are shown across network density thresholds as follows; a) .25, b) .30, c) .35, d) .40. **i)** The correlation between actual and predicted BRIEF scores based upon the PLS regression model, **ii)** the correlation between actual and predicted BRIEF scores based upon leave-one-out cross-validation of the PLS regression model. For **i)** and **ii)** the line represents $x = y$, indicative of perfect prediction of a model. **iii)** The bootstrapped (bias-corrected and accelerated) CI for PLS weightings for each ROI.

BRIEF scores predicted with Morphometric Similarity

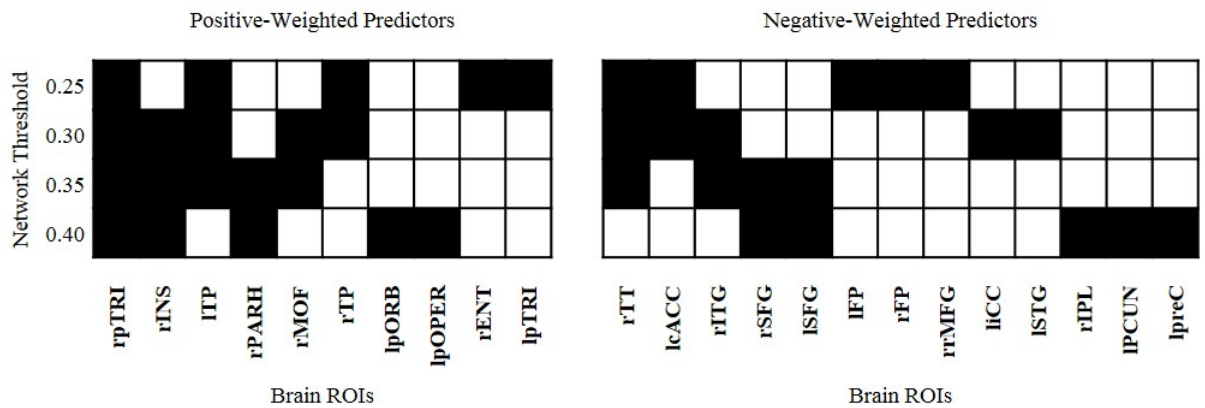


Figure 7.2. Plot of top five positive/negative weighted predictors (degree of ROIs) of BRIEF GEC across network thresholds from .25 density to .40. (*r* = right hemisphere, *l* = left hemisphere, *pTRI* = pars triangularis, *INS* = *r* insula, *TP* = temporal pole, *PARH* = parahippocampal gyrus, *MOF* = middle orbitofrontal, *pORB* = pars orbitalis, *pOPER* = pars opercularis, *ENT* = entorhinal, *TT* = transverse temporal, *cACC* = caudal anterior cingulate, *ITG* = inferior temporal gyrus, *SFG* = superior frontal gyrus, *FP* = frontal pole, *rMFG* = rostral middle frontal gyrus, *iCC* = isthmus cingulate, *STG* = superior temporal gyrus, *IPL* = inferior parietal lobule, *PCUN* = precuneus, *preC* = precentral sulcus)

7.5 Discussion

7.5.1 Patient-control differences in the magnitude of morphometric similarity

The current study adopts a morphometric similarity network approach (Seidlitz et al., 2018) to the investigation of the neuroanatomical correlates of later executive dysfunction following pTBI. However, we found no differences, across any of the morphometric similarity network thresholds tested. This was true at both the graph and ROI-level, between pTBI patients and controls. For these analyses, the entire patient group were considered as a single, homogenous group. However, we know that there are large heterogeneities in terms of structural damage post-pTBI (King et al., 2019), and in executive dysfunction outcomes (Ringdahl et al., 2019). In a previous study of the current dataset, we also showed that structural covariance derived from only cortical thickness measures, differed between patients and controls when patients were stratified based on an EF neuropsychological impairment rule (Beauchamp et al., 2015), with differences only being seen in those patients showing an impairment in EF (Chapter 4). Therefore, we compared morphometric similarity between groups derived from those with clinically relevant impairment or groups based on injury severity. We still found no significant group differences in the magnitude of morphometric similarity averaged across the cortex.

7.5.2 Predicting EF outcome using morphometric similarity in pTBI

Despite finding no group differences in the magnitude of morphometric similarity, we were able to predict later executive dysfunction in pTBI patients. We successfully built models that predicted BRIEF – GEC from the nodal degree of ROIs. This was across a collection of network densities across the middle of the range tested. This is unsurprising, given that at lower network densities the network would become sparse and contain much less information with which to predict outcome whilst at higher densities, there is a much greater propensity to the inclusion of false-positive edges, introducing error into the prediction algorithm. Our models performed relatively well, the correlation between actual and predicted scores, both in the training and LOO-CV sets were moderate.

Bootstrapping the predictor weightings highlighted strongest predictive utility (both positive and negatively weighted) across fronto-temporal regions. Of note were the high loadings across regions of the prefrontal cortex (inferior, superior and medial orbito- frontal gyri) which are particularly important for typical development of EFs (see Fiske and Holmboe (2019), for a review). The regions highlighted here consist of those that are commonly found to be smaller or reduced post pTBI compared to controls in terms of regional CT and GM volume, indicative of susceptibility to the pathologic effects of injury (Wilde et al. (2011), Merkle et al. (2008), Mayer et al. (2015), Wilde, Merkle, et al. (2012), Dennis, Faskowitz, et al. (2017), Dennis et al. (2016); see King et al. (2019) for a systematic review). Previous work investigating neuroanatomical correlates of the BRIEF-GEC post pTBI found no correlations with mean cortical thickness over multiple ROIs that were chosen a-priori due to their involvement in

mediating EFs (Vander Linden, Verhelst, Verleysen, et al., 2019). Our multivariate methodology, however, was able to identify a moderate relationship between patterns of morphometric similarity across the cortex and later EF. This suggests that not only has the current methodology replicated previous neuroanatomical differences post-TBI, but also the method is sensitive enough to functionally relevant morphometric variation.

Our results show convergence with previous work utilising multivariate methodologies to investigate the neuroanatomical correlates of EF. Ziegler, Dahnke, Winkler, and Gaser (2013) found that, in a child and adolescent cohort, a latent cognitive variable (onto which the BRIEF heavily loaded) was related to voxel-based morphometry of regions similar to those found in the current study, across regions of inferior frontal gyrus, insula, medial orbitofrontal, anterior cingulate cortices. DTI-derived connectivity of the anterior cingulate and superior frontal regions also distinguished a cluster of children characterised by a profile of elevated inattention, hyperactivity and EF symptoms, who also measured this using the BRIEF (Bathelt, Holmes, Astle, Centre for Attention, & Memory, 2018). Only one previous study has investigated the neuroanatomical correlates of executive functions utilising the morphometric similarity approach. He et al. (2019) specifically highlighted the role of right medial orbitofrontal cortex as a node of the morphometric similarity network specifically related to predicting inhibitory control performance in healthy adults. Overall, the neuroanatomical specificity of our predictions seems to be plausible in terms of EF maturation, correlates of EF problems in childhood and consistent with previous investigations using morphometric similarity. However, the current study expands these findings beyond the meso-scale architecture of individual regions and suggests that the meso-scale organisation of the cortex (indexed using morphometric similarity) in relation to these specific regions is important for subsuming later executive functioning.

EF measurements typically capture information about the performance of cognitive processing skills inherent to EFs, or the functional/behavioural manifestation of executive dysfunction. In the current study, an interesting pattern of findings emerged, along these lines. Specifically, whilst we show that morphometric similarity predicts BRIEF ratings of EF, which ascertain the functional consequences of executive impairments that manifest in everyday life, the same was not true for directly-measured, or performance-based, scores. The latter measures instead assess the cognitive aspects of executive impairments. Thus, the pattern of results reported here is perhaps unsurprising, given that the BRIEF has been shown to index different components of EF to typical performance-based measures (McCauley et al., 2010; Ten Eycke & Dewey, 2016) and has been shown to have differential neuroanatomical correlates (for instance Faridi et al. (2015) showed differences in neuroanatomical correlations of both performance-based and BRIEF measures of working memory). pTBI is also thought to be characterised by differential trajectories in terms of BRIEF and performance indexes of EF, although this may be due to practice effects (Anderson & Catroppa, 2005; Krasny-Pacini et al., 2017).

Another potential explanation for this pattern of results is that the BRIEF scores index a higher order, functional/behavioural manifestation of executive dysfunction in daily living, beyond that of individual EF skills. It is the common executive functions (working memory, inhibitory control & cognitive flexibility) that give rise to the more complex executive behaviours necessary for daily living, such as planning and reasoning. Therefore, it is likely that these complex behaviours recruit a diverse network of brain regions, beyond that of any one of the unitary executive skills that give rise to these higher order functions. It is therefore unsurprising that morphometric similarity, a model that investigates the integrative, interrelated nature of the structure of the cortex, is able to predict executive dysfunction related to daily living tasks, but not a measure of multiple performance-based EF skills.

Overall, these findings provide further evidence that the degree to which regions that typically play a role in supporting the acquisition of executive function skills are left-intact is associated with later executive dysfunction following pTBI (Anderson & Catroppa, 2005; Bettcher et al., 2016; Wilde et al., 2011). The current study expands these findings, suggesting that, not only is the post-injury structure of these regions prognostically important, but also how this structure is interrelated across all areas of the cortex. This further highlights the functional relevance of this cortex-wide organization of morphometric similarity. Nevertheless, there is no current understanding as to the ‘normative’ values for morphometric similarity across the developmental period and thus it is unclear if these inter-individual differences in this metric represent ‘damage’ or ‘abnormalities’ post-injury. Future research should be conducted to properly characterise the developmental trajectories of morphometric similarity across the developmental period.

The predictive validity of morphometric similarity occurred despite the lack of significant group differences across multiple comparisons of morphometric similarity outlined above. This may highlight the fact that damage following a pTBI is unlikely to occur to a single region in isolation. That is to say, the pathological effects of injury are diffuse in nature (Bigler, 2016; Bigler et al., 2010). One benefit of the PLS regression approach is that it allows us to better understand the multivariate pattern of the subtle changes that happen in the brain, beyond that of univariate approaches such as voxel-based morphometry that are biased towards detection of more spatially localized effects and neglect interactions between neuroanatomical features (Davatzikos, 2004; Levine et al., 2013; Sepehrband et al., 2018). However, it is important to note that accuracy of prediction based on supervised learning models does not necessarily confer evidence of causality; the predictive variables may carry intermediate ‘signal’ that is relevant to the measure of interest but is not directly related (Bzdok & Ioannidis, 2019). This is especially true in relation to models using morphometric similarity as predictive variables, as this is based on indirect measures of meso-scale features of the brain. Thus, inference from these models need to be considered with caution and tested within inferential statistical models.

7.5.3 Predicting EF outcome using individual morphometric features in pTBI

The current study expanded previous studies of neuroanatomical correlates of EF following pTBI by investigating previously unstudied structural features (i.e. curvature) but also using multivariate, rather than univariate approaches to structure. We generated models to predict both EF scores and BRIEF GEC from individual morphometric features to some success. Interestingly, despite previous work finding no significant neuroanatomical correlations between the BRIEF GEC and mean cortical thickness over multiple EF-subsuming ROIs post-pTBI (Vander Linden, Verhelst, Verleysen, et al., 2019), the PLS model was able to detect a meaningful, multivariate pattern of regional CT which was predictive of EF functioning. These predictions were despite an inability to predict EF scores from the morphometric similarity model.

We show a marked difference in the predictive performance of models using morphometric similarity vs. the individual morphometric features used to estimate morphometric similarity. For the BRIEF GEC, the morphometric similarity model explained a greater proportion of variance than the curvature index, folding index, CT and cortical volume models. However, across both morphometric similarity and individual feature models, the prediction error was similar in terms of MAE (difference in this error was less than a single point on the BRIEF measure). In addition, when we generated bootstrapped CIs of weightings of individual ROIs in terms of the PLS components, we found that these were wide, suggesting two things. Firstly the PLS model for these individual features is highly unstable and secondly, that there is little regional specificity of damage (as indexed by individual structural features) on the prediction of outcome, especially given the high overlap in CIs between regions. Overall, these findings are first evidence that morphometric similarity of regions may be more sensitive to the clinically relevant structural damage post-neurologic insult, compared to standard structural measures.

7.5.4 Limitations

One major strength in the current study is that, at the time of writing, it is the first study to investigate morphometric similarity in pTBI. However, it is also the first study to utilise PLS regression to investigate the neuroanatomical correlates of post-injury functioning in this clinical group. PLS is a powerful exploratory tool for such a task, allowing us to model even collinear or near-linearly dependant predictors as well as generating coefficients that are more stable and easier to interpret than other multivariate approaches such as canonical correlation analysis (Wegelin, 2000).

One potential limitation of the morphometric similarity approach is the evidence here which suggests that edge weights of the network based on morphometric similarity are not reliably estimated. It is important to note that the PLS regression only found models when utilising nodal degree to predict outcome. This binarises the network, thus removing a large amount of information from the network in the form of edge weights. Given that these edge weights did not result in a model with which to predict EF, it may be pertinent to assume that these edge weights contain more noise than predictive signal; potentially as the edge weights themselves cannot be reliably estimated. This may be because the edge

weighting is estimated from a correlation between seven morphometric features, a small number of observations with which to reliably estimate a correlation coefficient. This is further evidenced by the high SD of edge weights found by Seidlitz et al. (2018). However, some edge weighting information will inherently be retained in the binarised network, with retained edges (by definition) being those with a greater edge weight than the edges that were removed from the graph. More reliable estimation of morphometric similarity could result in more accurate predictive models. One potential solution for future research may be to generate/sample a larger number of morphometric, meso-scale features from the T1w image with which to estimate morphometric similarity (i.e. Klein et al. (2017)).

There are also some difficulties in testing the degree to which morphometric similarity predicts EF beyond individual structural features. Whilst our PLS models show that morphometric similarity seemingly contains prognostic information beyond individual features, this is a limited comparison. Morphometric similarity may only lead to greater prediction due to the fact it contains 'signal' from all features whilst we compared it a single individual feature at a time. A more sincere comparison for this hypothesis would be to compare the morphometric similarity model against a model that contains all features for all regions. This would allow us to assess whether the covariation structure between these features (as is represented by morphometric similarity) contains greater prognostic information than the features alone. However, this would result in a 7×68 predictor matrix, which far outstrips the number of observations we have, and may result in unstable and non-generalizable prediction models due to limited sample sizes. This in fact highlights a potential advantage to the use of morphometric similarity in research settings such as this, in populations where sample sizes are known to be limited (such as pTBI (King et al., 2019)). Morphometric similarity represents a low dimensional representation of the 7×68 matrix of individual features, and may in fact contain greater information than the individual features alone, and so is more appropriate for these populations where observation-predictor ratios would otherwise be suboptimal (such as clinical populations where larger sample sizes are harder to obtain).

7.6 Conclusion

The morphometric similarity approach is a methodology with which we can capture information about the brain's complex structural organisation. We posit this methodology can capture the disruption to the highly programmed organisation of the cortex in populations in which the normal developmental trajectories may be divergent. We have expanded the previous univariate investigations of the neuroanatomical correlates of executive functioning (which are inherently limited in detecting the diffuse effects of injury), utilising MS and PLS methods which are novel to the field of neuroimaging post pTBI. The current study shows that the complex, meso-scale organization of the morphometry of the cortex, namely the morphometric similarity between regions, not only provides additional insights

to brain morphometry compared to previous approaches but also possesses the potential to predict more accurately these clinically relevant, functional outcomes.

Chapter 8. General Discussion

8.1 Overview

There is a high prevalence of traumatic brain injuries in the paediatric population, and recent years have seen dramatic increases in survival rates. There has therefore, been a progressive move towards reducing the uncertainty surrounding the sequelae of an insult for children who have experienced a TBI, specifically in terms of later cognitive functioning. The current thesis used state-of-the-art, network-level analyses to investigate how the multivariate structural organisation of the brain post-injury relates to later cognitive function. This chapter discusses these findings within a wider context, and highlights potential directions for future research.

8.2 Findings and Thesis Aims

8.2.1 Current State of Morphometric Research in pTBI and Univariate Analyses of Morphometry

The first aim of the current thesis was to assess the current state of the field in regard to changes to brain morphometry post-pTBI and the subsequent neuroanatomical correlates of later executive functioning. In Chapter 2, a systematic review of the literature suggested that there is evidence of persistent, neuroanatomical consequences of pTBI. These changes are apparent cross-sectionally and longitudinally, suggesting these changes are long lasting. The systematic review also identified a lack of consensus on the relationship between morphometry and cognition. Specifically, in terms of executive functioning, there is little robust evidence of neuroanatomical relationships between sMRI measures and EF abilities. This thesis consolidated these previous findings; Chapter 4 investigated comparisons of CT between controls and patients who do or do not experience executive dysfunction at two years post injury and no significant differences were observed across the regions tested.

One key strength of this finding is that the current analyses account for frank parenchymal lesions which are present on T1w image for a subset of TBI cases. As highlighted in the systematic review, there is potential bias in previous pTBI research with many studies not acknowledging the potential effect of lesions on neuroimaging software used to analyse sMRI data. Chapter 3 provided evidence of a bias introduced to morphometric measures in the presence of frank parenchymal lesions, beyond the extent of the lesion. In analyses of CT data, these effects are controlled for using an adapted Freesurfer pipeline to reduce the impact of these biases. Previous studies do not seemingly account for these potential biases and therefore differences between patients and controls may specifically be misattributed to the effect of pTBI when in fact the differences are primarily error-driven due to this lesion-induced error. In the case of neuroanatomical correlates of cognition post-injury, this bias could have resulted in significant correlations between anatomy and function that were purely driven by the presence of these frank parenchymal lesions. Whilst this error was corrected for in these analyses, the approach in the current

this thesis subsequently followed the advice given in the systematic review and repeated analyses whilst excluding lesion cases, to ensure results are not biased by these cases.

However, whilst CT at the ROI-level was not associated with executive dysfunction, Chapter 7 highlights the predictive utility of a multivariate pattern of morphometry across the cortex in predicting later executive functioning. The current thesis adopted such an approach because of the spatial heterogeneity of damage and post-injury changes highlighted in the systematic review, as this may limit the potential of univariate approaches to morphometry to tell us about the subtleties of the more diffuse effects of an injury. Therefore, looking more widely at the global effects of injury may explain greater variance in functional outcomes post-injury.

In the existing pTBI literature, no previous studies have used such a multivariate approach to whole-brain anatomy. Some previous studies have adopted a voxel-based morphometry approach to capture the more diffuse effects of injury utilising a univariate approach (i.e. Bigler et al. (2013), Yeates et al. (2013)). However, it is important to note that these approaches have multiple limitations that make them unsuited to these research questions; they a) are biased towards detection of localized rather than spatially-complex group differences (Davatzikos, 2004), and b) are univariate in nature and therefore neglect interactions between neuroanatomical features across the cortex (Davatzikos, 2004; Sepehrband et al., 2018). Supervised learning approaches, such as partial least squares regression (utilised in the current thesis), is more suited to the investigation of diffuse effects of injury on the anatomy of the brain, especially since it allows for the high dimensional modelling of brain anatomy with significantly fewer observations than are required for more data-hungry approaches such as general linear modelling (Davatzikos, 2019; Sepehrband et al., 2018). In the adult TBI literature, PLS approaches to whole-brain neuroimaging have been utilised to successfully relate a pattern of brain volumetric changes to multiple domains of cognitive functioning (Esopenko & Levine, 2015, 2017; Fujiwara et al., 2008; Levine et al., 2013). In the paediatric TBI literature, no previous study has utilised supervised learning, multivariate approaches to capture the variance between regional-level structural indices and long term cognitive-behavioural outcome. One recent study utilised a support vector machine to predict change in post-concussive symptoms over four weeks for children in the acute stages of a mild-TBI however, they specifically focused on only two ROIs, rather than whole-brain morphometry data (Iyer, Zalesky, Barlow, & Cocchi, 2019). Other studies have harnessed the potential of multivariate PLS approaches in regard to brain and protein serum biomarkers and outcome (Wilkinson et al., 2017). The results of the current thesis, the complex pattern of morphometry found to be predictive of later executive functioning, and findings of no significant differences in cortical thickness at any one specific ROI, not only emphasise the subtle yet diffuse effect of pTBI on the brain but also indicate their relevance to uncovering the basis of poor functional outcomes.

One of the key goals for neuropsychological research of those children, who have experienced neurological insult, is to disentangle the effects of injury from normative maturational processes

between brain structure and cognitive functioning. It is important to note that, given the limited sample size of controls in the experimental cohort, it was not possible to test whether the predictive relationship between this multivariate pattern of injury and cognitive outcome differed in patients compared to controls. As highlighted previously, it is therefore difficult to ascertain definitively whether these relationships are the result of injury-related pathology or patterns of expected, developmental maturation between structure and function that occurs during the paediatric period.

The results of the current thesis make clear that the adopted multivariate approaches to neuroanatomical correlations between brain and behaviour post-injury (which are novel to the field of pTBI) are more sensitive at detecting the diffuse morphometric changes seen in acute phase of pTBI. Whilst univariate approaches have provided useful insights into the role brain structure plays in the subsiding of cognitive and behavioural functioning, these multivariate approaches may supersede these investigations in the field of pTBI and thus future studies in the field should begin to investigate how multivariate patterns of atrophy and damage across the cortex relate to post-injury functioning.

8.2.2 Network approaches to Neuroanatomical Correlates of EF post-pTBI

Previous evidence has highlighted disparate and inconsistent neuroanatomical correlates of executive dysfunction post-pTBI, potentially due to the vast heterogeneity of injury (Bigler et al., 2013). The assumption of the current thesis was that therefore the topography (the physical distribution across cortex) of morphometric insult or change being less sensitive to the relationships with functional outcomes.

The major aim of the current thesis was to validate and conduct novel experimental analyses of sMRI, investigating network-level, neuroanatomical correlates of future executive dysfunction in a pTBI population. Approaching the morphometry of the cortex as a complex network allows us to investigate additional information beyond that of univariate, local approaches to brain structure (Bullmore & Sporns, 2009; Pagani et al., 2016). Development of typical organisational principles of the healthy brain is likely genetically-mediated, and these enable the efficient, flexible and robust transmission of information (Lydon-Staley & Bassett, 2018). Given this highly coordinated development, there is strong theoretical support for the hypothesis that any neurological perturbation to the network-level organisation of the brain is likely to result in functionally-relevant and behaviourally-symptomatic phenotypes across neurological disorders (Aerts et al., 2016).

Given this, the current thesis takes the position that the topology, rather than the topography, of morphometric change post-injury, is more likely to be sensitive to detecting the neuroanatomical correlates of later executive functioning. At the level of the macroscopic cortical morphometry, as indexed with sMRI, the network-level organisation can be expressed as structural covariance (SC) or morphometric similarity (MS), and this organisation is likely driven by regional gene expression (Romero-Garcia et al., 2018; Seidlitz et al., 2018; Yee et al., 2017), and even axonal connectivity

(Goulas et al., 2017; Seidlitz et al., 2018; Wei et al., 2019). The current thesis expanded previous studies of pTBI that had begun to investigate interregional correlations of morphometry and atrophy (Drijkoningen et al., 2017; Spanos et al., 2007), by investigating the whole-brain SC and MSNs.

The current thesis highlights three key insights; i) pathology-related changes to neuroanatomy after pTBI load onto topologically important regions in those patients who experience executive dysfunction, ii) the magnitude to which the topology of the morphometric network differs from controls is related to the degree of dysfunction and iii) the topology of these morphometric networks is predictive of later executive dysfunction. Current network models of neurologic insult highlight the fact that the behavioural consequences of damage to the brain are highly dependent on the topological position of the damage within, and the organization of neural networks (Aerts et al., 2016; Hillary & Grafman, 2017). Overall, the results of the current thesis are in keeping with these models.

One potential reason for the increased sensitivity of these network level approaches to sMRI in detecting the neuroanatomical correlates of later cognition is change in how the approach models the effects of neurologic insult. In typical, whole-brain, ROI-level approaches to morphometry, only regions that experience insult (due to effects such as atrophy) are likely to show clinically-meaningful differences that are related to later functional outcome. Across a whole cohort where sites of primary insult are heterogeneous and diffuse effects of injury are subtle, it is unsurprising that neuroanatomical correlates of EF are not robustly found. In utilising the network-level approaches to sMRI, the insult is modelled in relation to the rest of the cortex, including tissue that remains undamaged. This therefore models the insult more diffusely across cortical ROIs. For instance, damage to region *i* will result in altered covariance between *i* and all other regions, thus the influence of this insult will be indexed in nodal metrics at all ROIs. This means that, because the effects of injury are measured at all nodes, there is greater spatial congruence of the effects of injury between patients with highly heterogeneous pathology. This makes network-level approaches to sMRI a highly useful approach for studying the neuroanatomical substrates of neurologic insult.

The benefits of these network-level approaches to sMRI are not only academic but also in relation to our theoretical understanding of neurological insult. There is a need to generate hypotheses about the mechanistic effects of neurological insult on the neural network biology, to improve clinically-relevant prognostic models (Aerts et al., 2016). The network-level structural changes in the current thesis provide observational support for these.

Neurologic insult during development is likely to divert the subsequent development of the cortex over the rest of the paediatric period (i.e. in pTBI King et al. (2019)) which can be observed as apparent change to the meso-scale organisation of morphometry across the cortex. This is evidenced by the fact that deviation of structural covariance varies as a function of the timing of insult in patients that experience malformations of cortical development (Hong et al., 2017). Developmental timing of this

divergence is likely to result in the biological and behavioural phenotypes seen in neurologic and neurodevelopmental disorders (Morgan, White, et al., 2018; Seidlitz et al., 2019).

Morgan, White, et al. (2018) highlights the importance of hub regions during development and their specific vulnerability during this period. Thus, atypical development of these hub regions is subsequently observed across multiple psychiatric and neurodevelopmental disorders (Morgan, White, et al., 2018). There is a very deliberate unfolding of morphometric covariance across the cortex (Váša et al., 2017), with hub regions experiencing fastest rates of cortical shrinkage and intracortical myelination (Whitaker et al., 2016). Overall, the results of the current thesis show that differences in the complex organization of the morphometry of the cortex, namely the SC and MS between regions, at the acute stage post injury is a potential substrate of later impaired functioning, and possesses the potential to better predict clinically-relevant functional outcomes than previous univariate approaches.

The network-level approaches to sMRI outlined in the current thesis are an exciting development in the field of developmental neuroscience. In a recent position piece, Dennis and colleagues (Dennis et al., 2019) highlighted the difficulty in MRI scanning of children with pTBI and made two recommendations to alleviate potential concerns regarding movement artefact and image quality; a) behavioural interventions such as mock scanning and b) optimized acquisitions for simultaneous multi-modal acquisition. The current thesis proposed an alternative approach, prioritising the advanced modelling and analysis of T1w sMRI, rather than utilising DTI or fMRI sequences that are standard approaches to estimate organisational principals across the cortex. The T1w acquisition sequence has reduced acoustic noise and a faster acquisition times. These factors make these scans more tolerable for vulnerable paediatric and clinical populations, making it easier to acquire high-quality, motion free images. Due to the quick acquisition times, these T1w MRI can also be repeated during a single acquisition session if necessary. These movement issues are not restricted to pTBI, in-scanner movement and quality concerns are common for both developing and clinical populations. The current thesis shows that, by analysing the meso-scale organisation of the morphometry of the cortex, there is additional prognostic information to be leveraged from the T1w sMRI, beyond that of commonly used current sMRI analysis approaches (such as univariate ROI analyses or even the multivariate approaches to standard morphometric measurements). Therefore, the SC and MSN methodologies are an attractive framework for future developmental neuroimaging studies of clinical populations where limitations to data quality (such as those outlined above) are common (Batalle et al., 2018), and are therefore generalizable beyond the analysis of pTBI presented in this thesis.

8.3. Strengths, Limitations and Open Questions in pTBI

8.3.1 Sample Size, Open Data and Normative Development

Sample sizes in the current thesis represent some of the largest in the field of neuroimaging of pTBI (King et al., 2019). This drives confidence in these findings compared to those studies with much more

limited/restricted sample sizes. However, for analyses such as whole-cortex ROI-level comparisons of CT such as those seen in Chapter 7, there remains limited statistical power, owing to the high number of multiple comparisons that have to be controlled for. Limited sample sizes are an even greater concern for network-level analyses compared to ROI-level approaches. Brain networks, irrespective of modality, are usually inferred from neuroimaging datasets where there are fewer participants than the number of cortical regions into which the cortex is parcellated. Therefore, the number of parameters to be estimated in the network model are greater than the number of independent observations; this is characterized as the ‘small n, large p’ problem (Romero-Garcia, Atienza, & Cantero, 2014; Romero-Garcia, Atienza, Clemmensen, & Cantero, 2012). This leads to the unreliable estimation of the network due to the overfitting of statistical models (Peng, Wang, Zhou, & Zhu, 2009; Romero-Garcia et al., 2014; Romero-Garcia et al., 2012). This may limit the inferences to be made from such models. The consequence of these small sample sizes in the field has more than academic consequences. The use of sMRI as a biomarker of injury is highly dependent on the discovery of robust effects across samples (Wilde, Dennis, & Tate, 2019) However, findings derived from small sample sizes are less likely to generalise beyond the sample under study. Reliable and reproducible biomarkers are most likely to have the potential to improve clinical assessment and guide intervention (Olsen et al., 2019).

One way to solve such an issue would be increased data-sharing within the field. With increased data-sharing within the field, a greater number of experimental hypotheses could be explored and be validated in independent, existing datasets. This is especially key if the field adopts the supervised, multivariate learning approaches (such as PLS regression) recommended by this thesis, in order to ascertain whether results are due to overfitting on the training data, rather than capturing a legitimate signal of interest in the data. Whilst the current thesis combats the effects of overfitting using leave-one-out cross validation approaches, testing on an independent dataset would offer much greater confidence in the resultant findings.

Many neuroimaging studies of pTBI have not sufficiently powered control groups to the same level as patient groups. Insufficiently powered control groups are a feature of many pTBI studies (Mayer et al., 2018). In the current thesis, robustness analyses using a large, open-access dataset (the ABIDE cohort (Di Martino et al., 2014)) were used to ensure that the studies included robust and reliable estimates of normative development, whilst still capturing variation due to individual differences. Multiple large-scale studies of normative development have provided critical data for comparison to development after brain-injury (Dennis et al., 2019) and additional, even larger, open-access datasets are also on the horizon (i.e. ABCD study (Casey et al., 2018) and HCP-Dev (Somerville et al., 2018)). Future studies should continue to use these larger datasets in a similar approach to that adopted by the current thesis, enabling dense phenotyping of the development of the brain over the paediatric period.

A criticism of this approach reflects the ‘super normal’ characteristics in such cohorts of normative development. Potential bias in sample recruitment may therefore mean that it is not possible to account

for many of the premorbid confounding factors that predispose individuals to injury (See Dennis et al 2019 for a brief commentary on this). This is one reason why many previous studies of TBI adopt orthopaedic-injury controls, in order to control for pre-morbid characteristics that may predispose a child to an injury requiring hospitalization (i.e. levels of impulsivity) but also ongoing environmental factors which may influence outcome (i.e. absence from school, family stress). This may be a concern when adopting analyses that utilise comparisons to these large, open-access control datasets, were differences between patients and these controls due to these predisposing characteristics, rather than due to pathological mechanisms. In spite of these issues, the magnitude of these cohorts offers unique opportunities to explore novel methods for indexing how the developmental trajectory of the brain changes post-insult, and the results of the current thesis highlight the prognostic utility of such approaches.

Another key benefit of some of these open access datasets is their focus on acquisition of large but high quality datasets. In a child-population, it is important to consider that children of a younger age seemingly exhibit greater motion, with ratings of motion significantly related to age at scan (Blumenthal, Zijdenbos, Molloy, & Giedd, 2002). This is echoed in Pardoe, Kucharsky Hiess, and Kuzniecky (2016) where an inverted-U relationship was seen between age and in-scanner motion with both children and over 40's exhibiting greater movement. These factors are likely to result in worse quality MRI however, these datasets have emphasised acquiring high-quality datasets, using behavioural techniques such as mock scanning to improve scan quality. The emphasis on sMRI and analysis quality in these open-access datasets is particularly pertinent given the disproportionate effect this may have on covariance approaches proposed by the current thesis. In a VBM or QDEC analysis, if motion systematically bias the estimations of two ROIs then the statistical results pertaining to those two regions are erroneous however, other regions can still be correctly interpreted in terms of statistical analyses. In the case of SCNs the effects of error-biased ROIs can propagate further through the analyses. For instance, the systematic bias would affect the entire vector of the correlation-matrix related to those ROIs. This example would invalidate the majority of network-derived metrics that either a) calculate an average network-level metric (i.e. global efficiency), b) nodal metrics derived from the biased-ROIs (i.e. degree, nodal efficiency) or c) those nodal metrics which, despite being calculated for a non-biased ROI, rely upon the path lengths of the entire network to be calculated (i.e. betweenness centrality). This is the major reason for stringent quality control mechanisms implemented in the current thesis. Therefore, whilst data-sharing and open datasets should be monopolised, this should not be at the expense of the age-old adage of 'junk in, junk out'.

Overall, given the limited sample sizes in the field of pTBI and the need to assess post-injury change in relation to normative developmental processes, it is highly recommended that future studies begin to utilise these open-access datasets. Neurological insult during development represents an acute deviation from the typically developing trajectory of the structure of the brain (King et al., 2019). These structural

changes and deviations are likely to be related to subsequent behavioural and cognitive sequelae. Thus, approaches such as those in the current thesis, which compare structure of brains post-insult to large healthy reference groups, are likely to have ongoing benefits to the fields of pTBI but also developmental neurology as a whole.

8.3.2 ‘Trajectories’ of development - beyond cross-sectional imaging

The current thesis rests on the assumption that cross-sectional difference in brain morphometry is due to some form of developmentally inappropriate atrophy or divergence from the typical developmental blueprint. Evidence derived from cross-sectional analyses limits the ability to disentangle whether the differences shown between patients and controls are in fact due to neurodevelopmental differences or age-related differences between samples (Kraemer et al., 2000; Vijayakumar et al., 2017). Cross-sectional approaches are also limited in their ability to capture the known variability in and dynamic evolution of pathology from the acute to chronic post-injury periods (Bigler, 2016). Conversely, truly developmental neuroimaging holds a central tenet of “the journey as well as the destination” (Giedd & Rapoport, 2010). Specifically, in adolescents, trajectories of CT over age are more relevant to explaining variation in IQ than absolute differences in CT (Shaw et al., 2006). This is especially important in the field of pTBI where changes to morphometry can be representative of both insult-related pathology but also due to later secondary pathology (i.e. Wallerian degeneration). There is evidence to suggest that maturational change of individual brain regions is different after injury, compared to controls (King et al., 2019). Longitudinal morphometric studies of paediatric cohorts have investigated morphometric change for both patients and controls across multiple time points post-injury (Dennis, Faskowitz, et al., 2017; Dennis et al., 2016; Mayer et al., 2015; Wilde, Merkley, et al., 2012; Wu et al., 2018; Wu et al., 2010). The majority of these studies show a reduction in volume or cortical thinning over time in the TBI group, as well as cross-sectional differences from controls. Interestingly however, they also show an interaction between group (patient vs. controls) and time post-injury on cortical thickness (CT) measures (Mayer et al., 2015; Wilde, Merkley, et al., 2012) and corpus callosum volumes (Wu et al., 2010), with greater atrophy over time seen post pTBI. This, alongside evidence of functionally-relevant developmental divergence in pTBI patients, suggests that there is developmental divergence from the normative developmental trajectory, and this is likely to be related to subsequent cognitive functioning. However, whilst longitudinal imaging is likely to tell us a great deal about the dynamic and evolving pathology due to injury, the current thesis did not take this approach, as it is in fundamental opposition to the aim at hand, early prediction of later cognitive functioning. In order to ensure the clinical benefit and applicability of such research, the focus of such longitudinal research should be to generate hypotheses about how spared networks and neuroanatomy at the time of injury seemingly still allow the unfolding of normative maturation of the brain to subsume healthy development and therefore recovery

from symptoms. This will give us a biological basis with which a priori prognostic models can be generated to effectively predict long-term outcome.

8.3.3 Graph Theory as a ‘language’ of opportunity?

No existing single imaging modality or diagnostic tool is sufficient for the prognostication and phenotyping of TBI (Amyot et al., 2015; Olsen et al., 2019). Chapters in the current thesis highlighted a novel network methodology with which to further interrogate the brain post-pTBI, however there is still a large proportion of variance in post-injury outcome which remains unexplained. Future work should investigate the potential for the integration of multiple modalities of MRI data, and graph theory may provide the ideal framework with which to interrogate this. One of the greatest strengths of the graph-theoretic framework outlined in the thesis is that it provides a common mathematical language with which to describe inter-relationships, irrespective of modality. This has been leveraged to analyse multi-modal, structure-function coupling, modelling sMRI, dMRI and fMRI within a common framework (Reid, Bzdok, et al., 2016; Reid, Lewis, et al., 2016). Other studies have been able to integrate extensive genomic expression data into analyses of the MSN (Seidlitz et al., 2019) due to this commonality of the network approach. This will provide multiple avenues of future discovery for the field of pTBI.

Such approaches may yield valuable insights into the role of structure-function decoupling, investigating how injury-mediated changes to the structural organisation of the brain has observable effects on the functional connectivity of the brain. This was first addressed in adult TBI by (Caeyenberghs, Leemans, Leunissen, Michiels, & Swinnen, 2013), but has not been addressed in the pTBI population. Further studies of structure-functional coupling in adult acquired brain injury (ABI) have shown that network propagation-time, a measure of how much of the structural network is utilised for the spread of functional activation, was greater in those with better recovery of consciousness (Kuceyeski et al., 2016). The two different connectivity modalities represented different phenotypes for recovery; with increased DTI-connectivity segregation and increased functional integration being related to better recovery in adult ABI (Kuceyeski, Jamison, Owen, Raj, & Mukherjee, 2019). Stam (2014) proposed a hub ‘overload and failure’ theory of neurological disease. Under this model, ‘functional hubs’ are regions which are particularly susceptible to damage. When a hub experiences structural damage then its incoming structural projections require functional redirection of information to hubs higher in the hierarchical organization of the brain network. Over time, these hubs higher in the functional hierarchy experience functional overload.

Given that functional activation between regions drives a proportion of the morphometric covariation between regions, likely due to the reciprocal effects of functional co-activation. and cortical structure constraining functional activity, the approaches in the current thesis may represent a novel substrate with which to investigate these functional changes.

Alternatively, by investigating the coupling between DTI-structural connectivity and SC between cortical regions it is possible to investigate how volume/cortical thickness changes distal to primary injury post-TBI may be due to the loss of connectivity between regions, with the connection dropout affecting the morphometry of once connected regions (Bigler, 2016). This highlights how the network-level approaches to brain morphometry may be further utilised for hypothesis testing within the field of pTBI.

A range of other medical and environmental factors also play a role in recovery and eventual impairments. That is to say, these injuries do not exist in a vacuum, and there are many factors, which may mediate outcome. For instance, family environment, such as socioeconomic status and parenting style, mediates some variation in behavioural outcomes for children post-TBI (see Li and Liu (2013) for a review). In regards to specifically EF outcomes, when aspects of the home environment, which are key for development, were of lower quality, long term EF skills were poorer (Durish et al., 2018). In the field of neuroimaging of pTBI, there is no current evidence that these clinical and environmental factors mediate injury-related changes in neuroanatomy as a substrate of later cognitive functioning. The post-injury factors may be key from a therapeutic standpoint, these are potential targets for intervention to improve outcome (Dennis et al., 2019). These types of variables are not investigated in the current thesis, as they were beyond the scope of the initial exploration of the appropriateness of network-level sMRI methodologies. A limited number of studies has examined how environmental factors can influence network-level changes in the brain, at the level of both structural and functional organisation (Lydon-Staley & Bassett, 2018), in pTBI or otherwise, especially within the context of SCN and MSN. Previous evidence suggests that CT in the neonatal period is associated with environmental maternal ethnicity and paternal education (Jha et al., 2018) there is also emerging evidence on the role of traffic-related air pollution on development and ageing-related changes to the morphometry of the brain (de Prado Bert, Mercader, Pujol, Sunyer, & Mortamais, 2018). Using SC approaches such as those highlighted in an earlier chapter, it has also been found that, in healthy adults, socioeconomic deprivation modulates covariance of brain morphometry, with the most deprived having a less modular organization of the SC network (Krishnadas et al., 2013). However, it is important to know whether changes to SC due to environmental factors are in fact functionally relevant. Given more powerful sample sizes with which to estimate these effects, this is an area which warrants further study.

8.4 Conclusion

Traumatic brain injury (TBI) is a common leading cause of disability for children and young adults. Such an insult during development leads to a cognitive-behavioural syndrome of impairments post-injury however, the trajectory and magnitude of this syndrome at an individual-patient level are unknown. The current thesis investigated novel network-level analyses of neuroanatomy, specifically whole-brain structural covariance and morphometric similarity approaches, and its relationship with

neuropsychological functioning, with a focus on executive functioning (EF) at 2 years post-injury. The current thesis further emphasised the role of deviation from the normative organisation of the morphometry of the brain post-insult, and its relationship with long term functioning, developing novel approaches to this important question.

The current thesis concludes that, regarding the neuropsychological sequelae post-neurological insult, quantification of the complex organisation of neuroanatomy across the cortex is a useful biomarker. The current results further motivate the use of neuroimaging and quantification of brain structure to supplement clinical evaluations in order to fully harness the prognostic value of these brain imaging approaches. Future investigations integrating neuropsychology and neuroimaging to understand brain structure-function relationships should continue to utilise modern network approaches which capture the diffuse, nature of injury.

Two major frontiers exist in the developmental neuroimaging fields; a) moving from the group to individual level, there is still large amounts of within group variation to account for (Giedd & Rapoport, 2010; Giedd et al., 2015) and b) moving from papers to people, ensuring that the vast numbers of publications can begin to have an impact on clinical practice (Giedd et al., 2015). The current thesis has addressed the first of these two points, specifically using methods to probe the network-level structure of the brain at the individual level, using large normative samples to estimate how a pTBI can influence the brain during development. The current thesis has also begun to address the second of these two points, the application of developmental neuroimaging to clinical practice, utilising these network-level approaches to morphometry as a biomarker of later cognitive functioning. Future work will be needed to validate these findings in independent cohorts and potentially monopolise on longitudinal imaging to understand how these measures of network-level organisation change over the post-injury period, both in terms of cognitive recovery, and decline. Overall, the network approaches in this thesis are a contemporary approach that appear to be a valuable addition to the toolbox of neuropsychologists, to quantitatively investigate symptomatic changes to neuroanatomy at the network-level post-brain insult.

References

- Adelson, P. D., & Kochanek, P. M. (1998). Head injury in children. *J Child Neurol*, *13*(1), 2-15.
doi:10.1177/088307389801300102
- Aerts, H., Fias, W., Caeyenberghs, K., & Marinazzo, D. (2016). Brain networks under attack: robustness properties and the impact of lesions. *Brain*. doi:10.1093/brain/aww194
- Akshoomoff, N., Beaumont, J. L., Bauer, P. J., Dikmen, S. S., Gershon, R. C., Mungas, D., . . . Heaton, R. K. (2013). VIII. NIH Toolbox Cognition Battery (CB): composite scores of crystallized, fluid, and overall cognition. *Monogr Soc Res Child Dev*, *78*(4), 119-132.
doi:10.1111/mono.12038
- Alexander-Bloch, A., Giedd, J. N., & Bullmore, E. (2013). Imaging structural co-variance between human brain regions. *Nat Rev Neurosci*, *14*(5), 322-336. doi:10.1038/nrn3465
- Alexander-Bloch, A., Raznahan, A., Bullmore, E., & Giedd, J. (2013). The convergence of maturational change and structural covariance in human cortical networks. *J Neurosci*, *33*(7), 2889-2899. doi:10.1523/JNEUROSCI.3554-12.2013
- Amann, M., Andelova, M., Pfister, A., Mueller-Lenke, N., Traud, S., Reinhardt, J., . . . Sprenger, T. (2015). Subcortical brain segmentation of two dimensional T1-weighted data sets with FMRIB's Integrated Registration and Segmentation Tool (FIRST). *Neuroimage-Clinical*, *7*, 43-52. doi:10.1016/j.nicl.2014.11.010
- Amyot, F., Arciniegas, D. B., Brazaitis, M. P., Curley, K. C., Diaz-Arrastia, R., Gandjbakhche, A., . . . Stocker, D. (2015). A Review of the Effectiveness of Neuroimaging Modalities for the Detection of Traumatic Brain Injury. *J Neurotrauma*, *32*(22), 1693-1721.
doi:10.1089/neu.2013.3306
- Andersen, S. M., Rapcsak, S. Z., & Beeson, P. M. (2010). Cost function masking during normalization of brains with focal lesions: still a necessity? *Neuroimage*, *53*(1), 78-84.
doi:10.1016/j.neuroimage.2010.06.003
- Anderson, P. (2002). Assessment and development of executive function (EF) during childhood. *Child Neuropsychology*, *8*(2), 71-82. doi:DOI 10.1076/chin.8.2.71.8724
- Anderson, S. W., Damasio, H., & Damasio, A. R. (2005). A neural basis for collecting behaviour in humans. *Brain*, *128*(Pt 1), 201-212. doi:10.1093/brain/awh329
- Anderson, V., Beauchamp, M. H., Yeates, K. O., Crossley, L., Hearps, S. J., & Catroppa, C. (2013). Social competence at 6 months following childhood traumatic brain injury. *J Int Neuropsychol Soc*, *19*(5), 539-550. doi:10.1017/S1355617712001543
- Anderson, V., Beauchamp, M. H., Yeates, K. O., Crossley, L., Ryan, N., Hearps, S. J. C., & Catroppa, C. (2017). Social Competence at Two Years after Childhood Traumatic Brain Injury. *J Neurotrauma*, *34*(14), 2261-2271. doi:10.1089/neu.2016.4692

- Anderson, V., & Catroppa, C. (2005). Recovery of executive skills following paediatric traumatic brain injury (TBI): A 2 year follow-up. *Brain Inj*, *19*(6), 459-470.
doi:10.1080/02699050400004823
- Anderson, V., Spencer-Smith, M., Coleman, L., Anderson, P., Williams, J., Greenham, M., . . . Jacobs, R. (2010). Children's executive functions: are they poorer after very early brain insult. *Neuropsychologia*, *48*(7), 2041-2050. doi:10.1016/j.neuropsychologia.2010.03.025
- Anderson, V., Spencer-Smith, M., Leventer, R., Coleman, L., Anderson, P., Williams, J., . . . Jacobs, R. (2009). Childhood brain insult: can age at insult help us predict outcome? *Brain*, *132*(Pt 1), 45-56. doi:10.1093/brain/awn293
- Anderson, V., Spencer-Smith, M., & Wood, A. (2011). Do children really recover better? Neurobehavioural plasticity after early brain insult. *Brain*, *134*(Pt 8), 2197-2221.
doi:10.1093/brain/awr103
- Andersson, J. L. R., Skare, S., & Ashburner, J. (2003). How to correct susceptibility distortions in spin-echo echo-planar images: application to diffusion tensor imaging. *Neuroimage*, *20*(2), 870-888. doi:10.1016/S1053-8119(03)00336-7
- Andersson, J. L. R., & Sotiropoulos, S. N. (2015). Non-parametric representation and prediction of single- and multi-shell diffusion-weighted MRI data using Gaussian processes. *Neuroimage*, *122*, 166-176. doi:10.1016/j.neuroimage.2015.07.067
- Andersson, J. L. R., & Sotiropoulos, S. N. (2016). An integrated approach to correction for off-resonance effects and subject movement in diffusion MR imaging. *Neuroimage*, *125*, 1063-1078. doi:10.1016/j.neuroimage.2015.10.019
- Ardila, A., Fatima, S., & Rosselli, M. (2019). *Dysexecutive Syndromes: Clinical and Experimental Perspectives*: Springer International Publishing.
- Babikian, T., & Asarnow, R. (2009). Neurocognitive outcomes and recovery after pediatric TBI: meta-analytic review of the literature. *Neuropsychology*, *23*(3), 283-296. doi:10.1037/a0015268
- Backhausen, L. L., Herting, M. M., Buse, J., Roessner, V., Smolka, M. N., & Vetter, N. C. (2016). Quality Control of Structural MRI Images Applied Using FreeSurfer-A Hands-On Workflow to Rate Motion Artifacts. *Front Neurosci*, *10*. doi:10.3389/Fnins.2016.00558
- Balardin, J. B., Comfort, W. E., Daly, E., Murphy, C., Andrews, D., Murphy, D. G., . . . Sato, J. R. (2015). Decreased centrality of cortical volume covariance networks in autism spectrum disorders. *J Psychiatr Res*, *69*, 142-149. doi:10.1016/j.jpsychires.2015.08.003
- Barch, D. M., Burgess, G. C., Harms, M. P., Petersen, S. E., Schlaggar, B. L., Corbetta, M., . . . Consortium, W.-M. H. (2013). Function in the human connectome: Task-fMRI and individual differences in behavior. *Neuroimage*, *80*, 169-189. doi:10.1016/j.neuroimage.2013.05.033
- Barr, D. J., Levy, R., Scheepers, C., & Tily, H. J. (2013). Random effects structure for confirmatory hypothesis testing: Keep it maximal. *Journal of Memory and Language*, *68*(3), 255-278.
doi:10.1016/j.jml.2012.11.001

- Bastien, P., Vinzi, V. E., & Tenenhaus, M. (2005). PLS generalised linear regression. *Computational Statistics & Data Analysis*, 48(1), 17-46. doi:10.1016/j.csda.2004.02.005
- Batalle, D., Edwards, A. D., & O'Muircheartaigh, J. (2018). Annual Research Review: Not just a small adult brain: understanding later neurodevelopment through imaging the neonatal brain. *J Child Psychol Psychiatry*, 59(4), 350-371. doi:10.1111/jcpp.12838
- Batalle, D., Munoz-Moreno, E., Figueras, F., Bargallo, N., Eixarch, E., & Gratacos, E. (2013). Normalization of similarity-based individual brain networks from gray matter MRI and its association with neurodevelopment in infants with intrauterine growth restriction. *Neuroimage*, 83, 901-911. doi:10.1016/j.neuroimage.2013.07.045
- Bates, D., Machler, M., Bolker, B. M., & Walker, S. C. (2015). Fitting Linear Mixed-Effects Models Using lme4. *Journal of Statistical Software*, 67(1), 1-48. doi:doi:10.18637/jss.v067.i01
- Bathelt, J., Holmes, J., Astle, D. E., Centre for Attention, L., & Memory, T. (2018). Data-Driven Subtyping of Executive Function-Related Behavioral Problems in Children. *J Am Acad Child Adolesc Psychiatry*, 57(4), 252-262 e254. doi:10.1016/j.jaac.2018.01.014
- Beauchamp, M., Catroppa, C., Godfrey, C., Morse, S., Rosenfeld, J. V., & Anderson, V. (2011). Selective Changes in Executive Functioning Ten Years After Severe Childhood Traumatic Brain Injury. *Dev Neuropsychol*, 36(5), 578-595. doi:10.1080/87565641.2011.555572
- Beauchamp, M. H., Aglipay, M., Yeates, K. O., Desire, N., Keightley, M., Anderson, P., . . . Zemek, R. (2018). Predictors of neuropsychological outcome after pediatric concussion. *Neuropsychology*, 32(4), 495-508. doi:10.1037/neu0000419
- Beauchamp, M. H., Brooks, B. L., Barrowman, N., Aglipay, M., Keightley, M., Anderson, P., . . . Zemek, R. (2015). Empirical Derivation and Validation of a Clinical Case Definition for Neuropsychological Impairment in Children and Adolescents. *Journal of the International Neuropsychological Society*, 21(8), 596-609. doi:10.1017/S1355617715000636
- Beauchamp, M. H., Ditchfield, M., Babl, F. E., Kean, M., Catroppa, C., Yeates, K. O., & Anderson, V. (2011). Detecting traumatic brain lesions in children: CT versus MRI versus susceptibility weighted imaging (SWI). *J Neurotrauma*, 28(6), 915-927. doi:10.1089/neu.2010.1712
- Beauchamp, M. H., Ditchfield, M., Maller, J. J., Catroppa, C., Godfrey, C., Rosenfeld, J. V., . . . Anderson, V. A. (2011). Hippocampus, amygdala and global brain changes 10 years after childhood traumatic brain injury. *Int J Dev Neurosci*, 29(2), 137-143. doi:10.1016/j.ijdevneu.2010.12.003
- Bellec, P., Yan, C., Milham, M., Li, Q., Lewis, J., Khundrakpam, B., . . . Craddock, C. (2013). The Neuro Bureau Preprocessing Initiative: open sharing of preprocessed neuroimaging data and derivatives. *Front Neuroinform*, 7. doi:10.3389/conf.fninf.2013.09.00041
- Benjamini, Y., & Hochberg, Y. (1995). Controlling the false discovery rate: a practical and powerful approach to multiple testing. *Journal of the Royal Statistical Society Series B-Methodological*, 57(1), 289-300.

- Bertrand, F., & Maumy-Bertrand, M. (2018). plsRglm: Partial least squares linear and generalized linear regression for processing incomplete datasets by cross-validation and bootstrap techniques with R. *Arxiv*. doi:arXiv:1810.01005.
- Bethlehem, R. A. I., Romero-Garcia, R., Mak, E., Bullmore, E. T., & Baron-Cohen, S. (2017). Structural Covariance Networks in Children with Autism or ADHD. *Cereb Cortex*, 1-10. doi:10.1093/cercor/bhx135
- Bettcher, B. M., Mungas, D., Patel, N., Eloffson, J., Dutt, S., Wynn, M., . . . Kramer, J. H. (2016). Neuroanatomical substrates of executive functions: Beyond prefrontal structures. *Neuropsychologia*, 85, 100-109. doi:10.1016/j.neuropsychologia.2016.03.001
- Bigler, (2007a). Neuroimaging correlates of functional outcome. In N. D. Zasler, D. I. Katz, & R. D. Zafonte (Eds.), *Brain injury medicine: Principles and practice* (pp. 225-246). New York: Demos Medical Publishing.
- Bigler, E. (2001). Quantitative magnetic resonance imaging in traumatic brain injury. *J Head Trauma Rehabil*, 16(2), 117-134.
- Bigler, E. D. (2007b). Anterior and middle cranial fossa in traumatic brain injury: relevant neuroanatomy and neuropathology in the study of neuropsychological outcome. *Neuropsychology*, 21(5), 515-531. doi:10.1037/0894-4105.21.5.515
- Bigler, E. D. (2013). Traumatic brain injury, neuroimaging, and neurodegeneration. *Front Hum Neurosci*, 7. doi:10.3389/Fnhum.2013.00395
- Bigler, E. D. (2016). Systems Biology, Neuroimaging, Neuropsychology, Neuroconnectivity and Traumatic Brain Injury. *Frontiers in Systems Neuroscience*, 10. doi:10.3389/Fnsys.2016.00055
- Bigler, E. D., Abildskov, T. J., Petrie, J., Farrer, T. J., Dennis, M., Simic, N., . . . Owen Yeates, K. (2013). Heterogeneity of brain lesions in pediatric traumatic brain injury. *Neuropsychology*, 27(4), 438-451. doi:10.1037/a0032837
- Bigler, E. D., Abildskov, T. J., Wilde, E. A., McCauley, S. R., Li, X. Q., Merkley, T. L., . . . Levin, H. S. (2010). Diffuse damage in pediatric traumatic brain injury: A comparison of automated versus operator-controlled quantification methods. *Neuroimage*, 50(3), 1017-1026. doi:10.1016/j.neuroimage.2010.01.003
- Bigler, E. D., & Maxwell, W. L. (2011). Neuroimaging and neuropathology of TBI. *NeuroRehabilitation*, 28(2), 63-74. doi:10.3233/NRE-2011-0633
- Bigler, E. D., & Maxwell, W. L. (2012). Neuropathology of mild traumatic brain injury: relationship to neuroimaging findings. *Brain Imaging Behav*, 6(2), 108-136. doi:10.1007/s11682-011-9145-0
- Bigler, E. D., & Wilde, E. A. (2010). Quantitative neuroimaging and the prediction of rehabilitation outcome following traumatic brain injury. *Front Hum Neurosci*, 4. doi:10.3389/Fnhum.2010.00228

- Bigler, E. D., Zielinski, B. A., Goodrich-Hunsaker, N., Black, G. M., Huff, B. S., Christiansen, Z., . . . Yeates, K. O. (2016). The Relation of Focal Lesions to Cortical Thickness in Pediatric Traumatic Brain Injury. *J Child Neurol, 31*(11), 1302-1311. doi:10.1177/0883073816654143
- Blair, C., & Razza, R. P. (2007). Relating effortful control, executive function, and false belief understanding to emerging math and literacy ability in kindergarten. *Child Dev, 78*(2), 647-663. doi:10.1111/j.1467-8624.2007.01019.x
- Blumenthal, J. D., Zijdenbos, A., Molloy, E., & Giedd, J. N. (2002). Motion artifact in magnetic resonance imaging: Implications for automated analysis. *Neuroimage, 16*(1), 89-92. doi:10.1006/nimg.2002.1076
- Bonilha, L., Tabesh, A., Dabbs, K., Hsu, D. A., Stafstrom, C. E., Hermann, B. P., & Lin, J. J. (2014). Neurodevelopmental alterations of large-scale structural networks in children with new-onset epilepsy. *Hum Brain Mapp, 35*(8), 3661-3672. doi:10.1002/hbm.22428
- Brett, M., Leff, A. P., Rorden, C., & Ashburner, J. (2001). Spatial normalization of brain images with focal lesions using cost function masking. *Neuroimage, 14*(2), 486-500. doi:10.1006/nimg.2001.0845
- Bullmore, E., & Sporns, O. (2009). Complex brain networks: graph theoretical analysis of structural and functional systems. *Nat Rev Neurosci, 10*(3), 186-198. doi:10.1038/nrn2575
- Buttram, S. D., Garcia-Filion, P., Miller, J., Youssfi, M., Brown, S. D., Dalton, H. J., & Adelson, P. D. (2015). Computed tomography vs magnetic resonance imaging for identifying acute lesions in pediatric traumatic brain injury. *Hosp Pediatr, 5*(2), 79-84. doi:10.1542/hpeds.2014-0094
- Bzdok, D., & Ioannidis, J. P. A. (2019). Exploration, Inference, and Prediction in Neuroscience and Biomedicine. *Trends in Neurosciences, 42*(4), 251-262. doi:10.1016/j.tins.2019.02.001
- Caeyenberghs, K., Leemans, A., De Decker, C., Heitger, M., Drijkoningen, D., Linden, C. V., . . . Swinnen, S. P. (2012). Brain connectivity and postural control in young traumatic brain injury patients: A diffusion MRI based network analysis. *Neuroimage Clin, 1*(1), 106-115. doi:10.1016/j.nicl.2012.09.011
- Caeyenberghs, K., Leemans, A., Leunissen, I., Michiels, K., & Swinnen, S. (2013). Topological correlations of structural and functional networks in patients with traumatic brain injury. *Front Hum Neurosci, 7*(726). doi:10.3389/fnhum.2013.00726
- Cao, M., Huang, H., Peng, Y., Dong, Q., & He, Y. (2016). Toward Developmental Connectomics of the Human Brain. *Front Neuroanat, 10*, 25. doi:10.3389/fnana.2016.00025
- Casey, B. J., Cannonier, T., Conley, M. I., Cohen, A. O., Barch, D. M., Heitzeg, M. M., . . . Workgroup, A. I. A. (2018). The Adolescent Brain Cognitive Development (ABCD) study: Imaging acquisition across 21 sites. *Dev Cogn Neurosci, 32*, 43-54. doi:10.1016/j.dcn.2018.03.001
- Catroppa, C., & Anderson, V. (2009). Neurodevelopmental outcomes of pediatric traumatic brain injury. *Future Neurology, 4*(6), 811-821. doi:10.2217/fnl.09.52

- Catroppa, C., Hearps, S., Crossley, L., Yeates, K., Beauchamp, M., Fusella, J., & Anderson, V. (2017). Social and Behavioral Outcomes following Childhood Traumatic Brain Injury: What Predicts Outcome at 12 Months Post-Insult? *J Neurotrauma*, *34*(7), 1439-1447. doi:10.1089/neu.2016.4594
- Cauda, F., Mancuso, L., Nani, A., & Costa, T. (2019). Heterogeneous neuroimaging findings, damage propagation and connectivity: an integrative view. *Brain*, *142*(5), e17. doi:10.1093/brain/awz080
- Chard, D. T., Jackson, J. S., Miller, D. H., & Wheeler-Kingshott, C. A. (2010). Reducing the impact of white matter lesions on automated measures of brain gray and white matter volumes. *J Magn Reson Imaging*, *32*(1), 223-228. doi:10.1002/jmri.22214
- Checa, P., & Rueda, M. R. (2011). Behavioral and brain measures of executive attention and school competence in late childhood. *Dev Neuropsychol*, *36*(8), 1018-1032. doi:10.1080/87565641.2011.591857
- Chen, T., Kendrick, K. M., Wang, J., Wu, M., Li, K., Huang, X., . . . Gong, Q. (2017). Anomalous single-subject based morphological cortical networks in drug-naive, first-episode major depressive disorder. *Hum Brain Mapp*. doi:10.1002/hbm.23534
- Chepkoech, J. L., Walhovd, K. B., Grydeland, H., Fjell, A. M., & Neuroimaging, A. D. (2016). Effects of change in FreeSurfer version on classification accuracy of patients with Alzheimer's disease and mild cognitive impairment. *Hum Brain Mapp*, *37*(5), 1831-1841. doi:10.1002/hbm.23139
- Cole, J. H., & Franke, K. (2017). Predicting Age Using Neuroimaging: Innovative Brain Ageing Biomarkers. *Trends in Neurosciences*, *40*(12), 681-690. doi:10.1016/j.tins.2017.10.001
- Cole, J. H., Leech, R., Sharp, D. J., & Alzheimer's Disease Neuroimaging, I. (2015). Prediction of brain age suggests accelerated atrophy after traumatic brain injury. *Ann Neurol*, *77*(4), 571-581. doi:10.1002/ana.24367
- Collette, F., Hogge, M., Salmon, E., & Van der Linden, M. (2006). Exploration of the neural substrates of executive functioning by functional neuroimaging. *Neuroscience*, *139*(1), 209-221. doi:10.1016/j.neuroscience.2005.05.035
- Consonni, V., Ballabio, D., & Todeschini, R. (2010). Evaluation of model predictive ability by external validation techniques. *Journal of Chemometrics*, *24*(3-4), 194-201. doi:10.1002/cem.1290
- Cook, L. G., Hanten, G., Orsten, K. D., Chapman, S. B., Li, X., Wilde, E. A., . . . Levin, H. S. (2013). Effects of moderate to severe traumatic brain injury on anticipating consequences of actions in adolescents: a preliminary study. *J Int Neuropsychol Soc*, *19*(5), 508-517. doi:10.1017/S1355617712001452
- Coulacoglou, C., & Saklofske, D. H. (2017). *Psychometrics and psychological assessment : principles and applications*. London, United Kingdom: Elsevier/AP, Academic Press, an imprint of Elsevier.

- Crinion, J., Ashburner, J., Leff, A., Brett, M., Price, C., & Friston, K. (2007). Spatial normalization of lesioned brains: performance evaluation and impact on fMRI analyses. *Neuroimage*, *37*(3), 866-875. doi:10.1016/j.neuroimage.2007.04.065
- Crossley, N. A., Mechelli, A., Scott, J., Carletti, F., Fox, P. T., McGuire, P., & Bullmore, E. T. (2014). The hubs of the human connectome are generally implicated in the anatomy of brain disorders. *Brain*, *137*, 2382-2395. doi:10.1093/brain/awu132
- Crowe, L. M., Catroppa, C., & Anderson, V. (2015). Sequelae in children: developmental consequences. *Handb Clin Neurol*, *128*, 661-677. doi:10.1016/b978-0-444-63521-1.00041-8
- Csardi, G., & Nepusz, T. (2006). The igraph software package for complex network research. *InterJournal, Complex Systems*, *1695*(5), 1-9.
- Csermely, P., London, A., Wu, L. Y., & Uzzi, B. (2013). Structure and dynamics of core/periphery networks. *Journal of Complex Networks*, *1*(2), 93-123. doi:10.1093/comnet/cnt016
- Cullen, D. K., Vernekar, V. N., & LaPlaca, M. C. (2011). Trauma-induced plasmalemma disruptions in three-dimensional neural cultures are dependent on strain modality and rate. *J Neurotrauma*, *28*(11), 2219-2233. doi:10.1089/neu.2011.1841
- Dale, A. M., Fischl, B., & Sereno, M. I. (1999). Cortical surface-based analysis - I. Segmentation and surface reconstruction. *Neuroimage*, *9*(2), 179-194. doi:DOI 10.1006/nimg.1998.0395
- Dale, A. M., & Sereno, M. I. (1993). Improved Localization of Cortical Activity by Combining Eeg and Meg with Mri Cortical Surface Reconstruction - a Linear-Approach. *Journal of Cognitive Neuroscience*, *5*(2), 162-176. doi:DOI 10.1162/jocn.1993.5.2.162
- Davatzikos, C. (2004). Why voxel-based morphometric analysis should be used with great caution when characterizing group differences. *Neuroimage*, *23*(1), 17-20. doi:10.1016/j.neuroimage.2004.05.010
- Davatzikos, C. (2019). Machine learning in neuroimaging: Progress and challenges. *Neuroimage*, *197*, 652-656. doi:10.1016/j.neuroimage.2018.10.003
- de Prado Bert, P., Mercader, E. M. H., Pujol, J., Sunyer, J., & Mortamais, M. (2018). The Effects of Air Pollution on the Brain: a Review of Studies Interfacing Environmental Epidemiology and Neuroimaging. *Current Environmental Health Reports*, *5*(3), 351-364. doi:10.1007/s40572-018-0209-9
- Delis, D. C., Kaplan, E., & Kramer, J. H. (Eds.). (2001). *Delis Kaplan Executive Function System (D-KEFS) Examiner's Manual*. San Antonio, TX: The Psychological Corporation.
- Dennis, E. L., Babikian, T., Giza, C. C., Thompson, P. M., & Asarnow, R. F. (2017). Diffusion MRI in pediatric brain injury. *Child's Nervous System*, *33*(10), 1683-1692. doi:10.1007/s00381-017-3522-y
- Dennis, E. L., Caeyenberghs, K., Asarnow, R. F., Asarnow, R. F., Bartnik-Olson, B., Bigler, E. D., . . . Wilde, E. A. (2019). Brain Imaging in Young Brain-Injured Patients: A Coordinated Effort

- Towards Individualized Predictors from the ENIGMA Pediatric msTBI Group. *PsyArXiv*. doi:10.31234/osf.io/y2txh
- Dennis, E. L., Faskowitz, J., Rashid, F., Babikian, T., Mink, R., Babbitt, C., . . . Asarnow, R. F. (2017). Diverging volumetric trajectories following pediatric traumatic brain injury. *Neuroimage Clin, 15*, 125-135. doi:10.1016/j.nicl.2017.03.014
- Dennis, E. L., Hua, X., Villalon-Reina, J., Moran, L. M., Kernan, C., Babikian, T., . . . Giza, C. C. (2016). Tensor-based morphometry reveals volumetric deficits in moderate/severe pediatric traumatic brain injury. *J Neurotrauma, 33*(9), 840-852.
- Dennis, E. L., & Thompson, P. M. (2013). Typical and atypical brain development: a review of neuroimaging studies. *Dialogues Clin Neurosci, 15*(3), 359-384.
- Dennis, M., Simic, N., Bigler, E. D., Abildskov, T., Agostino, A., Taylor, H. G., . . . Yeates, K. O. (2013). Cognitive, affective, and conative theory of mind (ToM) in children with traumatic brain injury. *Dev Cogn Neurosci, 5*, 25-39. doi:10.1016/j.dcn.2012.11.006
- Desikan, R. S., Segonne, F., Fischl, B., Quinn, B. T., Dickerson, B. C., Blacker, D., . . . Killiany, R. J. (2006). An automated labeling system for subdividing the human cerebral cortex on MRI scans into gyral based regions of interest. *Neuroimage, 31*(3), 968-980. doi:10.1016/j.neuroimage.2006.01.021
- Di Martino, A., Yan, C. G., Li, Q., Denio, E., Castellanos, F. X., Alaerts, K., . . . Milham, M. P. (2014). The autism brain imaging data exchange: towards a large-scale evaluation of the intrinsic brain architecture in autism. *Mol Psychiatry, 19*(6), 659-667. doi:10.1038/mp.2013.78
- Diamond, A. (2013). Executive functions. *Annu Rev Psychol, 64*, 135-168. doi:10.1146/annurev-psych-113011-143750
- Donders, J., & DeWit, C. (2017). Parental ratings of daily behavior and child cognitive test performance after pediatric mild traumatic brain injury. *Child Neuropsychol, 23*(5), 554-570. doi:10.1080/09297049.2016.1161015
- Downing, K. (2015). *An examination of three theoretical models of executive functioning*. (Doctor of Philosophy), Texas Woman's University. Retrieved from <https://twu-ir.tdl.org/handle/11274/7031?show=full>
- Drijckoningen, D., Chalavi, S., Sunaert, S., Duysens, J., Swinnen, S. P., & Caeyenberghs, K. (2017). Regional Gray Matter Volume Loss Is Associated with Gait Impairments in Young Brain-Injured Individuals. *J Neurotrauma, 34*(5), 1022-1034. doi:10.1089/neu.2016.4500
- Drijckoningen, D., Leunissen, I., Caeyenberghs, K., Hoogkamer, W., Sunaert, S., Duysens, J., & Swinnen, S. P. (2015). Regional volumes in brain stem and cerebellum are associated with postural impairments in young brain-injured patients. *Hum Brain Mapp, 36*(12), 4897-4909. doi:10.1002/hbm.22958

- Dubois, J., Benders, M., Borradori-Tolsa, C., Cachia, A., Lazeyras, F., Ha-Vinh Leuchter, R., . . . Huppi, P. S. (2008). Primary cortical folding in the human newborn: an early marker of later functional development. *Brain*, *131*(Pt 8), 2028-2041. doi:10.1093/brain/awn137
- Durish, C. L., Yeates, K. O., Stancin, T., Taylor, H. G., Walz, N. C., & Wade, S. L. (2018). Home Environment as a Predictor of Long-Term Executive Functioning following Early Childhood Traumatic Brain Injury. *J Int Neuropsychol Soc*, *24*(1), 11-21. doi:10.1017/S1355617717000595
- Erus, G., Battapady, H., Satterthwaite, T. D., Hakonarson, H., Gur, R. E., Davatzikos, C., & Gur, R. C. (2015). Imaging Patterns of Brain Development and their Relationship to Cognition. *Cereb Cortex*, *25*(6), 1676-1684. doi:10.1093/cercor/bht425
- Esopenko, C., & Levine, B. (2015). Aging, neurodegenerative disease, and traumatic brain injury: the role of neuroimaging. *J Neurotrauma*, *32*(4), 209-220. doi:10.1089/neu.2014.3506
- Esopenko, C., & Levine, B. (2017). Autobiographical memory and structural brain changes in chronic phase TBI. *Cortex*, *89*, 1-10. doi:10.1016/j.cortex.2017.01.007
- Esteban, O., Birman, D., Schaer, M., Koyejo, O. O., Poldrack, R. A., & Gorgolewski, K. J. (2017). MRIQC: Advancing the automatic prediction of image quality in MRI from unseen sites. *PLoS One*, *12*(9), e0184661. doi:10.1371/journal.pone.0184661
- Evans, A. C. (2013). Networks of anatomical covariance. *Neuroimage*, *80*, 489-504. doi:10.1016/j.neuroimage.2013.05.054
- Ewing-Cobbs, L., Prasad, M. R., Landry, S. H., Kramer, L., & DeLeon, R. (2004). Executive functions following traumatic brain injury in young children: a preliminary analysis. *Dev Neuropsychol*, *26*(1), 487-512. doi:10.1207/s15326942dn2601_7
- Fagerholm, E. D., Hellyer, P. J., Scott, G., Leech, R., & Sharp, D. J. (2015). Disconnection of network hubs and cognitive impairment after traumatic brain injury. *Brain*, *138*, 1696-1709. doi:10.1093/brain/awv075
- Fan, Y., Shi, F., Smith, J. K., Lin, W., Gilmore, J. H., & Shen, D. (2011). Brain anatomical networks in early human brain development. *Neuroimage*, *54*(3), 1862-1871. doi:10.1016/j.neuroimage.2010.07.025
- Farbota, K. D. M., Sodhi, A., Bendlin, B. B., McLaren, D. G., Xu, G. F., Rowley, H. A., & Johnson, S. C. (2012). Longitudinal Volumetric Changes following Traumatic Brain Injury: A Tensor-Based Morphometry Study. *Journal of the International Neuropsychological Society*, *18*(6), 1006-1018. doi:10.1017/S1355617712000835
- Faridi, N., Karama, S., Burgaleta, M., White, M. T., Evans, A. C., Fonov, V., . . . Waber, D. P. (2015). Neuroanatomical correlates of behavioral rating versus performance measures of working memory in typically developing children and adolescents. *Neuropsychology*, *29*(1), 82-91. doi:10.1037/neu0000079

- Fearing, M. A., Bigler, E. D., Wilde, E. A., Johnson, J. L., Hunter, J. V., Li, X. Q., . . . Levin, H. S. (2008). Morphometric MRI findings in the thalamus and brainstem in children after moderate to severe traumatic brain injury. *J Child Neurol*, *23*(7), 729-737.
doi:10.1177/0883073808314159
- Fischl, B. (2012). FreeSurfer. *Neuroimage*, *62*(2), 774-781. doi:10.1016/j.neuroimage.2012.01.021
- Fischl, B., & Dale, A. M. (2000). Measuring the thickness of the human cerebral cortex from magnetic resonance images. *Proc Natl Acad Sci U S A*, *97*(20), 11050-11055.
- Fischl, B., Liu, A., & Dale, A. M. (2001). Automated manifold surgery: Constructing geometrically accurate and topologically correct models of the human cerebral cortex. *Ieee Transactions on Medical Imaging*, *20*(1), 70-80. doi:Doi 10.1109/42.906426
- Fischl, B., Salat, D. H., Busa, E., Albert, M., Dieterich, M., Haselgrove, C., . . . Dale, A. M. (2002). Whole brain segmentation: automated labeling of neuroanatomical structures in the human brain. *Neuron*, *33*(3), 341-355.
- Fischl, B., van der Kouwe, A., Destrieux, C., Halgren, E., Segonne, F., Salat, D. H., . . . Dale, A. M. (2004). Automatically parcellating the human cerebral cortex. *Cereb Cortex*, *14*(1), 11-22.
- Fiske, A., & Holmboe, K. (2019). Neural substrates of early executive function development. *Dev Rev*, *52*, 42-62. doi:10.1016/j.dr.2019.100866
- Fjell, A. M., Grydeland, H., Krogsrud, S. K., Amlien, I., Rohani, D. A., Ferschmann, L., . . . Walhovd, K. B. (2015). Development and aging of cortical thickness correspond to genetic organization patterns. *Proc Natl Acad Sci U S A*, *112*(50), 15462-15467. doi:10.1073/pnas.1508831112
- Fornito, A., Zalesky, A., & Breakspear, M. (2013). Graph analysis of the human connectome: promise, progress, and pitfalls. *Neuroimage*, *80*, 426-444. doi:10.1016/j.neuroimage.2013.04.087
- Fornito, A., Zalesky, A., & Bullmore, E. (2016). *Fundamentals of Brain Network Analysis*: Academic Press.
- Fortin, J. P., Cullen, N., Sheline, Y. I., Taylor, W. D., Aselcioglu, I., Cook, P. A., . . . Shinohara, R. T. (2018). Harmonization of cortical thickness measurements across scanners and sites. *Neuroimage*, *167*, 104-120. doi:10.1016/j.neuroimage.2017.11.024
- Foulon, C., Cerliani, L., Kinkingnehun, S., Levy, R., Rosso, C., Urbanski, M., . . . Thiebaut de Schotten, M. (2017). Advanced Lesion Symptom Mapping Analyses And Implementation As BCBtoolkit. *bioRxiv*. doi:10.1101/133314
- Friedman, N. P., Miyake, A., Altamirano, L. J., Corley, R. P., Young, S. E., Rhea, S. A., & Hewitt, J. K. (2016). Stability and Change in Executive Function Abilities From Late Adolescence to Early Adulthood: A Longitudinal Twin Study. *Dev Psychol*, *52*(2), 326-340.
doi:10.1037/dev0000075
- Frisoni, G. B., Fox, N. C., Jack, C. R., Jr., Scheltens, P., & Thompson, P. M. (2010). The clinical use of structural MRI in Alzheimer disease. *Nature Reviews Neurology*, *6*(2), 67-77.
doi:10.1038/nrneurol.2009.215

- Fujiwara, E., Schwartz, M. L., Gao, F. Q., Black, S. E., & Levine, B. (2008). Ventral frontal cortex functions and quantified MRI in traumatic brain injury. *Neuropsychologia*, *46*(2), 461-474. doi:10.1016/j.neuropsychologia.2007.08.027
- Gaines, K. D., & Soper, H. V. (2018). Neuropsychological assessment of executive functions following pediatric traumatic brain injury. *Appl Neuropsychol Child*, *7*(1), 31-43. doi:10.1080/21622965.2016.1229406
- Galdi, P., Blesa, M., Sullivan, G., Lamb, G. J., Stoye, D. Q., Quigley, A. J., . . . Boardman, J. P. (2018). Neonatal Morphometric Similarity Networks Predict Atypical Brain Development Associated with Preterm Birth. *10842*, 47-57. doi:10.1007/978-3-030-00755-3_6
- Garcia-Ramos, C., Bobholz, S., Dabbs, K., Hermann, B., Joutsa, J., Rinne, J. O., . . . Group, T. S. (2017). Brain structure and organization five decades after childhood onset epilepsy. *Hum Brain Mapp*. doi:10.1002/hbm.23593
- Garcia-Ramos, C., Lin, J. J., Bonilha, L., Jones, J. E., Jackson, D. C., Prabhakaran, V., & Hermann, B. P. (2016). Disruptions in cortico-subcortical covariance networks associated with anxiety in new-onset childhood epilepsy. *Neuroimage Clin*, *12*, 815-824. doi:10.1016/j.nicl.2016.10.017
- Garren, S. T. (2019). jmuOutlier: Permutation Tests for Nonparametric Statistics (Version R Version 2.2).
- Genc, S., Anderson, V., Ryan, N. P., Malpas, C. B., Catroppa, C., Beauchamp, M. H., & Silk, T. J. (2017). Recovery of White Matter following Pediatric Traumatic Brain Injury Depends on Injury Severity. *J Neurotrauma*, *34*(4), 798-806. doi:10.1089/neu.2016.4584
- Geng, X., Li, G., Lu, Z., Gao, W., Wang, L., Shen, D., . . . Gilmore, J. H. (2017). Structural and Maturation Covariance in Early Childhood Brain Development. *Cereb Cortex*, *27*(3), 1795-1807. doi:10.1093/cercor/bhw022
- Giedd, J. N. (2004). Structural magnetic resonance imaging of the adolescent brain. *Ann N Y Acad Sci*, *1021*, 77-85. doi:10.1196/annals.1308.009
- Giedd, J. N., Blumenthal, J., Jeffries, N. O., Castellanos, F. X., Liu, H., Zijdenbos, A., . . . Rapoport, J. L. (1999). Brain development during childhood and adolescence: a longitudinal MRI study. *Nat Neurosci*, *2*(10), 861-863. doi:Doi 10.1038/13158
- Giedd, J. N., & Rapoport, J. L. (2010). Structural MRI of pediatric brain development: what have we learned and where are we going? *Neuron*, *67*(5), 728-734. doi:10.1016/j.neuron.2010.08.040
- Giedd, J. N., Raznahan, A., Alexander-Bloch, A., Schmitt, E., Gogtay, N., & Rapoport, J. L. (2015). Child psychiatry branch of the National Institute of Mental Health longitudinal structural magnetic resonance imaging study of human brain development. *Neuropsychopharmacology*, *40*(1), 43-49. doi:10.1038/npp.2014.236
- Gilmore, J. H., Lin, W., Prastawa, M. W., Looney, C. B., Vetsa, Y. S., Knickmeyer, R. C., . . . Gerig, G. (2007). Regional gray matter growth, sexual dimorphism, and cerebral asymmetry in the neonatal brain. *J Neurosci*, *27*(6), 1255-1260.

- Gioia, G. A., Isquith, P. K., Guy, S. C., & Kenworthy, L. (2000). *Behavior Rating Inventory of Executive Function*. Odessa, FL: Psychological Assessment Resources.
- Glasser, M. F., Sotiropoulos, S. N., Wilson, J. A., Coalson, T. S., Fischl, B., Andersson, J. L., . . . Consortium, W.-M. H. (2013). The minimal preprocessing pipelines for the Human Connectome Project. *Neuroimage*, *80*, 105-124. doi:10.1016/j.neuroimage.2013.04.127
- Glasser, M. F., & Van Essen, D. C. (2011). Mapping Human Cortical Areas In Vivo Based on Myelin Content as Revealed by T1- and T2-Weighted MRI. *Journal of Neuroscience*, *31*(32), 11597-11616. doi:10.1523/Jneurosci.2180-11.2011
- Gogtay, N., Giedd, J. N., Lusk, L., Hayashi, K. M., Greenstein, D., Vaituzis, A. C., . . . Thompson, P. M. (2004). Dynamic mapping of human cortical development during childhood through early adulthood. *Proc Natl Acad Sci U S A*, *101*(21), 8174-8179. doi:DOI 10.1073/pnas.0402680101
- Goh, S. Y., Irimia, A., Torgerson, C. M., & Horn, J. D. (2014). Neuroinformatics challenges to the structural, connectomic, functional and electrophysiological multimodal imaging of human traumatic brain injury. *Front Neuroinform*, *8*, 19. doi:10.3389/fninf.2014.00019
- Goldstrohm, S. L., & Arffa, S. (2005). Preschool children with mild to moderate traumatic brain injury: an exploration of immediate and post-acute morbidity. *Arch Clin Neuropsychol*, *20*(6), 675-695. doi:10.1016/j.acn.2005.02.005
- Gong, G., He, Y., Chen, Z. J., & Evans, A. C. (2012). Convergence and divergence of thickness correlations with diffusion connections across the human cerebral cortex. *Neuroimage*, *59*(2), 1239-1248. doi:10.1016/j.neuroimage.2011.08.017
- Gonzalez-Villa, S., Valverde, S., Cabezas, M., Pareto, D., Vilanova, J. C., Ramio-Torrenta, L., . . . Llado, X. (2017). Evaluating the effect of multiple sclerosis lesions on automatic brain structure segmentation. *Neuroimage Clin*, *15*, 228-238. doi:10.1016/j.nicl.2017.05.003
- Goulas, A., Uylings, H. B., & Hilgetag, C. C. (2017). Principles of ipsilateral and contralateral cortico-cortical connectivity in the mouse. *Brain Struct Funct*, *222*(3), 1281-1295. doi:10.1007/s00429-016-1277-y
- Griffiths, K. R., Grieve, S. M., Kohn, M. R., Clarke, S., Williams, L. M., & Korgaonkar, M. S. (2016). Altered gray matter organization in children and adolescents with ADHD: a structural covariance connectome study. *Translational Psychiatry*, *6*. doi:10.1038/tp.2016.219
- Gronenschild, E. H. B. M., Habets, P., Jacobs, H. I. L., Mengelers, R., Rozendaal, N., van Os, J., & Marcelis, M. (2012). The Effects of FreeSurfer Version, Workstation Type, and Macintosh Operating System Version on Anatomical Volume and Cortical Thickness Measurements. *PLoS One*, *7*(6). doi:10.1371/journal.pone.0038234
- Hahn, A., Lanzenberger, R., & Kasper, S. (2019). Making Sense of Connectivity. *International Journal of Neuropsychopharmacology*, *22*(3), 194-207. doi:10.1093/ijnp/pyy100

- Han, X., Jovicich, J., Salat, D., van der Kouwe, A., Quinn, B., Czanner, S., . . . Fischl, B. (2006). Reliability of MRI-derived measurements of human cerebral cortical thickness: the effects of field strength, scanner upgrade and manufacturer. *Neuroimage*, *32*(1), 180-194. doi:10.1016/j.neuroimage.2006.02.051
- Hannawi, Y., & Stevens, R. D. (2016). Mapping the Connectome Following Traumatic Brain Injury. *Current Neurology and Neuroscience Reports*, *16*(5). doi:10.1007/s11910-016-0642-9
- Hanten, G., Cook, L., Orsten, K., Chapman, S. B., Li, X., Wilde, E. A., . . . Levin, H. S. (2011). Effects of traumatic brain injury on a virtual reality social problem solving task and relations to cortical thickness in adolescence. *Neuropsychologia*, *49*(3), 486-497. doi:10.1016/j.neuropsychologia.2010.12.007
- Hayes, J. P., Bigler, E. D., & Verfaellie, M. (2016). Traumatic Brain Injury as a Disorder of Brain Connectivity. *J Int Neuropsychol Soc*, *22*(2), 120-137. doi:10.1017/S1355617715000740
- He, N., Rolls, E. T., Zhao, W., & Guo, S. (2019). Predicting human inhibitory control from brain structural MRI. *Brain Imaging Behav*. doi:10.1007/s11682-019-00166-9
- Heaton, R. K., Akshoomoff, N., Tulsky, D., Mungas, D., Weintraub, S., Dikmen, S., . . . Gershon, R. (2014). Reliability and Validity of Composite Scores from the NIH Toolbox Cognition Battery in Adults. *Journal of the International Neuropsychological Society*, *20*(6), 588-598. doi:10.1017/S1355617714000241
- Hedges, L. V., & Olkin, I. (2014). *Statistical methods for meta-analysis*. : Academic Press.
- Henry, L. A., & Bettenay, C. (2010). The Assessment of Executive Functioning in Children. *Child and Adolescent Mental Health*, *15*(2), 110-119. doi:10.1111/j.1475-3588.2010.00557.x
- Herting, M. M., Gautam, P., Spielberg, J. M., Dahl, R. E., & Sowell, E. R. (2015). A Longitudinal Study: Changes in Cortical Thickness and Surface Area during Pubertal Maturation. *PLoS One*, *10*(3). doi:10.1371/journal.pone.0119774
- Hillary, F. G., & Grafman, J. H. (2017). Injured Brains and Adaptive Networks: The Benefits and Costs of Hyperconnectivity. *Trends Cogn Sci*, *21*(5), 385-401. doi:10.1016/j.tics.2017.03.003
- Hong, S. J., Bernhardt, B. C., Gill, R. S., Bernasconi, N., & Bernasconi, A. (2017). The spectrum of structural and functional network alterations in malformations of cortical development. *Brain*, *140*(8), 2133-2143. doi:10.1093/brain/awx145
- Horowitz-Kraus, T., Holland, S. K., & Freund, L. (2016). Imaging executive functions in typically and atypically developed children. In J. A. Griffin, P. McCardle, & L. Freund (Eds.), *Executive Function in Preschool Age Children: Integrating Measurement, Neurodevelopment and Translational Research*. Washington, DC: American Psychological Association Press.
- Hunter, S. J., & Sparrow, E. P. (2012). *Executive function and dysfunction: Identification, assessment and treatment*. Cambridge: University Press.
- Huttenlocher, P. (1994). Synaptogenesis in human cerebral cortex. In G. Dawson & K. Fischer (Eds.), *Human Behavior and the Developing Brain* (pp. 137–152). New York, USA.: Guilford Press.

- Im, K., Lee, J. M., Lyttelton, O., Kim, S. H., Evans, A. C., & Kim, S. I. (2008). Brain size and cortical structure in the adult human brain. *Cereb Cortex*, *18*(9), 2181-2191.
doi:10.1093/cercor/bhm244
- Irimia, A., Chambers, M. C., Alger, J. R., Filippou, M., Prastawa, M. W., Wang, B., . . . Van Horn, J. D. (2011). Comparison of acute and chronic traumatic brain injury using semi-automatic multimodal segmentation of MR volumes. *J Neurotrauma*, *28*(11), 2287-2306.
doi:10.1089/neu.2011.1920
- Irimia, A., Chambers, M. C., Torgerson, C. M., Filippou, M., Hovda, D. A., Alger, J. R., . . . Van Horn, J. D. (2012). Patient-tailored connectomics visualization for the assessment of white matter atrophy in traumatic brain injury. *Front Neurol*, *3*, 10. doi:10.3389/fneur.2012.00010
- Irimia, A., Goh, S. M., Wade, A. C., Patel, K., Vespa, P. M., & Van Horn, J. D. (2017). Traumatic Brain Injury Severity, Neuropathophysiology, and Clinical Outcome: Insights from Multimodal Neuroimaging. *Front Neurol*, *8*, 530. doi:10.3389/fneur.2017.00530
- Irimia, A., Goh, S. Y., Torgerson, C. M., Vespa, P., & Van Horn, J. D. (2014). Structural and connectomic neuroimaging for the personalized study of longitudinal alterations in cortical shape, thickness and connectivity after traumatic brain injury. *J Neurosurg Sci*, *58*(3), 129-144.
- Irimia, A., Wang, B., Aylward, S. R., Prastawa, M. W., Pace, D. F., Gerig, G., . . . Van Horn, J. D. (2012). Neuroimaging of structural pathology and connectomics in traumatic brain injury: Toward personalized outcome prediction. *Neuroimage Clin*, *1*(1), 1-17.
doi:10.1016/j.nicl.2012.08.002
- Iyer, K. K., Zalesky, A., Barlow, K. M., & Cocchi, L. (2019). Default mode network anatomy and function is linked to pediatric concussion recovery. *bioRxiv*. doi:10.1101/795740
- Jacobs, R., Harvey, A. S., & Anderson, V. (2011). Are executive skills primarily mediated by the prefrontal cortex in childhood? Examination of focal brain lesions in childhood. *Cortex*, *47*(7), 808-824. doi:10.1016/j.cortex.2010.06.002
- Jenkinson, M., Bannister, P., Brady, M., & Smith, S. (2002). Improved optimization for the robust and accurate linear registration and motion correction of brain images. *Neuroimage*, *17*(2), 825-841. doi:10.1006/nimg.2002.1132
- Jenkinson, M., Beckmann, C. F., Behrens, T. E., Woolrich, M. W., & Smith, S. M. (2012). Fsl. *Neuroimage*, *62*(2), 782-790. doi:10.1016/j.neuroimage.2011.09.015
- Jenkinson, M., & Smith, S. (2001). A global optimisation method for robust affine registration of brain images. *Medical Image Analysis*, *5*(2), 143-156. doi:Doi 10.1016/S1361-8415(01)00036-6
- Jha, S. C., Xia, K., Ahn, M., Girault, J. B., Li, G., Wang, L., . . . Knickmeyer, R. C. (2018). Environmental Influences on Infant Cortical Thickness and Surface Area. *Cereb Cortex*, *29*(3), 1139-1149. doi:10.1093/cercor/bhy020

- Johnson, V. E., Stewart, W., & Smith, D. H. (2013). Axonal pathology in traumatic brain injury. *Exp Neurol*, 246, 35-43. doi:10.1016/j.expneurol.2012.01.013
- Johnson, V. E., Stewart, W., Weber, M. T., Cullen, D. K., Siman, R., & Smith, D. H. (2016). SNTF immunostaining reveals previously undetected axonal pathology in traumatic brain injury. *Acta Neuropathol*, 131(1), 115-135. doi:10.1007/s00401-015-1506-0
- Juranek, J., Johnson, C. P., Prasad, M. R., Kramer, L. A., Saunders, A., Filipek, P. A., . . . Ewing-Cobbs, L. (2012). Mean diffusivity in the amygdala correlates with anxiety in pediatric TBI. *Brain Imaging Behav*, 6(1), 36-48. doi:10.1007/s11682-011-9140-5
- Karr, J. E., Areshenkoff, C. N., Rast, P., Hofer, S. M., Iverson, G. L., & Garcia-Barrera, M. A. (2018). The Unity and Diversity of Executive Functions: A Systematic Review and Re-Analysis of Latent Variable Studies. *Psychol Bull*, 144(11), 1147-1185. doi:10.1037/bul0000160
- Karr, J. E., Hofer, S. M., Iverson, G. L., & Garcia-Barrera, M. A. (2019). Examining the Latent Structure of the Delis-Kaplan Executive Function System. *Arch Clin Neuropsychol*, 34(3), 381-394. doi:10.1093/arclin/acy043
- Kassambara, A. (2018). ggpubr: 'ggplot2' Based Publication Ready Plots (Version 0.1.8). Retrieved from <https://rpkgs.datanovia.com/ggpubr/>
- Katuwal, G. J., Baum, S. A., Cahill, N. D., Dougherty, C. C., Evans, E., Evans, D. W., . . . Michael, A. M. (2016). Inter-Method Discrepancies in Brain Volume Estimation May Drive Inconsistent Findings in Autism. *Front Neurosci*, 10. doi:10.3389/Fnins.2016.00439
- Keenan, H. T., Clark, A. E., Holubkov, R., Cox, C. S., & Ewing-Cobbs, L. (2018). Psychosocial and Executive Function Recovery Trajectories One Year after Pediatric Traumatic Brain Injury: The Influence of Age and Injury Severity. *J Neurotrauma*, 35(2), 286-296. doi:10.1089/neu.2017.5265
- Keightley, M. L., Sinopoli, K. J., Davis, K. D., Mikulis, D. J., Wennberg, R., Tartaglia, M. C., . . . Tator, C. H. (2014). Is there evidence for neurodegenerative change following traumatic brain injury in children and youth? A scoping review. *Front Hum Neurosci*, 8. doi:10.3389/Fnhum.2014.00139
- Khundrakpam, B. S., Lewis, J. D., Reid, A., Karama, S., Zhao, L., Chouinard-Decorte, F., . . . Brain Development Cooperative, G. (2017). Imaging structural covariance in the development of intelligence. *Neuroimage*, 144(Pt A), 227-240. doi:10.1016/j.neuroimage.2016.08.041
- Khundrakpam, B. S., Lewis, J. D., Zhao, L., Chouinard-Decorte, F., & Evans, A. C. (2016). Brain connectivity in normally developing children and adolescents. *Neuroimage*, 134, 192-203. doi:10.1016/j.neuroimage.2016.03.062
- Khundrakpam, B. S., Reid, A., Brauer, J., Carbonell, F., Lewis, J., Ameis, S., . . . Grp, B. D. C. (2013). Developmental Changes in Organization of Structural Brain Networks. *Cereb Cortex*, 23(9), 2072-2085. doi:10.1093/cercor/bhs187

- Kim, H. J., Shin, J. H., Han, C. E., Kim, H. J., Na, D. L., Seo, S. W., . . . Alzheimer's Disease Neuroimaging, I. (2016). Using Individualized Brain Network for Analyzing Structural Covariance of the Cerebral Cortex in Alzheimer's Patients. *Front Neurosci*, *10*(394), 394. doi:10.3389/fnins.2016.00394
- King, D. J., Ellis, K. R., Seri, S., & Wood, A. G. (2019). A systematic review of cross-sectional differences and longitudinal changes to the morphometry of the brain following paediatric traumatic brain injury. *NeuroImage: Clinical*, 101844. doi:10.1016/j.nicl.2019.101844
- King, D. J., Novak, J., Shephard, A., Beare, R., Anderson, V. A., & Wood, A. G. (In prep.). Lesion induced error on automated measures of brain volume: Data from a paediatric traumatic brain injury cohort.
- King, D. J., Seri, S., Beare, R., Catroppa, C., Anderson, V. A., & Wood, A. G. (2020). Developmental divergence of structural brain networks as an indicator of future cognitive impairments in childhood brain injury: Executive functions. *Dev Cogn Neurosci*, *42*, 100762. doi:10.1016/j.dcn.2020.100762
- King, D. J., & Wood, A. (2019). Clinically-Feasible Brain Morphometric Similarity Network Construction Approaches with Restricted Magnetic Resonance Imaging Acquisitions and their Relationship with Cognition. *PsyArXiv*. doi:10.31234/osf.io/vks3u
- Klapwijk, E. T., van de Kamp, F., van der Meulen, M., Peters, S., & Wierenga, L. M. (2019). Qoala-T: A supervised-learning tool for quality control of FreeSurfer segmented MRI data. *Neuroimage*, *189*, 116-129. doi:10.1016/j.neuroimage.2019.01.014
- Klein, A., Ghosh, S. S., Bao, F. S., Giard, J., Hame, Y., Stavsky, E., . . . Keshavan, A. (2017). Mindboggling morphometry of human brains. *PLOS Computational Biology*, *13*(2). doi:10.1371/journal.pcbi.1005350
- Knickmeyer, R. C., Gouttard, S., Kang, C., Evans, D., Wilber, K., Smith, J. K., . . . Gilmore, J. H. (2008). A structural MRI study of human brain development from birth to 2 years. *J Neurosci*, *28*(47), 12176-12182. doi:10.1523/JNEUROSCI.3479-08.2008
- Kochanek, P. M., Clark, R. S., Ruppel, R. A., Adelson, P. D., Bell, M. J., Whalen, M. J., . . . Jenkins, L. W. (2000). Biochemical, cellular, and molecular mechanisms in the evolution of secondary damage after severe traumatic brain injury in infants and children: Lessons learned from the bedside. *Pediatr Crit Care Med*, *1*(1), 4-19.
- Kong, X. Z., Liu, Z., Huang, L., Wang, X., Yang, Z., Zhou, G., . . . Liu, J. (2015). Mapping Individual Brain Networks Using Statistical Similarity in Regional Morphology from MRI. *PLoS One*, *10*(11), e0141840. doi:10.1371/journal.pone.0141840
- Kong, X. Z., Wang, X., Huang, L. J., Pu, Y., Yang, Z. T., Dang, X. B., . . . Liu, J. (2014). Measuring individual morphological relationship of cortical regions. *Journal of Neuroscience Methods*, *237*, 103-107. doi:10.1016/j.jneumeth.2014.09.003

- Konigs, M., Pouwels, P. J., Ernest van Heurn, L. W., Bakx, R., Jeroen Vermeulen, R., Goslings, J. C., . . . Oosterlaan, J. (2018). Relevance of neuroimaging for neurocognitive and behavioral outcome after pediatric traumatic brain injury. *Brain Imaging Behav*, *12*(1), 29-43. doi:10.1007/s11682-017-9673-3
- Konigs, M., van Heurn, L. W. E., Bakx, R., Vermeulen, R. J., Goslings, J. C., Poll-The, B. T., . . . Pouwels, P. J. W. (2017). The structural connectome of children with traumatic brain injury. *Hum Brain Mapp*. doi:10.1002/hbm.23614
- Kraemer, H. C., Yesavage, J. A., Taylor, J. L., & Kupfer, D. (2000). How can we learn about developmental processes from cross-sectional studies, or can we? *Am J Psychiatry*, *157*(2), 163-171. doi:10.1176/appi.ajp.157.2.163
- Krämer, N., & Sugiyama, M. (2011). The Degrees of Freedom of Partial Least Squares Regression. *Journal of the American Statistical Association*, *106*(494), 697-705. doi:10.1198/jasa.2011.tm10107
- Krasny-Pacini, A., Chevignard, M., Lancien, S., Escolano, S., Laurent-Vannier, A., De Agostini, M., & Meyer, P. (2017). Executive function after severe childhood traumatic brain injury - Age-at-injury vulnerability periods: The TGE prospective longitudinal study. *Ann Phys Rehabil Med*, *60*(2), 74-82. doi:10.1016/j.rehab.2016.06.001
- Krishnadas, R., Kim, J., McLean, J., Batty, D., McLean, J., Millar, K., . . . Cavanagh, J. (2013). The envirome and the connectome: exploring the structural noise in the human brain associated with socioeconomic deprivation. *Front Hum Neurosci*, *7*(722). doi:10.3389/fnhum.2013.00722
- Krishnan, A., Williams, L. J., McIntosh, A. R., & Abdi, H. (2011). Partial Least Squares (PLS) methods for neuroimaging: A tutorial and review. *Neuroimage*, *56*(2), 455-475. doi:10.1016/j.neuroimage.2010.07.034
- Kruschwitz, J. D., Waller, L., Daedelow, L. S., Walter, H., & Veer, I. M. (2018). General, crystallized and fluid intelligence are not associated with functional global network efficiency: A replication study with the human connectome project 1200 data set. *Neuroimage*, *171*, 323-331. doi:10.1016/j.neuroimage.2018.01.018
- Kuceyeski, A., Shah, S., Dyke, J. P., Bickel, S., Abdelnour, F., Schiff, N. D., . . . Raj, A. (2016). The application of a mathematical model linking structural and functional connectomes in severe brain injury. *Neuroimage Clin*, *11*, 635-647. doi:10.1016/j.nicl.2016.04.006
- Kuceyeski, A. F., Jamison, K. W., Owen, J. P., Raj, A., & Mukherjee, P. (2019). Longitudinal increases in structural connectome segregation and functional connectome integration are associated with better recovery after mild TBI. *Hum Brain Mapp*, *40*(15), 4441-4456. doi:10.1002/hbm.24713

- Kuperberg, G. R., Broome, M. R., McGuire, P. K., David, A. S., Eddy, M., Ozawa, F., . . . Fischl, B. (2003). Regionally localized thinning of the cerebral cortex in schizophrenia. *Arch Gen Psychiatry*, *60*(9), 878-888. doi:10.1001/archpsyc.60.9.878
- Lamblin, M., Murawski, C., Whittle, S., & Fornito, A. (2017). Social connectedness, mental health and the adolescent brain. *Neurosci Biobehav Rev*, *80*, 57-68. doi:10.1016/j.neubiorev.2017.05.010
- Lerch, J. P., van der Kouwe, A. J. W., Raznahan, A., Pans, T., Johansen-Berg, H., Miller, K. L., . . . Sotiropoulos, S. N. (2017). Studying neuroanatomy using MRI. *Nat Neurosci*, *20*(3), 314-326. doi:10.1038/nn.4501
- Lerman-Sinkoff, D. B., Sui, J., Rachakonda, S., Kandala, S., Calhoun, V. D., & Barch, D. M. (2017). Multimodal neural correlates of cognitive control in the Human Connectome Project. *Neuroimage*, *163*, 41-54. doi:10.1016/j.neuroimage.2017.08.081
- Levan, A., Black, G., Mietchen, J., Baxter, L., Brock Kirwan, C., & Gale, S. D. (2016). Right frontal pole cortical thickness and executive functioning in children with traumatic brain injury: the impact on social problems. *Brain Imaging Behav*, *10*(4), 1090-1095. doi:10.1007/s11682-015-9472-7
- Levin, H. S., Hanten, G., Roberson, G., Li, X., Ewing-Cobbs, L., Dennis, M., . . . Swank, P. (2008). Prediction of cognitive sequelae based on abnormal computed tomography findings in children following mild traumatic brain injury. *J Neurosurg Pediatr*, *1*(6), 461-470. doi:10.3171/PED/2008/1/6/461
- Levin, H. S., Song, J., Scheibel, R. S., Fletcher, J. M., Harward, H., Lilly, M., & Goldstein, F. (1997). Concept formation and problem-solving following closed head injury in children. *J Int Neuropsychol Soc*, *3*(6), 598-607.
- Levine, B., Kovacevic, N., Nica, E. I., Schwartz, M. L., Gao, F., & Black, S. E. (2013). Quantified MRI and cognition in TBI with diffuse and focal damage. *Neuroimage Clin*, *2*, 534-541. doi:10.1016/j.nicl.2013.03.015
- Li, L., & Liu, J. (2013). The effect of pediatric traumatic brain injury on behavioral outcomes: a systematic review. *Dev Med Child Neurol*, *55*(1), 37-45. doi:10.1111/j.1469-8749.2012.04414.x
- Li, W., Yang, C., Shi, F., Wu, S., Wang, Q., Nie, Y., & Zhang, X. (2017). Construction of Individual Morphological Brain Networks with Multiple Morphometric Features. *Front Neuroanat*, *11*, 34. doi:10.3389/fnana.2017.00034
- Liu, K., Shi, L., Chen, F., Wayne, M. M., Lim, C. K., Cheng, P. W., . . . Wang, D. (2015). Altered topological organization of brain structural network in Chinese children with developmental dyslexia. *Neurosci Lett*, *589*, 169-175. doi:10.1016/j.neulet.2015.01.037

- Luciana, M., & Nelson, C. A. (1998). The functional emergence of prefrontally-guided working memory systems in four- to eight-year-old children. *Neuropsychologia*, *36*(3), 273-293. doi:Doi 10.1016/S0028-3932(97)00109-7
- Lydon-Staley, D. M., & Bassett, D. S. (2018). Network Neuroscience: A Framework for Developing Biomarkers in Psychiatry. In J. Pratt & J. Hall (Eds.), *Biomarkers in Psychiatry* (pp. 79-109). Cham: Springer International Publishing.
- Madan, C. R. (2017). Advances in Studying Brain Morphology: The Benefits of Open-Access Data. *Front Hum Neurosci*, *11*, 405. doi:10.3389/fnhum.2017.00405
- Magnotta, V. A. (1999). Quantitative In Vivo Measurement of Gyrification in the Human Brain: Changes Associated with Aging. *Cereb Cortex*, *9*(2), 151-160. doi:10.1093/cercor/9.2.151
- Mak, E., Colloby, S. J., Thomas, A., & O'Brien, J. T. (2016). The segregated connectome of late-life depression: a combined cortical thickness and structural covariance analysis. *Neurobiol Aging*, *48*, 212-221. doi:10.1016/j.neurobiolaging.2016.08.013
- Mangeot, S., Armstrong, K., Colvin, A. N., Yeates, K. O., & Taylor, H. G. (2002). Long-term executive function deficits in children with traumatic brain injuries: assessment using the Behavior Rating Inventory of Executive Function (BRIEF). *Child Neuropsychol*, *8*(4), 271-284. doi:10.1076/chin.8.4.271.13503
- Manly, T., Robertson, I. H., Anderson, V., & Nimmo-Smith, I. (Eds.). (1999). *The Test of Everyday Attention for Children (TEA-Ch) Manual*. London: Harcourt Assessment.
- Mantel, N. (1967). The detection of disease clustering and a generalized regression approach. *Cancer research*, *27*(2 Part 1), 209-220.
- Marcus, D. S., Harwell, J., Olsen, T., Hodge, M., Glasser, M. F., Prior, F., . . . Van Essen, D. C. (2011). Informatics and data mining tools and strategies for the human connectome project. *Front Neuroinform*, *5*, 4. doi:10.3389/fninf.2011.00004
- Marek, S., Hwang, K., Foran, W., Hallquist, M. N., & Luna, B. (2015). The Contribution of Network Organization and Integration to the Development of Cognitive Control. *PLoS Biol*, *13*(12), e1002328. doi:10.1371/journal.pbio.1002328
- Marrus, N., Eggebrecht, A. T., Todorov, A., Elison, J. T., Wolff, J. J., Cole, L., . . . Pruett, J. R., Jr. (2018). Walking, Gross Motor Development, and Brain Functional Connectivity in Infants and Toddlers. *Cereb Cortex*, *28*(2), 750-763. doi:10.1093/cercor/bhx313
- Masel, B. E., & DeWitt, D. S. (2010). Traumatic brain injury: a disease process, not an event. *J Neurotrauma*, *27*(8), 1529-1540. doi:10.1089/neu.2010.1358
- Max, J. E., Wilde, E. A., Bigler, E. D., Thompson, W. K., MacLeod, M., Vasquez, A. C., . . . Levin, H. S. (2012). Neuroimaging correlates of novel psychiatric disorders after pediatric traumatic brain injury. *J Am Acad Child Adolesc Psychiatry*, *51*(11), 1208-1217. doi:10.1016/j.jaac.2012.08.026

- Maxwell, W. L. (2012). Traumatic brain injury in the neonate, child and adolescent human: an overview of pathology. *Int J Dev Neurosci*, *30*(3), 167-183.
doi:10.1016/j.ijdevneu.2011.12.008
- Maxwell, W. L., MacKinnon, M. A., Stewart, J. E., & Graham, D. I. (2010). Stereology of cerebral cortex after traumatic brain injury matched to the Glasgow Outcome Score. *Brain*, *133*, 139-160. doi:10.1093/brain/awp264
- Mayer, A. R., Hanlon, F. M., & Ling, J. M. (2015). Gray matter abnormalities in pediatric mild traumatic brain injury. *J Neurotrauma*, *32*(10), 723-730. doi:10.1089/neu.2014.3534
- Mayer, A. R., Kaushal, M., Dodd, A. B., Hanlon, F. M., Shaff, N. A., Mannix, R., . . . Meier, T. B. (2018). Advanced biomarkers of pediatric mild traumatic brain injury: Progress and perils. *Neurosci Biobehav Rev*, *94*, 149-165. doi:10.1016/j.neubiorev.2018.08.002
- McAuley, T., Chen, S., Goos, L., Schachar, R., & Crosbie, J. (2010). Is the behavior rating inventory of executive function more strongly associated with measures of impairment or executive function? *J Int Neuropsychol Soc*, *16*(3), 495-505. doi:10.1017/S1355617710000093
- McCauley, S. R., Wilde, E. A., Merkley, T. L., Schnelle, K. P., Bigler, E. D., Hunter, J. V., . . . Levin, H. S. (2010). Patterns of Cortical Thinning in Relation to Event-Based Prospective Memory Performance Three Months after Moderate to Severe Traumatic Brain Injury in Children. *Dev Neuropsychol*, *35*(3), 318-332. doi:10.1080/87565641003696866
- McCrorry, P., Collie, A., Anderson, V., & Davis, G. (2004). Can we manage sport related concussion in children the same as in adults? *Br J Sports Med*, *38*(5), 516-519.
doi:10.1136/bjism.2004.014811
- McKenna, R., Rushe, T., & Woodcock, K. A. (2017). Informing the Structure of Executive Function in Children: A Meta-Analysis of Functional Neuroimaging Data. *Front Hum Neurosci*, *11*.
doi:10.3389/Fnhum.2017.00154
- McKinlay, A., Grace, R. C., Horwood, L. J., Fergusson, D. M., Ridder, E. M., & Macfarlane, M. R. (2008). Prevalence of traumatic brain injury among children, adolescents and young adults: Prospective evidence from a birth cohort. *Brain Inj*, *22*(2), 175-181.
doi:10.1080/02699050801888824
- Mechelli, A., Friston, K. J., Frackowiak, R. S., & Price, C. J. (2005). Structural covariance in the human cortex. *J Neurosci*, *25*(36), 8303-8310. doi:10.1523/JNEUROSCI.0357-05.2005
- Merkley, T. L., Bigler, E. D., Wilde, E. A., McCauley, S. R., Hunter, J. V., & Levin, H. S. (2008). Diffuse changes in cortical thickness in pediatric moderate-to-severe traumatic brain injury. *J Neurotrauma*, *25*(11), 1343-1345. doi:10.1089/neu.2008.0615
- Mills, K. L., Goddings, A. L., Herting, M. M., Meuwese, R., Blakemore, S. J., Crone, E. A., . . . Tamnes, C. K. (2016). Structural brain development between childhood and adulthood: Convergence across four longitudinal samples. *Neuroimage*, *141*, 273-281.
doi:10.1016/j.neuroimage.2016.07.044

- Miyake, A., & Friedman, N. P. (2012). The Nature and Organization of Individual Differences in Executive Functions: Four General Conclusions. *Current Directions in Psychological Science*, *21*(1), 8-14. doi:10.1177/0963721411429458
- Miyake, A., Friedman, N. P., Emerson, M. J., Witzki, A. H., Howerter, A., & Wager, T. D. (2000). The unity and diversity of executive functions and their contributions to complex "frontal lobe" tasks: A latent variable analysis. *Cognitive Psychology*, *41*(1), 49-100. doi:10.1006/cogp.1999.0734
- Moher, D., Liberati, A., Tetzlaff, J., Altman, D. G., & Grp, P. (2009). Preferred Reporting Items for Systematic Reviews and Meta-Analyses: The PRISMA Statement. *Plos Medicine*, *6*(7). doi:10.1371/journal.pmed.1000097
- Morey, R. A., Petty, C. M., Xu, Y., Hayes, J. P., Wagner, H. R., Lewis, D. V., . . . McCarthy, G. (2009). A comparison of automated segmentation and manual tracing for quantifying hippocampal and amygdala volumes. *Neuroimage*, *45*(3), 855-866. doi:10.1016/j.neuroimage.2008.12.033
- Morgan, S. E., Seidlitz, J., Whitaker, K., Romero-Garcia, R., Clifton, N. E., Scarpazza, C., . . . Bullmore, E. T. (2018). Cortical patterning of abnormal morphometric similarity in psychosis is associated with brain expression of schizophrenia related genes. *bioRxiv*, 501494. doi:10.1101/501494
- Morgan, S. E., White, S. R., Bullmore, E. T., & Vertes, P. E. (2018). A Network Neuroscience Approach to Typical and Atypical Brain Development. *Biol Psychiatry Cogn Neurosci Neuroimaging*, *3*(9), 754-766. doi:10.1016/j.bpsc.2018.03.003
- Nachev, P., Coulthard, E., Jager, H. R., Kennard, C., & Husain, M. (2008). Enantiomorphic normalization of focally lesioned brains. *Neuroimage*, *39*(3), 1215-1226. doi:10.1016/j.neuroimage.2007.10.002
- Nie, J., Li, G., Wang, L., Shi, F., Lin, W., Gilmore, J. H., & Shen, D. (2014). Longitudinal development of cortical thickness, folding, and fiber density networks in the first 2 years of life. *Hum Brain Mapp*, *35*(8), 3726-3737. doi:10.1002/hbm.22432
- Niendam, T. A., Laird, A. R., Ray, K. L., Dean, Y. M., Glahn, D. C., & Carter, C. S. (2012). Meta-analytic evidence for a superordinate cognitive control network subserving diverse executive functions. *Cognitive Affective & Behavioral Neuroscience*, *12*(2), 241-268. doi:10.3758/s13415-011-0083-5
- Nomi, J. S., Vij, S. G., Dajani, D. R., Steimke, R., Damaraju, E., Rachakonda, S., . . . Uddin, L. Q. (2017). Chronnectomic patterns and neural flexibility underlie executive function. *Neuroimage*, *147*, 861-871. doi:10.1016/j.neuroimage.2016.10.026
- Nowrangi, M. A., Lyketsos, C., Rao, V., & Munro, C. A. (2014). Systematic Review of Neuroimaging Correlates of Executive Functioning: Converging Evidence From Different Clinical

- Populations. *Journal of Neuropsychiatry and Clinical Neurosciences*, 26(2), 114-125. doi:DOI 10.1176/appi.neuropsych.12070176
- Oldham, S., & Fornito, A. (2019). The development of brain network hubs. *Dev Cogn Neurosci*, 36. doi:10.1016/J.Dcn.2018.12.005
- Olsen, A., Asarnow, R. F., Bigler, E. D., Caeyenberghs, K., Conde, V., Dams-O'Connor, K., . . . Hillary, F. (2019). Toward a Global and Reproducible Science for Brain Imaging in Neurotrauma: The ENIGMA Adult Moderate/Severe Traumatic Brain Injury Working Group. *PsyArXiv*. doi:10.31234/osf.io/jnsb2
- Pagani, M., Bifone, A., & Gozzi, A. (2016). Structural covariance networks in the mouse brain. *Neuroimage*, 129, 55-63. doi:10.1016/j.neuroimage.2016.01.025
- Palacios, E. M., Sala-Llonch, R., Junque, C., Roig, T., Tormos, J. M., Bargallo, N., & Vendrell, P. (2013). White matter/gray matter contrast changes in chronic and diffuse traumatic brain injury. *J Neurotrauma*, 30(23), 1991-1994. doi:10.1089/neu.2012.2836
- Palaniyappan, L., Park, B., Balain, V., Dangi, R., & Liddle, P. (2015). Abnormalities in structural covariance of cortical gyrification in schizophrenia. *Brain Struct Funct*, 220(4), 2059-2071. doi:10.1007/s00429-014-0772-2
- Pardoe, H. R., Kucharsky Hiess, R., & Kuzniecky, R. (2016). Motion and morphometry in clinical and nonclinical populations. *Neuroimage*, 135, 177-185. doi:10.1016/j.neuroimage.2016.05.005
- Patenaude, B., Smith, S. M., Kennedy, D. N., & Jenkinson, M. (2011). A Bayesian model of shape and appearance for subcortical brain segmentation. *Neuroimage*, 56(3), 907-922. doi:10.1016/j.neuroimage.2011.02.046
- Peng, J., Wang, P., Zhou, N. F., & Zhu, J. (2009). Partial Correlation Estimation by Joint Sparse Regression Models. *Journal of the American Statistical Association*, 104(486), 735-746. doi:10.1198/jasa.2009.0126
- Penny, W. D., Friston, K. J., Ashburner, J. T., Kiebel, S. J., & Nichols, T. E. (2011). *Statistical parametric mapping: the analysis of functional brain images*: Elsevier.
- Pereira, J. B., Aarsland, D., Ginestet, C. E., Lebedev, A. V., Wahlund, L. O., Simmons, A., . . . Westman, E. (2015). Aberrant cerebral network topology and mild cognitive impairment in early Parkinson's disease. *Hum Brain Mapp*, 36(8), 2980-2995. doi:10.1002/hbm.22822
- Pereira, J. B., Mijalkov, M., Kakaei, E., Mecocci, P., Vellas, B., Tsolaki, M., . . . AddNeuroMed consortium, f. t. A. s. D. N. I. (2016). Disrupted Network Topology in Patients with Stable and Progressive Mild Cognitive Impairment and Alzheimer's Disease. *Cereb Cortex*, 26(8), 3476-3493. doi:10.1093/cercor/bhw128
- Perlaki, G., Horvath, R., Nagy, S. A., Bogner, P., Doczi, T., Janszky, J., & Orsi, G. (2017). Comparison of accuracy between FSL's FIRST and Freesurfer for caudate nucleus and putamen segmentation. *Sci Rep*, 7(1), 2418. doi:10.1038/s41598-017-02584-5

- Perone, S., Almy, B., & Zelazo, P. D. (2018). Toward an Understanding of the Neural Basis of Executive Function Development. In R. Gibb & B. Kolb (Eds.), *The Neurobiology of Brain and Behavioral Development* (pp. 291-314): Academic Press.
- Phan, T. G., Chen, J., Donnan, G., Srikanth, V., Wood, A., & Reutens, D. C. (2010). Development of a new tool to correlate stroke outcome with infarct topography: a proof-of-concept study. *Neuroimage*, *49*(1), 127-133. doi:10.1016/j.neuroimage.2009.07.067
- Pinto, P. S., Poretti, A., Meoded, A., Tekes, A., & Huisman, T. A. (2012). The unique features of traumatic brain injury in children. Review of the characteristics of the pediatric skull and brain, mechanisms of trauma, patterns of injury, complications and their imaging findings-- part 1. *J Neuroimaging*, *22*(2), e1-e17. doi:10.1111/j.1552-6569.2011.00688.x
- Polinder, S., Haagsma, J. A., van Klaveren, D., Steyerberg, E. W., & van Beeck, E. F. (2015). Health-related quality of life after TBI: a systematic review of study design, instruments, measurement properties, and outcome. *Popul Health Metr*, *13*, 4. doi:10.1186/s12963-015-0037-1
- Qi, T., Gu, B., Ding, G., Gong, G., Lu, C., Peng, D., . . . Liu, L. (2016). More bilateral, more anterior: Alterations of brain organization in the large-scale structural network in Chinese dyslexia. *Neuroimage*, *124*(Pt A), 63-74. doi:10.1016/j.neuroimage.2015.09.011
- R Core Team. (2016). R: A language and environment for statistical computing (Version 3.3.2). Vienna, Austria: R Foundation for Statistical Computing. Retrieved from <https://www.R-project.org/>
- Raamana, P. R., Weiner, M. W., Wang, L., Beg, M. F., & Alzheimer's Disease Neuroimaging, I. (2015). Thickness network features for prognostic applications in dementia. *Neurobiol Aging*, *36 Suppl 1*(S1), S91-S102. doi:10.1016/j.neurobiolaging.2014.05.040
- Raznahan, A., Lerch, J. P., Lee, N., Greenstein, D., Wallace, G. L., Stockman, M., . . . Giedd, J. N. (2011). Patterns of Coordinated Anatomical Change in Human Cortical Development: A Longitudinal Neuroimaging Study of Maturation Coupling. *Neuron*, *72*(5), 873-884. doi:10.1016/j.neuron.2011.09.028
- Raznahan, A., Shaw, P., Lalonde, F., Stockman, M., Wallace, G. L., Greenstein, D., . . . Giedd, J. N. (2011). How does your cortex grow? *J Neurosci*, *31*(19), 7174-7177. doi:10.1523/JNEUROSCI.0054-11.2011
- Reid, A. T., Bzdok, D., Langner, R., Fox, P. T., Laird, A. R., Amunts, K., . . . Eickhoff, C. R. (2016). Multimodal connectivity mapping of the human left anterior and posterior lateral prefrontal cortex. *Brain Struct Funct*, *221*(5), 2589-2605. doi:10.1007/s00429-015-1060-5
- Reid, A. T., Lewis, J., Bezgin, G., Khundrakpam, B., Eickhoff, S. B., McIntosh, A. R., . . . Evans, A. C. (2016). A cross-modal, cross-species comparison of connectivity measures in the primate brain. *Neuroimage*, *125*, 311-331. doi:10.1016/j.neuroimage.2015.10.057

- Resch, C., Anderson, V. A., Beauchamp, M. H., Crossley, L., Hearps, S. J. C., van Heugten, C. M., . . . Catroppa, C. (2019). Age-dependent differences in the impact of paediatric traumatic brain injury on executive functions: A prospective study using susceptibility-weighted imaging. *Neuropsychologia*, *124*, 236-245. doi:10.1016/j.neuropsychologia.2018.12.004
- Reuter, M., Tisdall, M. D., Qureshi, A., Buckner, R. L., van der Kouwe, A. J. W., & Fischl, B. (2015). Head motion during MRI acquisition reduces gray matter volume and thickness estimates. *Neuroimage*, *107*, 107-115. doi:10.1016/j.neuroimage.2014.12.006
- Riggs, N. R., Jahromi, L. B., Razza, R. P., Dillworth-Bart, J. E., & Mueller, U. (2006). Executive function and the promotion of social-emotional competence. *Journal of Applied Developmental Psychology*, *27*(4), 300-309. doi:10.1016/j.appdev.2006.04.002
- Ringdahl, E. N., Becker, M. L., Hussey, J. E., Thaler, N. S., Vogel, S. J., Cross, C., . . . Allen, D. N. (2019). Executive Function Profiles in Pediatric Traumatic Brain Injury. *Dev Neuropsychol*, *44*(2), 172-188. doi:10.1080/87565641.2018.1557190
- Romero-Garcia, R., Atienza, M., & Cantero, J. L. (2014). Predictors of Coupling Between Structural and Functional Cortical Networks in Normal Aging. *Hum Brain Mapp*, *35*(6), 2724-2740. doi:10.1002/hbm.22362
- Romero-Garcia, R., Atienza, M., Clemmensen, L. H., & Cantero, J. L. (2012). Effects of network resolution on topological properties of human neocortex. *Neuroimage*, *59*(4), 3522-3532. doi:10.1016/j.neuroimage.2011.10.086
- Romero-Garcia, R., Whitaker, K. J., Vasa, F., Seidlitz, J., Shinn, M., Fonagy, P., . . . Vertes, P. E. (2018). Structural covariance networks are coupled to expression of genes enriched in supragranular layers of the human cortex. *Neuroimage*, *171*, 256-267. doi:10.1016/j.neuroimage.2017.12.060
- Roncadin, C., Guger, S., Archibald, J., Barnes, M., & Dennis, M. (2004). Working memory after mild, moderate, or severe childhood closed head injury. *Dev Neuropsychol*, *25*(1-2), 21-36.
- Rosas, H. D., Liu, A. K., Hersch, S., Glessner, M., Ferrante, R. J., Salat, D. H., . . . Fischl, B. (2002). Regional and progressive thinning of the cortical ribbon in Huntington's disease. *Neurology*, *58*(5), 695-701.
- Rosen, A. F. G., Roalf, D. R., Ruparel, K., Blake, J., Seelaus, K., Villa, L. P., . . . Satterthwaite, T. D. (2018). Quantitative assessment of structural image quality. *Neuroimage*, *169*, 407-418. doi:10.1016/j.neuroimage.2017.12.059
- Rosnow, R. L., Rosenthal, R., & Rubin, D. B. (2000). Contrasts and correlations in effect-size estimation. *Psychological Science*, *11*(6), 446-453. doi:Doi 10.1111/1467-9280.00287
- Ross, D. E. (2011). Review of longitudinal studies of MRI brain volumetry in patients with traumatic brain injury. *Brain Inj*, *25*(13-14), 1271-1278. doi:10.3109/02699052.2011.624568
- Ryan, N. P., Beauchamp, M. H., Beare, R., Coleman, L., Ditchfield, M., Kean, M., . . . Anderson, V. A. (2016). Uncovering cortico-striatal correlates of cognitive fatigue in pediatric acquired

- brain disorder: Evidence from traumatic brain injury. *Cortex*, 83, 222-230.
doi:10.1016/j.cortex.2016.07.020
- Ryan, N. P., Catroppa, C., Beare, R., Silk, T. J., Crossley, L., Beauchamp, M. H., . . . Anderson, V. A. (2016). Theory of mind mediates the prospective relationship between abnormal social brain network morphology and chronic behavior problems after pediatric traumatic brain injury. *Soc Cogn Affect Neurosci*, 11(4), 683-692. doi:10.1093/scan/nsw007
- Ryan, N. P., Catroppa, C., Beare, R., Silk, T. J., Hearps, S. J., Beauchamp, M. H., . . . Anderson, V. A. (2017). Uncovering the neuroanatomical correlates of cognitive, affective and conative theory of mind in paediatric traumatic brain injury: a neural systems perspective. *Soc Cogn Affect Neurosci*, 12(9), 1414-1427. doi:10.1093/scan/nsx066
- Ryan, N. P., Catroppa, C., Cooper, J. M., Beare, R., Ditchfield, M., Coleman, L., . . . Anderson, V. A. (2015). The emergence of age-dependent social cognitive deficits after generalized insult to the developing brain: a longitudinal prospective analysis using susceptibility-weighted imaging. *Hum Brain Mapp*, 36(5), 1677-1691. doi:10.1002/hbm.22729
- Ryan, N. P., van Bijnen, L., Catroppa, C., Beauchamp, M. H., Crossley, L., Hearps, S., & Anderson, V. (2016). Longitudinal outcome and recovery of social problems after pediatric traumatic brain injury (TBI): Contribution of brain insult and family environment. *Int J Dev Neurosci*, 49, 23-30. doi:10.1016/j.ijdevneu.2015.12.004
- Saatman, K. E., Duhaime, A. C., Bullock, R., Maas, A. I., Valadka, A., Manley, G. T., . . . Advisory Panel, M. (2008). Classification of traumatic brain injury for targeted therapies. *J Neurotrauma*, 25(7), 719-738. doi:10.1089/neu.2008.0586
- Saggar, M., Hosseini, S. M., Bruno, J. L., Quintin, E. M., Raman, M. M., Kesler, S. R., & Reiss, A. L. (2015). Estimating individual contribution from group-based structural correlation networks. *Neuroimage*, 120, 274-284. doi:10.1016/j.neuroimage.2015.07.006
- Salat, D. H., Buckner, R. L., Snyder, A. Z., Greve, D. N., Desikan, R. S., Busa, E., . . . Fischl, B. (2004). Thinning of the cerebral cortex in aging. *Cereb Cortex*, 14(7), 721-730.
doi:10.1093/cercor/bhh032
- Santa-Cruz, C., & Rosas, R. (2017). Mapping of Executive Functions / Cartografía de las Funciones Ejecutivas. *Estudios de Psicología*, 38(2), 284-310. doi:10.1080/02109395.2017.1311459
- Schieber, T. A., Carpi, L., Diaz-Guilera, A., Pardalos, P. M., Masoller, C., & Ravetti, M. G. (2017). Quantification of network structural dissimilarities. *Nat Commun*, 8, 13928.
doi:10.1038/ncomms13928
- Schmitt, J. E., Wallace, G. L., Rosenthal, M. A., Molloy, E. A., Ordaz, S., Lenroot, R., . . . Giedd, J. N. (2007). A multivariate analysis of neuroanatomic relationships in a genetically informative pediatric sample. *Neuroimage*, 35(1), 70-82. doi:10.1016/j.neuroimage.2006.04.232

- Schneider, E. B., Sur, S., Raymont, V., Duckworth, J., Kowalski, R. G., Efron, D. T., . . . Stevens, R. D. (2014). Functional recovery after moderate/severe traumatic brain injury: a role for cognitive reserve? *Neurology*, *82*(18), 1636-1642. doi:10.1212/WNL.0000000000000379
- Seeley, W. W., Menon, V., Schatzberg, A. F., Keller, J., Glover, G. H., Kenna, H., . . . Greicius, M. D. (2007). Dissociable intrinsic connectivity networks for salience processing and executive control. *J Neurosci*, *27*(9), 2349-2356. doi:10.1523/JNEUROSCI.5587-06.2007
- Seghier, M. L., Ramlackhansingh, A., Crinion, J., Leff, A. P., & Price, C. J. (2008). Lesion identification using unified segmentation-normalisation models and fuzzy clustering. *Neuroimage*, *41*(4), 1253-1266. doi:10.1016/j.neuroimage.2008.03.028
- Segonne, F., Dale, A. M., Busa, E., Glessner, M., Salat, D., Hahn, H. K., & Fischl, B. (2004). A hybrid approach to the skull stripping problem in MRI. *Neuroimage*, *22*(3), 1060-1075. doi:10.1016/j.neuroimage.2004.03.032
- Segonne, F., Pacheco, J., & Fischl, B. (2007). Geometrically accurate topology-correction of cortical surfaces using nonseparating loops. *Ieee Transactions on Medical Imaging*, *26*(4), 518-529. doi:10.1109/Tmi.2006.887364
- Seidlitz, J., Nadig, A., Liu, S., Bethlehem, R. A. I., Vértes, P. E., Morgan, S. E., . . . Raznahan, A. (2019). Transcriptomic and Cellular Decoding of Regional Brain Vulnerability to Neurodevelopmental Disorders. *bioRxiv*. doi:10.1101/573279
- Seidlitz, J., Vasa, F., Shinn, M., Romero-Garcia, R., Whitaker, K. J., Vertes, P. E., . . . Bullmore, E. T. (2018). Morphometric Similarity Networks Detect Microscale Cortical Organization and Predict Inter-Individual Cognitive Variation. *Neuron*, *97*(1), 231-247 e237. doi:10.1016/j.neuron.2017.11.039
- Sepehrband, F., Lynch, K. M., Cabeen, R. P., Gonzalez-Zacarias, C., Zhao, L., D'Arcy, M., . . . Clark, K. A. (2018). Neuroanatomical morphometric characterization of sex differences in youth using statistical learning. *Neuroimage*, *172*, 217-227. doi:10.1016/j.neuroimage.2018.01.065
- Serra-Grabulosa, J. M., Junque, C., Verger, K., Salgado-Pineda, P., Maneru, C., & Mercader, J. M. (2005). Cerebral correlates of declarative memory dysfunctions in early traumatic brain injury. *Journal of Neurology Neurosurgery and Psychiatry*, *76*(1), 129-131. doi:10.1136/jnnp.2004.027631
- Sesma, H. W., Slomine, B. S., Ding, R., McCarthy, M. L., & Children's Health After Trauma Study, G. (2008). Executive functioning in the first year after pediatric traumatic brain injury. *Pediatrics*, *121*(6), e1686-1695. doi:10.1542/peds.2007-2461
- Shaw, P., Greenstein, D., Lerch, J., Clasen, L., Lenroot, R., Gogtay, N., . . . Giedd, J. (2006). Intellectual ability and cortical development in children and adolescents. *Nature*, *440*(7084), 676-679. doi:10.1038/nature04513

- Shaw, P., Kabani, N. J., Lerch, J. P., Eckstrand, K., Lenroot, R., Gogtay, N., . . . Wise, S. P. (2008). Neurodevelopmental trajectories of the human cerebral cortex. *J Neurosci*, *28*(14), 3586-3594. doi:10.1523/JNEUROSCI.5309-07.2008
- Shehzad, Z., Giavasis, S., Li, Q., Benhajali, Y., Yan, C., Yang, Z., . . . Craddock, C. (2015). The Preprocessed Connectomes Project Quality Assessment Protocol - a resource for measuring the quality of MRI data. *Front Neurosci*, *9*. doi:10.3389/conf.fnins.2015.91.00047
- Sherman, L. E., Rudie, J. D., Pfeifer, J. H., Masten, C. L., McNealy, K., & Dapretto, M. (2014). Development of the default mode and central executive networks across early adolescence: a longitudinal study. *Dev Cogn Neurosci*, *10*, 148-159. doi:10.1016/j.dcn.2014.08.002
- Sled, J. G., Zijdenbos, A. P., & Evans, A. C. (1998). A non-parametric method for automatic correction of intensity non-uniformity in MRI data. *Ieee Transactions on Medical Imaging*, *17*(1), 87-97.
- Slim, K., Nini, E., Forestier, D., Kwiatkowski, F., Panis, Y., & Chipponi, J. (2003). Methodological index for non-randomized studies (MINORS): development and validation of a new instrument. *ANZ Journal of Surgery*, *73*(9), 712-716. doi:10.1046/j.1445-2197.2003.02748.x
- Slomine, B. S., Gerring, J. P., Grados, M. A., Vasa, R., Brady, K. D., Christensen, J. R., & Denckla, M. B. (2002). Performance on measures of 'executive function' following pediatric traumatic brain injury. *Brain Inj*, *16*(9), 759-772. doi:10.1080/02699050210127286
- Smith, D. H., Johnson, V. E., & Stewart, W. (2013). Chronic neuropathologies of single and repetitive TBI: substrates of dementia? *Nature Reviews Neurology*, *9*(4), 211-221. doi:10.1038/nrneurol.2013.29
- Smith, S. M. (2002). Fast robust automated brain extraction. *Hum Brain Mapp*, *17*(3), 143-155. doi:10.1002/hbm.10062
- Smolker, H. R., Friedman, N. P., Hewitt, J. K., & Banich, M. T. (2018). Neuroanatomical Correlates of the Unity and Diversity Model of Executive Function in Young Adults. *Front Hum Neurosci*, *12*, 283. doi:10.3389/fnhum.2018.00283
- Somerville, L. H., Bookheimer, S. Y., Buckner, R. L., Burgess, G. C., Curtiss, S. W., Dapretto, M., . . . Barch, D. M. (2018). The Lifespan Human Connectome Project in Development: A large-scale study of brain connectivity development in 5-21 year olds. *Neuroimage*, *183*, 456-468. doi:10.1016/j.neuroimage.2018.08.050
- Sone, D., Matsuda, H., Ota, M., Maikusa, N., Kimura, Y., Sumida, K., . . . Sato, N. (2016). Graph Theoretical Analysis of Structural Neuroimaging in Temporal Lobe Epilepsy with and without Psychosis. *PLoS One*, *11*(7), e0158728. doi:10.1371/journal.pone.0158728
- Sosin, D. M., Sniezek, J. E., & Thurman, D. J. (1996). Incidence of mild and moderate brain injury in the United States, 1991. *Brain Inj*, *10*(1), 47-54.

- Sowell, E. R., Peterson, B. S., Kan, E., Woods, R. P., Yoshii, J., Bansal, R., . . . Toga, A. W. (2007). Sex differences in cortical thickness mapped in 176 healthy individuals between 7 and 87 years of age. *Cereb Cortex*, *17*(7), 1550-1560. doi:10.1093/cercor/bhl066
- Sowell, E. R., Thompson, P. M., Leonard, C. M., Welcome, S. E., Kan, E., & Toga, A. W. (2004). Longitudinal mapping of cortical thickness and brain growth in normal children. *Journal of Neuroscience*, *24*(38), 8223-8231. doi:10.1523/Jneurosci.1798-04.2004
- Spanos, G. K., Wilde, E. A., Bigler, E. D., Cleavinger, H. B., Fearing, M. A., Levin, H. S., . . . Hunter, J. V. (2007). cerebellar atrophy after moderate-to-severe pediatric traumatic brain injury. *AJNR Am J Neuroradiol*, *28*(3), 537-542.
- Spencer-Smith, M., & Anderson, V. (2009). Healthy and abnormal development of the prefrontal cortex. *Developmental Neurorehabilitation*, *12*(5), 279-297. doi:10.1080/17518420903090701
- Sporns, O., Tononi, G., & Kotter, R. (2005). The human connectome: A structural description of the human brain. *PLOS Computational Biology*, *1*(4), 245-251. doi:10.1371/journal.pcbi.0010042
- Staal, J. A., & Vickers, J. C. (2011). Selective vulnerability of non-myelinated axons to stretch injury in an in vitro co-culture system. *J Neurotrauma*, *28*(5), 841-847. doi:10.1089/neu.2010.1658
- Stam, C. J. (2014). Modern network science of neurological disorders. *Nature Reviews Neuroscience*, *15*(10), 683-695. doi:10.1038/nrn3801
- Stone, M. (1974). Cross-Validatory Choice and Assessment of Statistical Predictions. *Journal of the Royal Statistical Society Series B-Statistical Methodology*, *36*(2), 111-147.
- Taylor, S. J., Barker, L. A., Heavey, L., & McHale, S. (2015). The longitudinal development of social and executive functions in late adolescence and early adulthood. *Front Behav Neurosci*, *9*, 252. doi:10.3389/fnbeh.2015.00252
- Teasdale, G., & Jennett, B. (1974). Assessment of Coma and Impaired Consciousness - Practical Scale. *Lancet*, *2*(7872), 81-84.
- Teeuw, J., Brouwer, R. M., Koenis, M. M. G., Swagerman, S. C., Boomsma, D. I., & Hulshoff Pol, H. E. (2019). Genetic Influences on the Development of Cerebral Cortical Thickness During Childhood and Adolescence in a Dutch Longitudinal Twin Sample: The Brainscale Study. *Cereb Cortex*, *29*(3), 978-993. doi:10.1093/cercor/bhy005
- Ten Eycke, K. D., & Dewey, D. (2016). Parent-report and performance-based measures of executive function assess different constructs. *Child Neuropsychol*, *22*(8), 889-906. doi:10.1080/09297049.2015.1065961
- Tewarie, P., Steenwijk, M. D., Tijms, B. M., Daams, M., Balk, L. J., Stam, C. J., . . . Hillebrand, A. (2014). Disruption of Structural and Functional Networks in Long-Standing Multiple Sclerosis. *Hum Brain Mapp*, *35*(12), 5946-5961. doi:10.1002/hbm.22596
- Thomason, M. E., Dennis, E. L., Joshi, A. A., Joshi, S. H., Dinov, I. D., Chang, C., . . . Gotlib, I. H. (2011). Resting-state fMRI can reliably map neural networks in children. *Neuroimage*, *55*(1), 165-175. doi:10.1016/j.neuroimage.2010.11.080

- Thornhill, S., Teasdale, G. M., Murray, G. D., McEwen, J., Roy, C. W., & Penny, K. I. (2000). Disability in young people and adults one year after head injury: prospective cohort study. *British Medical Journal*, *320*(7250), 1631-1635. doi:DOI 10.1136/bmj.320.7250.1631
- Tijms, B. M., Series, P., Willshaw, D. J., & Lawrie, S. M. (2012). Similarity-based extraction of individual networks from gray matter MRI scans. *Cereb Cortex*, *22*(7), 1530-1541. doi:10.1093/cercor/bhr221
- Tijms, B. M., Sprooten, E., Job, D., Johnstone, E. C., Owens, D. G., Willshaw, D., . . . Lawrie, S. M. (2015). Grey matter networks in people at increased familial risk for schizophrenia. *Schizophr Res*, *168*(1-2), 1-8. doi:10.1016/j.schres.2015.08.025
- Tomson Reuters. (2013). Endnote.
- Toplak, M. E., West, R. F., & Stanovich, K. E. (2013). Practitioner review: do performance-based measures and ratings of executive function assess the same construct? *J Child Psychol Psychiatry*, *54*(2), 131-143. doi:10.1111/jcpp.12001
- Torgo, L., Branco, P., Ribeiro, R. P., & Pfahringer, B. (2015). Resampling strategies for regression. *Expert Systems*, *32*(3), 465-476. doi:10.1111/exsy.12081
- Tournier, J. D., Calamante, F., & Connelly, A. (2012). MRtrix: Diffusion tractography in crossing fiber regions. *International Journal of Imaging Systems and Technology*, *22*(1), 53-66. doi:10.1002/ima.22005
- Treble-Barna, A., Zang, H., Zhang, N., Taylor, H. G., Yeates, K. O., & Wade, S. (2017). Long-Term Neuropsychological Profiles and Their Role as Mediators of Adaptive Functioning after Traumatic Brain Injury in Early Childhood. *J Neurotrauma*, *34*(2), 353-362. doi:10.1089/neu.2016.4476
- Tulsky, D. S., Carlozzi, N. E., Chevalier, N., Espy, K. A., Beaumont, J. L., & Mungas, D. (2013). V. NIH Toolbox Cognition Battery (CB): measuring working memory. *Monogr Soc Res Child Dev*, *78*(4), 70-87. doi:10.1111/mono.12035
- Urban, K. J., Riggs, L., Wells, G. D., Keightley, M., Chen, J. K., Ptito, A., . . . Sinopoli, K. J. (2017). Cortical Thickness Changes and Their Relationship to Dual-Task Performance following Mild Traumatic Brain Injury in Youth. *J Neurotrauma*, *34*(4), 816-823. doi:10.1089/neu.2016.4502
- van den Heuvel, M. P., & Sporns, O. (2013). Network hubs in the human brain. *Trends Cogn Sci*, *17*(12), 683-696. doi:10.1016/j.tics.2013.09.012
- Van Essen, D. C., Smith, S. M., Barch, D. M., Behrens, T. E., Yacoub, E., Ugurbil, K., & Consortium, W. U.-M. H. (2013). The WU-Minn Human Connectome Project: an overview. *Neuroimage*, *80*, 62-79. doi:10.1016/j.neuroimage.2013.05.041
- Vander Linden, C., Verhelst, H., Deschepper, E., Vingerhoets, G., Deblaere, K., & Caeyenberghs, K. (2018). Cognitive training benefit depends on brain injury location in adolescents with traumatic brain injury: a pilot study. *Eur J Phys Rehabil Med*. doi:10.23736/S1973-9087.18.05548-X

- Vander Linden, C., Verhelst, H., Deschepper, E., Vingerhoets, G., Deblaere, K., & Caeyenberghs, K. (2019). Exploration of gray matter correlates of cognitive training benefit in adolescents with chronic traumatic brain injury. *Neuroimage Clin*, *23*, 101827. doi:10.1016/j.nicl.2019.101827
- Vander Linden, C., Verhelst, H., Verleysen, G., Caeyenberghs, K., Deblaere, K., & Vingerhoets, G. (2019). Prefrontal and temporal cortical thickness in adolescents with traumatic brain injury. *Dev Med Child Neurol*, *61*(6), 672-679. doi:10.1111/dmcn.14100
- Váša, F., Seidlitz, J., Romero-Garcia, R., Whitaker, K. J., Rosenthal, G., Vertes, P. E., . . . Bullmore, E. T. (2017). Adolescent Tuning of Association Cortex in Human Structural Brain Networks. *Cereb Cortex*, 1-14. doi:10.1093/cercor/bhx249
- Vijayakumar, N., Allen, N. B., Youssef, G., Dennison, M., Yucel, M., Simmons, J. G., & Whittle, S. (2016). Brain development during adolescence: A mixed-longitudinal investigation of cortical thickness, surface area, and volume. *Hum Brain Mapp*, *37*(6), 2027-2038. doi:10.1002/hbm.23154
- Vijayakumar, N., Mills, K. L., Alexander-Bloch, A., Tamnes, C. K., & Whittle, S. (2017). Structural brain development: A review of methodological approaches and best practices. *Dev Cogn Neurosci*. doi:10.1016/j.dcn.2017.11.008
- Walhovd, K. B., Krogstad, S. K., Amlien, I. K., Bartsch, H., Bjornerud, A., Due-Tonnessen, P., . . . Fjell, A. M. (2016). Neurodevelopmental origins of lifespan changes in brain and cognition. *Proc Natl Acad Sci U S A*, *113*(33), 9357-9362. doi:10.1073/pnas.1524259113
- Wallace, G. L., Eric Schmitt, J., Lenroot, R., Viding, E., Ordaz, S., Rosenthal, M. A., . . . Giedd, J. N. (2006). A pediatric twin study of brain morphometry. *J Child Psychol Psychiatry*, *47*(10), 987-993. doi:10.1111/j.1469-7610.2006.01676.x
- Wang, B., Prastawa, M., Awate, S. P., Irimia, A., Chambers, M. C., Vespa, P. M., . . . Gerig, G. (2012). Segmentation of Serial Mri of Tbi Patients Using Personalized Atlas Construction and Topological Change Estimation. *2012 9th Ieee International Symposium on Biomedical Imaging (Isbi)*, 1152-1155.
- Wang, B., Prastawa, M., Irimia, A., Chambers, M. C., Vespa, P. M., Van Horn, J. D., & Gerig, G. (2012). A Patient-Specific Segmentation Framework for Longitudinal MR Images of Traumatic Brain Injury. *Medical Imaging 2012: Image Processing*, 8314. doi:10.1117/12.911043
- Wang, H., Jin, X., Zhang, Y., & Wang, J. (2016). Single-subject morphological brain networks: connectivity mapping, topological characterization and test-retest reliability. *Brain Behav*, *6*(4), e00448. doi:10.1002/brb3.448
- Wannan, C. M. J., Cropley, V. L., Chakravarty, M. M., Bousman, C., Ganella, E. P., Bruggemann, J. M., . . . Zalesky, A. (2019). Evidence for Network-Based Cortical Thickness Reductions in Schizophrenia. *Am J Psychiatry*, *176*(7), 552-563. doi:10.1176/appi.ajp.2019.18040380

- Watson. (2016a). *Brain structural connectivity and neurodevelopment in post-Fontan adolescents*. (Doctor of Philosophy), Boston University.
- Watson. (2016b). brainGraph: Graph Theory Analysis of Brain MRI Data. (Version 2.7.0). Retrieved from <https://CRAN.R-project.org/package=brainGraph>
- Wechsler, D. (1999). *Manual for the Wechsler abbreviated intelligence scale (WASI)*. San Antonio, TX: The Psychological Corporation.
- Wechsler, D. (2008). *Wechsler adult intelligence scale–Fourth Edition (WAIS–IV)*. San Antonio, TX: NCS Pearson.
- Wechsler, D. (Ed.) (2003). *Wechsler Intelligence Scale for Children: Fourth Edition*. San Antonio, TX, : The Psychological Corporation
- Wegelin, J. A. (2000). A survey of Partial Least Squares (PLS) methods, with emphasis on the two-block case.
- Wei, Y. B., Scholtens, L. H., Turk, E., & van den Heuvel, M. P. (2019). Multiscale examination of cytoarchitectonic similarity and human brain connectivity. *Network Neuroscience*, 3(1), 124-137. doi:10.1162/netn_a_00057
- Welsh, J. A., Nix, R. L., Blair, C., Bierman, K. L., & Nelson, K. E. (2010). The Development of Cognitive Skills and Gains in Academic School Readiness for Children from Low-Income Families. *J Educ Psychol*, 102(1), 43-53. doi:10.1037/a0016738
- Westwater, M. L., Seidlitz, J., Diederer, K. M., Fischer, S., & Thompson, J. C. (2017). Alterations in cortical thickness and structural connectivity are associated with symptom severity in bulimia nervosa. *bioRxiv*. doi:10.1101/127910
- Whitaker, K. J., Notter, M., & Morgan, S. (2017). Brains For Publication (Version 0.2.1).
- Whitaker, K. J., Vertes, P. E., Romero-Garcia, R., Vasa, F., Moutoussis, M., Prabhu, G., . . . Bullmore, E. T. (2016). Adolescence is associated with genomically patterned consolidation of the hubs of the human brain connectome. *Proc Natl Acad Sci U S A*, 113(32), 9105-9110. doi:10.1073/pnas.1601745113
- Whitford, T. J., Rennie, C. J., Grieve, S. M., Clark, C. R., Gordon, E., & Williams, L. M. (2007). Brain maturation in adolescence: concurrent changes in neuroanatomy and neurophysiology. *Hum Brain Mapp*, 28(3), 228-237. doi:10.1002/hbm.20273
- Wickham, H. (2009). *ggplot2: Elegant Graphics for Data Analysis*. New York: Springer-Verlag.
- Wilde, E. A., Bigler, E. D., Haider, J. M., Chu, Z. L., Levin, H. S., Li, X. Q., & Hunter, J. V. (2006). Vulnerability of the anterior commissure in moderate to severe paediatric traumatic brain injury. *J Child Neurol*, 21(9), 769-776. doi:10.2310/7010.2006.00152
- Wilde, E. A., Bigler, E. D., Hunter, J. V., Fearing, M. A., Scheibel, R. S., Newsome, M. R., . . . Levin, H. S. (2007). Hippocampus, amygdala, and basal ganglia morphometrics in children after moderate-to-severe traumatic brain injury. *Dev Med Child Neurol*, 49(4), 294-299. doi:10.1111/j.1469-8749.2007.00294.x

- Wilde, E. A., Dennis, E. L., & Tate, D. F. (2019). The ENIGMA Brain Injury Working Group: Approach, Challenges, and Potential Benefits. *PsyArXiv*. doi:10.31234/osf.io/t96xb
- Wilde, E. A., Hunter, J. V., & Bigler, E. D. (2012). Pediatric traumatic brain injury: Neuroimaging and neurorehabilitation outcome. *NeuroRehabilitation*, 31(3), 245-260. doi:10.3233/Nre-2012-0794
- Wilde, E. A., Hunter, J. V., Newsome, M. R., Scheibel, R. S., Bigler, E. D., Johnson, J. L., . . . Levin, H. S. (2005). Frontal and temporal morphometric findings on MRI in children after moderate to severe traumatic brain injury. *J Neurotrauma*, 22(3), 333-344. doi:10.1089/neu.2005.22.333
- Wilde, E. A., Merkley, T. L., Bigler, E. D., Max, J. E., Schmidt, A. T., Ayoub, K. W., . . . Levin, H. S. (2012). Longitudinal changes in cortical thickness in children after traumatic brain injury and their relation to behavioral regulation and emotional control. *International Journal of Developmental Neuroscience*, 30(3), 267-276. doi:10.1016/j.ijdevneu.2012.01.003
- Wilde, E. A., Newsome, M. R., Bigler, E. D., Pertab, J., Merkley, T. L., Hanten, G., . . . Levin, H. S. (2011). Brain imaging correlates of verbal working memory in children following traumatic brain injury. *International Journal of Psychophysiology*, 82(1), 86-96. doi:10.1016/j.ijpsycho.2011.04.006
- Wilkinson, A. A., Dennis, M., Simic, N., Taylor, M. J., Morgan, B. R., Frndova, H., . . . The Canadian Critical Care Translational Biology, G. (2017). Brain biomarkers and pre-injury cognition are associated with long-term cognitive outcome in children with traumatic brain injury. *Bmc Pediatrics*, 17(1), 173. doi:10.1186/s12887-017-0925-6
- World Health Organization. (2006). Neurological disorders: Public health challenges. Retrieved from https://www.who.int/mental_health/neurology/neurodiso/en/
- Wu, K. K., Chan, S. K., Leung, P. W., Liu, W. S., Leung, F. L., & Ng, R. (2011). Components and developmental differences of executive functioning for school-aged children. *Dev Neuropsychol*, 36(3), 319-337. doi:10.1080/87565641.2010.549979
- Wu, T., Merkley, T. L., Wilde, E. A., Barnes, A., Li, X., Chu, Z. D., . . . Levin, H. S. (2018). A preliminary report of cerebral white matter microstructural changes associated with adolescent sports concussion acutely and subacutely using diffusion tensor imaging. *Brain Imaging Behav*, 12(4), 962-973. doi:10.1007/s11682-017-9752-5
- Wu, T. C., Wilde, E. A., Bigler, E. D., Li, X., Merkley, T. L., Yallampalli, R., . . . Levin, H. S. (2010). Longitudinal changes in the corpus callosum following pediatric traumatic brain injury. *Dev Neurosci*, 32(5-6), 361-373. doi:10.1159/000317058
- Yasuda, C. L., Chen, Z., Beltramini, G. C., Coan, A. C., Morita, M. E., Kubota, B., . . . Gross, D. W. (2015). Aberrant topological patterns of brain structural network in temporal lobe epilepsy. *Epilepsia*, 56(12), 1992-2002. doi:10.1111/epi.13225

- Yeates, K. O., Bigler, E. D., Abildskov, T., Dennis, M., Gerhardt, C. A., Vannatta, K., . . . Taylor, H. G. (2013). Social Competence in Pediatric Traumatic Brain Injury. *Clinical Psychological Science*, 2(1), 97-107. doi:10.1177/2167702613499734
- Yee, Y., Fernandes, D. J., French, L., Ellegood, J., Cahill, L. S., Vousden, D. A., . . . Lerch, J. P. (2017). Structural covariance of brain region volumes is associated with both structural connectivity and transcriptomic similarity. *bioRxiv*. doi:10.1101/183004
- Yu, K., Seal, M. L., Reyes, J., Godfrey, C., Anderson, V., Adamson, C., . . . Catroppa, C. (2018). Brain volumetric correlates of inhibition and cognitive flexibility 16 years following childhood traumatic brain injury. *J Neurosci Res*, 96(4), 642-651. doi:10.1002/jnr.24087
- Yu, K. X., Wang, X. T., Li, Q. L., Zhang, X. H., Li, X. W., Li, S. Y., & Initi, A. s. D. N. (2018). Individual Morphological Brain Network Construction Based on Multivariate Euclidean Distances Between Brain Regions. *Front Hum Neurosci*, 12. doi:10.3389/Fnhum.2018.00204
- Yuan, W., Treble-Barna, A., Sohlberg, M. M., Harn, B., & Wade, S. L. (2016). Changes in Structural Connectivity Following a Cognitive Intervention in Children With Traumatic Brain Injury: A Pilot Study. *Neurorehabil Neural Repair*. doi:10.1177/1545968316675430
- Yuan, W., Wade, S. L., & Babcock, L. (2015). Structural connectivity abnormality in children with acute mild traumatic brain injury using graph theoretical analysis. *Hum Brain Mapp*, 36(2), 779-792. doi:10.1002/hbm.22664
- Zelazo, P. D. (2006). The Dimensional Change Card Sort (DCCS): a method of assessing executive function in children. *Nat Protoc*, 1(1), 297-301. doi:10.1038/nprot.2006.46
- Zelazo, P. D., Anderson, J. E., Richler, J., Wallner-Allen, K., Beaumont, J. L., Conway, K. P., . . . Weintraub, S. (2014). NIH Toolbox Cognition Battery (CB): validation of executive function measures in adults. *J Int Neuropsychol Soc*, 20(6), 620-629. doi:10.1017/S1355617714000472
- Zhang, J., Cook, T. S., Goh, S.-Y. M., Irimia, A., Vespa, P. M., & Van Horn, J. D. (2016). Patient-tailored multimodal neuroimaging, visualization and quantification of human intra-cerebral hemorrhage. 9789, 978903. doi:10.1117/12.2216150
- Zhang, Z., Liao, W., Zuo, X.-N., Wang, Z., Yuan, C., Jiao, Q., . . . Liu, Y. (2011). Resting-State Brain Organization Revealed by Functional Covariance Networks. *PLoS One*, 6(12). doi:10.1371/journal.pone.0028817
- Zheng, W., Eilamstock, T., Wu, T., Spagna, A., Chen, C., Hu, B., & Fan, J. (2019). Multi-feature based network revealing the structural abnormalities in autism spectrum disorder. *IEEE Transactions on Affective Computing*, 1-1. doi:10.1109/taffc.2018.2890597
- Zheng, W., Yao, Z., Xie, Y., Fan, J., & Hu, B. (2018). Identification of Alzheimer's Disease and Mild Cognitive Impairment Using Networks Constructed Based on Multiple Morphological Brain Features. *Biol Psychiatry Cogn Neurosci Neuroimaging*, 3(10), 887-897. doi:10.1016/j.bpsc.2018.06.004

Ziegler, G., Dahnke, R., Winkler, A. D., & Gaser, C. (2013). Partial least squares correlation of multivariate cognitive abilities and local brain structure in children and adolescents. *Neuroimage*, 82, 284-294. doi:10.1016/j.neuroimage.2013.05.088

Appendices

Appendix A – Supplementary Materials for Chapter 2

Visualisation of study characteristics

Visualisation of dispersion of studies based upon sample characteristics of age at injury and injury-scan interval was achieved with the ggplot2 package in R (Wickham, 2009). Level of measurement across these two variables was standardized as years for both age at injury and injury-scan interval. Those studies using different levels of measurement (months and/or days) were converted (divided by 12 and 365 respectively). For studies reporting only ranges, the middle value was used.

Both mean values and standard deviations were used for visualisation. For studies that reported mean and standard deviation of these variables separately across injury severities, pooled mean and standard deviation were calculated. These were calculated in line with guidelines from the Cochrane handbook (Higgins & Green, 2011, Table 7.7.a) using the following formulae;

$$M_{pooled} = \frac{N_1M_1 + N_2M_2}{N_1 + N_2}$$
$$SD_{pooled} = \sqrt{\frac{(N_1 - 1)SD_1^2 + (N_2 - 1)SD_2^2 + \frac{N_1N_2}{N_1 + N_2}(M_1^2 + M_2^2 - 2M_1M_2)}{N_1 + N_2 - 1}}$$

where N_x is the sample size of the subgroup, M_x is the value and SD_x is the standard deviation of that mean. It is important to note that the pooled SD gives an approximation which is known to be a slight underestimation of the true SD however, for the purposes of visualisation, this is unlikely to be an issue.

All data used in the visualisation of studies are listed in the table below. It is important acknowledge that the use of multiple methods of imputation may slightly misrepresent the true data for studies. However, imputations and inferences made are fully transparent and are listed in the appendix (Table A.1), whilst the data actually reported in each paper can be seen in Table 2.2. Despite these caveats, Figure 2.2 provides a useful visualisation with which to grasp the extent of the current research in the field.

Table A.1 *Imputed data used for visualization of cross sectional studies*

Reference	Age at injury		Injury – MRI interval		Patient sample size (<i>n</i>)	Data-set
	Mean (years)	<i>SD</i>	Mean (years)	<i>SD</i>		
Beauchamp (2011)	6.58 ^a	3.19 ^a	10.40 ^a	1.45 ^a	49	NA
Dennis (2013)	7.80	2.00	2.60	1.20	82	4
Yeates (2014)	7.83	1.94	3.13 ^{b, c}	NA	82	4
Bigler (2013)	7.92 ^{a, e}	1.90 ^{a, e}	2.53 ^{a, e}	1.24 ^{a, e}	72	4
Bigler (2016)	7.92 ^f	NA	2.70	NA	72	4
Serra-Grabulosa (2005)	8.18	3.65	9.68	1.88	16	NA
Drijkoningen (2015)	9.30 ^b	NA	3.83 ^c	3.25 ^c	18	NA
Bigler (2010)	9.75	3.00	3.10	2.40	16	3
Wilde (2005)	9.75	3.00	3.10	2.40	16	3
Fearing (2008)	9.75	3.00	3.10	2.40	16	3
Wilde (2006)	9.75	3.00	3.10	2.40	16	3
Merkley (2008)	9.75	3.00	3.10	2.40	16	3 ^g
Wilde (2007)	9.75 ^f	NA	3.00 ^c	2.42 ^c	16	3
Spanos (2007)	9.75 ^f	NA	3.10	2.40	16	3
Ryan (2016, Cortex)	10.37 ^a	2.51 ^a	0.12 ^d	0.08 ^d	103	5
Ryan (2016, SCAN)	10.44 ^a	2.48 ^a	0.11 ^{a, d}	0.06 ^{a, d}	76	5
McCauley (2010)	12.00 ^b	NA	0.34 ^d	0.08 ^d	40	1
Wilde (2011)	12.00 ^f	NA	0.01 ^d	0.00 ^d	40	1
Max (2012)	13.40	3.00	0.25	NA	44	NA
Hanten (2011)	13.43	2.35	3.23 ^c	0.87 ^c	15	2
Cook (2013)	13.43	2.35	3.23 ^c	0.87 ^c	15	2
Krawczyk (2010)	13.86 ^h	NA	2.65	0.76	12	NA
Juranek (2012)	11.84 ^h	NA	0.24 ^{a, d}	0.11 ^{a, d}	21	NA
Konings (2017)	7.38 ^a	2.13 ^a	2.89 ^a	1.23 ^a	37	NA
Drijkoningen (2017)	10.08 ^c	3.40 ^c	3.67 ^c	3.40 ^c	19	NA
Urban (2017)	11.87 ^h	NA	0.33 ^d	0.01 ^d	13	NA
Ryan (2017)	10.31 ^a	2.50 ^a	0.12 ^f	NA	112	5

Note.

^a Pooled mean and *SD* from sub groups

^b Not available, middle value from reported range used for visualisation

^c Converted from months

^d Converted from days

^e Demographics refer to all participants in paper, not just those used for morphometry analyses

^f Inferred from other papers utilising dataset

^g Inferred from overlapping demographics with other papers from similar authors

^h Mean age imputed as the mean age at testing minus mean injury-MRI interval

Table A.2 Characteristics for all studies investigating relationship between cognition and morphometry included in the review by domain of cognitive functioning

Cognitive Domain	Reference	Measures Administered	Between-group performance	Design	Statistical Approach	Brain regions tested	Findings
IQ	Konigs et al (2017)	WISC-III short form FS-IQ	FS-IQ lower in Mild RF+ TBI and Moderate/severe TBI compared to controls.	Correlational	Pearsons correlations (only investigated in TBI group)	WM volume of 'affected' tracts	No significant relationships found between test and volume of WM regions
Executive Functioning	Wilde et al (2012)	BRIEF Behavioural regulation and emotional control indexes (at the 18 month timepoint)	Children with TBI were rated significantly more highly for both subscales than the OI group, suggesting greater behavioural problems for the patient group at 18 months post-injury.	Correlational	Vertex-wise correlations (only investigated in TBI group)	Vertex-wise longitudinal cortical thickness change	Emotional control index showed significant correlation with longitudinal cortical thickness change in right MFG and right anterior cingulate gyrus. The behavioral regulation index showed similar significant correlations but instead with the medial aspect of the left frontal lobe.
Processing Speed	Wu et al (2010)	Arrow-flanker task (baseline condition)	No differences were found between OI and TBI groups for processing speed at 3 or 18 months. However, the OI group saw a significant improvement with timepoint (from 3 to 18 months) but the TBI group did not	Cross-sectional (comparative)	Pearsons partial correlations (age at injury and SCI)	Total corpus callosum and sub-regions of corpus callosum	No significant relationship between processing speed and corpus callosum sub region volume at 3 or 18 months post injury for either group.
Working Memory	Konigs et al (2017)	WISC-III Digit Span test	Digit span scores lower Mild RF+ TBI and Moderate/severe TBI compared to controls.	Correlational	Pearsons correlations (only investigated in TBI group)	WM volume of 'affected' tracts	No significant relationships found between test and volume of WM regions
	Urban et al (2017)	N-back task and dual n-back task (with motor-task component)	Accuracy on n-back tasks in both conditions was not different between groups, however for reaction times there was an interaction of group and single vs dual task condition, with the mTBI group being slower for the dual task condition.	Cross-sectional (comparative)	Pearsons correlations (in both groups)	DLPFC and parietal cortices	In controls, better accuracy during single task condition 0-back, was associated with increased left DLPFC thickness and faster reaction times for single task 1-back was related to thicker anterior and posterior IPL. In patients, thicker DLPFC was related to poorer accuracy for 1-back single task condition. However, during the dual condition, thinner left DLPFC resulted in slower RT for all three n-back conditions. Also, thinner

anterior IPL was associated with slower performance in 2-back dual-task condition.

Wilde et al (2011)	SIRT	Only significant group difference (covarying for age) was found on the interaction of interference and on accuracy and reaction time, with the OI group showing a more negative effect of interference than the TBI group. No group differences in errors	Cross-sectional (comparative)	Pearsons correlations (in both groups)	Frontal and parietal lobes, middle frontal gyrus and cingulate gyrus	Significant negative correlations between right and left cingulate volumes as well as left parietal lobe volume with the non-interference condition reaction times in the TBI group, where smaller volume was associated with a longer RT. These relationships were not replicated, or new relationships found, in the OI group. Cortical thickness of bilateral caudal MFG, left SFG, SPG, and cuneas regions and right rostral MFG, preC, PCC, and PCUN regions was positively correlated with task errors in the OI group, whereas in the TBI group thickness of left parietal and inferior temporal regions and the right frontal, paracentral, rostral MFG and SPG regions was related to task errors. This difference in brain-cognition relationships was despite no differences in errors being found.
Merkley et al (2008)	BRIEF working memory scale	Not reported	Correlational	Pearsons correlations (unclear whether TBI group or whole sample)	Not reported	Significant correlations (no direction given) were found between working memory subscale and cortical thickness of bilateral inferior temporal, superior and inferior parietal as well as thickness of left FFG.
Fearing et al (2008)	SIRT	Not reported	Cross-sectional (statistical)	GLM (correcting for age and TIV) across groups	Total midbrain, total brainstem, total thalamus	Significant relation between decreased baseline (memory testing set of 1) reaction time and total brainstem volume. There was a significant interaction effect of group on the relationship between higher memory load (memory testing set of 6) reaction time and total midbrain, but total brainstem volume was marginally outside the alpha limit. Post-hoc tests for the total midbrain showed that only TBI children showed a significant relationship with higher memory load reaction time. This relationship persisted when

total lesion volume was also controlled for. No relationships were found for Thalamic volumes.

Memory	McCauley et al (2010)	Event-based prospective memory task	OI group significantly outperformed the TBI group on overall performance	Cross-sectional (statistical)	QDEC general linear model (controlling for age) across groups	Vertex-wise	Thinning of bilateral regions in middle and IFG, MTG and ITG, PARH and cingulate gyri contributed to group differences in performance
Overall Functioning (composite score)	Dennis et al (2017)	Composite score of WISC-IV processing speed index, WISC-IV working memory index, Trails 1-5 CVLT-C/II and Trails 4 DKEFS trail-making test	Not reported	Cross-sectional (comparative)	Voxel-wise linear regression (TBI and OI group investigated separately) of volume change against cognitive performance change	Voxel-wise analysis	Voxel-wise linear regression showed no relationship between longitudinal volume change and changes in cognition in the control group. In the TBI group (both IHTT slow and normal) there were a considerable number of diffuse clusters where morphometric change related to differences in the cognitive summary score. More generally, clusters which were positively associated with cognitive change (where greater volume was associated with better performance) were found across GM and WM tissues (n=18 clusters), whereas clusters where reduced volume was related to increased cognition were largely found in only GM regions (n=33 clusters).
	Dennis et al (2016)	Composite score of WISC-IV processing speed index, WISC-IV working memory index, Trails 1-5 CVLT-C/II and Trails 4 DKEFS trail-making test	Not reported	Cross-sectional (comparative)	Voxel-wise linear regression (TBI and OI group investigated separately)	Voxel-wise analysis	At timepoint 1, across all participants, there were significant regions of positive correlation between cognitive summary score and volume (bilateral ITG, OG, FFG and left STG) and multiple regions of negative correlation (lateral ventricles, left OG, left MTG and right cingulate gyrus). Correlations specific to the TBI-only analysis found specific regions of positive correlation between volume and performance (bilateral SFG, bilateral FFG, right OG, right SPL, right PCUN, right preC, left ITG and MFG) with less negative correlations found (lateral ventricles, the left OG, and left transverse temporal gyrus). At timepoint 2, positive correlations across all participants were found in bilateral postC, bilateral insula, right middle cerebellar peduncle, and left ITG, with TBI specific correlations being found in right middle cerebellar peduncle, right OrbG, and bilateral

FFG. Negative correlations were also found in lateral ventricles, left entorhinal cortex, left STG and IFG and specific TBI relationships found in bilateral MFG, right hippocampus, right STG, left amygdala, left fornix, left ITG, left supramarginal gyrus, left STG and IFG.

Theory of Mind (ToM)							
	Ryan et al (2017)	Jack and Jill task, Emotional and emotive faces task, Ironic criticism and empathic praise task (cognitive, affective and conative ToM)	No significant effect of group on Jack and Jill cognitive ToM, but for affective and conative ToM there was a main effect of severity group; for affective ToM the mild complicated group performed significantly worse than controls and severe injury, for conative ToM mild complicated TBI performed worse than control, mild and moderately injured groups.	Correlational	Multivariate regression (covarying for age, ICV, pre-injury ABAS, sex, SES, ToM control trial performance, and injury severity) Only investigated in TBI group.	CCMN, SN, MNEN, CEN and DMN network volumes (summed from ROIS)	For volumes of the networks hypothesized to be important for the different aspects of ToM, each regression model was significant. For cognitive ToM, the CCMN network volume was the only significant regressor, where reduced volume was associated with worse performance. Similar patterns were found for affective ToM and the SN, as well as conative ToM and the MNEN.
	Yeates et al (2014)	Jack and Jill task, Emotional and emotive faces task, Ironic criticism and empathic praise task (cognitive, affective and conative ToM)	Not reported	Cross-sectional (comparative)	Pearsons correlations controlling for age and group membership across all participants, only TBI and only controls, VBM	Global WM and GM volumes and voxel-wise	Conative ToM across groups was positively correlated with GM and WM volumes and negatively correlated with VBR when controlling for group. Conative ToM was positively correlated with GM in both groups but WM volume only in the TBI group. Cognitive and affective ToM was correlated positively with GM volume and negatively with VBR respectively. VBM identified significant clusters associated with ToM but only in the OI group, not TBI patients.
	Dennis et al (2013)	Jack and Jill task, Emotional and emotive faces task, Ironic criticism and empathic praise task (cognitive, affective and conative ToM)	Main effect of group on ToM performance, post-hoc tests showing that the OI group performed significantly better than severe TBI.	Cross-sectional (statistical)	MANOVA with group membership (TBI vs OI) as a between subjects and networks as within-subjects factor	CCMN, SN, MNEN, CEN and DMN network volumes (summed from ROIs)	Regression models were non-significant for cognitive or affective ToM but were significant for conative ToM. Individual predictors of the DMN, CEN and MNEN network were not individually significant, even though the overall model was. When these network volumes were decomposed, 8 out of 12 regions were significantly related to conative ToM outcome, with greater volume related to greater performance. After multiple correction, only

posterior cingulate/retrosplenial cortex and hippocampal formation survived.

Miscellaneous	Author	Task	Findings	Design	Analysis	Regions	Conclusions
	Konigs et al (2017)	RAVLT	Only encoding (not retrieval or consolidation subscores) was lower for Mild RF+ TBI and Moderate/severe TBI compared to controls	Correlational	Pearsons correlations (only investigated in TBI group)	WM volume of 'affected' tracts	No significant relationships found between test and volume of WM regions
	Cook et al (2013)	Anticipating consequences VR-task	The TBI group performed significantly worse on predicting long term outcomes compared to controls, but not short term consequences	Cross-sectional (Statistical)	QDEC general linear model (controlling for age) across groups	Vertex-wise	Between-group differences in performance of the overall measure were found to be significantly related to the CT of the medial PFC/FP region and bilateral PCUN. Stronger brain-behaviour relationships were found for the control group.
	Hanten et al (2011)	Social problem solving VR-task	Adolescents with TBI performed significantly poorer on the summary score of his task, across all processing load conditions, compared to controls	Cross-sectional (Statistical)	QDEC general linear model (controlling for age) across groups	Vertex-wise	There was a significant group difference in relationship between cortical thickness and performance measured by the task summary score in the right orbitomedial frontal cortex and cuneus. This showed a positive relationship (greater thickness related to greater performance) for the control group only. For the 'defining problem' step there was a significant group difference in relationship between cortical thickness and performance with decreased cortical thickness in temporal areas related to better performance. There were also group differences for the 'evaluate outcome' step, with better performance related to decreased cortical thickness in the bilateral medial prefrontal regions.
	Krawczyk et al (2010)	Picture analogy task	TD controls performed significantly better at reasoning analogous roles in scenes than the TBI patient group.	Cross-sectional (Statistical)	QDEC general linear model across groups	Vertex-wise	The strongest correlations were found in the control group, and inverse relationships between cortical thickness and accuracy on analogical reasoning tasks in anterior PFC, bilateral anterior and posterior lateral PFC, bilateral superior and inferior temporal gyri, and medial PFC. Relationships in the TBI group were less clear, but inverse relationships were seen in left medial OFC, and left SFG. Accuracy on trials with a distractor showed similar inverse relationships with clusters in the left STG and left MTG, right

IFG, and left PCC but additionally the anterior left dorsal PFC and right OFC in the TBI group.

Note. WISC=Wechsler Intelligence Scale for Children, FS-IQ=Full scale IQ, WASI=Wechsler abbreviated scale of Intelligence-, BRIEF=Behaviour rating inventory of executive functioning, CVLT-C/II= California verbal learning test, VR=Virtual reality, RAVLT= Rey auditory verbal learning test, DKEFS=Delis-Kaplan Executive Function System, SCI=Social composite index, SIRT=Sternberg item recognition task, ICV=Total intracranial volume, SES=Socio-economic status, ABAS=Adaptive Behaviour Assessment System, VBM=Voxel based morphometry

Appendix B – Supplementary Materials for Chapter 3

Generating simulated lesion cases

Lesions were simulated in control cases from real patient lesions as per previous methods (Brett et al., 2001; Gonzalez-Villa et al., 2017). Simulation approaches have been used to investigate the effectiveness of spatial normalization (Andersen, Rapcsak, & Beeson, 2010; Brett et al., 2001; Crinion et al., 2007) and segmentation (Seghier et al., 2008) using focal infarct, vascular event and atrophic lesions.

After initially skullstripping all cases (using *FSL*'s (Jenkinson et al., 2012) BET, (Smith, 2002)), non-linear warps from native space in the skullstripped control and patient cases to MNI-152 space were calculated using *FSL*'s FNIRT tool ((Jenkinson et al., 2012), initialised with an initial 12-DOF linear registration using FLIRT (Jenkinson & Smith, 2001) on the non-skullstripped T1w). For the lesioned cases, this was achieved using cost-function masking, using the inverse of the binary lesion mask (weighting the lesion as zero and the non-lesioned tissue as ones) in order to restrict the warp to being calculated using only healthy tissue. The warp from native control to MNI-152 space was then inverted to produce the warp necessary to move from MNI to control-case native space.

Using the *mrcalc* function within the *MRTrix* software, the binary lesion mask was multiplied by the lesioned T1w MRI, resulting in an image which included the lesion tissue only as an ROI. This “patch” was then moved into the native space of every control image, via the MNI-152 space, using the lesioned T1w to MNI-152 warp, followed by the inverse of the control T1w to MNI-152 warp as per below,

$$lesionROI^{targetspace} = lesionROI^{sourcespace} \times warp^{source \rightarrow MNI} \times$$

where the *source* image is the patient T1w and the *target* is the control T1w. In order to ensure that the lesions are realistic in intensities, we apply a simple intensity normalization procedure between the source and target T1w images. This involved calculation of a scaling factor (SF; as per (Brett et al., 2001)) as the ratio between the mean intensity of the target image and the source image (masked to avoid abnormal signal intensity due to the lesion), which was then applied to the lesion ROI as follows,

$$lesionROI^{targetintensity} = lesionROI^{sourceintensity} \times \frac{mean^{targetintensity}}{mean^{sourceintensity}}$$

Once the lesion ROI has been normalized to the target intensity and space, a binarized and inverted mask of this ROI is generated using *mrcalc* (where the lesion is zeros and the rest of the image is ones). The target control T1w image is then multiplied by this mask to remove the signal in the target location and then the lesioned ROI in target space and intensity is added to this image (similarly to Gonzalez-Villa et al. (2017)) as per below, and this final image is the simulated lesion case referred to in the rest of the paper;

$$\text{Simulatedlesion} = \text{lesionmask}^{\text{targetspace}} \times T_1W^{\text{target}} + \text{lesionROI}^{\text{targetspace/intensity}}$$

The resultant simulated dataset contained $n = 176$ cases, where every included lesion ($n = 16$) had been applied to every control image ($n = 11$) in all possible pairwise permutations. From here on, the control images with the simulated lesions applied will be referred to as the simulated lesion (Sim_{lesion}) cases ($n = 176$) and the control images without editing will be referred to as “ground truth” (GT) cases ($n = 11$). The entire pipeline is visualised in the below figure.

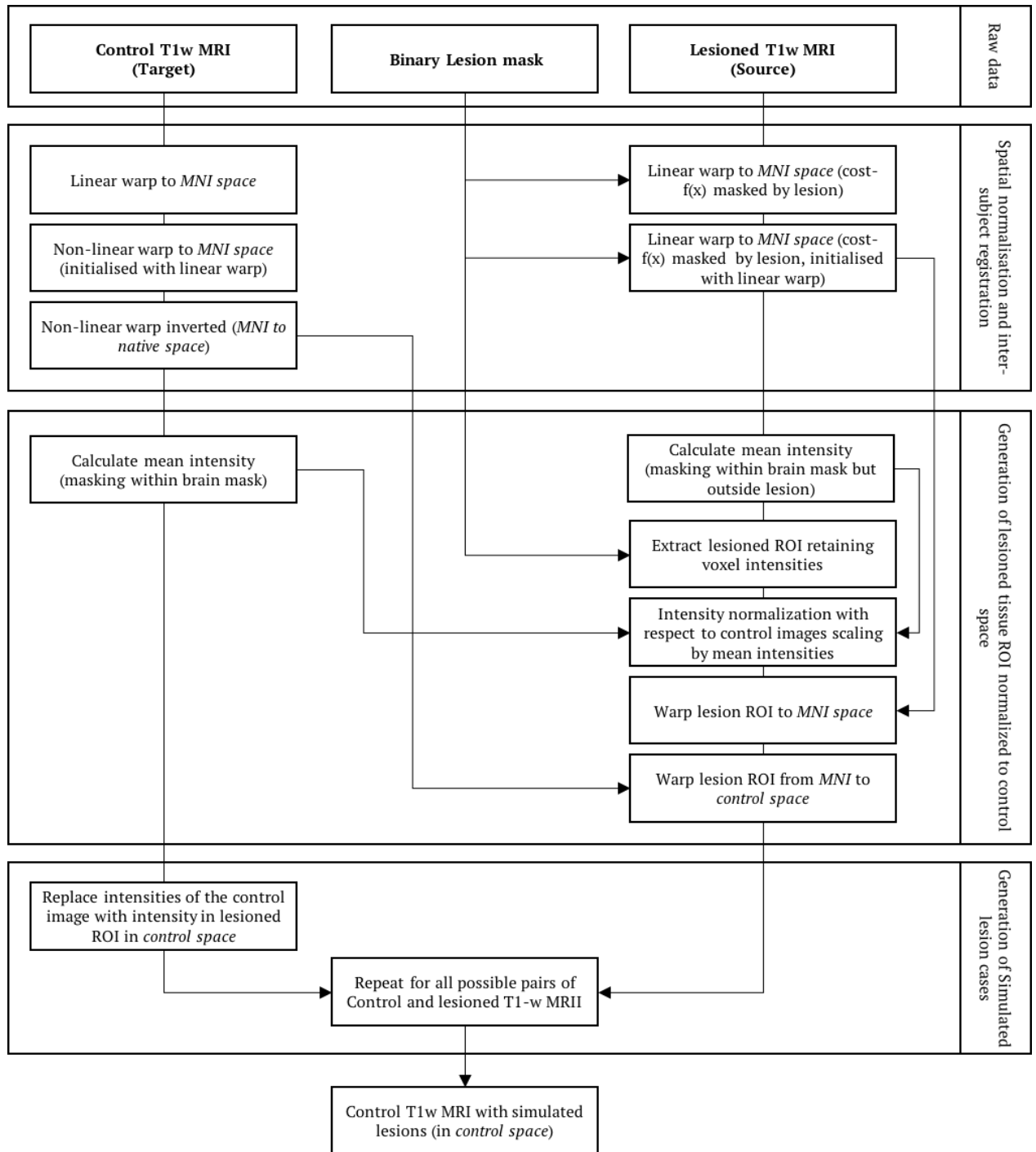


Figure B.1 Workflow for generating simulated lesions. Method adapted from Brett et al. (2001) and Gonzalez-Villa et al. (2017)

Results of Mixed Models

Table B.1. Outputs from linear mixed-models testing whether the difference in cortex volume between Sim_{lesion} and GT cases is significant across each hemisphere

Cortex Volume						
Predictors	Both Hemispheres ^a		Hemi _{lesion} ^b		Hemi _{contra} ^c	
	Estimates	std. Error	Estimates	std. Error	Estimates	std. Error
(Intercept)	299261.29 *** (288172.71 – 310349.88)	5657.55	299243.61 *** (287965.38 – 310521.84)	5754.30	299278.98 *** (288250.11 – 310307.84)	5627.08
Simulated Lesion	-942.61 (-1984.98 – 99.76)	531.83	-1324.46 (-3588.88 – 939.96)	1155.34	-560.76 *** (-828.23 – -293.29)	136.47
Random Effects						
	σ^2	4544617.35		1772686.02		1638835.43
	τ_{00}	0.00 Participant 241905.00 Lesion 349283191.51 Control_Image		2938645.92 Participant 1237325.29 Lesion 350327135.17 Control_Image		2404899.27 Participant 0.00 Lesion 348051258.85 Control_Image
	τ_{11}	0.00 Participant.LesionstatusSimulatedLesion				
	ρ_{01}					
	ICC	0.00 Participant 0.00 Lesion 0.99 Control_Image		0.01 Participant 0.00 Lesion 0.98 Control_Image		0.01 Participant 0.00 Lesion 0.99 Control_Image
	Observations	704		352		352
	Marginal R ² / Conditional R ²	NA		0.001 / 0.995		NA

Note. * $p < 0.05$ ** $p < 0.01$ *** $p < 0.001$, ^a CortexVol ~ Lesionstatus + (Lesionstatus|Participant) + (1|Lesion) + (1|Control_Image), ^b CortexVol ~ Lesionstatus + (1|Participant) + (1|Lesion) + (1|Control_Image), subset = (Hemi=='Lesion'), ^c CortexVol ~ Lesionstatus + (1|Participant) + (1|Lesion) + (1|Control_Image), subset = (Hemi=='Contralesion').

Table B.2. Outputs from linear mixed-models testing whether the difference in cortical white matter volume between Sim_{lesion} and GT cases is significant across each hemisphere

Predictors	cWM Volume					
	Both Hemispheres ^a		Hemi _{lesion} ^b		Hemi _{contra} ^c	
	Estimates	std. Error	Estimates	std. Error	Estimates	std. Error
(Intercept)	220026.04 *** (205476.56 – 234575.53)	7423.34	219983.31 *** (205388.05 – 234578.58)	7446.70	220068.77 *** (205511.02 – 234626.52)	7427.56
Simulated Lesion	-161.75 (-675.03 – 351.52)	261.88	-308.84 (-1522.33 – 904.65)	619.14	-14.66 (-212.62 – 183.29)	101.00
Random Effects						
σ^2	1463696.35		756656.02		897671.31	
τ_{00}	0.00 Participant		721818.41 Participant		606868.17 Participant	
	4521.04 Participant.1		352691.35 Lesion		0.00 Lesion	
	55625.95 Lesion		606014889.39 Control_Image		606761167.60 Control_Image	
	605508377.50 Control_Image					
τ_{11}	148203.23 Participant.1.LesionstatusSimulatedLesion					
ρ_{01}	-1.00 Participant.1					
ICC	0.00 Participant		0.00 Participant		0.00 Participant	
	0.00 Participant.1		0.00 Lesion		0.00 Lesion	
	0.00 Lesion		1.00 Control_Image		1.00 Control_Image	
	1.00 Control_Image					
Observations	704		352		352	
Marginal R ² / Conditional R ²	NA		0.000 / 0.999		NA	

Note. * $p < 0.05$ ** $p < 0.01$ *** $p < 0.001$, ^a cWMVol ~ Lesionstatus + (1|Participant) + (0 + Lesionstatus|Participant) + (1|Lesion) + (1|Control_Image), ^b cWMVol ~ Lesionstatus + (1|Participant) + (1|Lesion) + (1|Control_Image), subset = (Hemi=='Lesion'), ^c cWMVol ~ Lesionstatus + (1|Participant) + (1|Lesion) + (1|Control_Image), subset = (Hemi=='Contralesion').

Table B.3. Outputs from linear mixed-models testing whether the magnitude of PVD is significantly different between $hemi_{lesion}$ and $hemi_{contra}$

Predictors	Cortex PVD ^a		cWM PVD ^b	
	Estimates	std. Error	Estimates	std. Error
(Intercept)	0.48 *** (0.31 – 0.65)	0.09	0.44 *** (0.31 – 0.58)	0.07
Lesion	0.14 ** (0.05 – 0.23)	0.05	-0.01 (-0.08 – 0.07)	0.04
Random Effects				
	σ^2	0.20		0.14
	τ_{00}	0.02 Participant		0.02 Participant
		0.02 Lesion		0.01 Lesion
		0.06 Control_Image		0.04 Control_Image
	ICC	0.06 Participant		0.08 Participant
		0.08 Lesion		0.06 Lesion
		0.19 Control_Image		0.18 Control_Image
	Observations	352		352
	Marginal R ² / Conditional R ²	0.017 / 0.335		0.000 / 0.319

Note. * $p < 0.05$ ** $p < 0.01$ *** $p < 0.001$, ^a Cortex PVD ~ hemi + (1|Participant) + (1|Lesion) + (1|Control_Image), ^b cWM PVD ~ hemi + (1|Participant) + (1|Lesion) + (1|Control_Image).

Table B.4. Outputs from linear mixed-models testing whether lesion characteristics can significantly explain variance in PVD across $hemi_{lesion}$ and $hemi_{contra}$

Predictors	Cortex PVD				cWM PVD			
	Hemi _{lesion} ^a		Hemi _{lesion} ^b		Hemi _{contra} ^c		Hemi _{contra} ^d	
	Estimates	std. Error	Estimates	std. Error	Estimates	std. Error	Estimates	std. Error
(Intercept)	0.62 *** (0.48 – 0.76)	0.07	0.48 *** (0.36 – 0.60)	0.06	0.44 *** (0.31 – 0.56)	0.06	0.44 *** (0.31 – 0.57)	0.07
Mean Intensity	-0.14 (-0.31 – 0.04)	0.09	-0.01 (-0.17 – 0.15)	0.08	0.03 (-0.12 – 0.19)	0.08	0.02 (-0.14 – 0.19)	0.08
SD Intensity	-0.23 ** (-0.40 – -0.06)	0.09	-0.16 * (-0.32 – -0.00)	0.08	-0.00 (-0.16 – 0.15)	0.08	-0.11 (-0.28 – 0.05)	0.08
Volume	0.28 *** (0.20 – 0.35)	0.04	-0.00 (-0.06 – 0.06)	0.03	0.15 *** (0.09 – 0.21)	0.03	0.05 (-0.01 – 0.10)	0.03
Random Effects								
	σ^2	0.25		0.14		0.15		0.15
	τ_{00}	0.04 Control_Image		0.04 Control_Image		0.03 Control_Image		0.04 Control_Image
	ICC	0.13 Control_Image		0.20 Control_Image		0.18 Control_Image		0.20 Control_Image
	Observations	176		176		176		176
	Marginal R ² / Conditional R ²	0.274 / 0.370		0.121 / 0.294		0.112 / 0.269		0.085 / 0.271

Note. * $p < 0.05$ ** $p < 0.01$ *** $p < 0.001$, ^aCortex PVD ~ Mean_Intensity + SD_Intensity + Volume + (1|Control_Image), subset = (hemi=='Lesion'), ^bCortex PVD ~ Mean_Intensity + SD_Intensity + Volume + (1|Control_Image), subset = (hemi=='Contralesion'), ^ccWM PVD ~ Mean_Intensity + SD_Intensity + Volume + (1|Control_Image), subset = (hemi=='Lesion'), ^dcWM PVD ~ Mean_Intensity + SD_Intensity + Volume + (1|Control_Image), subset = (hemi=='Contralesion'),

Appendix C - Supplementary Materials for Chapter 4

Freesurfer Lesion Pipeline

We adapted the Freesurfer pipeline to mitigate some of the Issues surrounding surface-based parcellations in the presence of traumatic lesions, particularly the effect of lesions on the surface placement of contralateral region. The current paper utilises a new approach to Freesurfer segmentation in the presence of focal lesions. Lesions were identified in our dataset by a single rater and masks drawn where visible lesions could be identified by eye using T1w. Lesions were segmented manually (by JN) using the MRTrix (Tournier et al., 2012) software package, producing a binary lesion mask for each patient. These were used to enantiomorphically fill the lesions using the approach of Nachev et al. (2008). Briefly, this approach robustly registers the lesioned hemisphere to the non-lesioned hemisphere and fills the lesioned voxels (indicated by the lesion-mask) with healthy appearing signal intensities from the contra-lesional hemisphere. The output is an image with approximately-typical T1w voxel intensities in place of the lesioned tissue. This enanteomorphically generated T1w image was then processed using the Freesurfer cortical surface segmentation pipeline (with both -3T and -mprage flags). By processing this image rather than the original T1w MRI, we mitigate potential contrast-induced errors which may contribute to the lesion-induced error, even in the contralesional hemisphere.

As lesion masks were drawn in the native space directly into the T1w images, these could be projected onto the cortical surface vertices on the corresponding patient's Freesurfer surface model. This projected lesion ROI was filled (to avoid holes due to voxel-vertex mismatches) and was used as an ROI label for further analyses.

Individual-subject level atlas parcellations were then masked using the surface projected lesion masks. Thus, region labels that are completely or partially occluded by lesion tissue will be overwritten with the lesion label. Morphometric measures (such as cortical thickness, volume, etc) will be calculated using the standard Freesurfer approaches but due to this relabelling, no measures will be taken from tissue which is a) lesioned within the original image and b) filled with estimated voxel intensities in the enanteomorphically filled T1w images.

The output of this pipeline is cortical morphology measurements which are not contaminated by lesion tissue or the wider error associated with the processing of lesioned T1w images. For those regions which are completely occluded by the lesion label, morphological measures will be reported as zero. These will be recoded as NaN to ensure that when generating the covariance matrix we do not estimate covariance with this region.

ABIDE Dataset Quality Control

Quality assurance (QA) of ABIDE Imaging Data

The ABIDE pre-processed data provided by the PCP includes QA metrics as calculated using the Quality Assessment Protocol software (QAP, Shehzad et al. (2015)). We used the six spatial anatomical QA measures provided, to perform QA on the included data. Given that the ABIDE dataset includes data from 17 recruitment sites, there is potential for a ‘batch effect’ on QA seen between sites (Esteban et al., 2017). Hence, all QA metrics were centred (mean subtracted) and scaled (divided by Standard deviation) within-site. This results in metrics that are standardised and can be compared between sites. All metrics were also coded to ensure higher scores represented higher quality. We then calculated, per subject, how many of the QA metrics had a Zscore of below -1.5 (indicating quality which was 1.5SD below the mean). We included subjects if they had zero or one QA metric that fell below this quality metric. Of the ABIDE cases who were recorded as a) controls and b) being younger than 17 years of age at scanning (n=361), 14 subjects were removed due to having greater than one QA metric fall below the 1.5SD cut off (20 participants also had no Freesufer data available, resulting in the final ABIDE dataset of $n = 327$). Further details of the automated QA measures which are included can be found here: http://preprocessed-connectomes-project.org/abide/quality_assessment.html and <http://preprocessed-connectomes-project.org/quality-assessment-protocol>.

Site effects on cortical thickness within the ABIDE cohort

Given the control cases from the ABIDE dataset were recruited from multiple sites, it is important to control for potential site-effects on the cortical thickness measurements (Fortin et al., 2018). To account for these we adopt the residuals harmonization approach used by Fortin et al. (2018). Briefly, for each ROI, a linear model was defined with the site as a predictor and cortical thickness as the dependant measure. The vector of coefficients for each level of the site predictor was estimated, with the coefficient representing the site effects. For each site, this coefficient was subtracted from the individual subject’s cortical thickness values. This was done for each ROI independently.

Results when Lesion Cases (n=8) Excluded

Of the eight lesion cases removed five were assigned to the EF_{Good} subgroup, two to the EF_{Poor} and one had no EF data available. Analyses were repeated with these cases removed and results are outlined below.

Differences in CT between pTBI and Controls

Across all contrasts, no regional CT reductions in the TBI group compared to controls were significant (after FDR correction).

Differences in SC between pTBI and Controls

No significant difference in mean graph strength was found between patients and controls (observed difference (ObsDiff) = -11.5, $p_{\text{fdr}} = .063$). When investigating subgroups, significant differences were found between controls and EF_{poor} but not EF_{Good} (ObsDiff = -21.3, $p_{\text{fdr}} = .006$, and ObsDiff = -11.6, $p_{\text{fdr}} = .063$ respectively). After fdr correction no nodal differences remained significant between control and the whole pTBI group or EF_{Good} subgroups. However, when comparing the EF_{poor} group to controls, multiple regions (50/68) showed significantly greater nodal strength in the patient group.

SC between regions with CT reductions in pTBI

When considering the whole group of pTBI patients, for no value of n number of regions was the mean strength of regions significantly greater than that of n randomly selected regions. This was also true of the EF_{Good} subgroup.

However, for the EF_{poor} group, the mean strength of the greatest n nodes with cortical thickness reductions was significantly greater than the mean strength of n randomly selected regions for 36/67 values of n ($n = 10-11, 28-29, 31, 33-63$, p_{fdr} all $< .05$). When using the ABIDE dataset these results were largely repeated, with mean node strength being significantly greater than n randomly selected regions for multiple values of n (43/67) in the EF_{poor} group ($n = 23-24, 26-65, 67$, p_{fdr} all $< .05$), but neither the whole pTBI sample or the EF_{Good} subgroup.

List of ABIDE subject IDs included in the current study

Study.ID	MaxMun_d_0051356	NYU_0051091	Olin_0050113
KKI_0050772	MaxMun_d_0051357	NYU_0051093	Olin_0050116
KKI_0050773	MaxMun_d_0051358	NYU_0051094	Pitt_0050031
KKI_0050774	MaxMun_d_0051359	NYU_0051095	Pitt_0050033
KKI_0050775	MaxMun_d_0051360	NYU_0051096	Pitt_0050034
KKI_0050776	MaxMun_d_0051361	NYU_0051097	Pitt_0050036
KKI_0050777	NYU_0051036	NYU_0051098	Pitt_0050038
KKI_0050778	NYU_0051038	NYU_0051099	Pitt_0050043
KKI_0050779	NYU_0051039	NYU_0051100	Pitt_0050045
KKI_0050780	NYU_0051040	NYU_0051101	Pitt_0050047
KKI_0050781	NYU_0051041	NYU_0051102	Pitt_0050048
KKI_0050782	NYU_0051042	NYU_0051103	Pitt_0050049
KKI_0050783	NYU_0051044	NYU_0051104	Pitt_0050050
KKI_0050784	NYU_0051045	NYU_0051105	Pitt_0050051
KKI_0050785	NYU_0051046	NYU_0051106	Pitt_0050054
KKI_0050786	NYU_0051047	NYU_0051107	SDSU_0050193
KKI_0050788	NYU_0051048	NYU_0051109	SDSU_0050194
KKI_0050789	NYU_0051049	NYU_0051110	SDSU_0050195
KKI_0050790	NYU_0051050	NYU_0051111	SDSU_0050196
KKI_0050812	NYU_0051051	NYU_0051121	SDSU_0050198
KKI_0050814	NYU_0051052	NYU_0051122	SDSU_0050199
KKI_0050816	NYU_0051053	NYU_0051123	SDSU_0050200
KKI_0050817	NYU_0051054	NYU_0051124	SDSU_0050201
KKI_0050818	NYU_0051055	NYU_0051126	SDSU_0050202
KKI_0050819	NYU_0051064	NYU_0051127	SDSU_0050203
KKI_0050820	NYU_0051065	NYU_0051128	SDSU_0050204
KKI_0050821	NYU_0051069	NYU_0051159	SDSU_0050205
KKI_0050822	NYU_0051070	OHSU_0050157	SDSU_0050206
Leuven_2_0050722	NYU_0051071	OHSU_0050158	SDSU_0050208
Leuven_2_0050723	NYU_0051072	OHSU_0050159	SDSU_0050209
Leuven_2_0050724	NYU_0051073	OHSU_0050160	SDSU_0050210
Leuven_2_0050725	NYU_0051074	OHSU_0050161	SDSU_0050211
Leuven_2_0050726	NYU_0051075	OHSU_0050162	SDSU_0050213
Leuven_2_0050727	NYU_0051076	OHSU_0050163	SDSU_0050214
Leuven_2_0050728	NYU_0051078	OHSU_0050164	SDSU_0050215
Leuven_2_0050730	NYU_0051079	OHSU_0050166	SDSU_0050217
Leuven_2_0050731	NYU_0051080	OHSU_0050167	Stanford_0051180
Leuven_2_0050732	NYU_0051081	OHSU_0050168	Stanford_0051181
Leuven_2_0050733	NYU_0051082	OHSU_0050169	Stanford_0051182
Leuven_2_0050735	NYU_0051083	OHSU_0050170	Stanford_0051183
Leuven_2_0050736	NYU_0051084	OHSU_0050171	Stanford_0051184
Leuven_2_0050737	NYU_0051085	Olin_0050102	Stanford_0051185
Leuven_2_0050738	NYU_0051086	Olin_0050103	Stanford_0051186
Leuven_2_0050739	NYU_0051087	Olin_0050104	Stanford_0051187
Leuven_2_0050740	NYU_0051088	Olin_0050106	Stanford_0051188
Leuven_2_0050741	NYU_0051089	Olin_0050110	Stanford_0051189
Leuven_2_0050742	NYU_0051090	Olin_0050111	Stanford_0051190

Stanford_0051191	UCLA_1_0051280	UM_1_0050374
Stanford_0051192	UCLA_1_0051281	UM_1_0050375
Stanford_0051193	UCLA_1_0051282	UM_1_0050376
Stanford_0051194	UCLA_2_0051303	UM_1_0050377
Stanford_0051195	UCLA_2_0051304	UM_1_0050379
Stanford_0051196	UCLA_2_0051305	UM_1_0050381
Stanford_0051197	UCLA_2_0051306	UM_2_0050383
Stanford_0051198	UCLA_2_0051307	UM_2_0050387
Stanford_0051199	UCLA_2_0051308	UM_2_0050390
Trinity_0050257	UCLA_2_0051309	UM_2_0050414
Trinity_0050265	UCLA_2_0051311	UM_2_0050416
Trinity_0050266	UCLA_2_0051312	UM_2_0050417
Trinity_0050268	UCLA_2_0051313	UM_2_0050418
Trinity_0050269	UCLA_2_0051314	UM_2_0050419
Trinity_0051133	UCLA_2_0051315	UM_2_0050421
Trinity_0051134	UCLA_2_0051316	UM_2_0050422
Trinity_0051136	UM_1_0050327	UM_2_0050425
Trinity_0051137	UM_1_0050330	UM_2_0050426
Trinity_0051138	UM_1_0050332	UM_2_0050427
Trinity_0051140	UM_1_0050333	UM_2_0050428
Trinity_0051141	UM_1_0050334	USM_0050435
Trinity_0051142	UM_1_0050336	USM_0050436
UCLA_1_0051250	UM_1_0050337	USM_0050437
UCLA_1_0051251	UM_1_0050338	USM_0050438
UCLA_1_0051252	UM_1_0050340	USM_0050447
UCLA_1_0051253	UM_1_0050342	USM_0050448
UCLA_1_0051254	UM_1_0050343	USM_0050453
UCLA_1_0051255	UM_1_0050347	USM_0050470
UCLA_1_0051256	UM_1_0050350	Yale_0050551
UCLA_1_0051257	UM_1_0050351	Yale_0050552
UCLA_1_0051258	UM_1_0050352	Yale_0050556
UCLA_1_0051260	UM_1_0050353	Yale_0050559
UCLA_1_0051262	UM_1_0050354	Yale_0050563
UCLA_1_0051263	UM_1_0050355	Yale_0050564
UCLA_1_0051264	UM_1_0050357	Yale_0050565
UCLA_1_0051265	UM_1_0050358	Yale_0050566
UCLA_1_0051266	UM_1_0050359	Yale_0050568
UCLA_1_0051267	UM_1_0050360	Yale_0050569
UCLA_1_0051269	UM_1_0050362	Yale_0050571
UCLA_1_0051271	UM_1_0050363	Yale_0050572
UCLA_1_0051272	UM_1_0050364	Yale_0050573
UCLA_1_0051273	UM_1_0050365	Yale_0050574
UCLA_1_0051274	UM_1_0050366	Yale_0050576
UCLA_1_0051275	UM_1_0050367	Yale_0050577
UCLA_1_0051276	UM_1_0050369	
UCLA_1_0051277	UM_1_0050370	
UCLA_1_0051278	UM_1_0050371	
UCLA_1_0051279	UM_1_0050372	

Appendix D - Supplementary Materials for Chapter 5

List of ABIDE subject IDs included in the current study

Study.ID	Leuven_2_0050739	NYU_0051079	OHSU_0050161
KKI_0050772	Leuven_2_0050740	NYU_0051080	OHSU_0050162
KKI_0050773	Leuven_2_0050741	NYU_0051081	OHSU_0050163
KKI_0050774	Leuven_2_0050742	NYU_0051082	OHSU_0050164
KKI_0050775	MaxMun_d_005135	NYU_0051083	OHSU_0050166
KKI_0050776	6	NYU_0051084	OHSU_0050167
KKI_0050777	MaxMun_d_005135	NYU_0051085	OHSU_0050168
KKI_0050778	7	NYU_0051086	OHSU_0050169
KKI_0050779	MaxMun_d_005135	NYU_0051087	OHSU_0050170
KKI_0050780	8	NYU_0051088	OHSU_0050171
KKI_0050781	MaxMun_d_005135	NYU_0051089	Olin_0050102
KKI_0050782	9	NYU_0051090	Olin_0050103
KKI_0050783	MaxMun_d_005136	NYU_0051091	Olin_0050104
KKI_0050784	0	NYU_0051093	Olin_0050106
KKI_0050785	1	NYU_0051094	Olin_0050110
KKI_0050786	NYU_0051036	NYU_0051095	Olin_0050111
KKI_0050788	NYU_0051038	NYU_0051096	Olin_0050113
KKI_0050789	NYU_0051039	NYU_0051097	Olin_0050116
KKI_0050790	NYU_0051040	NYU_0051098	Pitt_0050031
KKI_0050812	NYU_0051041	NYU_0051099	Pitt_0050033
KKI_0050814	NYU_0051042	NYU_0051100	Pitt_0050034
KKI_0050816	NYU_0051044	NYU_0051101	Pitt_0050036
KKI_0050817	NYU_0051045	NYU_0051102	Pitt_0050038
KKI_0050818	NYU_0051046	NYU_0051103	Pitt_0050043
KKI_0050819	NYU_0051047	NYU_0051104	Pitt_0050045
KKI_0050820	NYU_0051048	NYU_0051105	Pitt_0050047
KKI_0050821	NYU_0051049	NYU_0051106	Pitt_0050048
KKI_0050822	NYU_0051050	NYU_0051107	Pitt_0050049
Leuven_2_0050722	NYU_0051051	NYU_0051109	Pitt_0050050
Leuven_2_0050723	NYU_0051052	NYU_0051110	Pitt_0050051
Leuven_2_0050724	NYU_0051053	NYU_0051111	Pitt_0050054
Leuven_2_0050725	NYU_0051054	NYU_0051121	SDSU_0050193
Leuven_2_0050726	NYU_0051055	NYU_0051122	SDSU_0050194
Leuven_2_0050727	NYU_0051064	NYU_0051123	SDSU_0050195
Leuven_2_0050728	NYU_0051065	NYU_0051124	SDSU_0050196
Leuven_2_0050730	NYU_0051069	NYU_0051126	SDSU_0050198
Leuven_2_0050731	NYU_0051070	NYU_0051127	SDSU_0050199
Leuven_2_0050732	NYU_0051071	NYU_0051128	SDSU_0050200
Leuven_2_0050733	NYU_0051072	NYU_0051159	SDSU_0050201
Leuven_2_0050735	NYU_0051073	OHSU_0050157	SDSU_0050202
Leuven_2_0050736	NYU_0051074	OHSU_0050158	SDSU_0050203
Leuven_2_0050737	NYU_0051075	OHSU_0050159	SDSU_0050204
Leuven_2_0050738	NYU_0051076	OHSU_0050160	SDSU_0050205
	NYU_0051078		

SDSU_0050206	Trinity_0051142	UCLA_2_0051315	UM_2_0050387
SDSU_0050208	UCLA_1_0051250	UCLA_2_0051316	UM_2_0050390
SDSU_0050209	UCLA_1_0051251	UM_1_0050327	UM_2_0050414
SDSU_0050210	UCLA_1_0051252	UM_1_0050330	UM_2_0050416
SDSU_0050211	UCLA_1_0051253	UM_1_0050332	UM_2_0050417
SDSU_0050213	UCLA_1_0051254	UM_1_0050333	UM_2_0050418
SDSU_0050214	UCLA_1_0051255	UM_1_0050334	UM_2_0050419
SDSU_0050215	UCLA_1_0051256	UM_1_0050336	UM_2_0050421
SDSU_0050217	UCLA_1_0051257	UM_1_0050337	UM_2_0050422
Stanford_0051180	UCLA_1_0051258	UM_1_0050338	UM_2_0050425
Stanford_0051181	UCLA_1_0051260	UM_1_0050340	UM_2_0050426
Stanford_0051182	UCLA_1_0051262	UM_1_0050342	UM_2_0050427
Stanford_0051183	UCLA_1_0051263	UM_1_0050343	UM_2_0050428
Stanford_0051184	UCLA_1_0051264	UM_1_0050347	USM_0050435
Stanford_0051185	UCLA_1_0051265	UM_1_0050350	USM_0050436
Stanford_0051186	UCLA_1_0051266	UM_1_0050351	USM_0050437
Stanford_0051187	UCLA_1_0051267	UM_1_0050352	USM_0050438
Stanford_0051188	UCLA_1_0051269	UM_1_0050353	USM_0050447
Stanford_0051189	UCLA_1_0051271	UM_1_0050354	USM_0050448
Stanford_0051190	UCLA_1_0051272	UM_1_0050355	USM_0050453
Stanford_0051191	UCLA_1_0051273	UM_1_0050357	USM_0050470
Stanford_0051192	UCLA_1_0051274	UM_1_0050358	Yale_0050551
Stanford_0051193	UCLA_1_0051275	UM_1_0050359	Yale_0050552
Stanford_0051194	UCLA_1_0051276	UM_1_0050360	Yale_0050556
Stanford_0051195	UCLA_1_0051277	UM_1_0050362	Yale_0050559
Stanford_0051196	UCLA_1_0051278	UM_1_0050363	Yale_0050563
Stanford_0051197	UCLA_1_0051279	UM_1_0050364	Yale_0050564
Stanford_0051198	UCLA_1_0051280	UM_1_0050365	Yale_0050565
Stanford_0051199	UCLA_1_0051281	UM_1_0050366	Yale_0050566
Trinity_0050257	UCLA_1_0051282	UM_1_0050367	Yale_0050568
Trinity_0050265	UCLA_2_0051303	UM_1_0050369	Yale_0050569
Trinity_0050266	UCLA_2_0051304	UM_1_0050370	Yale_0050571
Trinity_0050268	UCLA_2_0051305	UM_1_0050371	Yale_0050572
Trinity_0050269	UCLA_2_0051306	UM_1_0050372	Yale_0050573
Trinity_0051133	UCLA_2_0051307	UM_1_0050374	Yale_0050574
Trinity_0051134	UCLA_2_0051308	UM_1_0050375	Yale_0050576
Trinity_0051136	UCLA_2_0051309	UM_1_0050376	Yale_0050577
Trinity_0051137	UCLA_2_0051311	UM_1_0050377	
Trinity_0051138	UCLA_2_0051312	UM_1_0050379	
Trinity_0051140	UCLA_2_0051313	UM_1_0050381	
Trinity_0051141	UCLA_2_0051314	UM_2_0050383	

Quality assurance (QA) of ABIDE Imaging Data

The ABIDE pre-processed data provided by the PCP includes QA metrics as calculated using the Quality Assessment Protocol software (QAP, Shehzad et al. (2015)). We used the six spatial anatomical QA measures provided, to perform QA on the included data. Given that the ABIDE dataset includes data from 17 recruitment sites, there is potential for a ‘batch effect’ on QA seen between sites (Esteban et al., 2017). Hence, all QA metrics were centred (mean subtracted) and scaled (divided by Standard deviation) within site. This results in metrics which are standardised and can be compared between sites. All metrics were also coded to ensure higher scores represented higher quality. We then calculated, per subject, how many of the QA metric had a Zscore of below -1.5 (indicating quality which was 1.5SD below the mean). Subjects were excluded if they had more than one QA metric that fell below this quality metric. Of the ABIDE cases who were recorded as a) controls and b) being younger than 17 years of age at scanning (n=361), 14 subjects were removed due to having greater than one QA metric fall below the 1.5SD cut off (20 participants also had no FreeSurfer data available, resulting in the final ABIDE dataset of $n = 327$). Further details of the automated QA measures which are included can be found here: http://preprocessed-connectomes-project.org/abide/quality_assessment.html and <http://preprocessed-connectomes-project.org/quality-assessment-protocol>.

Site effects on cortical thickness within the ABIDE cohort and between cohorts

Given the control cases from the ABIDE dataset were recruited from multiple sites, it is important to control for potential site-effects on the cortical thickness measurements (Fortin et al., 2018). To account for these we adopt the residuals harmonization approach used by Fortin et al. (2018). Briefly, for each ROI, a linear model was defined with site as a predictor and cortical thickness as the dependant measure. The vector of coefficients for each level of the site predictor was estimated, with the coefficient representing the site effects. For each site, this coefficient was subtracted from the individual subject’s cortical thickness values. This was done for each ROI independently. Subsequently, this was repeated for the whole cohort to account for cohort effects (ABIDE cohort vs TBI cohort). The residuals harmonization approach was used to estimate the effect of cohort between control participants in the ABIDE and TBI cohorts (excluding TBI patients to ensure that this estimate is not confounded by the effect of injury). This estimate of cohort effect was subtracted from TBI cohort subject’s (patients and controls) cortical thickness values.

Selection of Appropriate Window-size for age-matched DDI

Optimal window-size was selected against a number of criteria: a) based on recommendations by Saggart et al. (2015) in relation to stability of their AOP metric, b) maximised the Mann-Whitney statistic for control vs TBI differences in DDI measure, and c) which resulted in an n^{th} window (where number of

windows is 1 : n) which was as close to the defined window size as possible. Saggari et al. (2015) investigated the stability of their AOP metric and found that a reference group of between 25 and 30 subjects ensured that there was a stable a) estimate of the AOP metric for the patient group, b) estimate of the correlation between AOP metric and behavioural measures and c) estimate of the correlation between AOP metric and behavioural measures in an external dataset.

Therefore we investigated 5 potential window sizes of varying number of subjects; $n = 22, 26, 30, 34,$ and 38. We did not vary step size, these windows remained half overlapping. We calculated the age-matched DDI for all subjects within this studies cohort and compared them between patients and controls using a Mann-Whitney test, due to the non-normal distribution of the data. Based on these given window sizes, we also calculated the size of the final sliding window. Both the Mann-Whitney statistics and final window sizes can be seen in Table D1

Post-hoc Exploratory Analyses

Differences in DDI over Severity

We investigated whether DDI_{inv} and DDI_{age} differed as a function of injury severity. To maintain statistical power, mild-complex, moderate and severe injury classifications were grouped into a ‘Moderate/Severe’ group for comparisons. Clinical presentation between injury severities is very different and thus treating the patient group as a single cohort in patient vs control analyses of the divergence index may miss clinically meaningful differences.

As can be seen in Table D2. across DDI_{inv} and DDI_{age} , for both the whole brain and CEN, non-parametric Kruskal-Wallis rank sum tests showed that the DDI measure did not change as a function of injury severity. This is further shown in Figure D1.

Table D1. *Details from analyses assessing appropriate window-size for primary analyses*

Window Size	Mann-Whitney Statistic	No. of windows	Final Window Size
22	1177	29	19
26	1237	25	15
30	1201	21	27
34	1210	20	21
38	1176	17	23

Table D2. *Differences in DDI between injury severity groups across whole-brain and CEN*

DDI Measure		Median Value			Difference ^b
		Controls (n = 33)	Mild TBI (n = 47)	Moderate/ Severe TBI ^a (n = 28)	
DDI _{inv.}	Whole-brain	3.97e-05	4.85e-05	5.2e-05	$\chi^2(2) = 1.96, p = .375$
	CEN	1.04e-05	1.39e-05	1.5e-05	$\chi^2(2) = .632, p = .729$
DDI _{age}	Whole-brain	4.14e-03	4.41e-03	5.01e-03	$\chi^2(2) = .991, p = .609$
	CEN	1.52e-03	1.12e-03	1.40e-03	$\chi^2(2) = .211, p = .900$

^a. Mild complicated TBI + Moderate TBI + Severe TBI, ^b. Kruskal-Wallis rank sum test. *p* values are uncorrected values.

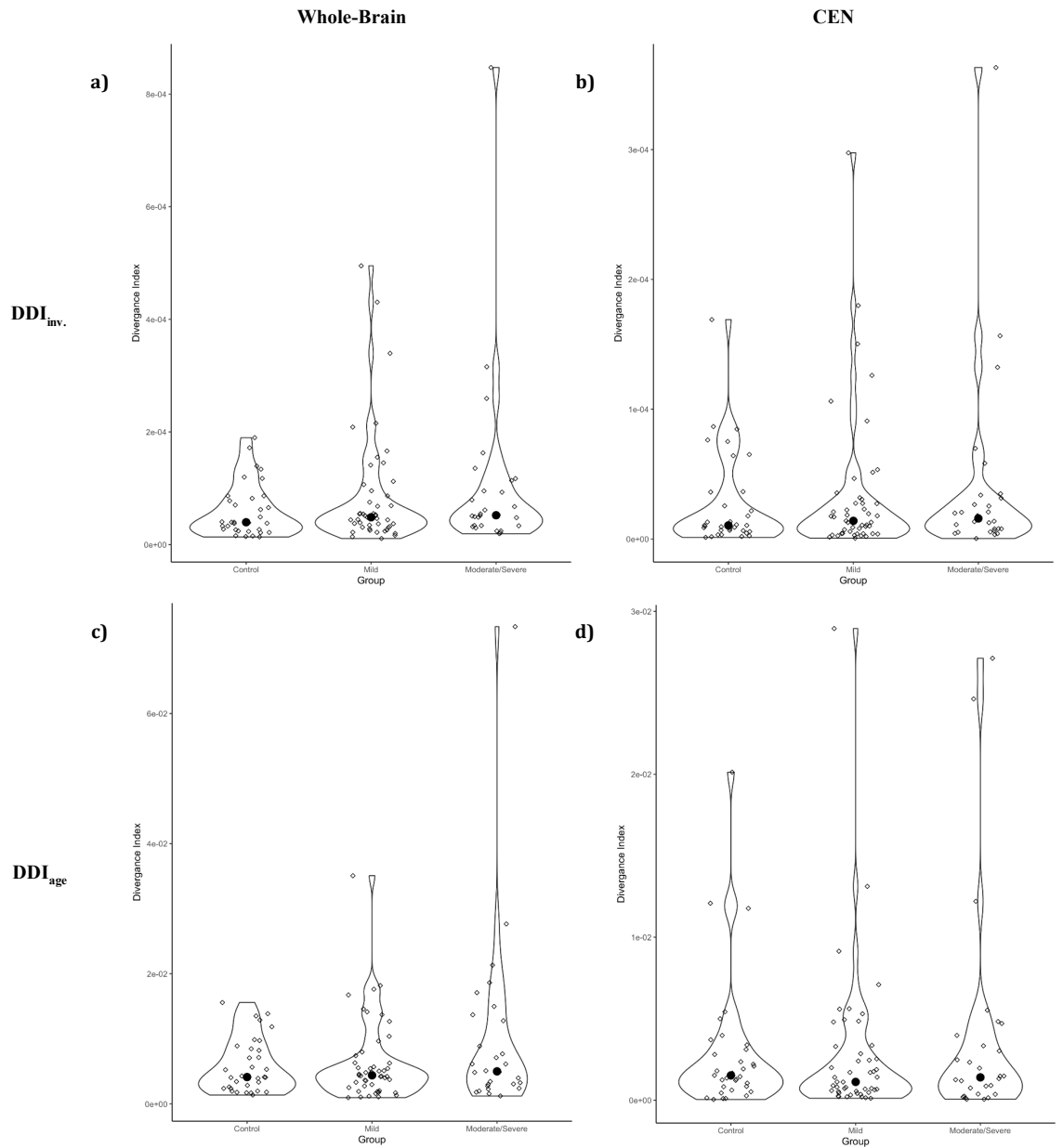


Figure D1. Differences in DDI_{inv} (top-row) and DDI_{age} (bottom-row) for both the whole brain (first column) and only the CEN (second column) across injury severities.

Partial correlations between DDI and EF

Partial correlations (Pearson's) were computed using the `jmuOutlier` (version 2.2) package in R (Garren, 2019) between whole-brain DDI_{inv}/DDI_{age} and EF/BRIEF whilst controlling for a) age at scanning (yrs), and b) both age at scanning (yrs) and the interval between MRI and EF assessment (days). This was to investigate whether the relationship between DDI_{inv}/DDI_{age} and EF/BRIEF was maintained whilst controlling for potentially confounding factors. As shown in Table S3, the results of these analyses were qualitatively the same, with very little changes to correlation coefficients. It is important to note that the p values reported in the table are uncorrected, parametric p values and therefore should be interpreted with caution.

Table D3. Pearson's partial correlation coefficients (*r*) between DDI and EF outcomes, controlling for age at MRI and interval between MRI and EF neuropsychological assessment with associated parametric *p*-values

DDI Measure	DV	Controlling for Age at MRI (yrs)						Controlling for Age at MRI (yrs) and MRI-EF assessment interval (days)					
		TBI Patients		Controls		Whole Sample		TBI Patients		Controls		Whole Sample	
		<i>r</i>	<i>p</i>	<i>r</i>	<i>p</i>	<i>r</i>	<i>p</i>	<i>r</i>	<i>p</i>	<i>r</i>	<i>p</i>	<i>r</i>	<i>p</i>
DDI _{inv.}	EF ^a	-.321	.021	-.064	.752	-.299	.007	-.321	.023	-.262	.196	-.273	.016
	BRIEF ^b	.272	.054	.413	.021	.296	.007	.270	.058	.447	.013	.284	.010
DDI _{age}	EF ^a	-.326	.020	-.084	.676	-.307	.006	-.326	.021	-.219	.283	-.288	.010
	BRIEF ^b	.254	.072	.314	.086	.270	.014	.254	.075	.325	.079	.263	.017

^a. Complete cases for correlation are n = 52 for TBI group and n = 28 for controls, ^b. complete cases for correlation are n = 52 for TBI group and n = 32 for controls. *p* values are raw, uncorrected values calculated using a parametric partial correlation approach.

Appendix E - Supplementary Materials for Chapter 6

Dimension reduction of Executive functioning task performance

A principal component analysis (PCA, using the 'prcomp' function in the base R 'stats' package (R Core Team, 2016)) was used to find a common EF component across all three EF measures. Data reduction using the PCA was done for two main reasons; a) to reduce dimensionality, and the number of multiple predictor models being built and b) to ensure that we were predicting (a latent variable of) executive functioning ability, rather than ability linked to task-specific performance.

The PCA suggested a three-component solution, however only the first component had an eigen-value > 1 (eigenvalue=1.607) and so only this component was retained. This component explained ~54% variance across our measures. All three measures; list-sort, card-sort and flanker, positively loaded onto this component (rotated sums of squares loading = .362, .673 and .646 respectively).

Appendix F - Supplementary Materials for Chapter 7

Differences in graph-level morphometric similarity across ROIs

When comparing pTBI patients against controls, mean difference in the magnitude of morphometric similarity (adjusted for age at scanning, sex, age*sex, and eTIV) across the brain was not significant following FDR correction, across all network thresholds tested (all $p_{\text{fdr}} > .05$). These can be seen below in Table F1. This was repeated for all ROIs of the unthresholded network to investigate the effect of group on nodal strength, and similar null results were found (all $p_{\text{fdr}} > .05$), which can be seen in Table F2.

Table F.1. Results of GLM to test the effect of group (TBI vs Controls) on average nodal strength, whilst controlling for age at scanning, sex, age*sex, and estimated total intracranial volume (eTIV).

Density Threshold	Mean Normalised Strength ^a		$p_{\text{fdr}}^{\text{b}}$	Hedges g^{c}
	Patient	Control		
0.05	3.23	3.23	0.75	0.09
0.1	6.25	6.25	0.98	0.01
0.15	9.02	9.03	0.75	-0.09
0.2	11.50	11.53	0.54	-0.20
0.25	13.64	13.71	0.37	-0.29
0.3	15.42	15.53	0.24	-0.36
0.35	16.81	16.98	0.22	-0.41
0.4	17.81	18.01	0.22	-0.44
1	-0.20	-0.13	0.54	-0.19

Note. ^a Mean values adjusted for covariates (age, sex, age*sex and eTIV), ^b False discovery rate corrected p values, ^c Corrected for unequal sample sizes

Table F.2. Results of GLM to test the effect of group (TBI vs Controls) on nodal strength, whilst controlling for covariates across all ROIs for the unthresholded network

ROI	p_{fdr}^a	Hedges g^b	ROI	p_{fdr}^a	Hedges g^b
lBSTS	0.46	-0.47	rBSTS	0.55	-0.27
lcACC	1.00	0.00	rcACC	0.76	-0.14
lcMFG	0.94	0.04	rcMFG	0.55	-0.24
lCUN	0.46	0.39	rCUN	0.46	0.40
lENT	0.55	0.26	rENT	0.55	0.23
lFUS	0.99	-0.01	rFUS	0.76	-0.15
lIPL	0.76	-0.13	rIPL	0.68	-0.19
lITG	0.50	-0.34	rITG	0.53	-0.30
liCC	0.94	-0.03	riCC	0.55	0.26
lLOG	0.90	-0.07	rLOG	0.90	0.09
lLOF	0.90	0.08	rLOF	0.94	-0.03
lLING	0.55	0.26	rLING	0.51	0.32
lMOF	0.94	0.03	rMOF	0.78	-0.12
lMTG	0.46	-0.39	rMTG	0.55	-0.23
lPARH	1.00	0.00	rPARH	0.55	-0.30
lparaC	0.90	-0.07	rparaC	0.51	0.32
lpOPER	0.68	-0.19	rpOPER	0.78	0.12
lpORB	0.46	0.42	rpORB	0.46	0.42
lpTRI	0.55	-0.27	rpTRI	0.55	0.28
lperiCAL	0.70	0.17	rperiCAL	0.51	0.32
lpostC	0.90	0.06	rpostC	0.46	-0.39
lPCC	0.90	0.09	rPCC	0.55	0.24
lpreC	0.70	-0.17	rpreC	0.50	-0.36
lPCUN	0.90	-0.06	rPCUN	0.46	-0.53
lrACC	0.50	-0.34	rrACC	0.90	0.06
lrMFG	0.55	-0.25	rrMFG	0.76	-0.14
lSFG	0.55	-0.25	rSFG	0.55	-0.23
lSPL	0.90	0.06	rSPL	0.90	0.06
lSTG	0.50	-0.36	rSTG	0.46	-0.44
lSMAR	0.94	-0.03	rSMAR	0.55	-0.26
lFP	0.50	0.34	rFP	0.55	0.23
lTP	0.76	0.14	rTP	0.74	0.16
lTT	0.99	0.01	rTT	0.70	0.17
lINS	0.55	-0.22	rINS	0.77	-0.13

Note. ^a False discovery rate corrected p values, ^b Corrected for unequal sample sizes

Exploratory Tests of Differences in graph-level morphometric similarity across multiple groupings

Given we found no significant differences between patients and controls for morphometric similarity, we post-hoc hypothesised that this may be due to the level inhomogeneous nature of the patient group. Thus, we conducted exploratory, post-hoc analyses of potential differences when splitting the patient group based on both outcome and clinical ratings of injury severity.

We firstly compared groups derived from injury severity. Injury severity was derived as described in previous publications of the current dataset (Anderson et al., 2013; Anderson et al., 2017; Catroppa et al., 2017), across severities of mild, mild-complex, moderate and severe. In order to reduce multiple comparisons and maintain reasonable group sample sizes, we divided the patients in to a mild group ($n=47$) and then a second group comprising all other severities (mild-complex, moderate and severe, $n=36$). We then conducted three-way comparisons between each of these groups and controls. We still found no significant differences in graph-level morphometric similarity across all network thresholds (all $p_{\text{fidr}} > .05$). These can be seen in Table F3.

We then divided the patient group based upon those exhibiting clinically relevant cognitive impairment in terms of executive (dys)function at 2 years post-injury. The current study adopted the neuropsychological impairment (NPI) rule proposed by Beauchamp et al. (2015) which has previously been used in regards to TBI (Beauchamp et al., 2015; Donders & DeWit, 2017; Beauchamp et al., 2018). Briefly, performance scores for the neuropsychological test batteries were converted to age-scaled scores ($M=10$, $SD=3$) and those assigned to the clinically impaired group were those who performed more than 1SD below average functioning on two or more individual EF measures (EF_{poor} , $n=17$), whereas those who were impaired on less than two measures were assigned to the without cognitive impairment group (EF_{good} , $n=42$). We only assigned group membership on the basis of the NPI rule for those cases who had the full battery of EF tests. When comparing morphometric similarity between those with and without impairment and those with controls again, we found no significant differences, and this can be seen in table F4. However, these results may be due to limited power due to the reduction in sample sizes.

Table F.3. Results of GLM to test differences across injury severity in average nodal strength, whilst controlling for age at scanning, sex, age*sex, and estimated total intracranial volume (eTIV).

Density Threshold	Mean Normalised Strength ^a			Hedges g ^c	Mean Normalised Strength ^a			Hedges g ^c
	Mild (n=47)	Control (n=33)	p_{fdr} ^b		Mod/Sev (n=36)	Control (n=33)	p_{fdr} ^b	
0.05	3.23	3.23	0.95	-0.02	3.23	3.23	0.71	-0.18
0.1	6.25	6.24	0.72	0.11	6.25	6.25	0.78	-0.13
0.15	9.03	9.01	0.61	0.19	9.03	9.03	0.94	-0.02
0.2	11.53	11.48	0.32	0.31	11.53	11.51	0.81	0.09
0.25	13.71	13.62	0.17	0.41	13.70	13.66	0.71	0.17
0.3	15.54	15.40	0.11	0.48	15.53	15.45	0.71	0.24
0.35	16.99	16.79	0.11	0.52	16.96	16.84	0.66	0.30
0.4	18.02	17.78	0.11	0.53	18.00	17.84	0.66	0.34
1	-0.11	-0.17	0.70	0.14	-0.15	-0.26	0.66	0.33

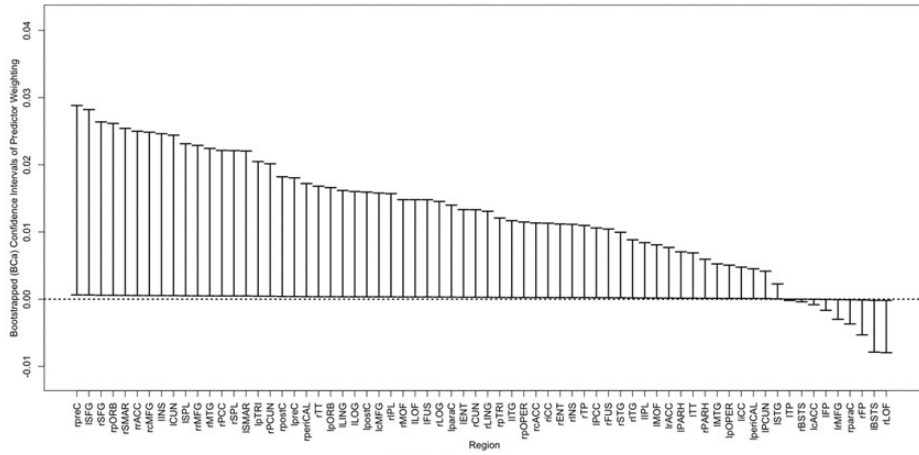
Note. ^a Mean values adjusted for covariates (age, sex, age*sex and eTIV), ^b False discovery rate corrected p values, ^c Corrected for unequal sample sizes

Table F.4. Results of GLM to test differences across EF impairment groups in average nodal strength, whilst controlling for age at scanning, sex, age*sex, and estimated total intracranial volume (eTIV).

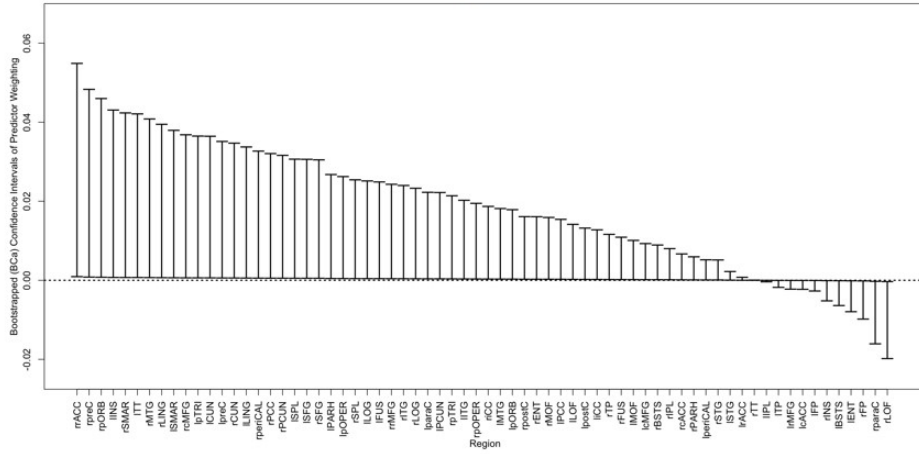
Density Threshold	Mean Normalised Strength ^a				Mean Normalised Strength ^a			
	EF _{poor} ^d		p_{fdr} ^b	Hedges g ^c	EF _{good} ^d		p_{fdr} ^b	Hedges g ^c
	(n=17)	Control (n=33)			(n=42)	Control (n=33)		
0.05	3.23	3.23	0.65	-0.28	3.23	3.23	0.64	-0.14
0.1	6.25	6.25	0.67	-0.19	6.25	6.25	0.97	0.01
0.15	9.02	9.02	0.89	0.04	9.03	9.01	0.64	0.13
0.2	11.53	11.50	0.67	0.20	11.53	11.49	0.37	0.27
0.25	13.71	13.64	0.65	0.29	13.70	13.62	0.24	0.38
0.3	15.53	15.43	0.65	0.35	15.53	15.39	0.17	0.45
0.35	16.97	16.83	0.65	0.37	16.97	16.78	0.17	0.49
0.4	18.01	17.83	0.65	0.39	18.00	17.78	0.17	0.50
1	-0.13	-0.09	0.78	-0.12	-0.14	-0.24	0.37	0.29

Note. ^a Mean values adjusted for covariates (age, sex, age*sex and eTIV), ^b False discovery rate corrected p values, ^c Corrected for unequal sample sizes, ^d Based on NPI rule where EF_{poor} represents those with clinically-relevant impairment

Curvature Index



Folding Index



Gaussian Curvature

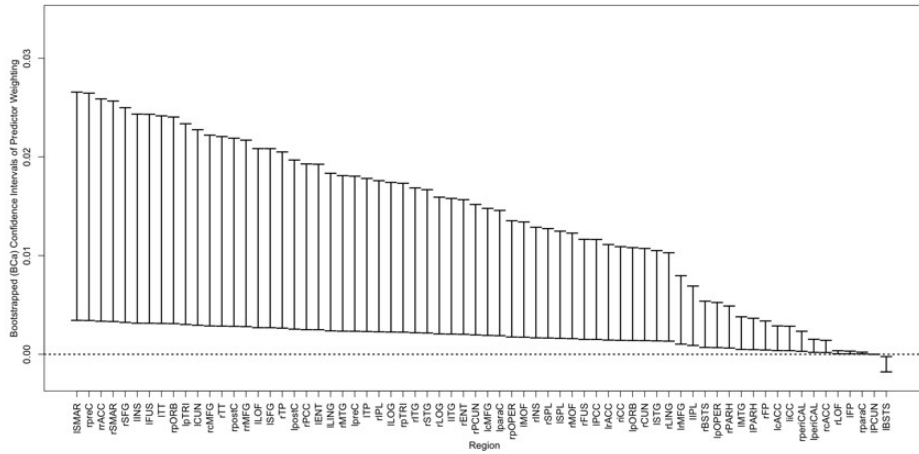


Figure F1. *Continued overleaf*

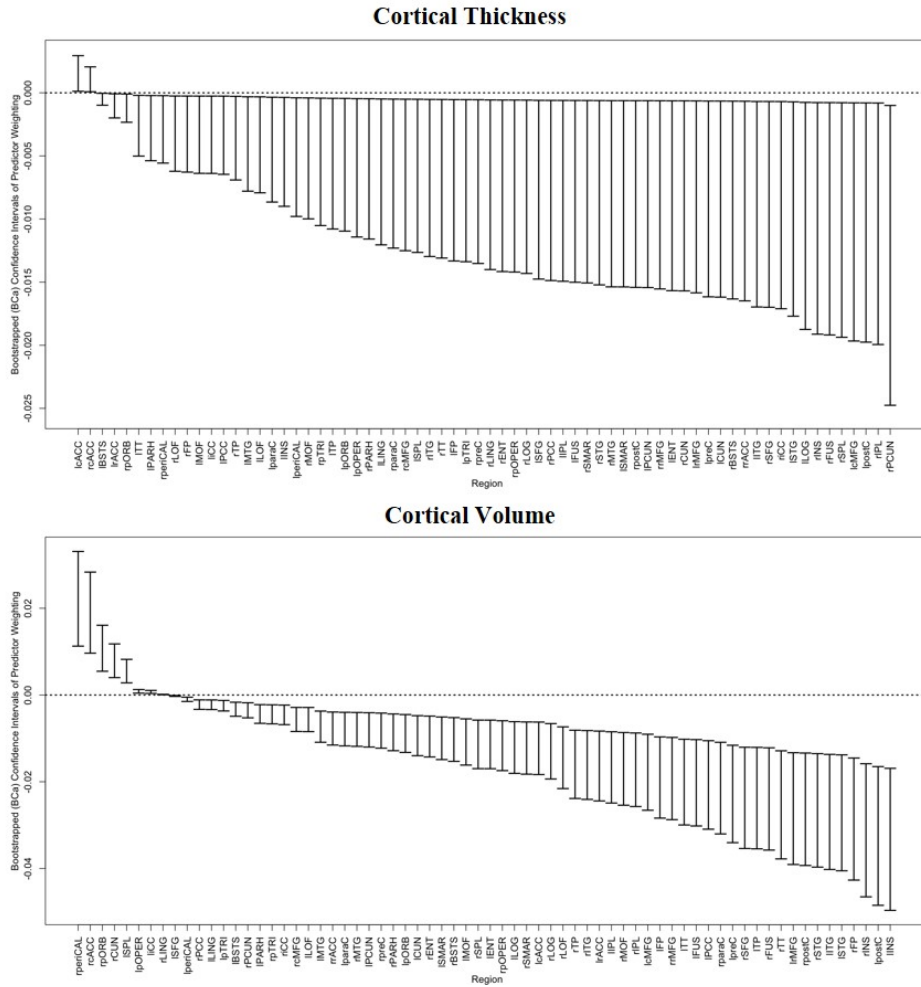


Figure F1. The bootstrapped (bias-corrected and accelerated) CI for PLS weightings for each ROI using individual morphometric features to predict BRIEF-GEC scores.

